XVI. WORKSHOP OF PHYSICAL CHEMISTS AND ELECTROCHEMISTS

BRNO, 6TH AND 7TH OF JUNE, 2016

BOOK OF ABSTRACTS

XVI. Workshop of Physical Chemists and Electrochemists

Book of abstracts

6th and 7th of June, 2016

Masaryk University

Brno 2016

THE ORGANIZATION HOSTING THE CONFERENCE

Faculty of Science, Masaryk University in Brno

Department of Chemistry

Kotlářská 2

611 37 Brno

http://www.sci.muni.cz

THE ORGANIZATIONAL SECURITY OF THE CONFERENCE

Libuše Trnková

libuse@chemi.muni.cz

(Department of Chemistry, Faculty of Science, Masaryk University)

The publication did not undergo the language control. All contributions are publicated in the form, in which they were delivered by the authors. Authors are also fully responsible for the material and technical accuracy of these contributions.

ISBN 978-80-210-8267-0

The Workshop of Physical Chemists and Electrochemists was supported by research organizations and projects:

The sponsors of the Workshop of Physical Chemists and Electrochemists:

The organizers thank a lot to all this year's sponsors for the support, which enabled to organize this traditional conference: Metrohm Czech Republic s.r.o., Eppendorf Czech & Slovakia s.r.o., DONAU LAB s.r.o, MANEKO spol. s r.o., ScienceTech s.r.o., CHROMSPEC spol. s r.o., Anamet s.r.o., Specion s.r.o., Pragolab s.r.o., Sigma-Aldrich spol. s r.o. and Czech Chemical Society, subdivision Brno.

Metrohm Česká republika

The main sponsor

eppendorf

DONAU LAB Prague
Member of LPPgroup

MANEKO
LABORATORNÍ POTŘEBY A TECHNIKA

Princeton Applied Research
solartron analytical

CHROMSPEC
SPOL. S R.O.

CHROMSERVIS®

ANAMET
ANALYTICAL & MEASURING & TESTING

SPECION, s.r.o.
LABORATORNÍ A ZKUŠEBNÍ TECHNIKA

pragolab

ČCHS

SIGMA-ALDRICH®

Úvodem...

Rok uběhl jako voda a opět si vás dovoluji přivítat na již 16. ročníku tradiční konference Workshop of Physical Chemists and Electrochemists pořádané na půdě Masarykovy univerzity v Brně. Oba konferenční dny budou naplněny sérií přednášek a soutěžními sekcemi, ať již Sekcí mladých studentů či Sekcí plakátových sdělení, v nichž mladí a nadaní vědci prezentují výsledky svého výzkumu s hlavním cílem podpořit výzkum v oblasti fyzikální chemie a elektrochemie a hlavně jejich aplikaci v biologických vědách a nanovědách. Jménem organizátorů bych vám chtěla všem popřát úspěšnou konferenci, která vás bude inspirovat k dalšímu vědeckému bádání společně s navázáním nové spolupráce.

Přeji vám příjemně strávené konferenční dny.

Libuše Trnková

Motto:

„Nejkrásnější, co můžeme prožívat, je tajemno. To je základní pocit, který stojí u kolébky pravého umění a vědy."

Albert Einstein

An introductory word...

One year is behind us and I would like to invite you to the 16th traditional conference Workshop of Physical Chemists and Electrochemists, which is held at Masaryk University in Brno. Both conference days will be filled-up with a sequence of lectures and competition sessions, such as The Young Scientists' Session or Poster Session, in which the young gifted scientists present the results of their research. The main idea is to support the research in the field of Physical Chemistry and Electrochemistry and its application in bio- and nanoscience. On behalf of the organizers I would like to wish you a successful conference that will inspire you in further scientific research supported by new cooperation.

Enjoy the conferece!

Libuše Trnková

Motto:

„The most beautiful thing we can experience is the mysterious. This is the fundamental emotion that stands at the cradle of true art and science.“

Albert Einstein

Table of contents

NANO IN ELECTROCHEMISTRY 11

ELECTROCHEMISTRY AND SURFACE ACTIVITY OF NUCLEIC ACIDS: EFFECTS OF SEQUENCE, STRUCTURE, CHEMICAL MODIFICATION AND NON-COVALENT INTERACTIONS 14

NANO – TODAY'S FASCINATING PHENOMENON 19

WHAT IS SO COOL ON ICE? 24

EFFECT OF CdS QUANTUM DOTS ON DNA DEGRADATION UNDER UV ILLUMINATION 25

ELECTROCHEMICAL BEHAVIOUR OF [N]HELICENES 28

BIOLOGICAL ACTIVITY OF MANGANESE(II) TRITHIOCYANURATE COMPLEXES 31

GRAPHENE AND GARPHENE OXIDE FOR BIOSENSING 38

REDOX-PAIR DEFINED ELECTROCHEMICAL DETECTION – BIAMPEROMETRIC SET-UP EXHIBITING "INTERFERENCES-FREE" PERFORMANCE 45

ATOMIC FORCE MICROSCOPY – TOOL TO STUDY NANOMECHANICAL PROPERTIES OF LIVING CELLS AND BIOMATERIALS 48

ENHANCEMENT OF ELECTROCHEMICAL DETECTION IN CAPILLARY ELECTROPHORESIS USING NANOMATERIALS 55

GAS SENSITIVE STRUCTURES WITH N-N NANOJUNCTIONS BASED ON WO_{3-x} NANONEEDLES AND Fe_2O_3 NANOPARTICLES 58

APOFERRITIN AS A NANOCARRIER FOR ACTIVE TARGETING OF DOXORUBICIN TOWARDS CANCER CELLS 62

ELECTROCHEMICAL IMPEDANCE SPECTROSCOPY BASED BIOSENSOR FOR RAPID DETECTION OF *SALMONELLA* 66

STUDY OF SURFACE EFFECTS OF SELECTED BIMETALLIC NANOPARTICLES 70

SYNTHESIS OF COPPER COMPLEXES AND THEIR ANTIMICROBIAL ACTIVITY 73

ELECTROCHEMICAL PROPERTIES OF CONFORMATIONAL DERIVATIVES OF (N-FERROCENYLIMINOMETHYL)PHENYLBORONIC ACID 78

ELECTROSPINNING OF POLY(VINYL) ALCOHOL AND HYALURONIC ACID 80

STATISTICAL PROCESSING OF EXPERIMENTAL DATA FROM TESTING FULLY AUTOMATED ELECTROCHEMICAL APPARATUS FOR APLICATION IN EXTREME CONDITIONS 84

ELECTROCHEMICAL DETERMINATION OF CADMIUM AND TELLURIUM IN BIOSYNTHESIZED AND MICROWAVE OVEN PREPARED CdTe QUANTUM DOTS 89

ELECTROCHEMICAL DETECTION OF ZINC IONS USING GLASSY CARBON ELECTRODE MODIFIED WITH ELECTROCHEMICALLY REDUCED GRAPHENE OXIDES 96

GOLD NANOSTRUCTURED SURFACES BASED ON ALUMINA TEMPLATE 100

SOLID-STATE SYNTHESIS OF GOLD NANOPARTICLES FILMS FOR SPECTROSCOPIC MEASUREMENT ENHANCEMENT 104

ZINC-SCHIFF BASE-NOVICIDIN COMPLEX AS A POTENTIAL ANTITUMOR DRUG FOR PROSTATE CANCER THERAPY 108

STUDDING OF QDS FLUORSCENCE QUENCHING EFFECT CAUSED BY COVALENT CONJUGATION WITH BSA 115

SYNTHESIS OF SILVER NANOPARTICLES AS ANTIMICROBIAL COATING FOR ION EXCHANGE MEMBRANE 119

STRUCTURAL AND THERMODYNAMIC PROPERTIES OF THE QUADRUPLEX IN THE PROMOTER OF THE POU5F1 GENE 125

ELECTROCHEMICAL DEPOSITION OF GOLD NANORODS FOR VOCS SENSING 128

THE EFFECT OF WATER CONTAMINATED BY HEAVY METALS ON *TRAMETES VERSICOLOR* 131

EFFECT OF HYALURONAN ON DIFFUSION PROPERTIES OF ARTIFICIAL CELL MEMBRANE STUDIED BY FLUORESCENCE CORRELATION SPECTROSCOPY 135

EXPOSURE OF RATS TO A MIXTURE OF ARISTOLOCHIC ACID I AND II INFLUENCES GENOTOXICITY OF THESE PLANT ALKALOIDS 139

NATURALLY OCCURRING BASE LESIONS EFFECT THE FOLDING AND THE STABILITY OF THE HUMAN TELOMERE G-QUADRUPLEX 143

FLUORESCENCE CHEMOSENSORS FOR GAS PHASE DETECTION BASED ON NAPHTHALIMIDE DERIVATIVES 146

A NEW APPROACH TO PRETREATMENT OF A PENCIL GRAPHITE ELECTRODE SURFACE FOR 3N-METHYLADENINE DETERMINATION 149

XVI. WORKSHOP OF PHYSICAL CHEMISTS AND ELECTROCHEMISTS

FLUORESCENCE PROBE STUDY OF INTERACTIONS BETWEEN CATIONIC MICELLES AND NEGATIVELY CHARGED POLYELECTROLYTE 154

PREPARATION OF SILVER NANORODS VIA TEMPLATE BASED METHOD 157

CYTOCHROME B_5 PLAYS A DUAL ROLE IN THE REACTION CYCLE OF CYTOCHROME P450 3A4 DURING OXIDATION OF AN ANTICANCER DRUG ELLIPTICINE 161

SPECTROELECTROCHEMISTRY OF RHENIUM-CATECHOL COMPLEX 164

EFFECT OF ANTI-PAIIL ANTIBODY ON *PSEUDOMONAS AERUGINOSA* INFECTION IN CELLULAR AND ANIMAL MODELS 168

EFFECT OF LIPOPHILIC MEMBRANE ON PENETRATION OF POTASSIUM LIGNOHUMATE 172

FABRICATION AND CHARACTERIZATION OF SELF-ORDERED MERMISTIVE TiO_2 WITH ANODIC OXIDATION 176

DIHYDROMYRICETIN AND EXPRESSION OF CYTOCHROMES P450 1A1/2 AND CYTOCHROME B_5 ON TRANSCRIPTIONAL LEVELS IN RATS 180

EFFICIENCIES OF HUMAN CYTOCHROME P450 3A4 ENCAPSULATED IN LIPOSOMAL AND MICROSOMAL NANOPARTICLES TO ACTIVATE ELLIPTICINE TO FORM COVALENT DNA ADDUCTS 183

STUDY OF EFFECT OF HYALURONAN ADDITION TO SEPTONEX MICELLAR SOLUTION 187

AB INITIO STUDY OF SURFACE OF NANOPARTICLES Ag AND Ni 190

EFFECT OF PREPARATION PARAMETERS ON SHORT TiO_2 NANOTUBES 194

EFFICIENCIES OF HUMAN CYTOCHROME P450 1A1 EXPRESSED IN EUKARYOTIC AND PROKARYOTIC SYSTEMS IN OXIDATION AND DNA ADDUCT FORMATION BY BENZO[A]PYRENE: A COMPARATIVE STUDY 198

DNA BASED BIOSENSOR FOR ELECTROCHEMICAL STUDY OF AROMATIC COMPOUNDS IN BIOLOGICAL MATRIX 201

MATRA-A REAGENT/POLYETHYLENEIMINE COMPLEX TRANSFECTION FOR LOW TOXIC DNA PLASMID DELIVERY 205

THE ELECTROCHEMICAL ANALYSIS OF DNA HEXAMER d(GCGAGC) 209

STUDY OF THE GLASS TRANSITION OF CO-AMORPHOUS DRUG BY DMA 212

GENERATION OF OXIDATION DOUBLE PEAK OF GUANINE IN URACIL SUBSTITUTED DNA FRAGMENT 215

GET TO KNOW METROHM 218

REAL-TIME MONITORING OF INTERACTIONS BY EC-MP-SPR 219

NANO IN ELECTROCHEMISTRY

Jana DRBOHLAVOVÁ[1,2*], Hana KYNCLOVÁ[1,2], Radim HRDÝ[1,2],
Kateřina PŘIKRYLOVÁ[1] , Milena ŠETKA[2], Jaromír HUBÁLEK[1,2]

[1] *Department of Microelectronics, Faculty of Electrical Engineering and Communication, Brno University of Technology, Technická 3058/10, 616 00 Brno, Czech Republic*

[2] *Central European Institute of Technology, Brno University of Technology, Purkyňova 123, 612 00 Brno, Czech Republic*

**drbohla@feec.vutbr.cz*

Abstract

Nanostructured electrodes are very promising in many fields thanks to their unique properties raising from the ability to control the architecture of the electrode interface at nanoscale in both, vertical and lateral direction [1]. These electrodes find application in material sciences, especially in devices such as solar cells, high-power lithium ion batteries [2, 3] and supercapacitors due to better cyclic stability, higher energy and power density. The nanostructured electrodes become also extremely popular in life sciences, mainly in bioelectronics and (bio)sensors for hand-held devices used in medical diagnosis and immunoassays [4]. The main advantage is their high surface area enhancing the electrode sensitivity via improved immobilization of biorecognition molecule into nanomaterial matrices [5]. We summarize and discuss the various methods of nanostructured electrode fabrication together with modification of surface chemistry and crystallinity.

1. CURRENT STATE OF ART

Many materials, such as silver, gold, platinum, palladium, ruthenium, copper, nickel and bimetallic nanoparticles with different structures, such as dendrites, nanorods, or nanotubes, have been already used for fabrication of nanostructured electrodes [6, 7]. Nevertheless, carbon in its various forms (e.g. glassy carbon, graphite, graphene, or carbon nanotubes) still belongs to the most frequently studied one. The deposition of noble metal nanoparticles onto electrode surface may contribute to a substantially higher density of carriers of free loads and hence to enhanced electrical conductivity [8]. However, the electrode structures become random and untailored after their typical electrode fabrication process (mixing with polymer binder and conductive additives). So far very little work has yet been done in systematically studying the principles for optimizing electrode architectures, especially those involving

redox reactions. The overview of materials used for electrode nanostructuring together with fabrication methods and final electrode application is listed in Table 1.

Table 1.: List of few basic materials and methods currently used for nanostructured electrodes fabrication

Material	Nanostructure morphology	Fabrication methods	Application	Reference
Carbon	Multiwalled carbon nanotubes	CVD method	Hybrid supercapacitors	[9]
	Nanoporous graphene	Flame treatment of graphene oxide	Electrode for lithium-ion batteries	[10]
Gold	Nanorods	Dip coating of colloidal Au nanorods	Electrocatalytic reduction of oxygen	[11]
	Nanoparticle arrays	Pulsed laser nanostructuring	Electrochemical detection of glucose	[12]
	Nanorods	Electrochemical deposition via AAO	Electrochemical detection of guanine	[13]
Platinum	Nanowires	Electrochemical deposition	Nanoelectronics, gas sensors and biosensors	[14]
ZnO/Pd	Nanoparticles	Dip coating, chemical reduction	Electrochemical analysis	[15]
RuO_2	Nanoparticles	Corrosion of Ni foam in $RuCl_3$ presence	Water splitting	[16]
TiO_2	Nanotubes, nanopores	Anodic oxidation	Photocatalysis, electrocatalysis	[17]

It is shown that particle size and packing density of the nanostructures array are important factors which determine the electrode performance. In general, the modification of electrode surface can be performed by four approaches which are (1) the direct attachment of nanoparticles onto an electrode, (2) templating with membranes such as polycarbonates or alumina, (3) the use of lyotropic liquid crystals as templates and (4) colloidal templating. Self-assembled monolayers (SAMs) and templated methods offer the greatest possible control over how an electrode interface can be modified. Namely, the electrodeposition method using nanoporous anodic aluminium oxide (AAO) template is versatile tool which enables to achieve appropriately designed nanostructures, interfaces and crystallinity [18] as illustrated in Figure 1.

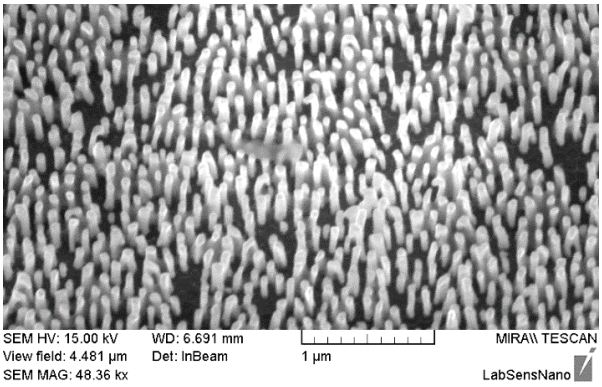

Figure 1.: SEM image of electrode with electrodeposited gold nanorods using AAO template.

2. CONCLUSION

This paper provides short review work done on nanostructuring electrodes using variety of materials and methods. Even the majority of published works shows significant improvement of electrode behaviour thanks to their nanostructuring, there are still some serious problems which have to be eliminated. In this field, the research efforts should be further devoted to the development and fabrication of thin film electrodes in maximally simplified way, with regard to consumption of precious starting materials and mainly with increased reproducibility, so that the technology can be directly used on an industrial level.

3. ACKNOWLEDGEMENT

The work has been supported by IGA FEKT/STI-J-16-3625 and IGA FEKT-S-14-2300 research grants.

4. REFERENCES

[1] Alkire RC, Kolb DM, Lipkowski J, et al.: Chemically Modified Electrodes, Wiley2009
[2] Mukherjee R, Krishnan R, Lu T-M, et al.: Nano Energy, 1 (2012), 4, 518-533
[3] Liu D, Cao G: Energy & Environmental Science, 3 (2010), 9, 1218-1237
[4] Sage AT, Besant JD, Lam B, et al.: Accounts Chem. Res., 47 (2014), 8, 2417-2425
[5] Prakash PA, Yogeswaran U, Chen S-M: Sensors, 9 (2009), 3, 1821
[6] Campbell FW, Compton RG: Analytical and Bioanalytical Chemistry, 396 (2010), 1, 241-259
[7] Rackus DG, Dryden MDM, Lamanna J, et al.: Lab Chip, 15 (2015), 18, 3776-3784
[8] Dobrzanska-Danikiewicz A, Lukowiec D, Kubacki J: J. Nanomater., (2016), 8
[9] Zuo W, Wang C, Li Y, et al.: Scientific Reports, 5 (2015),
[10] Jiang HB, Zhang YL, Zhang Y, et al.: Scientific Reports, 5 (2015), 8
[11] Di Bari C, Shleev S, De Lacey AL, et al.: Bioelectrochemistry, 107 (2016), 30-36
[12] Grochowska K, Siuzdak K, Karczewski J, et al.: Appl. Surf. Sci., 357 (2015), 1684-1691
[13] Hrdy R, Kynclova H, Drbohlavova J, et al.: Int. J. Electrochem. Sci., 8 (2013), 4, 4384-4396
[14] Nerowski A, Opitz J, Baraban L, et al.: Nano Res., 6 (2013), 5, 303-311
[15] Bakare FO, Mahfoz W, Aziz MA, et al.: J. Electrochem. Soc., 163 (2016), 2, H24-H29
[16] Lee J, Lim GH, Lim B: Chem. Phys. Lett., 644 (2016), 51-55
[17] Přikrylová K, Drbohlavová J, Svatoš V, et al.: Monatshefte für Chemie - Chemical Monthly, 147 (2016), 5, 943-949
[18] Drbohlavova J, Kynclova H, Hrdy R, et al.: Analytical Letters, 49 (2016), 1, 135-151

ELECTROCHEMISTRY AND SURFACE ACTIVITY OF NUCLEIC ACIDS: EFFECTS OF SEQUENCE, STRUCTURE, CHEMICAL MODIFICATION AND NON-COVALENT INTERACTIONS

Miroslav FOJTA[*1,2], Jan ŠPAČEK[1,2], Pavlína VIDLÁKOVÁ[1], Zdenka DUDOVÁ[1], Medard PLUCNARA[1], Aleš DAŇHEL[1], Hana PIVOŇKOVÁ[1] and Luděk HAVRAN[1]

[1] *Institute of Biophysics of the AS CR, v.v.i., Královopolská 135, 612 65 Brno, Czech Republic*

[2] *CEITEC-Central European Institute of Technology, Masaryk University, Kamenice 5, CZ-62500, Brno, Czech Republic*

** fojta@ibp.cz*

Abstract

Nucleic acid (NA) electrochemistry has been developing for last six decades, during which a lot of knowledge on electrochemical and surface activity of NA components has been collected. Structure sensitivity of electrochemical responses of NAs, particularly their sensitivity to helix opening transitions, has been utilized in a number of analytical applications. Recent data has extended this knowledge towards effects of nucleotide sequence on the behavior of single-stranded NAs at electrodes, effects of the formation of alternative (non-canonical) DNA structures, as well as effects of chemical modification. In this contribution, these phenomena will be presented along with potential applications in DNA and RNA studies.

1. INTRODUCTION

Electrochemical methods are well-suited for studies of nucleic acid (NA) structure and interactions [1]. In aqueous media, cytosine (C) and adenine (A) residues in their protonated states are irreversibly reduced at mercury and some types of amalgam electrodes. Reduction of G at the mercury-based electrodes takes place at more negative potentials to give 7,8-dihydroguanine. The latter compound can be oxidized back to G close to -0.25 V [in 0.3 M ammonium formate, 50 mM sodium phosphate pH around 6.9 (AFP) against Ag|AgCl|3 M KCl], giving rise to an anodic signal. All standard NA bases have been reported to undergo oxidation at carbon electrodes. The behavior of natural DNA at electrodes is dictated by the accessibility of nucleobase residues for interaction with the electrode surfaces. In duplex (double-stranded, ds) DNA, the nucleobases (base pairs) are located inside the double helix, making their communication with electrodes relatively difficult. Particularly reduction of

cytosine and adenine residues at the mercury-based electrodes (which takes place in sites involved in the Watson-Crick base pairing) strongly depends on formation (or denaturation) of the DNA double helix. On the other hand, redox processes in the imidazole ring of guanine (G) (reduction/oxidation at mercury or oxidation at carbon electrodes) are relatively feasible in the double-stranded DNA due to accessibility of this site via major groove. Base-specific and structure-selective electrochemical responses of DNA, either label-free or based on a redox DNA labelling [2], have been utilized in a variety of applications oriented towards detecting DNA damage [3], analysis of nucleotide sequences, protein-DNA interactions [4] and others.

2. EFFECTS OF NUCLEOTIDE SEQUENCE ON INTRINSIC NA RESPONSES

In unmodified single-stranded (ss; unstructured) random-sequence NAs, typically represented by denatured natural chromosomal or plasmid DNAs, relative intensities of reduction or oxidation signals proportionally reflect the relative contents of the respective bases. Moreover, reduction of cytosine and adenine in such DNAs give a single common peak CA. However, experiments with specifically designed oligodeoxynucleotides (ODNs) revealed effects of nucleotide sequence on their electrochemical responses. First, homonucleotide blocks dA_n and dC_n produce two distinguishable reduction signals at the mercury electrodes, with C residues being reduced at less negative potentials than A residues. In short ODNs, separation of the C and A signals has been observed even for CC and AA dinucleotides, particularly with the help of elimination voltammetry [5]. For longer homonucleotide blocks the peak separation is more pronounced. Since homopyrimidine (but not homopurine) ODNs were shown to form condensed layers at the negatively charged electrode surface [6], different adsorption modes of dA_n and dC_n clusters may at least partly be involved in this effect. Second, oxidation of G at carbon electrodes has been shown to be influenced by sequence context in which the G residues occur, particularly by the presence of C next to G ([7] and our recent more systematic study, unpublished). Sequence effects on the peak G measured at HMDE (i.e., signal due to 7,8-dihydroguanine oxidation) have recently been reported as well [8].

3. ALTERNATIVE DNA STRUCTURES

In addition to differentiation between ds and ss DNA, which has been utilized in a number of analytical applications mostly related to detecting DNA damage [3], electrochemical methods

have recently been applied also in studies of other (alternative, non-canonical) DNA structures. Some of them (such as G quadruplexes) are based on Hoogsteen base pairing that involves the imidazole rings of purine bases, where primary reduction and oxidation processes of G occur. Recently, oxidation of guanine residues in the G-quadruplexes at glassy carbon electrodes has been reported to take place at a potential by about 100 mV more positive, compared to guanines in single-stranded or duplex oligonucleotides, suggesting more difficult electrode process in the case of the quadruplex structure [9]. Our more recent data [10] revealed formation of quadruplex structures in homo-guanine blocks longer than 5 nucleotides, which were stable in solution as well as in adsorbed state at the negatively charged mercury surface. Hoogsteen-paired guanine residues in the quadruplexes exhibited only limited accessibility for reduction at the negatively charged surface of the mercury electrode from which these rigid structures were repelled. On the contrary, the oxidation process of guanine at a carbon electrode took place at positively charged surface to which the oligodeoxynucleotide molecules were attracted.

4. NUCLEIC ACIDS MODIFIED WITH REDOX LABELS

Labeling of the NAs with electroactive moieties has been introduced as a way to more specific and more sensitive sequence-specific electrochemical analysis of the NAs [2]. Compared to natural (unmodified) NAs, the labeled ones contain extra redox center(s) producing additional, label-specific signal(s). For example, chemical modification of NAs with oxoosmium complexes in the presence of bidentate nitrogenous ligands such as 2,2'-bipyridine or 1,10-phenanthroline derivatives. Reagents based on osmium tetroxide have proved to be suitable for the modification of unpaired or mispaired pyrimidine (primarily thymine) residues, with applications not only in DNA labeling as such, but also for probing perturbations in dsDNA structure [11]. Analogous complexes of six-valent osmium have been applied for labeling of 3'-terminal ribose in RNA [12]. Other redox labels have been introduced in DNA via enzymatic (polymerase) incorporation of labeled nucleotides using modified deoxynucleotide triphosphates bearing the respective redox moieties, e.g., ferrocene, anthraquinone, nitrophenyl, benzofurazan, azidophenyl [13], but also simple analogues of natural bases such as 7-deazapurines [14]. Combination of labels differing in their potentials of reduction and/or oxidation (and differing from those of the natural nucleobases) provide versatile multipotential NA labeling scheme, which has further been enhanced by electrochemical [13c] or chemical [13b] transformations of the primarily introduced labels.

Applications in the areas of SNP typing, ratiometric analysis of nucleotide sequences as well as studies of protein-DNA binding have been demonstrated.

5. ADSORPTION/DESORPTION PROCESSES OF NATURAL AND MODIFIED DNA

It has been shown that in weakly alkaline media, tensammetric signals of NAs sensitively reflecting their structure can be observed at the mercury-based electrodes. In ssDNA, hydrophobic nucleobases are strongly adsorbed at the electrode surface even at highly negative potentials: a tensammetric peak due to reorientation of DNA segments adsorbed via bases ("peak 3") is observed around –1.4 V vs. Ag|AgCl|3M KCl. Duplex B-form DNA, in which the bases are not freely accessible, undergoes the reorientation processes at significantly less negative potential (peak 1 around -1.2 V); appearance of the peak 3 thus indicates a duplex opening transition [1]. Moreover, distorted (partially unwound, e.g. due to intercalation of planar molecules between DNA base pairs [15]) dsDNA produces another tensammetric signal at intermediate potential (peak 2). Our recent studies with double-stranded DNA bearing extrinsic hydrophobic moieties, e.g., extra aromatic groups attached to bases in the duplex major groove, revealed a strong influence of these modifications on the tensammetric properties of DNA.

6. CONCLUSION

Nucleic acids electrochemistry has been developing for decades, resulting in design of a number of applications in DNA and RNA studies. Recent progress in the field has extended our knowledge on the behavior of NAs at electrodes, namely about the effects of nucleotide sequence, formation of alternative structures and chemical modification. Based on these new data, extending of the application area of NA electrochemistry can be expected.

7. ACKNOWLEDGEMENT

Financial support by the Czech Science Foundation (16-01625S) and from the ASCR (RVO 68081707) is gratefully acknowledged. The authors thank members of Prof. Michal Hocek group (IOCB ASCR, Prague) for providing modified deoxynucleotide triphosphates used in part of this work.

8. REFERENCES

[1] E. Palecek and M. Bartosik, Chem Rev 2012, 112, 3427-3481.
[2] M. Hocek and M. Fojta, Chem Soc Rev 2011, 40, 5802-5814.
[3] M. Fojta, A. Daňhel, L. Havran and V. Vyskočil, TrAC – Trends Anal Chem 2016, published online (2015), doi:10.1016/j.trac.2015.11.018.
[4] R. P. Bowater, A. M. Cobb, H. Pivonkova, L. Havran and M. Fojta, Monatsh Chem 2015, 146, 723-739.
[5] L. Trnkova, F. Jelen and I. Postbieglova, Electroanalysis 2006, 18, 662-669.
[6] S. H. Hason, V. Vetterl and M. Fojta, Electrochim Acta 2008, 53, 2818-2824.
[7] R. J. Toh, A. Bonanni and M. Pumera, Electrochem Commun 2012, 22, 207-210.
[8] I. Triskova, L. Gurecky and L. Trnkova, Monatsh Chem 2016, 147, 857-864.
[9] A.-M. Chiorcea-Paquim and A. M. Oliveira-Brett, Electrochim Acta 2014, 126, 162-170.
[10] P. Vidlakova, H. Pivonkova, I. Kejnovska, L. Trnkova, M. Vorlickova, M. Fojta and L. Havran, Anal Bioanal Chem 2015, 407, 5817-5826.
[11] M. Fojta, P. Kostecka, H. Pivonkova, P. Horakova and L. Havran, Curr Anal Chem 2011, 7, 35-50.
[12] M. Bartosik, R. Hrstka, E. Palecek and B. Vojtesek, Anal Chim Acta 2014, 813, 35-40.
[13] a) J. Balintova, M. Plucnara, P. Vidlakova, R. Pohl, L. Havran, M. Fojta and M. Hocek, Chem-Eur J 2013, 19, 12720-12731; b) J. Balintova, J. Spacek, R. Pohl, M. Brazdova, L. Havran, M. Fojta and M. Hocek, Chem Sci 2015, 6, 575-587; c) J. Balintova, R. Pohl, P. Horakova, P. Vidlakova, L. Havran, M. Fojta and M. Hocek, Chem-Eur J 2011, 17, 14063-14073.
[14] a) H. Pivonkova, P. Horakova, M. Fojtova and M. Fojta, Analy Chem 2010, 82, 6807-6813; b) Z. Dudova, J. Spacek, M. Tomasko, L. Havran, H. Pivonkova and M. Fojta, Monatsh Chem 2016, 147, 3-11.
[15] M. Fojta, L. Havran, J. Fulneckova and T. Kubicarová, Electroanalysis 2000, 12, 926-934.

NANO – TODAY'S FASCINATING PHENOMENON

Anton FOJTÍK[1*]

[1] Faculty of Biomedical Engineering, Czech Technical University, Prague, Czech Republic

**fojtiant@fbmi.cvut.cz*

Abstract

During the past several decades, "small-particle" research has become quite popular in various fields of physics and chemistry. By "small particles" are meant clusters of atoms or molecules of metals, semiconductors and others materials, ranging in size between single atoms or molecules and bulk materials.

1. INTRODUCTION

In the very early stages of "Nano" science I had an opportunity to participate in the experimental shaping of this area. At the beginning, we stepped into nanostructure research, which was completely unexplored area, with a significant risk of failure and misunderstanding. This note presents the area of quantum nanoparticles from the perspective of one of the founders of the experimental study of nanotechnology and nanostructures as a completely new field of research, including subsequent unique applications.

At the beginning of the eighties, the team of prof. A. Henglein, (director of Hahn-Meitner Institute, HMI) in TU (West) Berlin, perform investigation of small colloidal particles.

Ambitious objective of project EUREKA (EU and Germany1980) was to end the domination of U.S. and Japan in the field of chip technology. To obtain chip units with a density record 10 ÷ 100 Mb/cm^2 was to ensure necessary material base. HMI in Berlin has become in the being a major centre for research and training materials for miniaturisation particles technology. We had an inconsiderable share in the preparation and study of metal and semiconductor colloidal materials. The work has gradually started to depend on the area of study super small particles, currently known as quantum nanostructures. The development of the nanostructural world and problem ignition began, when the systematic research of small particles run in laboratories in Hahn-Meitner Institute in Berlin - prof. Henglein[1,2], and at Bell Telephone Laboratories, NY USA - prof. L. E. Brus.. The results of this research are dozens of original work in the field of training and study nanoparticles, nanostructures and nanotechnology[3]. We will try to illustrate the way, how the research and development in

this area went. Practical and theoretical problems, which had to be faced on infancy of this new science industry, will be presented.

In this short note, we point out several key moments, which played in the development of this area decisive role.

The findings of the effect of space restrictions of colloidal particles (i)

The findings of absorption of exciton status in a normal temperature (ii)

Confirmation of the higher excited states on one particle (iii)

Surface and internal conditions of charge carriers in nanoparticles (iv)

The dimensional quantization effect, which caused unprecedented interest in the world in the research of this kind, appeared as a remarkable feature. Band structure of metals and semiconductors is also dependent on the number and arrangement of atoms in the crystalline grid, i.e. in quantum properties, there is considerable dimensional function of microcrystal when in semiconductors, or in metal occurs in the nanometre area a gradual transition from the macroscopic voluminous characteristics to quantum characteristics of molecules. Optical, photocatalytic and fotophysical characteristics of semiconductors are significantly changed and there were observed interesting electrochemical and physical effects.

A progress has been made in improving the properties of particles by surface modification[4,5,6] and by the preparation of composite structures ("sandwiches"), in which the particle consist of two semiconductor components[7].

2. METHODS

Approach to Nanoparticles and Nanostructures

Measuring system

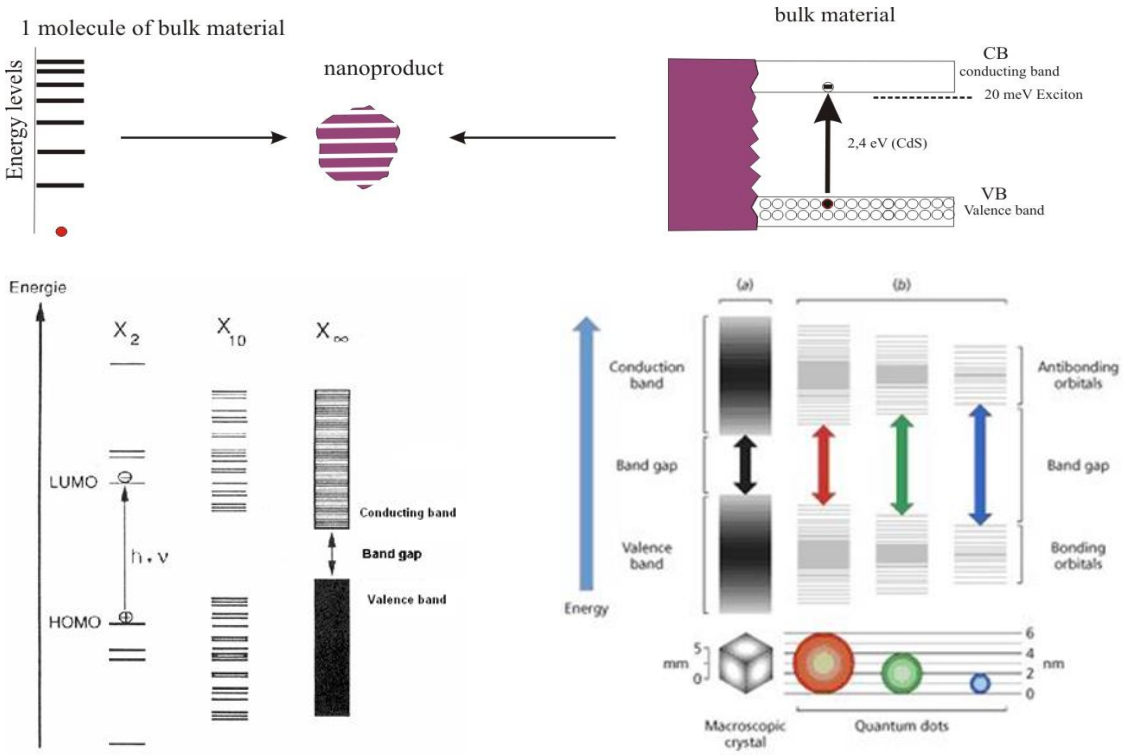

Fojtik A.: Quantum State of Small Semiconductor Clusters – „Exciton".
Radiat. Phys. Chem. Vol. 28, No 5/6 (1986) p. 463

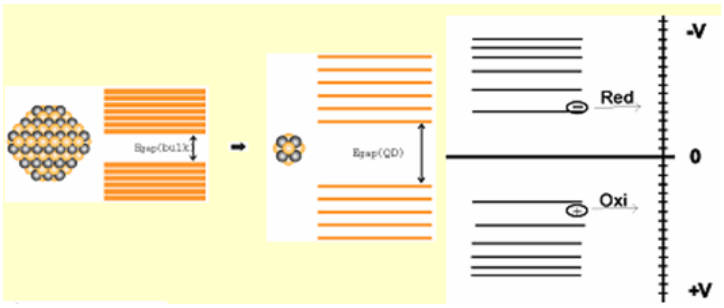

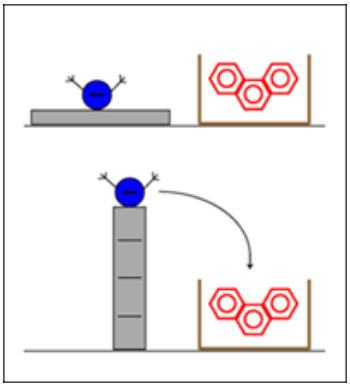

Managing the band-gap extent by particle size.

The phenomena arise when the size of the particle becomes comparable to the DeBroglie wavelength of the carriers.

(Some) Methods for nanoparticles preparation.

1. Laser ablation, 2. Low frequency heating, 3. Thermal deposition
4. RF plasma deposition, 5. Molecular beam epitaxy, 6. Chemical methods
7. Pulls radiolysis

3. RESULTS

(i) It was found that the start of absorption shifted to the shorter wavelengths depending on the size of particles

(ii) During a more detailed study of the absorption spectra of CdS colloidal solutions, a stronger local maximum suddenly appeared. The situation was highly reminiscent of the absorption curves of Cu_2O and GaAs measured at a temperature of 21 K (their structures were successfully explained using the concept of the existence of excitons - special quasiparticles-). Possible explanation even in the case of the absorption spectra shape measured by us. Speculation about the possible effective existence of an exciton at room temperature, .however, met from the beginning with a strictly negative reaction among experts. The main reason given for this rejection was, that the low temperatures would be necessary to reduce lattice vibration, since it was known that at room temperature this vibration fundamentally disrupts the exciton's realization abilities on the absorption processes, due to the close proximity of the exciton energy level and the lower edge of the conduction band. At room temperature, the exciton energy level was simply too close to the lower edge of the conduction band for it to be able to exist as an independent level.

(iii) The absorption spectra of particles from one fraction always showed two peaks. It was shown that these two peaks always belonged to one particle. If the concentration of particles of this size decreased, the sizes of both absorption peaks decreased simultaneously. This was the first direct proof that it was possible excite Q-particles to a higher state. The experimental result was confirmed by a theoretical calculation. All sizes of observed particles conformed to the observed results.

(iv) Charge separation in AgI/Ag_2S colloidal nanoparticles for photosensitive layers. Pure AgI colloid solution exhibits strong blue luminiscence with maximum of 420 nm. The

addition of sulphur in the solution of AgI caused qualitative changes in the luminiscence of AgI – small concentration of the sulphur quenched the blue luminiscence and subsequent addition of sulphur introduced new luminiscence peak at 900 nm which was moving towards longer wavelengths. Numerical calculations of the charge carrier motion inside of AgI/Ag_2S heterostructures with different properties was performed. We have presented a detailed description of the mechanism of charge separation in these heterostructures and its effect on the luminiscent properties.

4. ACKNOWLEDGEMENT

The work has been design at Hahn-Meitner Institute, Berlin, thank to Prof. Arnim Henglein, director of Institute.

5. REFERENCES

[1] Fojtik A, Weller H, Koch U, Henglein A.:Ber.Buns.Phys.Chem.88, 1984, 969.
[2] Weller H, Schmidt H.M, Koch U, Fojtik A, Henglein A.: Chem.Phys.Letters 124, 1986, 557.
[3] Fojtik A, Henglein A.: Ber. Buns.Phys.Chem.Vol.97, No.9, 1993, p.252
[4] Weller H, Koch D, Gutierrez M, Henglein A.: Ber.Bunsen-Ges. Phys. Chem. 1984,88,649
[5] Spanhel L, Haase M, Weller H, Henglein A.: J. Am. Chem. Soc. 1987, 106, 5649.
[6] Fojtik A, Henglein A.: J. Phys. Chem. B, Vol. 110, No.5, 2006, p.1994-1998.
[7] Henglein A, Guttietez M, Weller H, Fojtik A, Jirkovsky J.: Ber.Buns.Phys.Chem. 93, 1989, 593.

WHAT IS SO COOL ON ICE?

Dominik HEGER[1,2*]

[1] *Department of Chemistry, Faculty of Science, Masaryk University, Kamenice 5/A8, Brno 602 00, Czech Republic*

[2] *Research Centre for Toxic Compounds in the Environment, Faculty of Science, Masaryk University, Kamenice 3, 625 00 Brno, Czech Republic*

**hegerd@chemi.muni.cz*

Abstract

Ice is seemingly simple solid form of water, yet, it has plenty of interesting properties whose effects in various fields we are still only finding[1]. In the talk, I will introduce the topic of I_h ice and mention also new findings about other crystal and amorphous modification[2]. Then, I will focus on the results of our scientific group[3-5]. Recently, we researched the influence of ice on the biochemical compounds being frozen. The molecules being frozen are exposed to various stresses as increased concentration, high ionic strength and pH jumps. The consequences of these stresses and possibility of their eliminations will be shown.

REFERENCES

[1] Bartels-Rausch, T.; Jacobi, H. W.; Kahan, T. F.; Thomas, J. L.; Thomson, E. S.; Abbatt, J. P. D.; Ammann, M.; Blackford, J. R.; Bluhm, H.; Boxe, C.; Domine, F.; Frey, M. M.; Gladich, I.; Guzmán, M. I.; Heger, D.; Huthwelker, T.; Klán, P.; Kuhs, W. F.; Kuo, M. H.; Maus, S.; Moussa, S. G.; McNeill, V. F.; Newberg, J. T.; Pettersson, J. B. C.; Roeselová, M.; Sodeau, J. R., A review of air–ice chemical and physical interactions (AICI): liquids, quasi-liquids, and solids in snow. Atmos. Chem. Phys. 2014, 14, 1587-1633.

[2] Fuentes-Landete, V.; Mitterdorfer, C.; Handle, P. H.; Ruiz, G. N.; Bernard, J.; Bogdan, A.; Seidl, M.; Amann-Winkel, K.; Stern, J.; Stephan, F.; Loerting, T., Crystalline and amorphous ices. Proceedings of the International School of Physics "Enrico Fermi" 2015, 187: Water: Fundamentals as the Basis for Understanding the Environment and Promoting Technology, SIF 2015, 173–208.

[3] Krausko, J.; Ondrušková, G.; Heger, D., Comment on “Photolysis of Polycyclic Aromatic Hydrocarbons on Water and Ice Surfaces” and on “Nonchromophoric Organic Matter Suppresses Polycyclic Aromatic Hydrocarbon Photolysis in Ice and at Ice Surfaces”. The Journal of Physical Chemistry A 2015, 119, 10761-10763.

[4] Krausko, J.; Malongwe, J. K. E.; Bičanová, G.; Klán, P.; Nachtigallová, D.; Heger, D., Spectroscopic Properties of Naphthalene on the Surface of Ice Grains Revisited: A Combined Experimental–Computational Approach. The Journal of Physical Chemistry A 2015, 119, 8565-8578.

[5] Krausko, J.; Runštuk, J.; Neděla, V.; Klán, P.; Heger, D., Observation of a Brine Layer on an Ice Surface with an Environmental Scanning Electron Microscope at Higher Pressures and Temperatures. Langmuir 2014, 30, 5441-5447.

EFFECT OF CdS QUANTUM DOTS ON DNA DEGRADATION UNDER UV ILLUMINATION

Jana BLAŠKOVIČOVÁ[1*], Monika TEKEĽOVÁ[1], Veronika SVITKOVÁ[1], Ján LABUDA[1]

[1] *Institute of Analytical Chemistry, Faculty of Chemical and Food Technology, Slovak University of Technology in Bratislava, Radlinského 9, 812 37 Bratislava, Slovakia*

**jana.blaskovicova@stuba.sk*

Abstract

Quantum dots (QDs) are frequently used in many areas of technique, technology and daily life, due to their unique and advantageous properties of different kind. Together with the advantages, their potential risk properties on living organisms have been reported and thus the investigation of QDs with respect to human health became a subject of great interest. The effect of CdS QDs of various properties and sizes on integrity of DNA-based electrochemical biosensor under UV illumination has been investigated in this study.

1. INTRODUCTION

Metallic nanomaterials and quantum dots are known to influence yields of irradiation by light. QDs can be broadly classified into chemicaly induced and photoinduced energy donors [1]. QDs can transfer energy inducing the generation of reactive oxygen species (ROS) [2]. CdS quantum dots are representative semiconductor metal chalcogenide based QDs posessing unique size dependent and optoelectronic properties [3]. In this work, the effect of CdS QDs of various sizes on integrity of salmon sperm double stranded DNA attached to the surface of glassy carbon electrode under the UV-C light (λ = 254 nm) irradiation has been determined.

2. MATERIAL AND METHODS

Voltammetric measurements were performed using the potentiostat Autolab PGSTAT-100 and the software NOVA 1.10.13 (Metrohm Autolab, Netherlands). All measurements were carried out in three-electrode system using a glassy carbon working electrode (GCE), a silver|silver chloride reference electrode (Ag|AgCl) and a platinum counter electrode. dsDNA was from Sigma-Aldrich (USA), CdS QDs were prepared at and obtained from the Mendel University in Brno (Czech Republic).

The cyclic voltammetric (CV) response of the $[Fe(CN)_6]^{3-/4-}$ redox indicator, electrochemical impedance spectroscopy (EIS) and square-wave voltammetric (SWV) intrinsic signal of the DNA base moieties were utilized at the detection of damage to DNA.

3. RESULTS AND DISCUSSION

CdS QDs of various sizes (type 80 of 4.0 nm, type 100 of 5.5 nm, and type 120 of 10.5 nm) and optoelectronic properties present on the surface of the DNA biosensor exhibited significant and time dependent effects on the salmon sperm (ssp) dsDNA layer under UV irradiation. The portion of survived ssp DNA is shown in Figure 1. The results were verified by experiments with the UV irradiation of the ssp DNA and CdS QDs mixture in the phase of solution (Figure 2) and by gel electrophoresis.

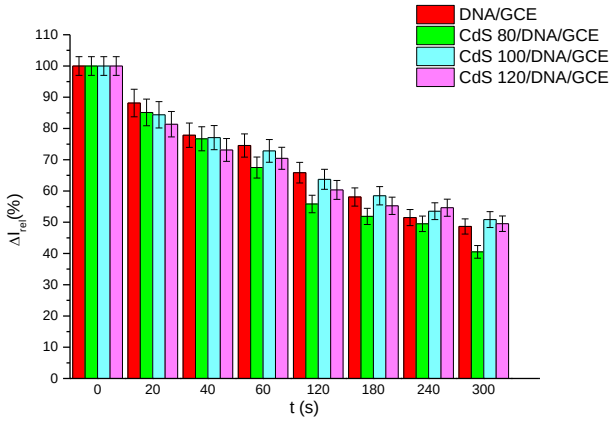

Figure 1.: Portion of survived DNA present at the DNA electrode surface after the UV irradiation in the presence of CdS QDs (biosensor).

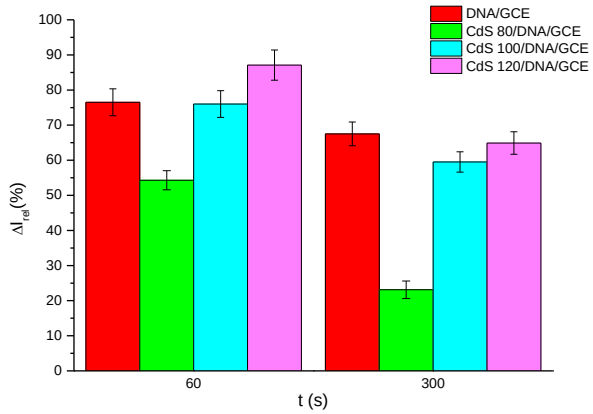

Figure 2.: Portion of survived DNA after the UV irradiation of mixture of ssp DNA and CdS QDs in the phase of solution (biosensing).

4. CONCLUSION

The DNA-based electrochemical biosensor is demonstrated as an effective warning device for tests of damage to DNA. The results indicate a significant effect of nanoparticles fluorescence properties and size on depth of the UV damage to the DNA structure.

5. ACKNOWLEDGEMENT

This work was supported by the by the Scientific Grant Agency VEGA of the Ministry of Education of the Slovak Republic (Project No. 1/0361/14).

6. REFERENCES

[1] Petersen EJ, Nelson BC: Analytical and Bioanalytival Chemistry, 398 (2010), 613-650
[2] Chen N, He Y, Su Y, Li X, Huang Q, Wang H, Zheng X, Tai R, Fan C: Biomaterials, 33 (2012), 1238-1244
[3] Chen Q, Chen F, Yan Y: BioResources, 8 (2013), 6-7

ELECTROCHEMICAL BEHAVIOUR OF [N]HELICENES

Jan HRBÁČ[1*], Jan STORCH[2], Libuše TRNKOVÁ[1], Jan VACEK[3]

[1] *Department of Chemistry, Masaryk University, Kamenice 5, Brno 625 00, Czech Republic*

[2] *Institute of Chemical Process Fundamentals of the AS CR, v.v.i., Praha 6, 165 02, Czech Republic*

[3] *Department of Medical Chemistry and Biochemistry, Faculty of Medicine and Dentistry, Palacky University, Hnevotinska 3, 775 15 Olomouc, Czech Republic*

[*] *jhrbac@atlas.cz*

Abstract

Electrochemical behaviour of [*n*]helicenes (*n*=5,6,7) was investigated using cyclic voltammetry.

1. INTRODUCTION

Helicenes are ortho-condensed polycyclic aromatic compounds, in which benzene rings are angularly annulated to give helically-shaped molecules. The chemistry of helicenes attracts continuing attention because of their unique structural, spectral and optical features. Synthetic approaches are continuously developed allowing the syntheses of these unique compounds in higher amounts and with greater yields. The aim of this work is to investigate basic redox behaviour of [5]helicene, [6]helicene and [7]helicene in acetonitrile solutions using cyclic voltammetry.

2. MATERIALS AND METHODS

Acetonitrile, p.a. (Sigma-Aldrich), tetrabutylammonium perchlorate – TBAP (Fluka) were used as the supporting electrolytes in electrochemical experiments. [5]helicene, [6]helicene and [7]helicene were prepared according to a previously reported protocol with slight modifications [1]. Voltammetric analyses were conducted using Nanoampere electrochemical workstation (L-Chem, Czech Republic) in three-electrode configuration, where alumina polished CHI MF-2012 glassy carbon electrode (disc, 3 mm in diameter) or indium tin oxide (ITO) coated glass sq slide with surface resistivity of 8-12 Ω/sq, (Sigma Aldrich) were used as the working electrodes, Ag/AgCl/3M KCl (RE-5B, Bioanalytical Systems, Inc., IN, USA) and a platinum wire served as the reference and auxiliary electrodes, respectively. The use of an aqueous reference electrode for measurement in non-aqueous electrolytes was justified by

recording the cyclic voltammogram of ferrocene. The solutions were deoxygenated by argon prior to recording of cyclic voltammograms.

3. RESULTS AND DISCUSSION

Under given experimental conditions, irreversible anodic reactions were found to occur in the region of potentials of 1500-2500 mV vs. Ag/AgCl for [5]helicene, [6]helicene and [7]helicene (Figure 1). If repeated anodization of the electrode immersed in 1 mM helicene solution is performed between 0 and 2500 mV, a decrease in CV peak heights are observed for all three studied helicenes, indicating the passivation of the electrode surface and formation of a polymeric deposit on the GCE. The aforementioned polymeric layers were prepared on the ITO electrode and subjected to spectroscopic and microscopic (SEM) characterization according to the methodology given in [2] (not shown).

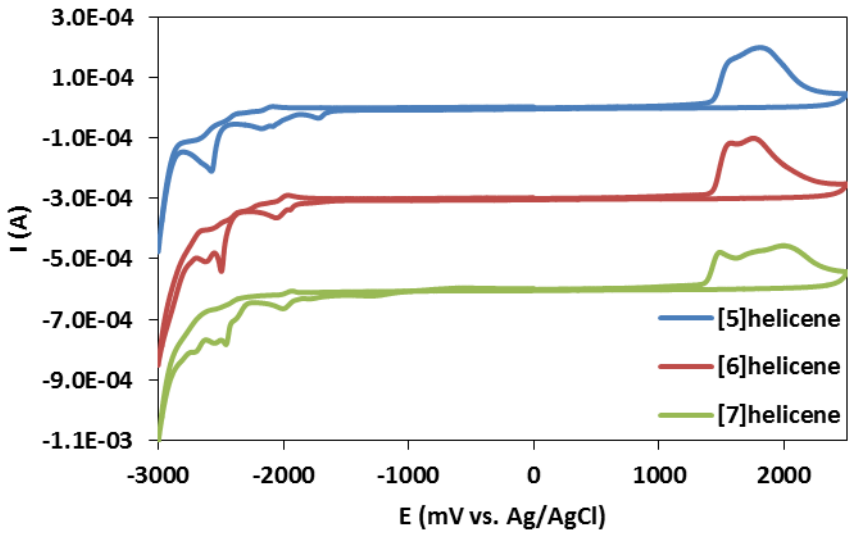

Figure 1.: Cyclic voltammograms of helicenes (1 mM solutions in deaerated acetinitrile containing 0.1 M TBAP), recorded on alumina polished GC electrode. 100 mV/s, voltammograms of 6- and 7- helicene are shifted on y-scale for clarity of presentation.

It has been confirmed that it is possible to fabricate helicene thin films on conductive substrates by this way. Such behaviour is not observed if the potential is reversed in the far negative region of potentials, where complex (multi-step) cathodic reactions occur, distinct for each helicene in the study (Figure 1). Cathodic reactions include two main processes, a quasireversible peak at ca. -2000 mV and a cluster of peaks around -2400 mV, where the number of individual peaks increases with increasing number of benzene rings in a given helicene.

4. CONCLUSION

By using cyclic voltammetry in acetonitrile solutions, [5]helicene, [6]helicene and [7]helicene was shown to provide irreversible anodic peaks with the onsets at ca. 1500 mV vs. Ag/AgCl, a quasireversible peak at ca. -2000 mV and a cluster of peaks around -2400 mV. In case the potential excursions of the electrode in helicene solutions are limited only to anodization, the formation of helicene films occurs.

5. ACKNOWLEDGEMENTS

This work was supported by the Ministry of Education, Youth and Sports of the Czech Republic, COST Action EU-ROS, BM1203 (project No. LD14033, J.V.).

6. REFERENCES

[1] Storch J, Sykora J, Cermak J, Karban J, Cisarova I, Ruzicka A, J. Org. Chem. 74 (2009) 3090.
[2] Hrbac J, Storch J, Halouzka V, Cirkva V, Matejka P, Vacek J, RSC Adv. 4 (2014) 46102.

BIOLOGICAL ACTIVITY OF MANGANESE(II) TRITHIOCYANURATE COMPLEXES

Pavel KOPEL[1,2*], Dagmar HEGEROVA[1,2], Vratislav LANGER[3]

[1] *Department of Chemistry and Biochemistry, Faculty of Agronomy, Mendel University in Brno, Zemedelska 1, CZ-613 00 Brno, Czech Republic*

[2] *Central European Institute of Technology, Brno University of Technology, Technicka 3058/10, CZ-616 00 Brno, Czech Republic*

[3] *Environmental Inorganic Chemistry, Department of Chemical and Biological Engineering, Chalmers University of Technology, SE-412 96 Göteborg, Sweden*

**paulko@centrum.cz*

Abstract

Binuclear and trinuclear Mn(II) complexes $[Mn_2(phen)_4(\mu\text{-ttc})](ClO_4)$ (**1**), $[Mn_3(nphen)_6(\mu\text{-ttc})](ClO_4)_3$ (**2**) and $[Mn_3(bphen)_6(\mu\text{-ttc})](ClO_4)_3$ (**3**) (phen = 1,10-phenanthroline, nphen = 5-nitro-1,10-phenanthroline, bphen = 4,7-diphenyl-1,10-phenanthroline, ttc^{3-} = $trithiocyanurate^{3-}$ anion) have been prepared and characterized by elemental analyses. The X-ray structure of **1** revealed two hexacoordinated manganese cations connected by trithiocyanuarate bridge. Their potential antimicrobial and antifungal activity on a wide range of strains including clinical species have been evaluated.

1. INTRODUCTION

Trithiocyanuric acid ($ttcH_3$), also referred as trimercaptotriazine, has a symmetric structure with three nitrogen atoms and three sulphur atoms (see Figure 1).

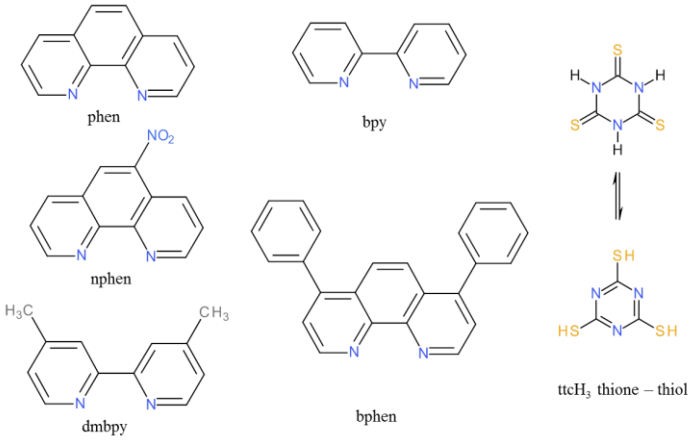

Figure 1.: The structures of ligands (phen = 1,10-phenanthroline, bpy = 2,2′-dipyridyl, nphen = 5-nitro-1,10-phenanthroline, dmbpy = 4,4′-dimethyl-2,2′-dipyridyl, bphen = 4,7-diphenyl-1,10-phenanthroline and $ttcH_3$ = trithiocyanuric acid).

The structure of $ttcH_3$ is similar to biomolecules and that is why the biological activity was studied. It was found that it can be applied as a ligand of *Toxoplasma gondii* orotate phosphoribosyltransferase [1]. The antitumor and antimicrobial activities were evaluated for Ni(II), Fe(II) and Mn(II) trithiocyanurate complexes [2]. The complexes of Fe(II), Mn(II) and Ni(II) with a combination of a Schiff base, nitrogen-donor ligand or macrocyclic ligand and trithiocyanuric acid were prepared and their anticholinesterase activity was studied [3]. It was shown that the tested compounds inhibit cholinesterases and can be considered as potential drugs for Alzheimer's disease or as prophylactics in the case of nerve agent exposure or poisoning by pesticides. The trinuclear complex $[Ni_3(abb)_3(H_2O)_3(\mu\text{-ttc})](ClO_4)_3$ (abb = 1-(1*H*-Benzimidazol-2-yl)-*N*-(1*H*-benzimidazol-2-ylmethyl)methanamine) was prepared and its structure proved by X-ray analysis [4]. The complex shows very good antimicrobial and antifungal activity on a wide spectrum of bacterial and yeast strains.

Here, we present crystal and molecular structure of manganese (II) complex with trithiocyanurate bridge. Two new trinuclear Mn(II) have been prepared and characterized by different techniques. Moreover, the potential biological activity of complexes was tested on *Staphylococcus aureus*, *Escherichia coli* and *Saccharomyces cerevisiae* and three bacterial strains isolated from patients from non-healing wounds infected by bacterial strains (*Streptococcus agalactiae*, *Corynebacterium striatum* and *Serratia marcescens*). Already known and characterized trinuclear complexes $[Mn_3(phen)_3(\mu\text{-ttc})](ClO_4)_3$ (**4**), $[Mn_3(bpy)_3(\mu\text{-ttc})](ClO_4)_3$ (**5**) and $[Mn_3(dmbpy)_3(\mu\text{-ttc})](ClO_4)_3$ (**6**), where bpy = 2,2′-dipyridyl, dmbpy =

4,4′-dimethyl-2,2′-dipyridyl, were also prepared according to Cermakova *et al.* [5], and used for the biological activity testing.

2. MATERIAL AND METHODS

Synthesis

[Mn_2(phen)$_4$(μ-ttc)](ClO_4) (**1**)

The complex **1** was obtained by recrystallization of [Mn_3(phen)$_6$(μ-ttc)](ClO_4)$_3$ (**4**) [5] from DMSO and slow diffusion of diethylether. After a week yellow crystals (suitable for X-ray analyses) were collected on a frit, washed with methanol and dried in air.

[Mn_3(nphen)$_6$(μ-ttc)](ClO_4)$_3$ (**2**)

The nphen (0.45 g, 2 mmol) dissolved in 40 ml of EtOH was added to a 10 ml EtOH solution of Mn(ClO_4)$_2$.6H_2O (0.36g, 1 mmol) with stirring. Yellow milky precipitate formed was dissolved by addition of 20 ml of nitromethane. A solution of ttcNa_3·9H_2O (0.14 g, 0.33 mmol) in water (5 ml) was added to the reaction mixture with stirring. Yellow precipitate was collected on frit and washed several times with small portions of EtOH and finally by Et_2O and dried under an infra lamp.

[Mn_3(bphen)$_6$(μ-ttc)](ClO_4)$_3$ (**3**)

The bphen (0.33 g, 1 mmol) dissolved in 40 ml of EtOH was added to a 5 ml EtOH solution of Mn(ClO_4)$_2$.6H_2O (0.18g, 0.5 mmol) with stirring. Yellow solution was obtained after boiling. A solution of ttcNa_3·9H_2O (0.07 g, 0.16 mmol) in water (3 ml) was added to the cooled reaction mixture with stirring. Yellow precipitate was collected on frit and washed several times with small portions of EtOH and finally by Et_2O and dried under an infra lamp.

Crystal structure determination

X-ray data of **1** were collected on a SMART CCD diffractometer (Siemens, Madison, WI, USA) with Mo-Kα radiation. X-ray data of **1**: Important crystallographic parameters are as follows: $C_{51}H_{32}N_{11}O_4S_3ClMn_2$, triclinic, space group Pī, a = 10.4687(4), b = 15.1594(5), c = 16.8970(6) Å, α = 110.553(1)°, β = 90.129(1)°, γ = 109.802(1)°, volume 2339.93(14) Å^3, Z = 2, density (calc.) 1.567 Mg/m^3, absorption coefficient 0.792 mm^{-1}, F(000) = 1124, crystal size 0.20 mm × 0.11 mm × 0.09 mm, index ranges $-13 \leq h \leq 13$, $-18 \leq k \leq 18$, $-21 \leq l \leq 21$,

reflections collected/independent 28848/9593 (R_{int} = 0.0335), data/restraints/parameters 9593/6/682, goodness-of fit on F^2 = 1.018, final R_1 (I > 2σ(I) data) = 0.0475, wR_2 = 0.1257, final R_1 (all data) = 0.0680, wR_2 = 0.1385. The largest peak and hole on the final difference map were 0.872 and −0.612 e.Å^{-3}.

Biological Activity Testing

Staphylococcus aureus (NCTC 8511), *Escherichia coli* (NCTC 13216) and *Saccharomyces cerevisiae* (ATCC 9763) were obtained from the Czech Collection of Microorganisms, Faculty of Science, Masaryk University (Brno, Czech Republic). Smears were collected from the infected wounds with the agreement of the patients. The swab samples were cultivated on blood agar with 10% of NaCl, blood agar with no other compounds, Endo agar and blood agar with amikacin [4]. The procedure for the evaluation of the antimicrobial effect of tested compounds consisted in measuring of the absorbance using the apparatus Multiskan EX (Thermo Fisher Scientific, Vantaa, Finland) and subsequent analysis in the form of growth curves. The software STATISTICA (data analysis software system), version 10.0 (Statsoft Inc. ed., Tulsa, OK, USA) was used for the data processing.

3. RESULTS AND DISCUSSION

Structural description

The molecular structure of **1** is shown in Figure 2. The crystal structure is stabilized by weak hydrogen bonds and π-π interactions among phenanthroline rings of neighbouring molecules. The molecular structure of **1** consists of dinuclear manganese(II) complex and perchlorate anion. Two central manganese atoms are coordinated by four N atoms of phen and the S,N-donor set of a ttc trianion in a deformed octahedral arrangement. The ttc trianion forms a bridge connecting the manganese centers.

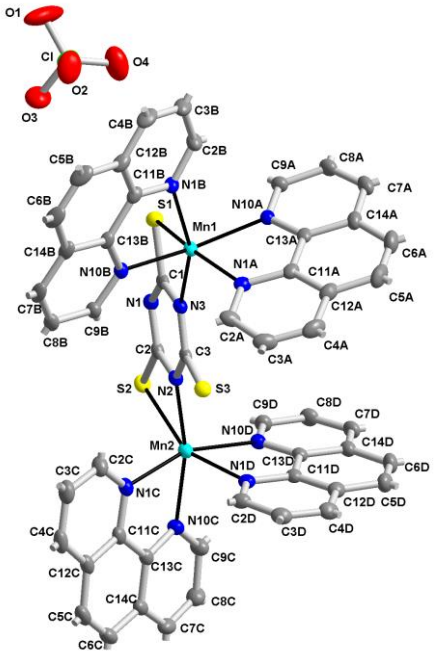

Figure 2.: The molecular structure of compound **1** with atom numbering, plotted with 30% probability of displacement ellipsoids. The hydrogen atoms are omitted for clarity.

Biological activity

The biological activity of complexes **1** – **6** and control (manganese perchlorate) was studied. The results of the study are presented in Figure 3.

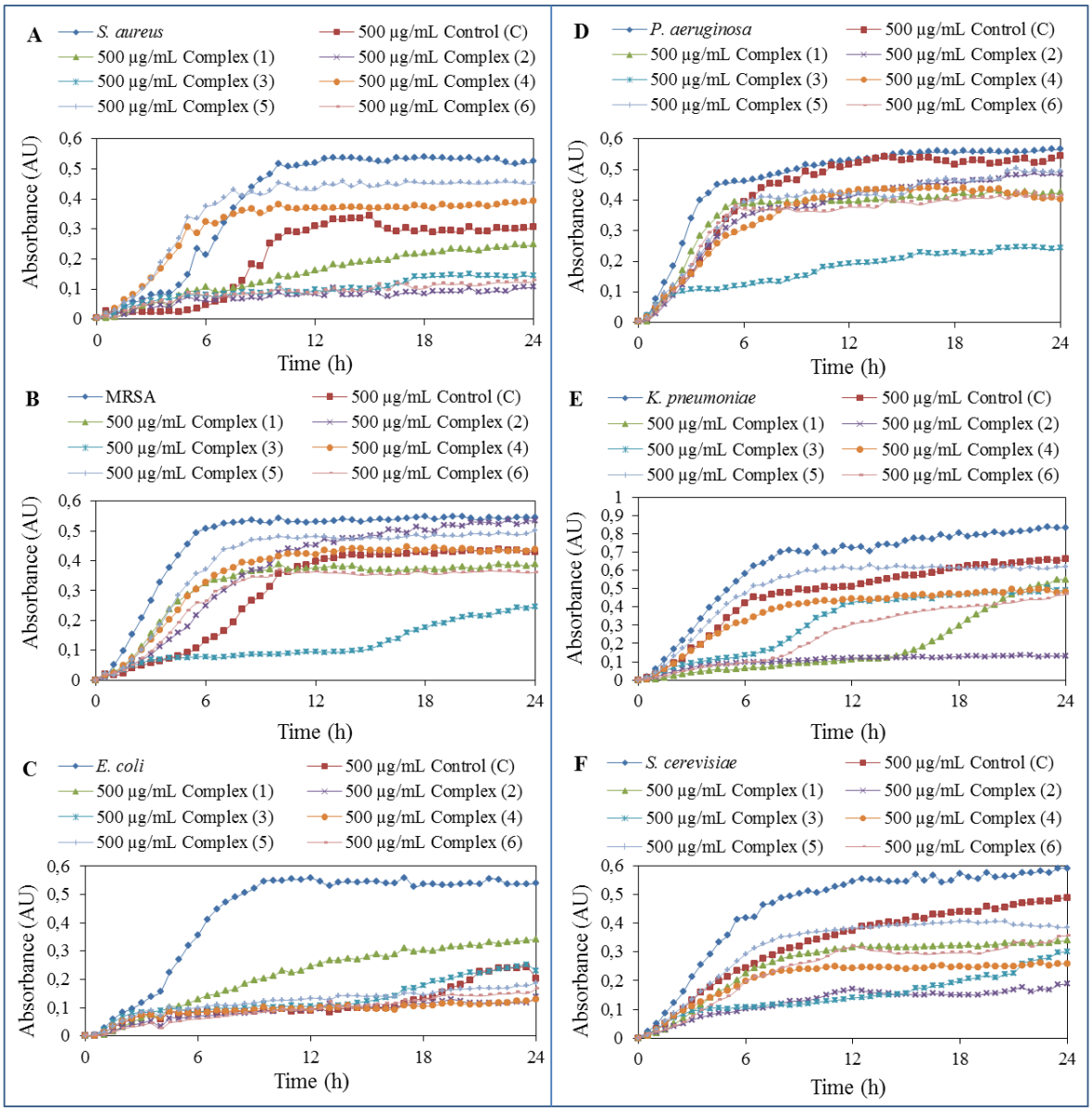

Figure 3.: Testing of antimicrobial activity of 500 µg/mL concentrations of tested complexes after 24 h of treatment on: (**A**) *S. aureus*; (**B**) MRSA; (**C**) *E. coli*; (**D**) *P. aeruginosa*; (**E**) *K. pneumoniae*; (**F**) *S. cerevisiae*.

Antimicrobial effect of tested complexes was tested on six different bacterial and yeast strains. Commercially available and explored in detail strains represented *Staphylococcus aureus* (*S. aureus*), *Escherichia coli* (*E. coli*) and methicillin-resistant *Staphylococcus aureus* (MRSA). Other strains, *Pseudomonas aeruginosa* (*P. aeruginosa*), *Klebsiella pneumoniae* (*K. pneumoniae*), and *Saccharomyces cerevisiae* (*S. cerevisiae*), were isolated from the patients with serious infected wounds on the skin surface.

The complexes were applied in 0; 7.8; 15.6; 31.3; 62.5; 125; 250 and 500 μg/mL concentrations on the three model organisms and three isolates. Antimicrobial effect of tested compounds was evaluated by basic microbiological method of growth curves based on the decrease of absorbance values in comparison with the control strains without the treatment. Graphs (Figure 3 A-F) show the highest inhibition effect by using of complex **2** except resistant strain of *S. aureus* - MRSA (*S. aureus* – 80.7 %, *E. coli* – 77.9 %, *P. aeruginosa* – 65.8 %, *K. pneumoniae* – 81.4 %, and *S. cerevisiae* – 64.8 %) and complex **6** also except MRSA (*S. aureus* – 76.8 %, *E. coli* – 71.8 %, *P. aeruginosa* – 62.4 %, *K. pneumoniae* – 68.1 %, and *S. cerevisiae* – 74.8 %).

4. CONCLUSION

Binuclear and trinuclear Mn(II) complexes bridged by the ttc^{3-} were prepared and characterized. From the results of biological testing it is obvious that the compounds can be potentially used for healing of infectious wounds of patients. The next step will be anticancer activity testing.

5. ACKNOWLEDGEMENT

The work has been supported by the project CEITEC CZ.1.05/1.1.00/02.0068.

6. REFERENCES

[1] M. H. Iltzsch and K. O. Tankersley, Biochemical Pharmacology, 48 (1994) 781.
[2] P. Kopel, K. Dolezal, L. Machala and V. Langer, Polyhedron, 26 (2007) 1583.
[3] P. Kopel, K. Dolezal, V. Langer, D. Jun, V. Adam, K. Kuca and R. Kizek, Molecules, 19 (2014) 4338.
[4] P. Kopel, D. Wawrzak, V. Langer, K. Cihalova, D. Chudobova, R. Vesely, V. Adam and R. Kizek, Molecules, 20 (2015) 10360.
[5] S. Cermakova, R. Herchel, Z. Travnicek and M. Sebela, Inorganic Chemistry Communications, 13 (2010) 778.

GRAPHENE AND GARPHENE OXIDE FOR BIOSENSING

Ondrej KUBESA[1*], Veronika HORNAKOVA[2], Zdenek MORAVEC[2], Petr SKLADAL[1,2]

[1] *Department of Biochemistry, Faculty of Science, Masaryk University in Brno, Kamenice 5, 625 00 Brno, Czech Republic*

[2] *Department of Chemistry, Faculty of Science, Masaryk University in Brno, Kamenice 5, 625 00 Brno, Czech Republic*

**268876@mail.muni.cz*

Abstract

In this work, different sizes of graphite flakes for preparation of graphene oxide were tested. Smaller particles resulted in bigger yield with higher stage of oxidation. The final characterization of the resulting graphene oxide was focused onquick and reliable methods such as Raman spectroscopy, UV-Vis spectroscopy and atomic force microscopy. Graphene oxide suitable for bioelectrochemical applications was prepared, with typical single layer thickness of ~1 nm; further treatment with ascorbic acid graphene with similar thickness.

1. INTRODUCTION

Graphene based materials have attracted wide attention in the last few years in many scientific fields. Graphene is a two-dimensional single-layered structure of carbon atoms with sp^2 configuration and many derivatives such as graphene nanoribbon, graphene oxide, doped graphene materials and reduced graphene oxide. Graphene has shown many interesting properties such as big surface area (~2630 $m^2 \cdot g^{-1}$ for single-layered graphene), high electrical conductivity, unique optical, thermal and mechanical properties [1–3].

Although graphene based materials have many potential applications in capacitors, e.g. drug delivery, electronic nanosystems and chemistry, they also became very popular in biosensing and electrochemistry in general, due to their mentioned properties, but also because they have relatively low production cost and similar potential window as graphite (2.5 V in 0.1 M PBS, pH = 7.0) [2, 4, 5].

Several methods for graphene preparation are known. The most common ones include mechanical exfoliation, epitaxial growth and various reductions of graphene oxide (GO) [5]. It is mostly GO which attracted big attention since it contains several oxygen functional groups such as hydroxyl, carboxylic and epoxide which make GO attractive for further modifications and applications [6, 7].

Graphene oxide was firstly reported by Schafhaeutl (1840) and by Brodie (1859). Since then many approaches for GO synthesis were developed, mostly based on the Hummers and Offeman method - strong oxidation of graphite flakes with acid. In order to retrieve graphene, further reduction is usually needed. Many strategies have been reported such as thermal reduction, microwave reduction, chemical reduction (hydrazine, $NaBH_4$, pyrogallol, KOH, HI or ascorbic acid), photo catalyst reduction, electrochemical reduction or multi-step reduction approaches [8, 9]. Reduction of graphene oxide leads to a reduced graphene oxide which exhibits similar properties as graphene but lacks its structural perfection. Oxidation and reduction usually leave us with structural defects and some residual functional groups which cause partial loss in electron mobility [5, 8, 10, 11].

Since most approaches for graphene oxide synthesis and reduction are still experimental, further characterization is needed. In this work, atomic force microscopy was mostly used, as well as UV-Vis spectroscopy and Raman spectroscopy.

2. MATERIAL AND METHODS

Graphite powders -20+100 mesh (~150-850 μm), -100 mesh (~150 μm) and -200 mesh (~74 μm) (Alfa Aesar; www.alfa.com), hydrochloric acid, phosphoric acid, potassium permanganate, ethanol, diethyl ether, hydrogen peroxide, sulfuric acid, ascorbic acid (Lach:ner; www.lach-ner.com), , mica grade V-1 muscovite was purchased from SPI Supplies (www.2spi.com).

PREPARATION OF GRAPHENE OXIDE Samples of graphene oxide were synthesized according to the Improved Hummers method (IHM) as reported by Marcano at al.[12] Graphene oxide was then diluted in acidified pH 3.0 water, sonicated for 2 hours and centrifuged for 10 minutes at 4 000 rpm in order to remove bigger particles and stored in the fridge when not in use.

AFM Atomic force microscope Dimension FastScan (Bruker, Santa Barbara, CA USA) was used to carry out the measurement of topography of graphene oxide. The FastScan-A probe (Bruker) with spring constant 18 N/m and resonance frequency of cantilever 1400 kHz was used. The mica (1.5 cm x 1.5 cm) was cleaned with adhesive tape and remaining microelements were removed by compressed air. For imaging, a drop (5 μl) of diluted graphene oxide was deposited on the surface and let to dry.

RAMAN SPECTROSCOPY Raman spectra were recorded using micro-Raman spectrometer Horiba Labram HR Evolution with a 532-nm laser as excitation source. Samples were deposited in dry state on microscope slides.

CHEMICAL REDUCTION Chemical reduction of GO using ascorbic acid (AA, 2 mM) was carried out at pH 9-10 (25% amonia) water [13, 14], concentration of graphene oxide was 0.5 $mg \cdot ml^{-1}$. The whole mixture was then tempered under stirring at 90 °C. The reduction process was monitored using UV-Vis absorption spectroscopy.

UV-Vis SPECTROSCOPY For UV-Vis measurements, the microtitre plate reader Synergy 2 BioTec (Winooski, USA) was used. All measurements were recorded as a function of time. Every 15 min, an aliquot of 300 µl was used for recording spectra.

3. RESULTS AND DISCUSSION

Three different types of graphite flakes were used, -200 mesh, -100 mesh and -20+100 mesh in order to prepare various types / grades of graphene oxide using IHM [12]. Table 1 shows comparison of the yields when using different sizes of graphite flakes. The best results were reached when using graphite flakes of -100 mesh (F2), approximately the same size of particles used by Marcano et al. The total yield of this reaction was 5.6 g from 3.0 g of graphite flakes, on the other hand when bigger particles were used such as -20+100 mesh (F3) the resulted product was mostly graphitic oxide with black-brownish colour (Figure 1), also the total yield of this reaction was very small.

Table 1.: Comparison of yields when using different grades of graphite flakes

	Amount of graphite flakes used	Gained amount of Graphene oxide	Gained amount of Graphene oxide in %
F1: -200 mesh (~74 microns)	3.0 g	4.4 g	+47
F2: -100 mesh (~150 microns)	3.0 g	5.6 g	+87
F3: -20+100 mesh (~150-850 microns)	3.0 g	X1.2 g	-60

Figure 1.: Graphene oxide – two different products; Left (F3) from -20+100 mesh graphite flakes; Right (F1) from -200 mesh graphite flakes.

Thus prepared GO was then characterised using Raman spectroscopy. As a very simple and nondestructive method, Raman spectroscopy provides characterization of carbon-based materials. Figure 2 displays, that typical D and G bands for graphene oxide were observed with their intensity ratio of 0.93.

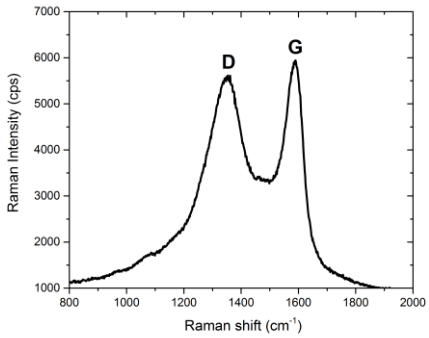

Figure 2.: Recorded Raman spectra for the GO based on the graphite type F2 – D-band of shift 1348 cm^{-1} and intensity 5632 cps and G-band of shift 1585 cm^{-1} and intensity 6041 cps.

UV-Vis spectroscopy was used in order to observe direct chemical reduction of graphene oxide using ascorbic acid. The position of absorption peak is well known to be around 231 nm and it becomes red-shifted from this value as the reduction proceeds. Basically, the more this peak red-shifts, the more efficient the reductant is. AA was used as an alternative to toxic hydrazine which leads to peak maximum around 268 nm. In our measurements (Figure 3) GO suspension showed the initial absorption maximum at 229 ±1 nm and after the treatment with AA, the chemically reduced GO maximum shifted to 266 ±1 nm.

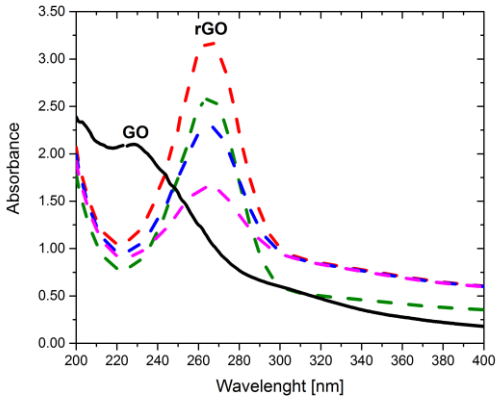

Figure 3.: Absorption spectra of the graphene oxide solution (GO – full line) with maximum at 229 ±1 nm and by AA reduced graphene oxide (rGO – dashed lines, green – 15 min, red – 30 min, blue – 45 min, pink – 60 min) with maximum at 266 ±1 nm.

The atomic force microscopy is very powerful method for getting surface topography information about graphene / graphene oxide. Main reason to implement AFM measurements was to observe the structural changes, size and shape of graphene nanosheets and to observe the differences between graphene oxide and chemically reduced graphene oxide.

It is well known that the amount of functional groups varies depending on the method used for preparation of graphene oxide. The corresponding ratio C/O within the 4:1-2:1 interval was reported for GO preparations. Even after the reduction the ratio was usually 12:1. The main problem is that different reduction processes lead to different extent of oxygen functional groups removal [8].

A typical pristine graphene sheet is atomically flat with reported thickness of ~0.34 nm. Graphene oxide, on the other hand, is expected to be thicker due to functional groups, ruptures and various displacements of sp^3-hybridized carbon atoms above and below the graphene sheets. Typical reported thickness when using AFM in tapping mode is approximately ~1.1 nm [8, 10, 12, 15, 16]. Thanks to the AFM, there was confirmed that the size of graphene oxide nanosheets significantly varies, although there were neither thinner nor thicker sheets than ~1.1 nm (Figure 4); multiples of this value are obtained for several overlaid layers.

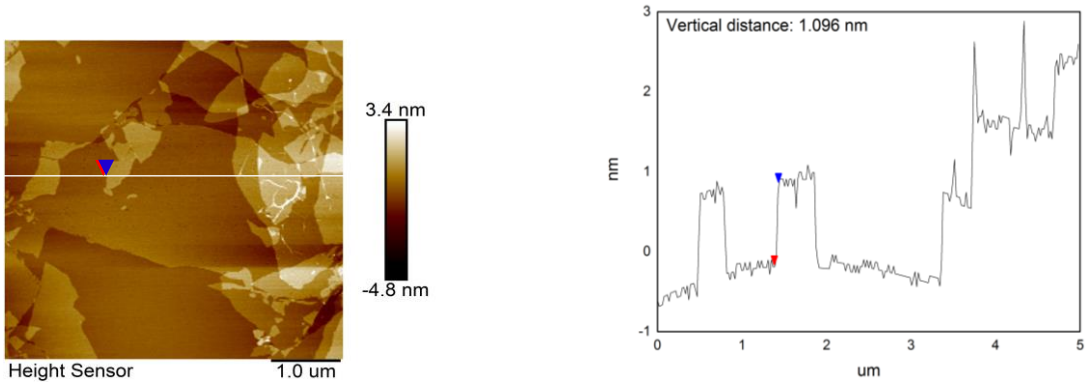

Figure 4.: Atomic force microscopy results for graphene oxide deposited on mica, average thickness ~1 nm.

GO chemically reduced by AA showed no big difference. In fact, several chemical approaches were tested (not shown), all resulted in visible change in colour of the suspension from yellow-brownish GO to dark-grey, but still transparent suspension of chemically reduced graphene oxide. However, the thickness remained the same. This supports previously reported observations [13] of remaining functional groups and disturbances in such prepared graphene sheets. Similar effect as mentioned at Yongchao Si et. al. was also observed, small holes and disruptions inside the graphene sheets probably caused by sonification or / and reduction process [16].

4. CONCLUSION

The preparation of reduced graphene oxide through its intermediate graphene oxide is very complicated process with many steps. As it seems, even small changes in the conditions usually lead to different results. For the preparation of graphene oxide itself, small graphite particles seem to be much better precursor than bigger ones.

Several fractions of graphene oxide with different results and of different quality were prepared for further electrochemical applications.

Graphene oxide is definitely very interesting material which provides many options and capabilities. Although for many scientific fields pristine graphene layer is demanded, for electrochemistry and biochemistry laboratory the prepared graphene oxide has many potential applications. Disorders in the sheet structure are sources of various functional groups even after reduction of graphene oxide, several functional groups still remain, which provides possibilities for further modifications.

Since the laboratory preparation of graphene oxide is still very experimental, proper description and characterization of obtained graphene oxide is always needed. Raman spectra and UV-Vis spectroscopy give us very quick results, but it is atomic force microscopy which can reliably provide information on thickness, disorders in the structure, size and many other properties needed for further electrochemical applications.

5. ACKNOWLEDGEMENT

The work has been supported by MUNI/A/1265/2015 – Support of biochemical research at MU.

6. REFERENCES

[1] Geim AK (2009) Graphene: Status and Prospects. Science 324:1530–1534.
[2] Stankovich S, Dikin DA, Dommett GHB, et al (2006) Graphene-based composite materials. Nature 442:282–286.
[3] Pumera M, Ambrosi A, Bonanni A, et al (2010) Graphene for electrochemical sensing and biosensing. TrAC Trends Anal Chem 29:954–965.
[4] Zhou M, Zhai Y, Dong S (2009) Electrochemical Sensing and Biosensing Platform Based on Chemically Reduced Graphene Oxide. Anal Chem 81:5603–5613.
[5] Wang Z, Zhou X, Zhang J, et al (2009) Direct Electrochemical Reduction of Single-Layer Graphene Oxide and Subsequent Functionalization with Glucose Oxidase. J Phys Chem C 113:14071–14075.
[6] Robinson JT, Perkins FK, Snow ES, et al (2008) Reduced Graphene Oxide Molecular Sensors. Nano Lett 8:3137–3140.
[7] Szabó T, Berkesi O, Dékány I (2005) DRIFT study of deuterium-exchanged graphite oxide. Carbon 43:3186–3189.
[8] Pei S, Cheng H-M (2012) The reduction of graphene oxide. Carbon 50:3210–3228.
[9] Pei S, Zhao J, Du J, et al (2010) Direct reduction of graphene oxide films into highly conductive and flexible graphene films by hydrohalic acids. Carbon 48:4466–4474.
[10] Stankovich S, Dikin DA, Piner RD, et al (2007) Synthesis of graphene-based nanosheets via chemical reduction of exfoliated graphite oxide. Carbon 45:1558–1565.
[11] Park S, Ruoff RS (2009) Chemical methods for the production of graphenes. Nat Nanotechnol 4:217–224.
[12] Marcano DC, Kosynkin DV, Berlin JM, et al (2010) Improved Synthesis of Graphene Oxide. ACS Nano 4:4806–4814.
[13] Fernández-Merino MJ, Guardia L, Paredes JI, et al (2010) Vitamin C Is an Ideal Substitute for Hydrazine in the Reduction of Graphene Oxide Suspensions. J Phys Chem C 114:6426–6432.
[14] Zhang J, Yang H, Shen G, et al (2010) Reduction of graphene oxide viaL-ascorbic acid. Chem Commun 46:1112–1114.
[15] Sheshmani S, Amini R (2013) Preparation and characterization of some graphene based nanocomposite materials. Carbohydr Polym 95:348–359.
[16] Si Y, Samulski ET (2008) Synthesis of Water Soluble Graphene. Nano Lett 8:1679–1682.

REDOX-PAIR DEFINED ELECTROCHEMICAL DETECTION – BIAMPEROMETRIC SET-UP EXHIBITING "INTERFERENCES-FREE" PERFORMANCE

Karel LACINA,[1*], Petr VANÝSEK[2], Libuše TRNKOVÁ[3], Petr SKLÁDAL[1,4]

[1] *CEITEC – Central European Institute of Technology, Masaryk University, Kamenice 5, Brno, 625 00, (Czech Republic)*

[2] *Department of Chemistry and Biochemistry, 418 La Tourette Hall, Northern Illinois, University DeKalb, IL 60115-2862 (U.S.A.) and*
CEITEC – Central European Institute of Technology, Brno University of Technology, Technická 10, Brno, 616 00 (Czech Republic)

[3] *Department of Chemistry, Faculty of Science, Masaryk University, Kamenice 5, Brno, 625 00 (Czech Republic)*

[4] *Department of Biochemistry, Faculty of Science, Masaryk University Kamenice 5, Brno, 625 00 (Czech Republic)*

**lacinak@chemi.muni.cz*

Abstract

A routine, large scale monitoring, such as point-of-care systems, requires inexpensive and simple analytical schemes. An electroanalytical concept of biamperometry for such sensing systems has been overlooked due to the widespread potentiostat-controlled experiments.

We have previously designed a simple detection platform[1,2] where the analyte dependent electrolytic current has been amplified by a bipolar transistor resulting in a glow of a light emitting diode. The inexpensive four-component electronic circuit has been able to sensitively determine presence of H_2O_2 and glucose without any additional instrumentation[1,2]. In the course of the characterization of this system[7a], we found out that it works on the basis of an electrolytic cell, i.e. application of a voltage between two electrodes is followed by electrochemical reactions - reduction on cathode and oxidation on anode - analogously to biamperometric cell.

We have already exemplified technique of biamperometry as a powerful electroanalytical tool suitable especially for the enzyme-based biosensing[3]. The putative application of the studied biamperometric cell set-up for applied electroanalytical purposes is demonstrated in Figure 1, left. The current flowing through the system was followed using a potentiostat where the gold anode and cathode were connected as the working and the combined reference/auxiliary electrodes, respectively. Different combinations of electrolytes (either a

buffer or $[Fe(CN)_6]^{4-/3-}$) in spatially separated electrode compartments were tested. A current signal is detected only in the case in which both redox partners are in the contact with the corresponding electrode – $[Fe^{II}(CN)_6]^{4-}$ above the anode and $[Fe^{III}(CN)_6]^{3-}$ above the cathode. In the presence of only one partner of a particular redox pair, a redox reaction cannot occur and hence the current does not flow, so if there is no available suitable redox pair combination, then the resulting response is zero.

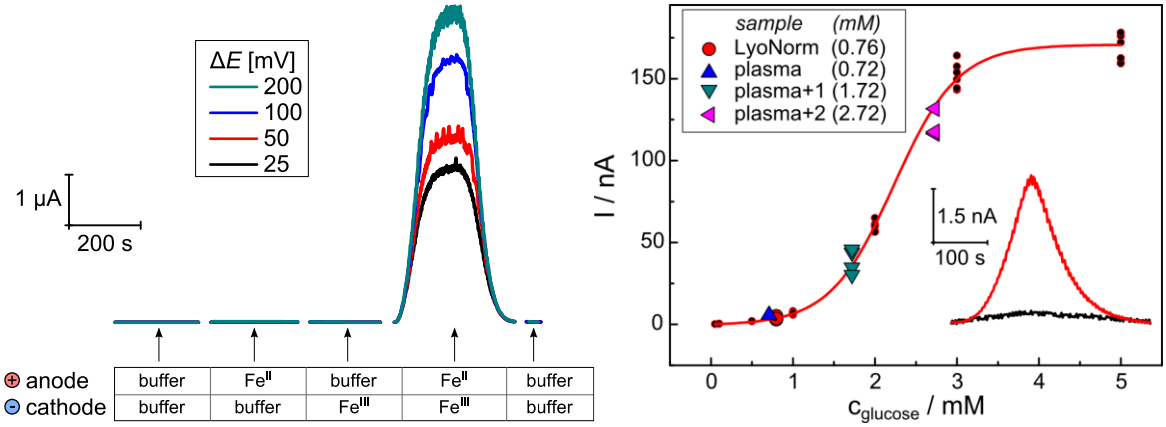

Figure 1.: Biamperometric detection using a flow-through cell where the compartments of the anode (⊕) and the cathode (⊖) are spatially separated. The table in the graph corresponds to the combinations of the electrolytes (either buffer or $[Fe(CN)_6]^{4-/3-}$) in contact with a particular electrode. The response was measured upon several differences of a potential applied to the electrochemical cell (ΔE) (left). Calibration curve for the glucose biamperometric biosensor. Blood plasma samples were 1:4 diluted with buffer containing 5 mM $Ru(NH_3)_6^{3+}$, Sample of blood plasma was fortified with glucose to obtain higher concentrations of glucose in real samples. Content of glucose in real samples is depicted in legend in mM. Difference of potential between anode and cathode was ΔE=50 mV. Right lower corner: comparison of the signal of GOD (red curve) and BSA (black curve) modified electrodes to plasma sample (0.72 mM glucose) is depicted. No significant interference signal is observed. (right)

The possible utilization of the introduced concept was proved on the case of a glucose determination (Figure 1, right). In this case glucose was specifically and precisely determined in the environment of 5-times diluted blood plasma. The detection system consisted only of a gold anode and a cathode modified by glucose oxidase and BSA, respectively. It should be emphasized that no diffusion barrier or any electrocatalytic materials (nanoparticles or graphene, etc.) were employed. The experiment was performed with the redox system $Ru(NH_3)_6^{2+/3+}$. In the presence of excess of Ru(III), Ru(II) is generated from the enzymatic reaction of reduction of glucose. Generated Ru(II) is than oxidized on the anode.

Calibration curve for the glucose is depicted in Figure 1, right, showing also responses of real samples. These correspond well to the concentrations determined by standard analytical

methods (glucometer and a kit for photometric determination). The signal from the matrix of the sample was negligible (nearly zero) at the particular experimental conditions.

Thus, we have shown that the principles of biamperometry can be advantageously utilized for the rejection of electrochemical interferents. Moreover, as the utilization of mediators is widespread for redox enzymes (e.g. glucose oxidase and alike), the possibilities of uniquely specific signal generation are apparent – only enzyme reaction converts redox substrate to the detectable complementary redox partner (zero-background signal if a compound with a suitable redox potential is initially absent).

ACKNOWLEDGEMENT

This work was realized in CEITEC - Central European Institute of Technology with research infrastructure supported by the project CZ.1.05/1.1.00/02.0068 financed from European Regional Development Fund. Furthermore, the SIX (Sensor, Information and Communication Systems) CZ.1.05/2.1.00/03.0072 is acknowledged.

REFERENCES

[1] Lacina K., Skládal P., Sensors & Actuators B: Chemical, 210 (2015), 183-189.
[2] K. Lacina, P. Skládal, [In Czech] Systém pro převod elektrochemického signálu na vizuální vjem, Czech Republic utility patent CZ 28142, 28-4-2015.
[3] Lacina K., Vanýsek P., Bednář P., Trnková L., Skládal P., ChemElectroChem, 2016, *in press*.

ATOMIC FORCE MICROSCOPY – TOOL TO STUDY NANOMECHANICAL PROPERTIES OF LIVING CELLS AND BIOMATERIALS

Mapping the mechanical properties of biomaterials on different length scales: Depth-sensing indentation and AFM based nanoindentation

Jan PŘIBYL[1*], Petr SKLÁDAL[1,2], Pavel BOUCHAL[2], Irena KRATOCHVÍLOVÁ[4]

[1] *Central European Institute of Technology,* [2] *Department of Biochemistry, Faculty of Science, Masaryk university, Kamenice 5, 625 00 Brno, Czech Republic*

[2] *Institute of Physics, Academy of Sciences of the Czech Republic, Na Slovance 2, Prague 8, 182 21, Czech Republic*

**pribyl@nanobio.cz*

Abstract

Mechanical properties (elasticity and adhesivity) of cells, tissues and biomaterials play important roles in many biological and biotechnological processes including cell differentiation, tumor formation, metastatic processes and/or plant development. Changes in stiffness of cells are often signs of changes in cell physiology or phenotype. Thereofre, cell stiffness is an index to evaluate the status of cell cultures. Atomic Force Microscopy (AFM) operated in spectroscopic mode provides a way to reliably measure the stiffness of living cells and biomaterials suitable for cell treatment. This method has been widely applied to map stiffness of various materials with nanometer resolution. The AFM tip indents studied material and the applied force is measured. Fitting the force-indentation curve to either Hertz or Sneddon model can give quantitative measurements of material stiffness. Application of AFM spectroscopy (nanoindentation) for mapping of stiffness is demonstrated, when stem cells, cancer cell, plant tissues and layers of glycosaminoglycans were investigated.

1. INTRODUCTION

AFM is a three-dimensional high resolution topographic technique. It is suitable for biological applications in native conditions with the ability to measure bending of the cantilever probe with extremely high precision. This allows AFM to be used as a mechanical nanosensor, in cell based biosensing of drug effects and in study of growth factor effects on cells. Among the multitude of methods applied to measure the stiffness of cells and tissues,

micro-indentation using an Atomic Force Microscopy (AFM) provides a way to reliably measure the stiffness of living cells and other biomaterials.

A variety of biophysical techniques such as atomic force microscopy (AFM) [1,2], cytoindentation [3], magnetic twisting cytometry [4], optical tweezers [4] and micropipette aspiration [5] have been used to probe the mechanical properties of cells. A change in the biophysical properties of cells has recently emerged as an indication of disease [6,7]. Specifically, cell elasticity or deformability has been recognized as a marker for cellular phenotypic events associated with alteration in cytoarchitecture and adhesion during malignant transformation [8–10].

Application of AFM spectroscopy (nanoindentation) for mapping of stiffness changes is demonstrated, when stem cells, cancer cell, fibroblasts, plant tissues and layers of glycosaminoglycans were investigated.

2. MATERIAL AND METHODS

2.1. Young's modulus mapping by Atomic Force Microscope

Standard bioAFM microscope JPK NanoWizard 3 from JPK (JPK, Berlin, Germany) was used to perform force mapping procedure. The scanning by probe head (maximal visualization range 100 100 15 μm in X Y Z axis) of AFM microscope was placed on inverted optical microscope Olympus IX 81, 10x objective was used to find proper area covered with cells and to place cantilever in the proper position for force mapping procedure. Plastic Petri dish (TPP, Trasadingen, Switzerland) with either the distilled water for instrument calibration or with the fibroblast culture was placed inside the Petri dish heater (JPK) preheated to 37 oC.

Non coated silicon nitride AFM cantilever Hydra 2R 100N (AppNano, Mountain View, CA, United States) equipped with pyramidal silicon tip was used for all the experiments. The probe was calibrated prior every experiment as described in the below text.

The calibration procedure was done in double distilled water, when the whole setup was preheated (Petri dish heater) to 37 oC for 30 minutes. Then the laser reflection sum was maximized, followed by centering of the laser detector. The AFM probe was introduced in contact with the surface during a standard process of landing. The sensitivity of the AFM setup was determined as a slope of the force distance curve measured by lifting the cantilever with Z height of 450 nm, time per curve was 3 seconds. The sensitivity was found in the range 15.07 15.37 nm/V, cantilever stiffness was calibrated by measurement of its thermal noise and proceeded between 17.34 and 19.19 nN/m for different days of experiments.

The bioAFM setting was identical for all the force mapping procedure. SetPoint value was 1.0 nN (relative to baseline value), time per curve 0.45 sec, Z length 15.0 μm, speed of curve recording 33.3 μm/sec, the force distance curves were recorded with data sample rate of 2 kHz. The force mapping procedure was performed as step by step recording of force distance curves in the network of 64x64 points on 55x55 μm covering area of single fibroblast cell.

2.2. Long term monitoring of cell growth

Surface stiffness of the fibroblasts cultured on a Petri dish shortly (25 minutes) after thawing process was monitored during overnight nanomechanical mapping of the fibroblast cell. Petri dish containing freshly thawed suspension of cells was for a short period pre incubated in a standard CO2 incubator (see chapter Short term incubation). When first cells started to adhere, culturing medium in the dish was completely exchanged and force mapping process was started immediately. Nanomechanical measurement was performed during 14 hours continuous experiment of repeated force mapping process on identical place (scanning over the identical cell). Parameters identical to other mapping processes were used also in this case. Neither media exchange nor AFM instrument adjustment was involved during the repeated mapping procedure.

2.3. Process of cells thawing

Fibroblast suspension (about 1 ml in a standard plastic tube) was taken out from liquid nitrogen (Dewar flask), transported to place of thawing on an ice bath. The cell suspension was then quickly thawed in stream of hot water until the point, where a few remaining crystals were visible in the tube. The whole volume was immediately transported into the 15 ml standard Falcon tube and 12 ml of cold (4 oC) MEF media (mouse embryonal feed) was added by drop wising from Pasteur pipette. The tube was centrifuged (200 g, 4 oC) for 5 minutes, the excess of MEF media above the cell pellet was removed by pipette, cells were re suspended in 1 ml of MEF media (37 oC) and distributed into the 3 plastic Petri dishes (3 cm in diameter). The dishes were placed inside the standard CO2 incubator for either short or long term incubation.

2.4. Immobilization of glycosaminoglycans

Mica surface (2SPi, West Chester, PA, USA) was cleaned by scotch tape and stream of compressed air. Clean surface was afterwards silanized by vapours of (3-aminopropyl)-

dimethyl-ethoxysilane (APDMES) for 2 hours. Monolayer of glycosaminoglycan (hyaluronic acid, chondroitin sulfate, heparin) was formed, when solution of appropriate compound in PBS buffer was incubated on the surface for 24 hours, formation of covalent bond was catalyzed by addition of fresh N-(3-Dimethylaminopropyl)-N′-ethylcarbodiimide hydrochloride (EDAC).

3. RESULTS AND DISCUSSION

The bioAFM microscope was used to study surface elasticity of cancer cell lines known to have different stiffness. This method is based on measurement of force distance curves of cantilever lifted above the cell surface in a defined pattern of 64x64 points thus providing force maps. Such a curve is fitted to Hertzian Sneddon model (Figure 1) in order to get exact value of Young's modulus (YM).

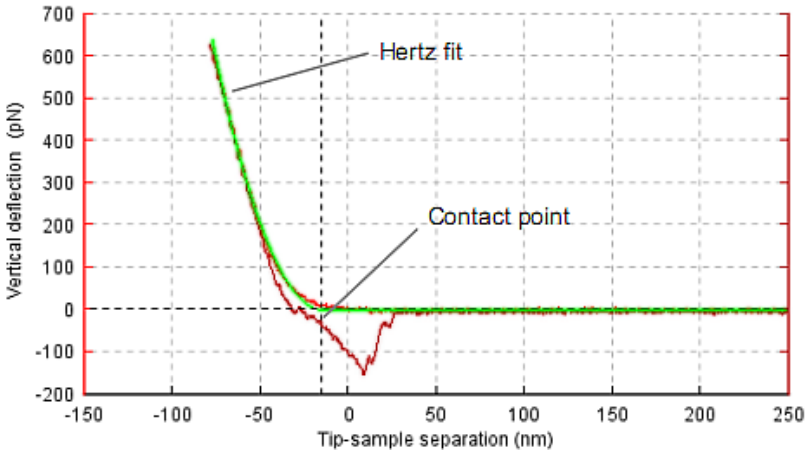

Figure 1.: Example of force-distance curve, green curve shows the Hertz fit used to calculate Young's modulus of indented material.

Changes in stiffness of cells are often signs of changes in cell physiology or phenotype. Thereofre, cell stiffness is an index to evaluate the status of cell cultures. Atomic Force spectroscopy was used to monitor changes in stiffness of stem cells (Figure 2). Height profile and adhesion properties of studied surface can be estimated, too.

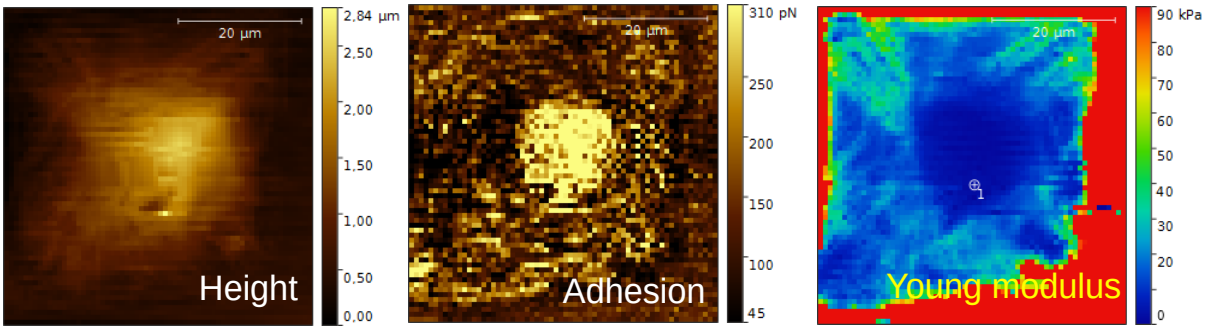

Figure 2.: Process of nanomechanical mapping is based on evaluation of FD curves. Height profile and adhesion properties of studied surface can be estimated, too.

Young's modulus mapping of two cell lines (with expressed vs. non-expressed protein, i.e. specific vs. control line) was studied, when the above described method was used. Significant difference in stiffness values between the two cell lines were found (Figure 3), when the average Young's modulus value of the MCF7 control line and MCF7 with transfected siRNA was 0.858±0.398 kPa and 2.72±0.85 kPa, respectively. Similarly, the stiffness value found for the cell line MCF7_PDZIM was 8.96±1.60 kPa, which is significantly higher value comparing to the control line - 1.67±0.70 kPa.

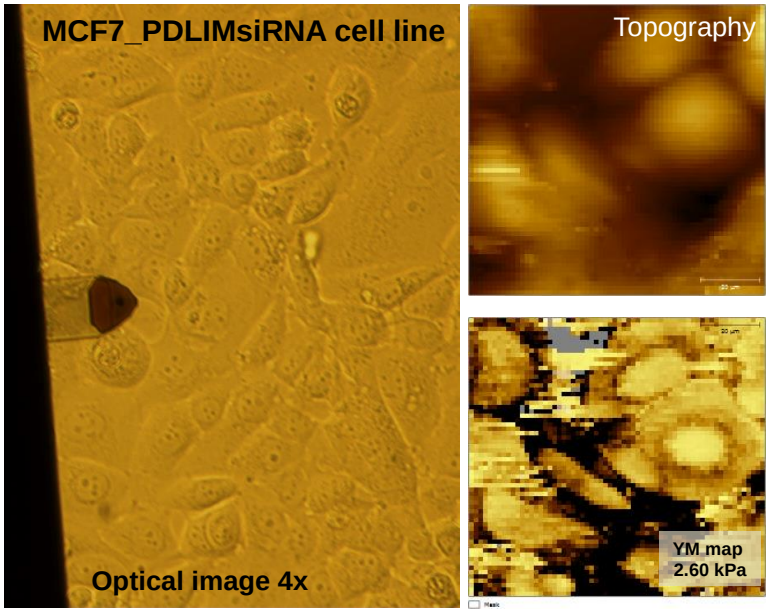

Figure 3.: Procedure of nanomechanical mapping of the cell culture. Real optical image on the left shows AFM cantilever above the cells, the up right image topography based on FD curves and bottom left image final YM map with average value of stiffness.

Process of interaction between immobilized hyaluronane layer and myeloperoxidase resulting in rapid changes in layer stiffness was monitored AFM spectroscopy in a real time (Figure 4).

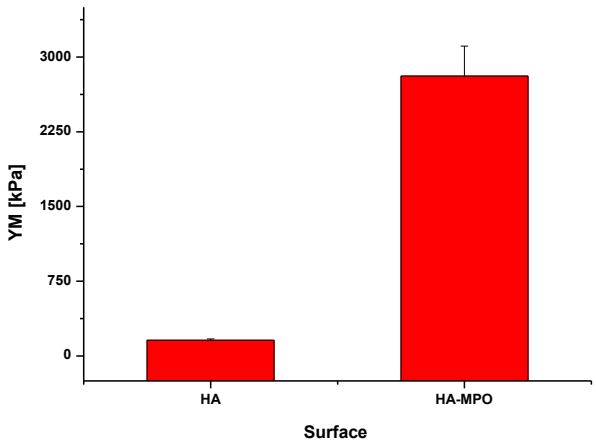

Figure 4.: Change of layer stiffness as effect of hyaluronan (HA) intraction with myeloperoxidase molecules, thus forming hyaluronan-myeloperoxidase complex (HA-MPO).

4. CONCLUSION

In conclusion, we present application of AFM spectroscopy (nanoindentation) for mapping of stiffness changes for various stem cell lines, cancer cell line. Moreover, process of fibroblast grow following the cell thawing was characterized. Ability of the method to study changes in plant tissues is demonstrated, too. Process of interaction between immobilized hyaluronane layer and myeloperoxidase resulting in rapid changes in layer stiffness was monitored AFM spectroscopy in a real time.

5. ACKNOWLEDGEMENT

The work has been supported by CEITEC - Central European Institute of Technology (CZ.1.05/1.1.00/02.0068 and LQ1601), the European Regional Development Fund and the National Program of Sustainability II.

6. REFERENCES

[1] I. Crha, J. Pribyl, P. Skladal, J. Zakova, P. Ventruba, M. Pohanka, Determination of the surface pathology of human sperm by atomic force microscopy, Hum. Reprod. 25 (2010) I122–I122.

[2] M. Pesl, I. Acimovic, J. Pribyl, R. Hezova, A. Vilotic, J. Fauconnier, J. Vrbsky, P. Kruzliak, P. Skladal, T. Kara, V. Rotrekl, A. Lacampagne, P. Dvorak, A.C. Meli, Forced aggregation and defined factors allow highly uniform-sized embryoid bodies and functional cardiomyocytes from human embryonic and induced pluripotent stem cells, Heart Vessels. 29 (2014) 834–846. doi:10.1007/s00380-013-0436-9.

[3] [3] A.X. Cartagena-Rivera, W.-H. Wang, R.L. Geahlen, A. Raman, Fast, multi-frequency, and quantitative nanomechanical mapping of live cells using the atomic force microscope, Sci. Rep. 5 (2015) 11692. doi:10.1038/srep11692.

[4] V.M. Laurent, S. Hénon, E. Planus, R. Fodil, M. Balland, D. Isabey, F. Gallet, Assessment of mechanical properties of adherent living cells by bead micromanipulation: comparison of magnetic twisting cytometry vs optical tweezers, J. Biomech. Eng. 124 (2002) 408–421.

[5] L.M. Lee, A.P. Liu, The Application of Micropipette Aspiration in Molecular Mechanics of Single Cells, J. Nanotechnol. Eng. Med. 5 (2014) 0408011–0408016. doi:10.1115/1.4029936.

[6] J. Bercoff, S. Chaffai, M. Tanter, L. Sandrin, S. Catheline, M. Fink, J.L. Gennisson, M. Meunier, In vivo breast tumor detection using transient elastography, Ultrasound Med. Biol. 29 (2003) 1387–1396. doi:10.1016/S0301-5629(03)00978-5.

[7] D.E. Discher, P. Janmey, Y. Wang, Tissue Cells Feel and Respond to the Stiffness of Their Substrate, Science. 310 (2005) 1139–1143. doi:10.1126/science.1116995.

[8] S. Suresh, J. Spatz, J.P. Mills, A. Micoulet, M. Dao, C.T. Lim, M. Beil, T. Seufferlein, Connections between single-cell biomechanics and human disease states: gastrointestinal cancer and malaria, Acta Biomater. 1 (2005) 15–30. doi:10.1016/j.actbio.2004.09.001.

[9] S. Suresh, Biomechanics and biophysics of cancer cells, Acta Mater. 55 (2007) 3989–4014. doi:10.1016/j.actamat.2007.04.022.

[10] J. Guck, S. Schinkinger, B. Lincoln, F. Wottawah, S. Ebert, M. Romeyke, D. Lenz, H.M. Erickson, R. Ananthakrishnan, D. Mitchell, J. Käs, S. Ulvick, C. Bilby, Optical Deformability as an Inherent Cell Marker for Testing Malignant Transformation and Metastatic Competence, Biophys. J. 88 (2005) 3689–3698. doi:10.1529/biophysj.104.045476.

ENHANCEMENT OF ELECTROCHEMICAL DETECTION IN CAPILLARY ELECTROPHORESIS USING NANOMATERIALS

Marketa VACULOVICOVA[1,2*], Vojtech ADAM[1,2]

[1] *Department of Chemistry and Biochemistry, Mendel University in Brno, Zemedelska 1, 613 00 Brno, Czech Republic*

[2] *Central European Institute of Technology, Brno University of Technology, Purkynova 123, 612 00 Brno, Czech Republic*

** marketa.vaculovicova@mendelu.cz*

Abstract

Nanotechnology has been defined as a technology in which dimensions and tolerances within the range of 0.1–100 nm play a critical role. Nanomaterials have greatly influenced numerous scientific fields, and these influences can be observed in different ways. Their influence on capillary electrophoresis will be discussed in this lecture.

1. INTRODUCTION

The NANO phenomenon has clearly influenced the entire scientific world, including instrumental analytical chemistry; therefore, scientists are not only developing new approaches and assays using nanotechnologies, they are also upgrading standard techniques. One of the methods most influenced by this phenomenon is capillary electrophoresis (CE).

In general, the connection between nanomaterials and CE can be viewed from two broad perspectives I) CE of nanomaterials and II) nanomaterials in CE. The first category focuses on the application of CE for characterization used during nanomaterial synthesis and modification and for the monitoring of properties and interactions with other molecules. The second category addresses applications of nanomaterials to improve CE performance, mainly by enhancing separation efficiency and by increasing detection sensitivity and/or selectivity.

In particularly, the electrochemical detection in CE is benefiting from utilization of nanomaterials.

2. DISCUSSION

The electrochemical detection can be performed in three modes: potentiometric, conductometric and amperometric. Conductometric and potentiometric detectors provide a bulk property response with good sensitivity. By contrast, amperometric detection is selective

and can be tuned to the analyte of interest. One of the main differences of this approach versus the optical detection modes is the fact that electrochemical detection is mostly performed by off-column, end-capillary, destructive means. To overcome these limitations, interest in contactless conductometric detection has been growing steadily over the past decade.[1-4] The application of nanomaterials for electrochemical detection encompasses a notably broad area. Due to their electrochemical properties, nanomaterials have been applied for electrochemical analysis of numerous analytes, including nucleic acids,[5-7] proteins,[8, 9] secondary metabolites,[10, 11] and metals.[12] The important functions provided by nanoparticles include the immobilization of biomolecules, catalysis of electrochemical reactions, enhancement of electron transfer between electrode surfaces and proteins, labeling of biomolecules, and even participation as a reactant.[13] In addition to the relatively low costs of electrochemical detection compared with those of optical instrumentation, other advantages such as the possibility of miniaturization and in-field applications are important.

Due to the great breadth of this area, it is not surprising that reviews have been published. Pumera and Escarpa[14] summarized the different approaches for constructing nanomaterial-based detectors for conventional CE and microchip electrophoresis and mostly focused on three main types of nanomaterials, i.e., carbon nanotubes, nanoparticles, and nanorods, in various designs. The advantages and disadvantages of the selected detectors have been discussed. From the materials viewpoint, reviews by Chen[15] and Martin[16] were focused on carbon. That review was directed at CNTs and boron-doped diamond and covered CNT-based electrochemical detectors in microchip CE, CNT-based electrochemical detectors in conventional CE, boron-doped diamond electrochemical detectors in microchip CE, and boron-doped diamond electrochemical detectors in conventional CE.

3. CONCLUSION

In summary, the use of nanomaterials in electromigration methods offers new perspectives in the field of clinical use because these advanced materials can lower detection limits while simultaneously enhancing separation effectiveness. The combination of the miniaturization potential of CE with the abilities of nanomaterials to improve the overall performance might increase the possibility of development and practical application of a portable and cost-effective device that is applicable in point-of-care areas suitable for personalized diagnostics. And especially in this area, the electrochemical detection is of a great potential because it

mainly benefits from applications of nanomaterials that enable increasingly sensitive detection. Moreover, in combination with advances in microfluidics, the separation power of electrophoretic analysis, which is further enhanced by nanomaterial-based stationary and pseudostationary phases, promises increasingly effective analyses of complex biological samples.

4. ACKNOWLEDGEMENT

The work has been supported by project CEITEC 2020 (LQ1601) with financial support from the Ministry of Education, Youth and Sports of the Czech Republic under the National Sustainability Programme II. The financial support for Grant Agency of Czech Republic (16-23647Y) is highly acknowledged.

5. REFERENCES

[1] Elbashir, A. A., Aboul-Enein, H. Y., Biomed. Chromatogr. 2010, 24, 1038-1044.
[2] Elbashir, A. A., Aboul-Enein, H. Y., Biomed. Chromatogr. 2012, 26, 990-1000.
[3] Kuban, P., Hauser, P. C., Electroanalysis 2004, 16, 2009-2021.
[4] Zemann, A. J., Electrophoresis 2003, 24, 2125-2137.
[5] Erdem, A., Talanta 2007, 74, 318-325.
[6] Liu, X. G., Cheng, Z. Q., Fan, H., Ai, S. Y., Han, R. X., Electrochim. Acta 2011, 56, 6266-6270.
[7] Mao, X., Liu, G. D., J. Biomed. Nanotechnol. 2008, 4, 419-431.
[8] Rusling, J. F., Chem. Rec. 2012, 12, 164-176.
[9] Rusling, J. F., Sotzing, G., Papadimitrakopoulosa, F., Bioelectrochemistry 2009, 76, 189-194.
[10] de Andres, F., Zougagh, M., Castaneda, G., Rios, A., J. Chromatogr. A 2008, 1212, 54-60.
[11] Songa, E. A., Waryo, T., Jahed, N., Baker, P. G. L., et al., Electroanalysis 2009, 21, 671-674.
[12] Aragay, G., Merkoci, A., Electrochim. Acta 2012, 84, 49-61.
[13] Luo, X. L., Morrin, A., Killard, A. J., Smyth, M. R., Electroanalysis 2006, 18, 319-326.
[14] Pumera, M., Escarpa, A., Electrophoresis 2009, 30, 3315-3323.
[15] Chen, G., Talanta 2007, 74, 326-332.
[16] Martin, A., Lopez, M. A., Gonzalez, M. C., Escarpa, A., Electrophoresis 2015, 36, 179-194.

GAS SENSITIVE STRUCTURES WITH N-N NANOJUNCTIONS BASED ON WO_{3-x} NANONEEDLES AND Fe_2O_3 NANOPARTICLES

Stella VALLEJOS[1]*, Isabel GRÀCIA[2]

[1] *SIX Research Centre, Brno University of Technology, Brno, Technická 10, CZ-61600, Czech Republic*

[2] *Instituto de Microelectrónica de Barcelona (IMB-CNM, CSIC), Campus UAB, 08193, Barcelona, Spain*

**vargas@feec.vutbr.cz*

Abstract

Gas sensitive structures with n-n nanjunctions based on WO_{3-x} nanoneedles (NNs) and Fe_2O_3 nanoparticles (NPs) are synthetised using a co-deposition method *via* aerosol assisted chemical vapour deposition (AACVD). These structures demonstrate enhanced gas sensor performance compared to pristine WO_{3-x} NNs, particularly towards toluene.

1. INTRODUCTION

Nanostructured semiconducting metal oxides (SMOX) such as NNs have demonstrated exceptional chemical and physical properties, due to their large number of surface sites, which facilitate surface reactions and electron/phonon confinement. These characteristics have favored the use of these materials in different solid-state devices, including gas sensors. Due to the increasing demand of more sensitive, selective and stable gas sensors, the optimization of SMOX as gas sensitive material is still largely studied, and previous studies have shown that incorporating two ot more SMOX to form a heterojunction interface can have possitive effects on gas sensor performance.[1] Here we synthetise an n-n heterojunction gas sensitive material based on WO_{3-x} NNs functionalized with Fe_2O_3 NPs, i.e., Fe_2O_3@WO_{3-x}, and analyze its gas sensing properties to various reducing gases.

2. MATERIAL AND METHODS

Fe_2O_3@WO_{3-x} were co-deposited at 390 °C *via* aerosol-assisted CVD of $W(CO)_6$ and $FeCl_3$•$6H_2O$ dissolved in methanol. Deposition were carried out on flexible-transducing platforms developed previously.[2] The morphology of the films was examined using SEM and HRTEM, whereas the film structure and the surface were examined using XRD and XPS. Gas sensors were tested towards the gaseous analytes using a continuous flow test chamber, and the sensor response (R) was defined as $R= R_a/R_g$, where R_a is the sensor resistance in air at stationary state and R_g represents the sensor resistance after 10 minutes of analyte exposure.

3. RESULTS AND DISCUSSION

SEM of the films showed uniform non-aligned NNs, and TEM of a single NNs displayed NPs at the surface of the NNs. HRTEM revealed crystalline structures, with the NPs displaying planar spacing of 2.81±0.15 Å, consistent with the internal lattice spacing of the cubic Fe_2O_3 (ICCD card no. 39-1346), and the NNs displaying planar spacing of 3.55±0.16 Å, consistent with a monoclinic phase of a tungsten oxide (ICCD card no. 72-0677), also identified *via* XRD (Figure 1).

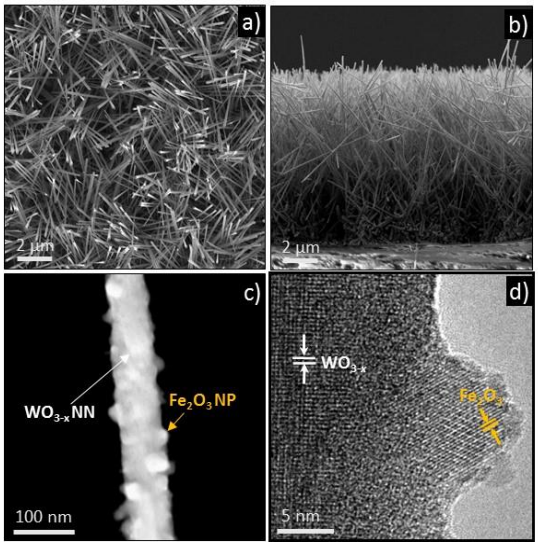

Figure 1.: Top (a) and cross-sectional (b) SEM, and TEM (c) and HRTEM (d) images of the Fe_2O_3@WO_{3-x} NNs

XPS exhibited typical W 4f and Fe 2p core-level peaks in the spectra, indicating the presence of Fe^{3+} species. Comparison of the valence-band (VB) recorded on the Fe_2O_3@WO_{3-x} structures and pristine WO_{3-x} or Fe_2O_3 (Figure 2) indicated the formation of a staggered type of heterojunction at the interface of the WO_{3-x} NNs and the Fe_2O_3 NPs, by considering the literature energy gaps for Fe_2O_3 (2.1 eV) and WO_{3-x} (2.6 eV). This spectra also suggested the formation of new electronic states above the VB maximum of the Fe_2O_3@WO_{3-x}, which could be increasing the density of electronic states near the Fermi energy level of this material.

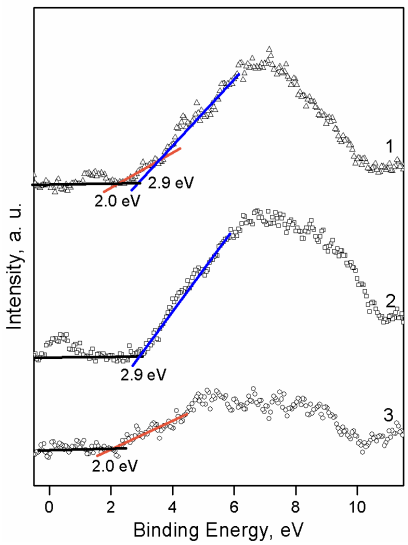

Figure 2.: XPS valence-band spectra of the Fe_2O_3@WO_{3-x} NNs(1), WO_{3-x} NNs (2) and Fe_2O_3 NPs (3)

Test to various concentrations of toluene, ethanol and hydrogen showed typical direct dependence of the response to analyte concentration, with noticeable higher and faster responses of the functionalized NNs compared to pristine NNs (Figure 3).

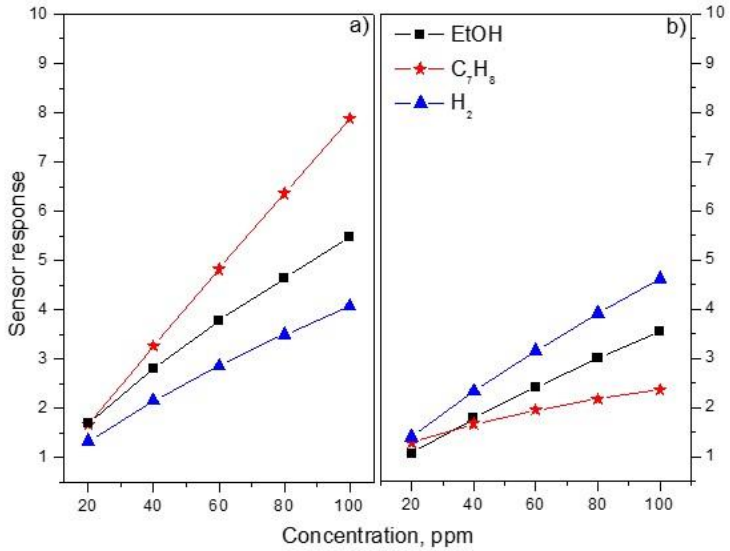

Figure 3.: Sensor response at 220 °C towards varios concentrations of toluene, hydrogen and ethanol

4. CONCLUSION

Gas sensitive structures based on WO_{3-x} NNs and Fe_2O_3 NPs were synthetised using a co-deposition method *via* AACVD. The gas sensing properties of these modified nanostructures demonstrated improved responses particularly to toluene, with up to six-fold increase in sensitivity, compared to structures based on only WO_{3-x} NNs. This improvement is attributed to the formation of n-n nanojunctions within the sensitive structure.

5. ACKNOWLEDGEMENT

This work has been supported, in part, by the SoMoPro II Programme, cofinanced by the European Union and the South-Moravian Region, via Grant 4SGA8678, and the Spanish Ministry of Science and Innovation via Grant TEC-2013-48147. Part of this research has used the infrastructures of the SIX Research Centre.

6. REFERENCES

[1] D. R. Miller, S. A. Akbar, P. A. Morris, Sens. Actuator, B, 204 (2014) 250-272.
[2] S. Vallejos, I. Gràcia, E. Figueras, J. Sánchez, R. Mas, O. Beldarrain, C. Cané, Sens. Actuators A, 219 (2014), 0, 88-93.

APOFERRITIN AS A NANOCARRIER FOR ACTIVE TARGETING OF DOXORUBICIN TOWARDS CANCER CELLS

Simona DOSTALOVA[1], Tereza CERNA[2,3], Marketa VACULOVICOVA[1], Zbynek HEGER[1], Tomas ECKSCHLAGER[2], Marie STIBOROVA[3], Vojtech ADAM[1,4*]

[1] *Department of Chemistry and Biochemistry, Faculty of Agronomy, Mendel University in Brno, Zemedelska 1, 613 00 Brno, Czech Republic*

[2] *Department of Pediatric Hematology and Oncology, 2nd Faculty of Medicine, Charles University in Prague and University Hospital Motol, V Uvalu 84/1, CZ-150 06 Prague 5, Czech Republic.*

[3] *Department of Biochemistry, Faculty of Science, Charles University in Prague, Hlavova 2030/8, CZ-128 43 Prague 2.*

[4] *Central European Institute of Technology, Brno University of Technology, Purkynova 123, 612 00 Brno, Czech Republic*

**vojtech.adam@mendelu.cz*

Abstract

A novel approach for targeting of apoferritin protein encapsulating doxorubicin (DOX) to prostate cancer cells using antibodies against prostate-specific membrane antigen (PSMA) is described in this work. The prostate cancer-targeted and non-targeted nanocarriers were tested using LNCaP and HUVEC cell lines. The effect on LNCaP cells was comparable for free DOX and DOX in non-targeted and prostate cancer-targeted apoferritin. With non-malignant cells, free DOX also showed high toxicity; however, the toxicity was lowered after treatment with APO-encapsulated DOX (APODOX) and even more in prostate cancer-targeted APODOX.

1. INTRODUCTION

Nanomedicine is a fast developing field that employs nanoscopic carriers for the targeted drug delivery to diseased tissue. It can be especially convenient in the treatment of heterogeneous diseases, such as cancer [1]. The encapsulation of drug molecules inside a suitable nanocarrier can offer multiple advantages compared with the administration of free drug. One of the advantages is the ability to dissolve otherwise water insoluble drugs [2]. The encapsulation can also increase biocompatibility of the drug and its shelf life, while also protecting the cargo from degradation prior to the diseased site [3]. The main advantage of nanomedical approach is the ability to lower the adverse side effects that conventional drugs often cause [1].

One of the principles that caused the boom of nanomedicine was the discovery of the Enhanced Permeability and Retention (EPR) effect. This effect leads to increased accumulation of nanoparticles in tumours which then causes the increase of drug concentration in tumour by up to 400%. It is caused by irregularly dilated angiogenic blood vessels with relatively large pores as well as the lack of lymphatic vessels in the tumour site.

Nanocarriers can be composed from a wide variety of organic and inorganic materials. Each material offers some advantages but also suffers from some drawbacks [4]. Currently, the structure with perfect properties is being sought for. Our approach uses the ubiquitous 480 kDa apoferritin (APO) protein, which forms a hollow icosahedral cage with internal diameter of 8 nm and external diameter of 12 nm. The huge advantage of this protein is its structural responsiveness to the surrounding environment [1, 4]. Its 24 subunits can be reversibly disassembled in low pH which enables the drug encapsulation while at neutral pH they are again reassembled, entrapping the drug molecules inside the apoferritin structure [4].

2. MATERIAL AND METHODS

The influence of nanocarrier on non-malignant and prostate cancer cell lines.

xCELLigence RTCA DP instrument (Roche Diagnostics GmbH, Basel, Switzerland) was used to evaluate the in vitro cytotoxicity of APODOX, APODOX-anti-PSMA and free DOX. The background impedance signal was measured using 100 µL cell culture media with cytostatics. Then $1.5 \cdot 10^4$ HUVEC or LNCaP cells were seeded in each well of 16-well plates (E-plates, Roche Diagnostics GmbH) followed by incubation at 37 °C with 5% CO_2. Final concentrations of APODOX, APODOX-anti-PSMA and DOX were 0.50 µM for HUVEC and 0.25 µM for LNCaP in 200 µL total volume in each well. Proliferation, spreading and cell attachment kinetics were monitored every 30 s for first 10 min, then every 30 min for 72 h. Experiments were performed in three independent repetitions.

3. RESULTS AND DISCUSSION

xCELLigence The proliferation, spreading and cell attachment kinetics of HUVEC and LNCaP cell lines after treatment with free DOX, APODOX and APODOX-anti-PSMA during 72 h was studied with real-time cell impedance analyzer xCELLigence. The obtained results proved similar sensitivity of LNCaP cancer cell line to all forms of DOX – free DOX, non-targeted APODOX and prostate cancer-targeted APODOX-anti-PSMA (Figure 1A.c). However, the toxicity of different forms of DOX to non-malignant HUVEC cells showed

significant differences (Figure 1B.c). Free DOX was highly toxic to non-malignant cells; however, the cells treated with non-targeted APODOX were spared from the DOX toxicity and even further spared using APODOX modified with anti-PSMA antibodies.

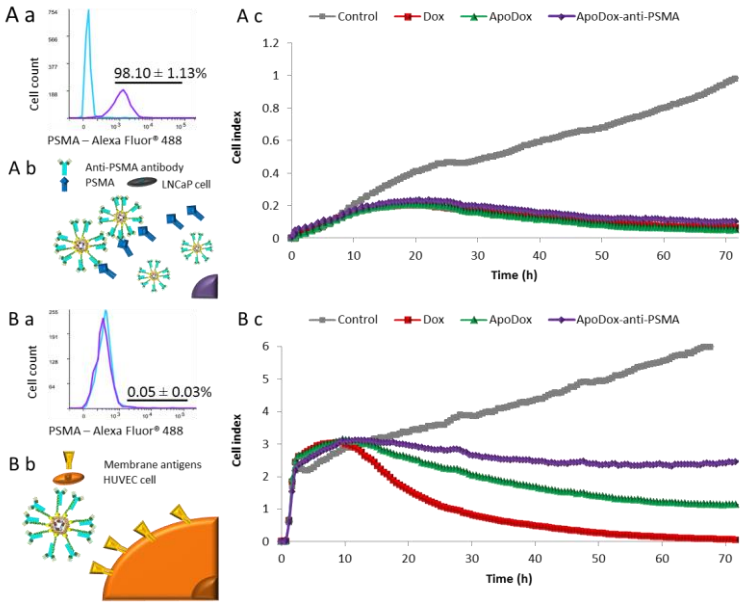

Figure 1.: The influence of prostate cancer-targeted and non-targeted nanocarriers on prostate cancer (LNCaP, A) and non-malignant (HUVEC, B) cell lines. a: The quantitative expression of PSMA in the membranes of used cells investigated by flow cytometry after incubation of cells with anti-PSMA-Alexa Fluor® 488 conjugate for 15 min at 20 °C in dark. Cyan line – unstained cells. Purple line – cells with antibody. b: The schematic depiction of interactions between nanocarrier and cell membranes. c: The proliferation, spreading and cell attachment kinetics of $1.5 \cdot 10^4$ of cells after treatment with 0.25 µM DOX, APODOX and APODOX-anti-PSMA revealed by real-time measurement using XCELLigence instrument.

4. CONCLUSION

In conclusion, apoferritin can serve as a suitable and universal nanocarrier for anticancer drugs. It provides easy encapsulation and modification protocol, it is naturally found in human body and it can encapsulate wide variety of drugs and target wide variety of cells. The encapsulated drug also retains its properties and is released in endosomes after the nanocarrier enters target cells.

5. ACKNOWLEDGEMENT

The work has been supported by the Grant Agency of the Czech Republic (NANOCHEMO GA CR 14-18344S) and IGA MENDELU IP_28/2016.

6. REFERENCES

[1] Blazkova, I., Nguyen, H. V., Dostalova, S., Kopel, P., et al., Int. J. Mol. Sci. 2013, 14, 13391-13402.
[2] Duncan, R., Gaspar, R., Mol. Pharm. 2011, 8, 2101-2141.
[3] Svenson, S., Curr. Opin. Solid State Mat. Sci. 2012, 16, 287-294.
[4] Tmejova, K., Hynek, D., Kopel, P., Dostalova, S., et al., Int. J. Electrochem. Sci. 2013, 8, 12658-12671.

ELECTROCHEMICAL IMPEDANCE SPECTROSCOPY BASED BIOSENSOR FOR RAPID DETECTION OF *SALMONELLA*

Zdeněk FARKA[1*], Tomáš JUŘÍK[1], Matěj PASTUCHA[1], Petr Skládal[1,2]

[1] *CEITEC MU, Masaryk University, Kamenice 5, 625 00 Brno, Czech Republic*

[2] *Department of Biochemistry, Faculty of Science, Masaryk University, Kotlářská 2, 611 37 Brno, Czech Republic*

**farka@mail.muni.cz*

Abstract

A label-free biosensor based on electrochemical impedance spectroscopy (EIS) was developed for the detection of *Salmonella* Typhimurium in milk. Specific antibody was immobilized on a screen-printed electrode, the electrode was incubated directly with the sample and binding of bacteria was measured as a change of impedance. Different procedures for sample treatment (combinations of heat and sonication) were tested and their impact on the assay performance was compared. Atomic force microscopy (AFM) was used to study the effect of the treatment on the cell shape and to confirm the specific binding of *Salmonella* to the sensing surface. The immunosensor allowed detection of 1×10^3 CFU·mL^{-1} in 20 min with negligible interference from other bacteria. A wide linear response was obtained in the range between 10^3 and 10^8 CFU·mL^{-1}.

1. INTRODUCTION

Rapid detection and identification of low levels of bacterial cells integrated into a portable device remains challenging for point-of-care clinical diagnosis, food testing and environmental screening. Conventional methods for the detection of bacteria comprise the cell culturing, ELISA and PCR. These approaches provide high sensitivity, but the analysis is rather slow (several hours), which is a major drawback in situations when spreading of the pathogen has to be prevented. Besides the traditional methods, biosensor technologies have been extensively developed as an alternative for rapid (in minutes) and sensitive detection. EIS represents an efficient method capable of detecting small changes occurring on the electrode-solution interface. The EIS based biosensors for the bacterial detection are generally based on the immobilization of antibodies on the electrode leading to a specific binding of the target cells. Thus, the label-free operation may be attained, which brings important benefits as simplicity and robustness.

2. MATERIAL AND METHODS

Microorganisms and antibodies

Salmonella Typhimurium (ATCC 14028) was aerobically cultivated overnight at 37 ºC, and the bacteria were resuspended in PBS. The samples were optionally heat-treated on Thermomixer Comfort or homogenized using sonicator Q700 (Qsonica, USA) [1]. Monoclonal anti-*Salmonella* antibody ab8274 specific against the lipopolysaccharides (LPS) of *S*. Typhimurium was obtained from Abcam (UK).

Preparation of biosensor

The electrochemical measurements were performed using a 2-channel gold screen-printed electrode (SPE). In the first step of immobilization, a self-assembled monolayer of cysteamine was formed followed by binding of glutaraldehyde. The sensor was then incubated with antibody overnight at 4 ºC. Blocking of free reactive groups was done by BSA [2].

Electrochemical immunoassay

The EIS measurements were carried out using PGSTAT302N (Autolab, Netherlands). For the binding of bacteria, the electrode was placed inside a microtube with sample and incubated for 15 min. The sensor was then thoroughly washed, placed inside the measuring solution (5 mM ferro/ferricyanide in 0.1 M KCl) and EIS spectra were acquired. The results were evaluated in Nova software (Autolab, Netherlands) using the Randles equivalent circuit. The attachment of bacteria to the electrode results in the increase of charge transfer resistance.

3. RESULTS AND DISCUSSION

The affinity of antibody to the bacteria significantly depends on the condition of antigenic determinants on the cell surface. After incubation of native cells with the sensor, only small change of impedance was observed, which indicates low binding affinity. After the treatment of microbe by heat, the affinity significantly increased. The EIS spectra for the detection of heat-treated cells are depicted in Figure 1A. AFM was used to confirm the presence of cells on the sensor surface (Figure 1B). The limit of detection (LOD) of 7×10^4 CFU·mL^{-1} and wide linear range up to 10^8 CFU·mL^{-1} was achieved. The heat-treatment does not pose a major technical complication for the potential analysis of real samples. Furthermore, the manipulation with killed or weakened bacteria can be even advantageous because of the reduced pathogenicity.

To further improve sensitivity, sonication of the heat-treated and native *Salmonella* was tested. In this case, the antibody has shown considerably higher affinity compared to the whole cells. The evaluated LOD was 1×10^3 CFU·mL^{-1}. Real samples of milk were spiked by bacteria and analyzed on electrodes blocked by milk. Thorough washing of sensors after incubation in real samples was crucial, insufficient washing resulted in gradual non-specific increases of impedance. The analysis in real samples was realized with the LOD of 9×10^3 CFU·mL^{-1} [3].

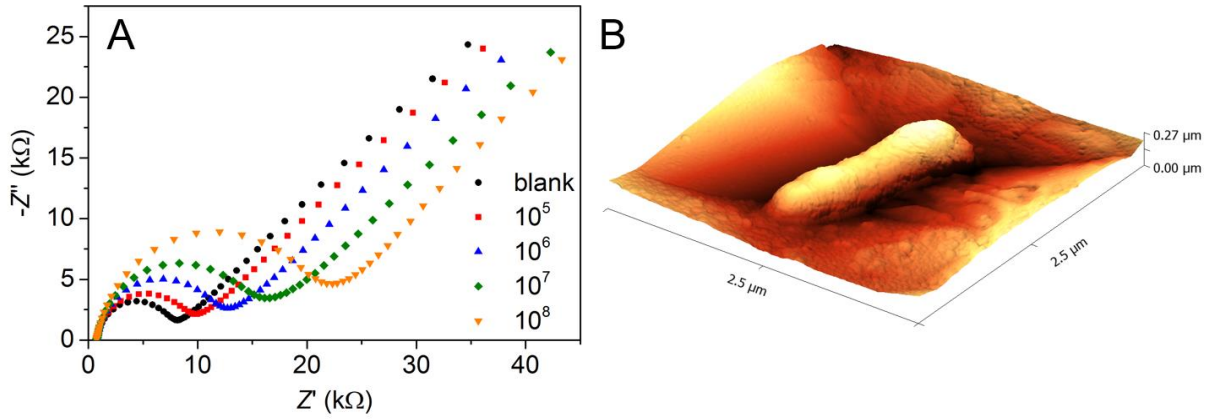

Figure 1.: A) EIS response of immunosensor to heat-treated *Salmonella* (concentrations in CFU·mL^{-1}). B) AFM image of sensor with specifically bound *Salmonella*.

4. CONCLUSION

Label-free immunosensor based on EIS was developed for the detection of *S.* Typhimurium. The specific antibody was immobilized to the SPE and the impedance was measured between two gold electrodes. Microbial cells were treated by heat and sonication and the effect of treatment was studied using AFM and EIS. The optimal results were achieved with the heat-treated and sonicated *Salmonella*, which provided LOD of 1×10^3 CFU·mL^{-1}. The analysis (including incubation of sensor with sample) was carried out within 20 min. The sensor demonstrated a great possibility of *Salmonella* detection in real samples.

5. ACKNOWLEDGEMENT

This research has been financially supported by the Ministry of Education, Youth and Sports of the Czech Republic under the project CEITEC 2020 (LQ1601).

6. REFERENCES

[1] Farka Z, Kovář D, Skládal P: Sensors, 15 (2015), 1, 79-92.
[2] Farka Z, Kovář D, Přibyl J, Skládal P: Int. J. Electrochem. Sci., 8 (2013), 1, 100-112.
[3] Farka Z, Juřík T, Pastucha M, Kovář D, Lacina K, Skládal P: Electroanalysis, 2016, accepted manuscript.

STUDY OF SURFACE EFFECTS OF SELECTED BIMETALLIC NANOPARTICLES

Martina HEJDUKOVÁ[1], Pavel BROŽ[1,2*], Ondřej ZOBAČ[1], Vít VYKOUKAL[1]

[1] *Department of Chemistry, Faculty of Science, Masaryk University, Kotlářská 2, 611 37 Brno, Czech Republic*

[2] *Central European Institute of Technology, CEITEC, Masaryk University, Kamenice 753/5, 625 00 Brno, Czech Republic*

**broz@chemi.muni.cz*

Abstract

AgCu and AgNi bimetallic nanoparticles (NPs) were synthesized by solvothermal synthesis in nature of oleylamine (OAm), which works as a slightly reducing agent and as a capping agent [1]. Thermal stability and catalytic properties of these systems were investigated by Knudsen effusion mass spectrometry (KEMS). Results are summarized and discussed in a view of previous study [2].

1. INTRODUCTION

Bimetallic nanoparticles (NPs) are currently the subject of intensive investigation and research. These NPs generally exhibit different physicochemical behavior from the bulk material [2]. Due to their unique physical, electronic and thermodynamic properties they are considered as potential candidates for applications across a diverse range of fields, including catalysis. AgCu and AgNi nanoparticle systems which were selected for the study have catalytic properties and moreover, AgCu may be a good candidate as a catalyst for oxygen reduction reaction (ORR) [3,4]. It is one of the systems which could replace platinum catalyst in fuel cells. Both systems are weakly miscible systems and form core-shell structure in which the core is made of the more cohesive element and the shell of the less cohesive one [3]. In this case silver is less cohesive than copper or nickel [3]. Properties of these NPs are, therefore, strongly influenced by their structure.

2. MATERIAL AND METHODS

AgCu NPs were synthesized in non-aqueous environment of OAm from silver malonate and copper (II) acetylacetonate. AgNi NPs were synthesized in non-aqueous environment of OAm from silver nitrate and nickel (II) acetylacetonate. Both the systems were investigated by KEMS on a Netzsch STA 409 CD/3/403/5/ G apparatus, a specially-adapted type of the

commercial STA 409 CD-QMS403/5 Skimmer Coupling Instrument [5]. Mass spectra were obtained during slow heating from 30 °C to 1000 °C with the heating rate 5 °C · min^{-1}.

3. RESULTS AND DISCUSSION

OAm works as capping agent which protects NPs against coagulation. As can be seen from Figures 1 and 2, both systems work as a catalyst. A fast and quantitative evaporation of the organic protection layer taking place at elevated temperatures during a slow heating is accompanied by its oxidation which is visible from evolution of carbon dioxide at 44 amu in the mass spectra. The quantitative evaporation of the organic substance from the AgCu NPs was already found before [2].

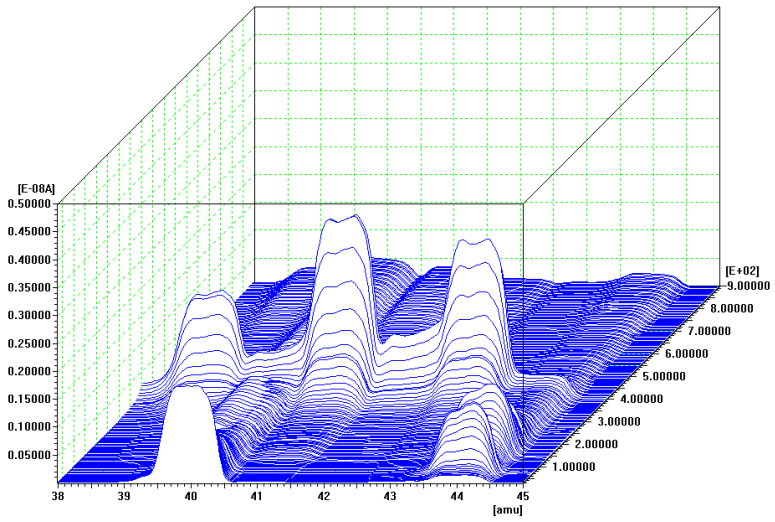

Figure1.: Selected part of mass spectral data of AgCu NPs capped by OAm

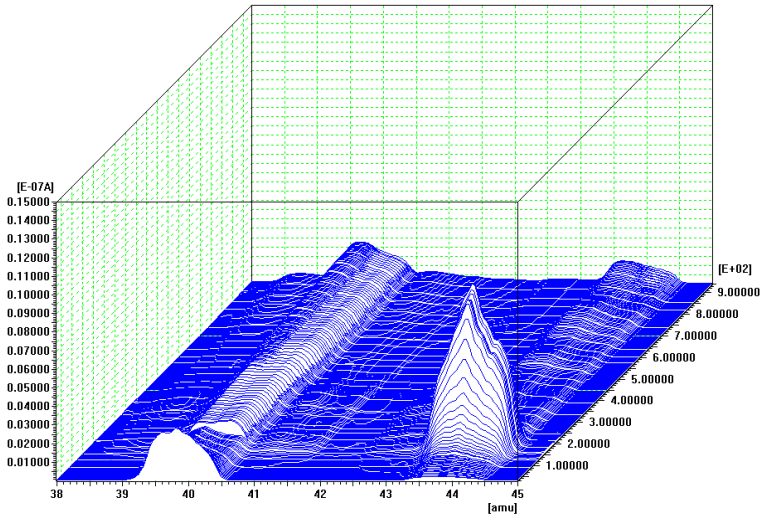

Figure 2.: Selected part of mass spectral data of AgNi NPs capped by OAm

4. CONCLUSION

Study of thermal stability and surface effects on AgCu NPs capped by OAm shows the stability of this system to be up to 250 °C. Similarly, study of AgNi NPs capped by OAm shows the stability of this system to be up to 290 °C. At these temperatures a quantitative removal of the OAm was observed, accompanied by simultaneous oxidation of OAm which follows from carbon dioxide production detectable as a strong signal at 44 m/z in the mass spectra. The AgNi NPs system has stronger catalytic behavior than the AgCu NPs system.

5. ACKNOWLEDGEMENT

This work has been supported by the project CEITEC 2020 (LQ1601) from the Ministry of Education, Youth and Sports of the Czech Republic under the National Sustainability Programme II as well as by the Grant Agency of the Czech Republic under the project GA 14-12653S.

6. REFERENCES

[1] Mourdikoudis S., Liz-Marzán L. M.: *Chemistry of Materials*, 25 (2013), 9, 1465-1476.
[2] Sopoušek J., Pinkas J., Brož P., et all.: *Journal of Nanomaterials*, (2014), Article Number: 638964, 1-13.
[3] Laasonen K., Panizon E., Bochicchio D., et all.: *The Journal of Physical Chemistry C*, 117 (2013), 49, 26405-26413.
[4] Bochicchio D, Ferrando R.: *Physical Review B*, 87 (2013), 165435-1 - 165435-1.
[5] Brož P., Sopoušek J., Vřešťál J., et all.: *ECS Transactions*, 46 (2013), 1, 69-76.

SYNTHESIS OF COPPER COMPLEXES AND THEIR ANTIMICROBIAL ACTIVITY

Pavlína JELÍNKOVÁ[1], Rafal KRUSZYNSKI[2], Vojtěch ADAM[1,3*]

[1] *Department of Chemistry and Biochemistry, Faculty of Agronomy, Mendel University in Brno, Zemedelska 1, 613 00 Brno, Czech Republic*

[2] *Department of X-ray Crystallography and Crystal Chemistry, Institute of General and Ecological Chemistry, Lodz University of Technology, Zeromskiego 116, 90-924, Lodz, Poland*

[3] *Central European Institute of Technology, Brno University of Technology, Technicka 3058/10, 616 00 Brno, Czech Republic*

** vojtech.adam@mendelu.cz*

Abstract

Copper complexes with potential antimicrobial activity have been prepared and characterised using single crystal X-ray analysis. The complexes are binuclear with thiodipropionate or hydroxo bridges, respectively. The copper atoms are coordinated by chelate amines. The main aim of this study was to test the antimicrobial activity of the prepared complexes. The antibacterial activities of copper complexes (0; 10; 20; 41; 83; 166; 333 μM) were tested against one Gram-positive - *Staphylococcus aureus*; one Gram-negative - *Escherichia coli*; and one resistant strain of bacteria - MRSA (*Methicillin-Resistant Staphylococcus aureus*). It has been found that the copper complexes showed increased antimicrobial effect on *S. aureus*, *E. coli and MRSA.*

1. INTRODUCTION

Infectious diseases are included amongst one of the greatest health problems worldwide. To the major bacterial pathogens causing infection belong *E. coli* and *S. aureus*. [1] Due to the rapidly spreading bacterial resistance to antibiotics, the various alternative antimicrobial materials are implemented for testing. [2] Methicillin-resistant Staphylococcus aureus (MRSA) is a dangerous pathogen resistant to ß-lactam antibiotics. Due to its resistance, it is difficult to manage the infections caused by this strain. [3] Due to the outbreak of infectious diseases, researchers are searching for new antibacterial agents. Therefore, new antimicrobial agents and materials have to be synthesized for the treatment of resistant bacterial diseases. There is a real perceived need for the discovery of new compounds endowed with antimicrobial activities. The newly prepared compounds should be more effective and

possibly act through a distinct mechanism from those of well-known classes of antimicrobial agents to which many clinically relevant pathogens are now resistant. [4]

2. MATERIAL AND METHODS

2.1. Preparation of the compounds

2.1.1. $[Cu_2(pmdien)_2(H_2O)_2(\mu\text{-}tdp)](ClO_4)_2 \cdot (H_2O)$ (1)

Pmdien (0.42 cm^3, 2 mmol) was added to a solution of $Cu(ClO_4)_2.6H_2O$ (0.74 g, 2 mmol) in methanol (50 cm^3). Consecutively, a solution of 3,3´-thiodipropionic acid $tdpH_2$ (0.18 g, 1 mmol) in water (10 cm^3) neutralised with KOH (0.11 g, 2 mmol) was slowly added. White precipitate was removed by filtration and blue-violet solution was left for crystallization. The deep blue crystals obtained after a week were collected on a frit, washed with water and dried in air. Yield: 54%.

2.1.2. $[Cu_2(tmen)_2(H_2O)_2(\mu\text{-}OH)_2](ClO_4)_2$ (2)

N,N,N',N'-tetramethylethane-1,2-diamine (tmen) (0.6 cm^3, 2 mmol) was added to a solution of $Cu(ClO_4)_2.6H_2O$ (0.74 g, 2 mmol) in methanol (50 cm^3). Consecutively, a solution of 2,2´-thiodiacetic acid $tdaH_2$ (0.15 g, 1 mmol) in water (10 cm^3) neutralised with KOH (0.11 g, 2 mmol) was slowly added. White precipitate was removed by filtration and blue solution was left for crystallization. The deep blue crystals obtained after a week were collected on a frit, washed with water and dried in air. Yield: 68%.

2.2. Cultivation of bacteria strains

Staphylococcus aureus (NCTC 8511), *Escherichia coli* (NCTC 13216) and MRSA (ST239) were obtained from the Czech Collection of Microorganisms, Faculty of Science, Masaryk University (Brno, Czech Republic). Cultivation media (Luria Bertani) were inoculated with bacterial culture and were cultivated for 24 h on a shaker at 600 rpm and 37 °C.

2.3. Testing of antimicrobial activity

Bacterial culture was diluted by cultivation medium to OD600 = 0.1 for the following experiments. The concentrations of copper complexes were 0, 10; 20; 41; 83; 166 and 333 μM. The total volume in the microplate wells was always 300 μL. The measurements were carried out at time 0, then each half-hour for 24 h at 37 °C and a wavelength of 600 nm. Evaluation of the antimicrobial effect of the tested compounds was performed by

measurement of the absorbance using the apparatus Multiskan EX (Thermo Fisher Scientific, Bremen, Germany) and subsequent analysis in the form of growth curves.

2.4. Statistical analyses

The software STATISTICA (data analysis software system), version 10.0 (Statsoft Inc. ed., Tulsa, OK, USA) was used for the data processing. The half-maximal concentrations (IC_{50}) were calculated from logarithmic regression of sigmoidal dose-response curve. The general regression model was used to analyse differences between the combinations of the compounds.

3. RESULTS AND DISCUSSION

A perspective view of compound **1** and **2** molecular structures are shown in Figure 1 and 2, respectively. In both compounds all atoms occupy the general positions. One asymmetric unit of compound **1** contains one dinuclear complex cation, two perchlorate anions and one outer coordination sphere water molecule. The complex cation of **1** is composed from one bridging difunctional thiodipropionate anion (each carboxylate group acts in monodendate mode), two copper cations, two water molecules and two N,N,N´,N´´,N´´-pentamethyldiethylenetriamine molecules. The each metal cation is five coordinated by one water molecule, one trifunctional pentamethyldiethylenetriamine and one monodendate carboxylate group of thiodipropionate anion. The complex cation of **2** consists of two bridging hydroxide anions, two copper cations, two water molecules and two N,N,N',N'-tetramethylethane-1,2-diamine molecules. The each copper ion is five coordinated by one water molecule, one difunctional tetramethylethanediamine and hydroxide anions (acting as monodendate ones toward one specific copper cation).

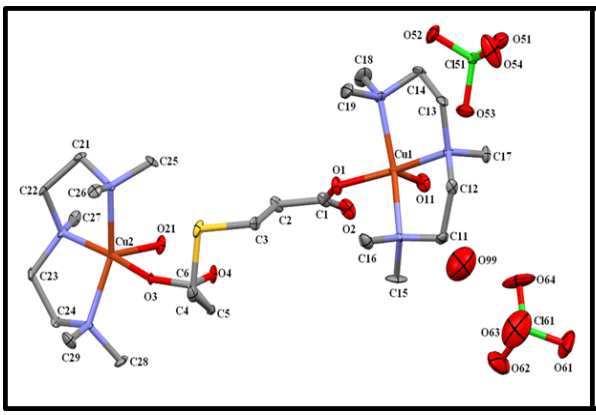

Figure 1.: Molecular structure of the complex **1**

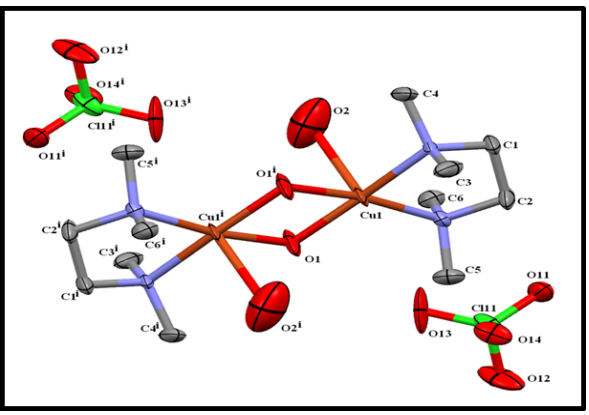

Figure 2.: Molecular structure of the complex **2**

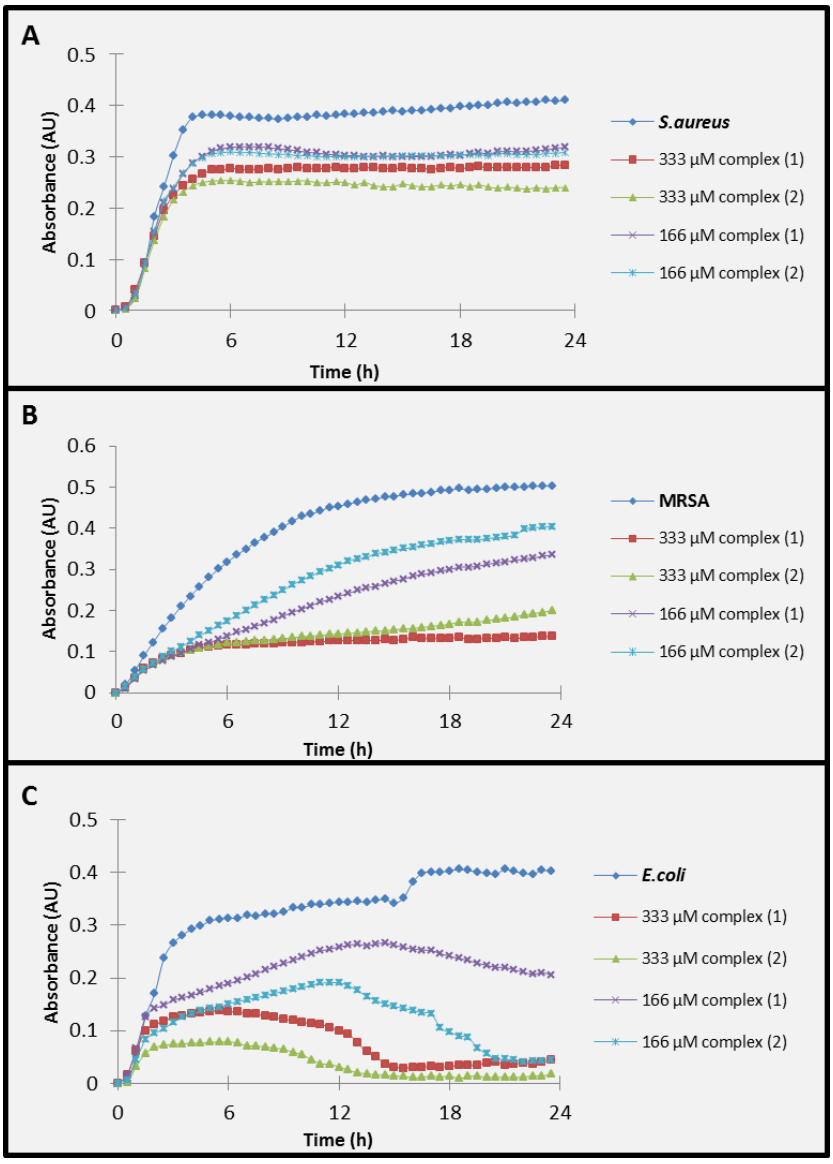

Figure 3.: Testing of antimicrobial activity of 166 µM and 333 µM concentration of complexes after 24 h of treatment on: (**A**) *S. aureus*; (**B**) MRSA; (**C**) *E. coli*

For testing the antimicrobial activity of the copper complex were selected three types of commercial bacteria, namely: *S. aureus*, *E. coli*, *MRSA*. Copper complexes were applied in contrentrations of 0, 10; 20; 41; 83; 166, 333 µM. The effect was subsequently evaluated using growth curve compared with measurements of the samples of bacteria without complex. Both copper complexes have shown inhibitory effect on all bacterial strains in this study. The inhibition of bacterial growth was achieved at a 166 µM concentration of complex.

Table 1.: Statistical calculation of IC_{50} by the STATISTICA software version 10.0 from absorbance values after the application of 0; 10; 20; 41; 83; 166 and 333 μM concentrations of tested compounds.

	IC_{50} (μM) Measurement after 24 h		
Compounds	*S. aureus*	MRSA	*E. coli*
Complex **1**	199.9	165.7	176.2
Complex **2**	209.9	213.0	25.4

The increasing concentrations (0; 10; 20; 41; 83; 166; 333 μM) of complexes were used to observe antimicrobial effect of each tested compounds for the statistical analysis of the viability of bacterial cells. The IC_{50} values were calculated from the absorbance measurements after the application of the concentration range in 24 h of measurements (Table 1). By these values, the previous results of antimicrobial activity were confirmed.

4. CONCLUSION

In this study, we presented our results for copper complexes and their effect on bacterial strains, such as antimicrobial substances. We have synthesized two types of copper compounds. Both tested copper complexes showed inhibitory effect on three selected bacterial strains (*S. aureus; E. coli; MRSA).*

5. ACKNOWLEDGEMENT

The work has been supported by the project CEITEC CZ.1.05/1.1.00/02.0068.

6. REFERENCES

[1] B. Heydari, H. Khalili, I. Karimzadeh and H. Emadi-Kochak, Iranian Journal of Pharmaceutical Research, 15 (2016) 347.
[2] C.-W. Cho, J.-S. Park, S. Stolte and Y.-S. Yun, Journal of hazardous materials, 311 (2016) 168.
[3] K. Cihalova, D. Chudobova, P. Michalek, A. Moulick, R. Guran, P. Kopel, V. Adam and R. Kizek, International Journal of Molecular Sciences, 16 (2015) 24656.
[4] M. Rizzotto, Metal complexes as antimicrobial agents, INTECH Open Access Publisher, 2012.

ELECTROCHEMICAL PROPERTIES OF CONFORMATIONAL DERIVATIVES OF (N-FERROCENYLIMINOMETHYL)PHENYLBORONIC ACID

Martin KONHEFR[1*], Karel LACINA[2], Monika LANGMAJEROVÁ[1], Petr SKLÁDAL[1,2], Ctibor MAZAL[3]

[1] *Department of Biochemistry, Faculty of Science, Masaryk University, Kamenice 5, 625 00 Brno, Czech Republic*

[2] *Central European Institute of Technology, Masaryk University, Kamenice 5, 625 00 Brno, Czech Republic*

[3] *Department of Chemistry, Faculty of Science, Masaryk University, Kamenice 5, 625 00 Brno, Czech Republic*

**379848@mail.muni.cz*

Abstract

An electrochemically active synthetic receptor for saccharides consists of two connected parts – boronic acid is able to directly interact with an analyte, a diol-containing compound and a ferrocenyl residue provides electrochemical response on this binding event [1,2]. These two parts joined together represent the probe - a receptor for the detection of saccharides. Throughout our way towards the saccharide-sensitive receptor, we synthesized three new derivatives (N-ferrocenyliminomethyl)phenylboronic acids (FcPBAi). These were characterized by nuclear magnetic resonance, mass spectrometry, infrared spectroscopy and their electrochemical properties were studied by cyclic voltammetry. The results show some different behavior of the iminic *ortho* derivative due to intramolecular interactions of boronate functional group and iminic nitrogen atom.

FcPBAi derivatives (Figure 1) were synthesized from equimolar amount of aminoferrocene and related formylphenylboronic acid (*ortho*-, *meta*- or *para*-) in solution of toluene:ethanol (9:1) using azeotropic dehydration on rotational vacuum evaporator up to 40°C. These conditions enabled quantitative progress of the reaction.

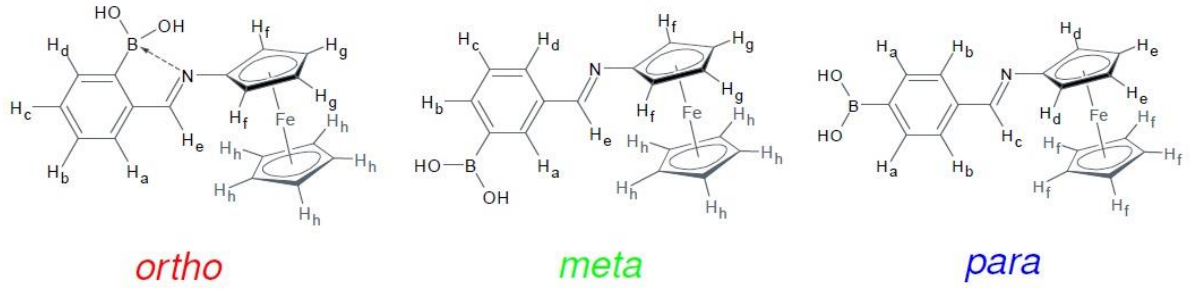

Figure 1.: Three new conformational FcPBA derivatives joining together ferrocenyl and boronic acid residues

Due to the instability of FcPBA imines in the presence of nucleophiles (e.g. water, physiologic solution), interaction between boronic acid and saccharide could not probed. As the main aim was the comparison of behavior of all imines, we studied their fundamental behavior and their electrochemical properties.

NMR results show structural differences in *ortho* imine in contrast to *meta* and *para* derivatives. The free electron pair of nitrogen atom interacts with free p-orbital of boron atom in structurally near boronic acid functional group. Thus the different behavior of *ortho* imine was observed also in all electrochemical measurements.

Ortho imine exhibited poor stability at pH around 7 in aqueous solution, it partly decomposed immediately back to the reactants (an equilibria was set up) as studied by cyclic voltammetry. According to computations conducted by Cal et. al., this could be caused by proximity of boronic group near imine group leading to the facilitated attack of imine bond by one hydroxyl from near boronic acid group [3]. The speed of decomposition of *meta* and *para* imines was substantially lower although increasing of pH (to around 10), where should imines decompose rapidly by hydroxide attack on C=N bond.

Acknowledgement

This research has been financially supported by the Ministry of Education, Youth and Sports of the Czech Republic under the project CEITEC 2020 (LQ1601).

References

[1] Wang, B.; Takahashi, S.; Du, X.; Anzai, J.; Biosensors, 2014, 4, 243–256.
[2] Norrild, J. C.; Søtofte, I.; J. Chem. Soc., Perkin Trans. 2, 2001, 727–732.
[3] Cal, P. M. S. D.; Vicente, J. B.; Pires, E.; Coelho, A. V.; Veiros, L. F.; Cordeiro, C.; Gois, P. M. P.; J. Am. Chem. Soc., 2012, 134, 10299–10305.

ELECTROSPINNING OF POLY(VINYL) ALCOHOL AND HYALURONIC ACID

Adéla KOTZIANOVÁ[1,2,*], Marek POKORNÝ[1], Jan HRBÁČ[2]

[1] *Contipro a.s., R&D Department, CZ-56102 Dolni Dobrouc, Czech Republic*

[2] *Masaryk University, Faculty of Science, Department of Chemistry, Kamenice 5, CZ-62500 Brno, Czech Republic*

**kotzianova@sci.muni.cz*

Abstract

Poly(vinyl) alcohol is a hydrophilic semi-crystalline polymer soluble in water that exhibits great chemical and thermal stability. This polymer is biodegradable, biocompatible and non-toxic. Due to these properties as well as the ease of its processing, it is widely used in many fields – from papermaking to the production of cosmetics, where it is used as a binding agent, emulsifier and a thickening agent. PVA is available in a variety of degrees of hydrolysis (DH) and molecular weights because it is derived from the hydrolysis (or alcoholysis) of poly(vinylacetate). Its properties are therefore dependent on the degree of hydrolysis. Hyaluronic acid (HA) is a naturally occurring polysaccharide commonly found in the connective tissues of higher animals. HA is a linear polymer belonging to the glycosaminoglycan family. HA solutions have a relatively high conductivity, which increases in direct proportion to their concentration. HA solutions also have a high viscosity and surface tension, even at relatively low concentrations. Like PVA, HA is currently widely used in cosmetics and also in the pharmaceutical industry.

The aim of this work is to use the electrostatic spinning method to produce nanofibrous materials containing exclusively PVA and HA. The influence of polymer tye and solution characteristics on the preparation of nanofibrous materials will be discussed.

1. INTRODUCTION

The field of nanotechnology has undergone unprecedented development in the recent decades. Nanofibres and nanofibrous structures are still in the focus of attention. Due to a huge surface-area-to-volume ratio, nanofibres have a potential to significantly improve existing technologies and are continuously finding use in new areas. One of the most important fields of use for nanofibrous materials comprises biomedical applications. Out of all nanofibrous patents, biomedicine accounts for 2/3 of nanofibrous product applications [1]. A greater

degree of biocompatibility in biomedical applications is ensured by using natural biopolymers instead of synthetic polymers. The disadvantages of nanofibrous materials produced from natural polymers are their inadequate mechanical properties and short degradation time. A natural biopolymer is usually more difficult to convert into nanofibres by electrostatic spinning than a synthetic polymer.

One of the natural polymers most commonly used in biomedical applications is hyaluronic acid (HA) [2]. Its unique rheological properties and biocompatibility make HA suitable for biomedical applications in numerous areas including ophthalmology, dermatology, surgery, drug distribution, medical implants and wound healing [3, 4].

This paper aims to describe the unique process of fabrication of nanofibrous materials from HA mixed with PVA in a single solution system from the water and thus without the use of any organic solvents. A material prepared in this way could find use above all in the areas of biomedicine and cosmetics.

2. MATERIAL AND METHODS

Materials

Hyaluronic acid (HyActive 220514-E1, 82 kDA) was produced in the Contipro a.s. company (Czech Republic). Poly(vinyl) alcohole (PVA) with different degree of hydrolysis and various molecular weight was purchased from Sigma-Aldrich (St. Louis, USA) and SCIENTIFIC POLYMER PRODUCTS, INC. (Ontario, USA). The HA/PVA nanofibrous layers were prepared using a blend of HA and PVA dissolved in distilled water with different wt.% of polymers.

Methods

The commercially available laboratory device 4SPIN® LAB1 (Pokorny, Novak, Rebicek, Klemes & Velebny, 2015) by Contipro a.s. (Dolni Dobrouč, Czech Republic) was used to prepare the samples.

3. RESULTS AND DISCUSSION

We measured solution properties to find out the best solution for the electrospinning of HA and PVA blend. We also tested three different PVA (different Mw and degree of hydrolysis) to determine best polymer type. From our measurement it is obvious that the higher the degree of hydrolysis is, the higher concentration of PVA has to be used for electrospinning. Using higher molecular weight and partially hydrolyse PVA enables to use lower concentrations. These facts are depicted on the right figure. Moreover, higher Mw of PVA supports HA spinning. Molecular weight is related to the viscosity of solution. If viscosity is too low, the surface tension is dominant factor and beads are formed. On the other hand, if viscosity is too high, it is hard to eject jet from solution (Figure 1).

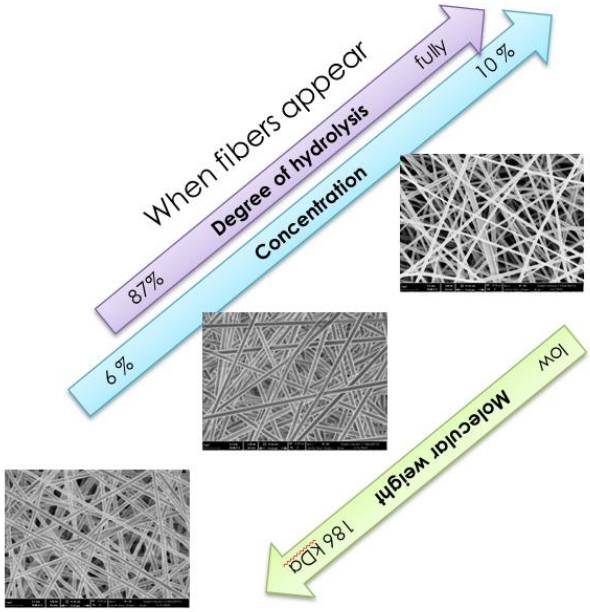

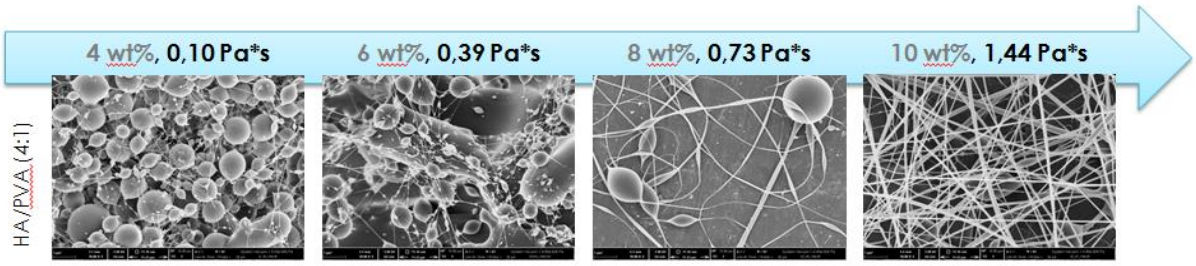

Figure 1.: Relation between viscosity, weight concentration and spinnability.

4. CONCLUSION

We prepared nanofibers made of hyaluronic acid and a synthetic polymer suitable for cosmetic purposes using as high HA content as possible. We estimated best parameters of solutions for spinning – viscosity, surface tension – as well as best PVA type.

5. ACKNOWLEDGEMENT

This research project was conducted under financial support provided by the Ministry of Industry and Trade of the Czech Republic (FR-TI2/246).

6. REFERENCES

[1] Bhardwaj, N. & Kundu, S. C.: Biotechnoogy. Advances, 28 (2010), 325-347.
[2] Collins, M. N.; Birkinshaw C.: Carbohydrate Polymers, 92 (2013), 1262-1279.
[3] Kogan, G.; Šoltés, L.; Stern, R.; Gemeiner, P.: Biotechnology Letter, 29 (2007), 17-25.
[4] Zahedi, P.; Rezaeian, I.; Ranaei-Siadat, S. O.; Jafari, S. H.; Supaphol, P.: Polymers for Advance Technology, 21 (2010), 77-95.

STATISTICAL PROCESSING OF EXPERIMENTAL DATA FROM TESTING FULLY AUTOMATED ELECTROCHEMICAL APPARATUS FOR APLICATION IN EXTREME CONDITIONS

Zuzana KOUDELKOVA[1], Jan ZITKA[1], Michal PLATENIK[1], Lukas RICHTERA[1,2], Rene KIZEK, Vojtech ADAM*[1,2]

[1] *Department of Chemistry and Biochemistry, Faculty of Agronomy, Mendel University in Brno, Zemedelska 1, 613 00 Brno, Czech Republic*

[2] *Central European Institute of Technology, Brno University of Technology, Purkynova 123, 612 00 Brno, Czech Republic*

**vojtech.adam@mendelu.cz*

Abstract

For routine analysis of environmental samples (e.g. contaminated water or soil) in badly accessible areas, and locations it is not only advantageous to have the option of automatic sample collection (which is sometimes impractical), but also the possibility of carrying out the basic analysis in real time, on real place and in massive scale of hundreds or even of thousands of analyses in one single action. Even to obtain samples from inaccessible places such as highly contaminated or dangerous areas (for example radiation contamination or toxic waste contamination) or from volcanic craters. The aim of our study was to design and test fully automated compact and portable electrochemical apparatus which would be able to quickly measure required analyte, e.g. heavy metal, concentrations of in little or inaccessible areas. Small, compact, easy to repair and to manufacture and inexpensive apparatus was designed, which is fully able to collect, store and evaluate data automatically. This device was tested under various unfavourable conditions, to determine its resistance and stability. The obtained data were statistically processed.

1. INTRODUCTION

Nowadays, the main objective is to introduce rapid, sensitive and cheap techniques for the detection of different multiple substances. Remote analysis *in situ* will be much more desirable due to the development of technology in the future. One of the objectives of scientists is to get these devices to be fully automated and thus remove human factor [1-3]. Such devices also enable the collection and detection of samples in difficult to reach areas. The advantage of electrochemical methods is their high sensitivity, selectivity, possibility of

miniaturization [4]. Thanks to electrochemical methods can detect most metals, metalloid and biomolecules (especially nucleic acids and proteins) [1-3,5,6]. It is important that our proposed device is arranged as multifunctional and allow users to change easily the setting of measurement method and types of used electrodes.

2. MATERIAL AND METHODS

2.1. Chemicals and material

All chemicals used in this study were purchased from Sigma Aldrich (St. Louis, USA) in ACS purity unless noted otherwise. Pipetting was performed by pipettes from Eppendorf (Hamburg, Germany). Stock solutions were prepared with ACS water.

2.2. Fabrication of the automatic electrochemical apparatus

The electrochemical cell was made of resin. The size of the measuring cell is 2.0 × 1.2 × 2.5 cm. The electrochemical cell has three gaps enabling the classic three-electrode wiring. As an auxiliary electrode the platinum electrode was used, Ag/AgCl/3M KCl reference electrode (both CH Instruments, Austin, USA) and the working electrode was amalgam electrode. The actual cell was inserted in a special insulated plastic housing (6.0 × 12.0 × 13.5 cm). This part was printed using 3D printer, profi 3D maker (Aroja, Czech Republic). Measurement was performed using a transferable potentiostat 910 PSTAT mini (Metrohm, Switzerland). Potentiostat is connected to minicomputer and it is energized by batteries, GENS ACE Li-Po battery (5000 mAh, 18.5 V, Acepow Electronics, China). Minicomputer is serviced by our created scripts. For the electrochemical measurements, the script was created to control the correct run of PSTAT software 1.0 (Metrohm, Switzerland). During the planned duration of the experiment, hundred voltamograms are measured and saved. For their evaluation after the measurement, other scripts were created that are used for the fully automated. This script also ensures data transcription into spreadsheet templates which are subsequently used for the final statistical data processing and data send via internet to another computer.

2.3. Electrochemical determination of cadmium using amalgam electrode

For measuring were selected ten methods of cyclic voltammetry with these parameters. Initial potential was −1.2 V end potential −0.3 V, step was 3 mV and potential of deposition −1 V. In case of methods 0 – 5 were deposition time 15 seconds, their scanrates were 0.05 V/s, 0.1 V/s,

0.2 V/s, 0.3 V/s, 0.4 V/s and 0.5 V/s. It was done about fifty measurements in one run. Scanrate of methods 6 – 9 was 0.2 V/s, their deposition time were 0, 7.5, 22.5 and 30 seconds.

2.4. Fabrication of the working amalgam electrode

For amalgam modification, copper wire (Thermo scientific, UK) was used. The copper wire was immersed into 0.01M $Hg(NO_3)_2$ solution for 10 minutes. This solution was prepared by dissolving of 0.086 g mercury(II) nitrate in 25 mL of acidified (5% HNO_3, v/v) ACS water.

3. RESULTS AND DISCUSSION

We evaluated the peak height of cadmium and its potential under different temperatures (0 °C, 5 °C, 10 °C, 15 °C, 20 °C and 25 °C) and in time (0 – 250 minutes), in order to investigate the stability of the entire system. Acetate buffer (0.2M CH_3COONa + 0.2M CH_3COOH, pH 5) was used as a supporting electrolyte. Different working electrodes were used, silver electrode, carbon electrode, amalgam electrode and copper electrode were tested. As reference electrode Ag/AgCl/3M KCl electrode and carbon electrode was tested. All electrodes were stable in our device throughout the experiment. It followed that the user can choose any type of electrode and any type of buffer according to the type of sample. Our proposed cell is resistant to effects of different electrolytes and can be used repeatedly, for example for fluid arrangement.

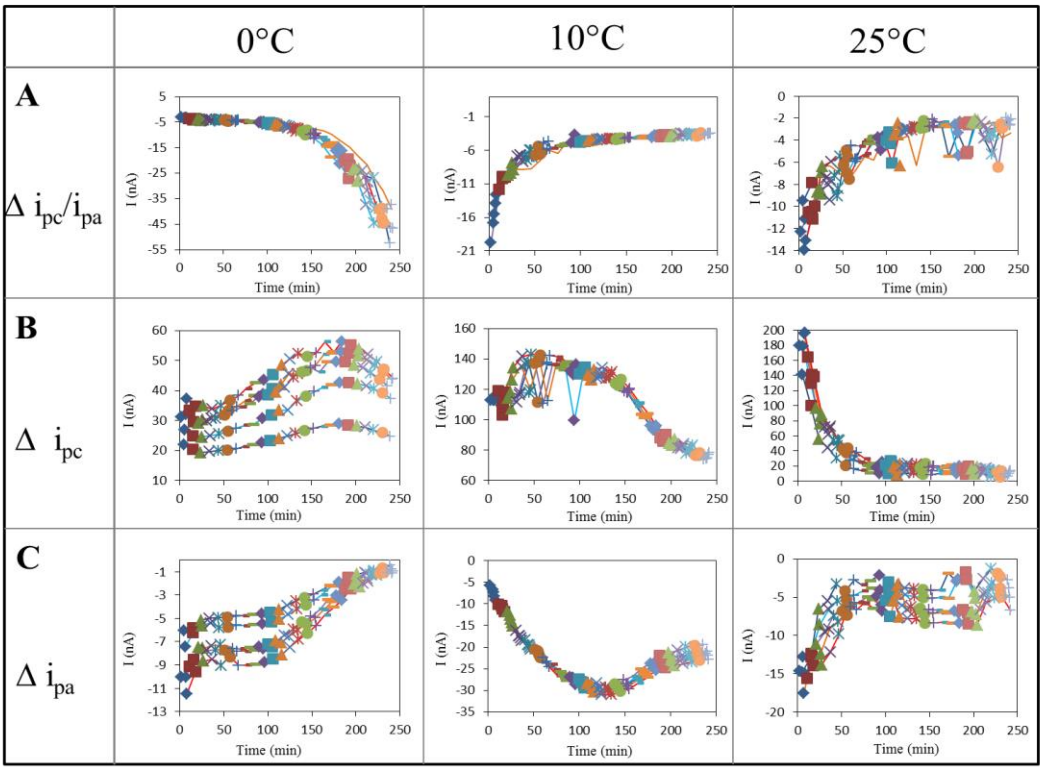

Figure 1.: Measurement using cyclic voltammetry under different temperatures (0 °C, 10 °C and 25 °C): (A) change the aspect ip_c / ip_a in time, (B) ip_c change in time, (C) ip_a change in time.

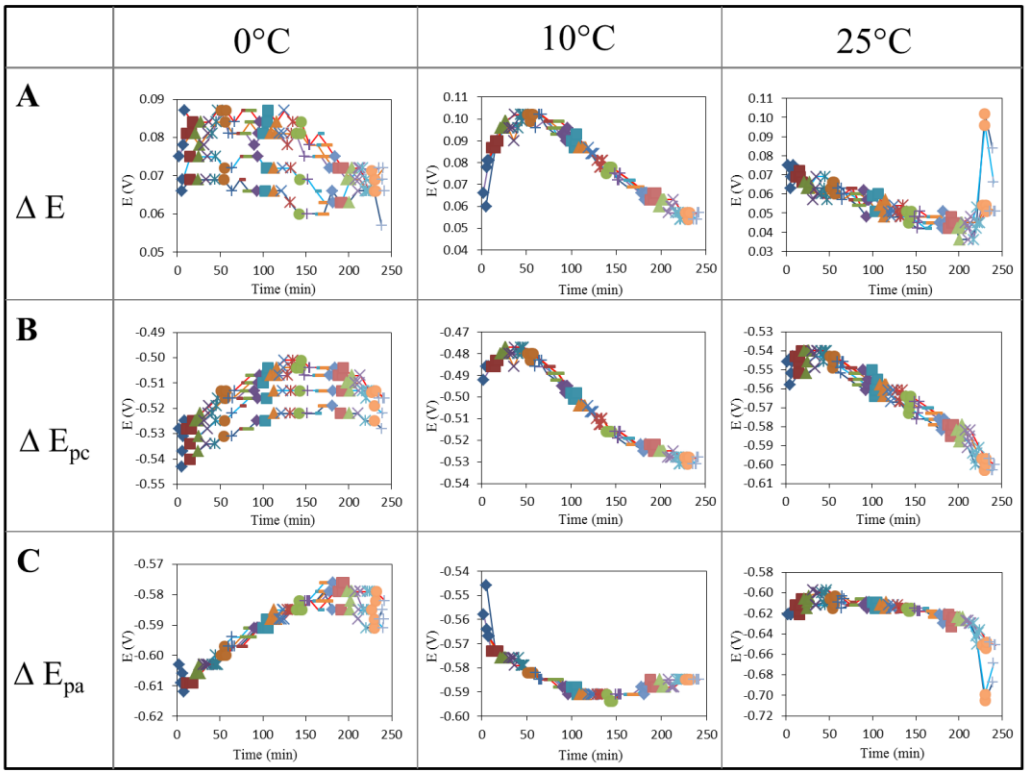

Figure 2.: Measurement using cyclic voltammetry under different temperatures (0 °C, 10 °C and 25 °C): (A) change the aspect E_{pc} / E_{pa} in time, (B) E_{pc} change in time, (C) E_{pa} change in time.

4. CONCLUSION

The electrochemical apparatus was tested under different conditions and it was found to be stable in wide ranch of temperatures and it is possible to make measurement for a long time. The cell is accordingly applicable in a wide range of temperatures, there is no problem to temper it due to its small dimensions, thereby maintaining constant conditions during the whole measurement. Our system is fully automated, it is able to measure, store and evaluate hundreds or thousands of voltamograms in one run. Our designed and tested device is transferable and offers wide customization possibilities for performing various analyzes.

5. REFERENCES

[1] M. A. Baldo, S. Daniele, I. Ciani, C. Bragato and J. Wang, Electroanalysis, 16 (2004) 360.
[2] L. Nejdl, J. Kudr, B. Ruttkay-Nedecky, Z. Heger, L. Zima, L. Zalud, S. Krizkova, V. Adam, M. Vaculovicova and R. Kizek, Int. J. Electrochem. Sci, 10 (2015) 3635.
[3] M. L. Tercier and J. Buffle, Electroanalysis, 5 (1993) 187.
[4] G. Hanrahan, D. G. Patil and J. Wang, Journal of Environmental Monitoring, 6 (2004) 657.
[5] D. Hynek, J. Prasek, P. Businova, J. Zak, J. Drbohlavova, J. Chomoucka, J. Kynicky, M. Konecna, M. Brnicky and J. Hubalek, INTERNATIONAL JOURNAL OF ELECTROCHEMICAL SCIENCE, 8 (2013) 4441.
[6] L. Nejdl, J. Kudr, K. Cihalova, D. Chudobova, M. Zurek, L. Zalud, L. Kopecny, F. Burian, B. Ruttkay–Nedecky and S. Krizkova, Electrophoresis, 35 (2014) 2333.

ELECTROCHEMICAL DETERMINATION OF CADMIUM AND TELLURIUM IN BIOSYNTHESIZED AND MICROWAVE OVEN PREPARED CdTe QUANTUM DOTS

Ludmila KREJCOVA[1,2*], Lukas RICHTERA[1,2], Vojtech Adam[1,2]

[1] *Department of Chemistry and Biochemistry, Faculty of Agronomy, Mendel University in Brno, Zemedelska 1, 613 00 Brno, Czech Republic*

[2] *Central European Institute of Technology, Brno University of Technology, Purkyňova 123, 616 00 Brno, Czech Republic*

**lidakrejcova@seznam.cz*

Abstract

The aim of this study was to develop the simple and fast method, that would allow characterization of CdTe quantum dots (QDs). Two different CdTe QDs (biosynthesized and microwave prepared) were undergone of the stripping voltametry analysis. Using the proposed method simultaneous detection of cadmium and tellurium in both of selected QDs were provided. Results from newly established method were compared with previously published methods for apart detection of cadmium and tellurium.

1. INTRODUCTION

Cadmium telluride (CdTe) quantum dots (QDs) are semiconductor materials with a diameter ranging from 2 to 100 nm, which boasts a wide range of applications from photovoltaics [1,2] thought imaging and sensing [3,4] to health care [5,6]. Ever growing range of their applications is given by their unique optical properties such as a broad excitation spectrum and a narrow emission spectrum as well as photostability, long fluorescent lifetime and low susceptibility to photobleaching [7,8,9]. All these features are particularly useful for fluorescence detection [10,11], or the other frequently used chemiluminescence detection[12]. Across these we decided to take advantage of electroactivity as the target property for detection of both compounds of CdTe QDs. Electrochemical approach was selected hence electroanalytical methos provide a sensitive, reasonable cost and reliable detection of trace quantity of different elements.

Two types of QDs were subjected to electrochemical study. First one were prepared by the classical way (microwave preparation) and a second one by alternative way (biosynthesis). Firstly, both of QDs types were characterized using previously published methods for

tellurium [13] and cadmium [14], subsequently we proposed a modified method that allows detection of both component of QDs simultaneously in one sample and during one scan.

Cathodic stripping differential pulse voltammetry (CSV DPV) was applied for the determination of CdTe QDs, as the working electrode the hanging mercury drop electrode (HMDE) was employed, and as an efficient ligand for stripping voltammetry oxine (8-hydroxyquinoline) was used. This technique was firstly published by Wang *et al.* [13], he described the selective adsorptive collection of the tellurium-8-quinolinol (oxine) complex on a hanging mercury drop electrode followed by cathodic stripping voltammetry. Five years later Yang *et al.* described method for determination Te(IV) using a Tosflex/8-quinolinol (oxine) coated mercury film electrode by square-wave cathodic voltammetry [15], their also highlight that peak of Te(IV) is suppressed by the presence of cadmium(II) in the solution, they resolve this problem by addition of EDTA and they completely eliminated the interference from cadmium(II) [16]. In our study we decide take advantage of this disadvantage and merge detection tellurium and cadmium in one procedure.

2. MATERIAL AND METHODS

2.1. Chemicals and material

All chemicals mentioned in our study were purchased from Sigma-Aldrich (St. Louis, MO, USA), meeting the specification of American Chemical Society (ACS), unless noted otherwise. As standards of tellurium and cadmium atomic absorption spectroscopy (AAS) standard from Sigma-Aldrich (St. Louis, MO, USA) were used. The deionized water was prepared using reverse osmosis equipment Aqual 25 (Aqual s.r.o., Brno, Czech Republic), and it was subsequently purified by apparatus Milli-Q Direct QUV (Billerica, MA, USA), exhibiting a resistance of 18 MΩ. Stock solutions were prepared with ACS water. The pH was measured using pH meter WTW inoLab (Weilheim, Germany). Pipetting was performed by pipettes from Eppendorf (Hamburg, Germany).

2.2. Synthesis of CdTe QDs

Biosynthesis of QDs by Escherichia coli

The LB culture media were inoculated with bacterial cultures (*E. coli*). Suspension of *E. coli* (OD600 = 0.6) was diluted and then cadmium chloride ($CdCl_2$), trisodium citrate dihydrate, sodium tellurite (Na_2TeO_3), mercaptosuccinic acid (MSA) and sodium borohydride ($NaBH_4$)

were added under constant stirring, followed by an incubation, methods for biosynthesis of QDs was taken from Bao *et al.* [17]. Biosynthesis was followed by centrifugation and precipitation of QDs using 50% isopropanol, and repetitive centrifugation. The pellet was dissolved in Milli-Q water and analyzed.

Microwave preparation of QDs

Cadmium telluride CdTe QDs were prepared using followed chemicals: Cd $(OAc)_2 \cdot 2H_2O$, $C_6H_5Na_3O_7 \cdot 2H_2O$, Na_2TeO_3, and $NaBH_4$. Solution were transferred into a vials, which were heated at 90 ° C, 300 W for 10 min (ramping time 10 min) under microwave irradiation (Multiwave3000, Anton-Paar GmbH, Graz, Austria). Prepared CdTe QDs were stored in dark at 4 °C. Methods for microwave preparation of CdTe was published previously [18].

2.3. Electrochemical detection of cadmium and tellurium of CdTe QDs

The above mentioned method (Wang et al.) which utilizes formation of Te - oxine complex and its determination using CSV DPV, was assume and employed for detection of tellurium in both of QDs without any further modifications. Cadmium, Cd(II) was determined by method which we published in our previou study [14], method was slightly modified, deposition time was set up at 120 s, due to reduction of the time required for analysis.

2.4. Proposal and optimization of method for simultaneously detection of cadmium and tellurium of CdTe QDs

The parameters of the method for simultaneous detection of cadmium and tellurium using metal - oxine complexation, followed by CSV DPV detection, were further optimized. Influence of three parameters (start potential, depostion potential and time of deposition) on Cd and Te peak height were observed. Firstly parameters were optimized for deterimention of cadmium and tellurium individually, therafter optimized parameters were adapted to detection of both of metal ions simultaneously during one scan.

2.5. Detection of cadmium and tellurium of real sample of CdTe QDs

Newly estabilished method was employed under optimized conditions for determination of quantities of cadium and tellurium in QDs. As real samples biosynthesized and microwave prepared CdTe QDs were used.

3. RESULTS AND DISCUSSION

3.1. Electrochemical detection of cadmium and tellurium of CdTe QDs

Two previously published methods for separate detection cadmium and tellurium were used for creating of calibration curves of tellurium and cadmium standards. Under same conditions were also detected quantities of Cd and Te in both of QDs. Obtained results were compared with data form AAS detection. Calibration curves of Cd and Te standards measured by stripping voltammetry in presence of different electrolytes are shown on Figure 1.

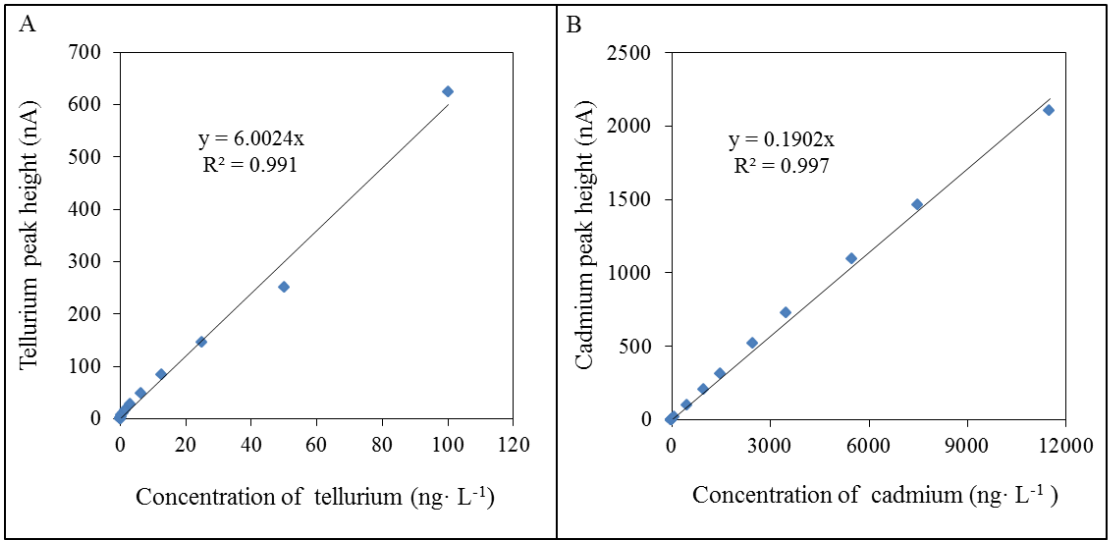

Figure 1.: Calibration curves of tellurium (**A**) an cadmium (**B**). All of measurements were provided by stripping voltametry coupled with differential pulse voltametry, as working electode HMDE was employed. Tellurium was measured in presence of oxine buffer, as an electrolyte for cadmium detection acetate buffer was used.

3.2. Optimization of newly established method

The method for the simultaneous determination of both of elements was subjected to optimization. At first three different parameters were optimized using Cd and Te standards. Optimized parameters were: start potential, deposition potential, and time of deposition. As optimal parametres were selected: start potential −0.35 V (compromise between −0.40 V for Cd and −0.30 V for Te), as deposition potential was selected same potential as the start potential (−0.35 V), again as a compromise between the optimum for both of the elements. As optimal deposition time 120 s were selected, because longer deposition will make method more time consuming.

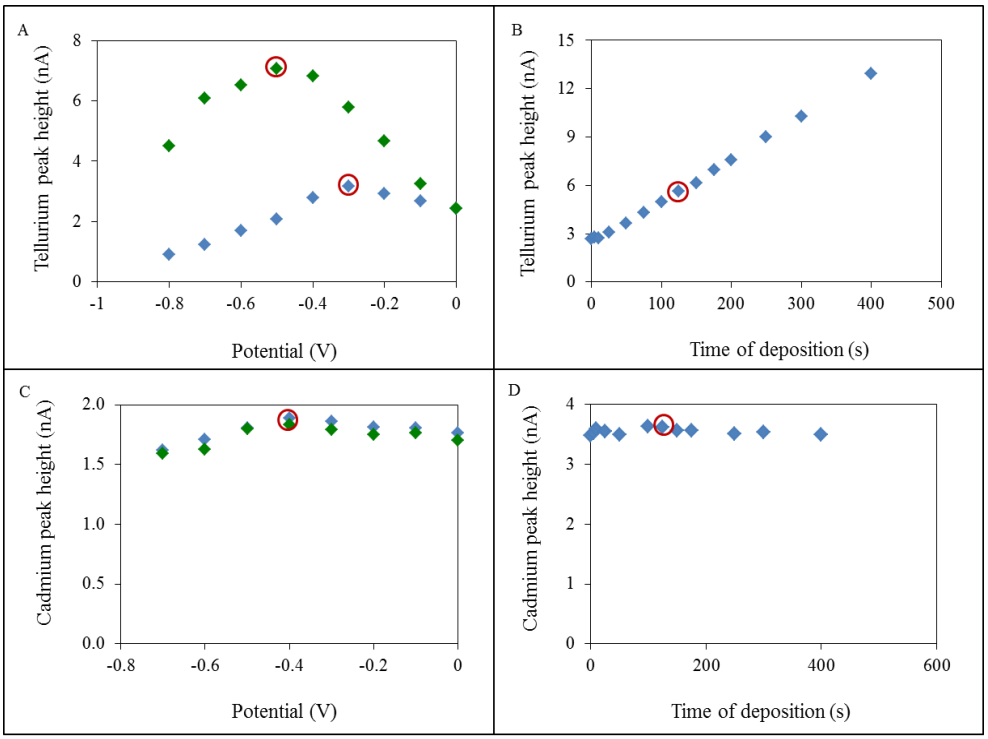

Figure 2.: Optimization of electrochemical detection of tellurium (**A**, **B**) and cadmium (**C**, **D**) of microwave prepared CdTe QDs. Three parameters for detection both of metal ions were optimized: start potential (blue dots, **A** and **B**), deposition potential (green dots, **A** and **B**), and time of deposition (**B**, **D**). CSV DPV was employed, oxine buffer as supporting electrolyte was used.

3.3. Detection of cadmium and tellurium of real sample of CdTe QDs

CSV DPV under optimized conditions was used for cahracterization of both of QDs (biosynthesized and microwave prepared). Moreover both of QDs were characterised before and after mineralization. As was expected, mineralization was necessary toward deeper insight into formation of QDs. Mineralization allow the identification of a amount of different oxidation states of both of the elements. As shows Figure 3 micowave prepared QDs contain far less Cd than bio QDs, the difference between the content before and after mineralization is negligible. Regarding the content of Te, there is a much bigger difference. Micowave prepared have higher levels of Te than bio QDs. It was also observed different amounts of Te in both of QDs samples before and after digestion. Electrochemical analysis will be compared with AAS.

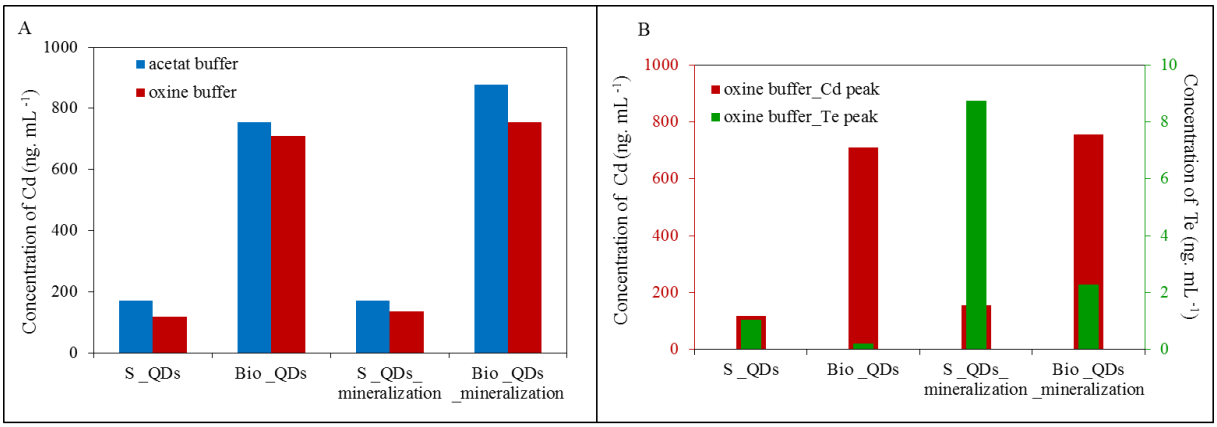

Figure 3.: A Comparison of detection of Cd in both of QDs using previously described method in acetate buffer (blue) and the newly estabilished method in oxine (red). **B** Cathodic stripping voltammetry coupled with differential pulse voltammetry (CSV DPV) was used for cahracterization of amount of cadmium and tellurium in biosynthesized (Bio QDs) and micro wave prepared (S QDs) CdTe QDs. Also influence of mineralization on the contents of both of elements were taken into account.

4. CONCLUSION

Cathodic stripping differential pulse voltammetry (CSV DPV) was applied for the determination of CdTe QDs, a good linear relationship of the catalytic peak current and the concentrations of both of analytes were achieved. The results provided an insight into the hidden properties structure of CdTe QDs and the potency of QDs for real life applications. Suggested method could be used to decide about the applicability of concrete QDS for concrete purposes, or for monitoring of changes both of elements in the form of QDs during and after their applications. The method could also help in solving the problems of toxicity and recycling CdTe QDs.

5. ACKNOLEDGEMENT

The authors would like to thank Marketa Kominkova for preparation biosynthesized QDs and Vedran Milosavljevic for microwave prepared QDs.

6. REFERENCES

[1] Rugen-Hankey SL, Clayton AJ, Barrioz V, Kartopu G, Irvine SJC, et al. (2015) Improvement to thin film CdTe solar cells with controlled back surface oxidation. Solar Energy Materials and Solar Cells 136: 213-217.

[2] Antanovich AV, Prudnikau AV, Melnikau D, Rakovich YP, Chuvilin A, et al. (2015) Colloidal synthesis and optical properties of type-II CdSe-CdTe and inverted CdTe-CdSe core-wing heteronanoplatelets. Nanoscale 7: 8084-8092.

[3] Du JH, Wang CL, Xu XJ, Wang ZY, Xu SH, et al. (2016) Assembly of light-emitting diode based on hydrophilic CdTe quantum dots incorporating dehydrated silica gel. Luminescence 31: 419-422.

[4] Tang TT, Deng JJ, Zhang M, Shi GY, Zhou TS (2016) Quantum dot-DNA aptamer conjugates coupled with capillary electrophoresis: A universal strategy for ratiometric detection of organophosphorus pesticides. Talanta 146: 55-61.
[5] Lin Y, Ramirez-Giraldo JC, Gauthier DJ, Stierstorfer K, Samei E (2014) An angle-dependent estimation of CT x-ray spectrum from rotational transmission measurements. Medical Physics 41.
[6] Wang K, Qian J, Jiang D, Yang ZT, Du XJ (2015) Onsite naked eye determination of cysteine and homocysteine using quencher displacement-induced fluorescence recovery of the dual-emission hybrid probes with desired intensity ratio. Biosensors & Bioelectronics 65: 83-90.
[7] Gao X, Zhao Y, Zhang B, Tang YW, Liu XY, et al. (2016) Highly-sensitive organophosphorus pesticide biosensors based on CdTe quantum dots and bi-enzyme immobilized eggshell membranes. Analyst 141: 1105-1111.
[8] Ensafi AA, Kazemifard N, Rezaei B (2015) A simple and rapid label-free fluorimetric biosensor for protamine detection based on glutathione-capped CdTe quantum dots aggregation. Biosensors & Bioelectronics 71: 243-248.
[9] Chao MR, Hu CW, Chen JL (2014) Comparative syntheses of tetracycline-imprinted polymeric silicate and acrylate on CdTe quantum dots as fluorescent sensors. Biosensors & Bioelectronics 61: 471-477.
[10] Rao HB, Liu W, Lu ZW, Wang YY, Ge HW, et al. (2016) Silica-coated carbon dots conjugated to CdTe quantum dots: a ratiometric fluorescent probe for copper(II). Microchimica Acta 183: 581-588.
[11] Amjadi M, Jalili R, Manzoori JL (2016) A sensitive fluorescent nanosensor for chloramphenicol based on molecularly imprinted polymer-capped CdTe quantum dots. Luminescence 31: 633-639.
[12] Taokaenchan N, Tangkuaram T, Pookmanee P, Phaisansuthichol S, Kuimalee S, et al. (2015) Enhanced electrogenerated chemiluminescence of tris(2,2 '-bipyridyl) ruthenium(II) system by L-cysteine-capped CdTe quantum dots and its application for the determination of nitrofuran antibiotics. Biosensors & Bioelectronics 66: 231-237.
[13] Wang J, Lu JM (1994) ADSORPTIVE STRIPPING VOLTAMMETRIC DETERMINATION OF TRACE TELLURIUM IN THE PRESENCE OF OXINE. Electroanalysis 6: 405-408.
[14] Krejcova L, Nejdl L, Hynek D, Krizkova S, Kopel P, et al. (2013) Beads-Based Electrochemical Assay for the Detection of Influenza Hemagglutinin Labeled with CdTe Quantum Dots. Molecules 18: 15573-15586.
[15] Yang HY, Sun IW (1999) Cathodic stripping voltammetric determination of tellurium(IV) in chloride media using a Tosflex/8-quinolinol mercury film electrode. Electroanalysis 11: 195-200.
[16] Yang HY, Sun IW (1998) Cathodic stripping voltammetric determination of tellurium(IV) at a Nafion/8-quinolinol mercury film modified electrode. Analytica Chimica Acta 358: 285-290.
[17] Bao HF, Lu ZS, Cui XQ, Qiao Y, Guo J, et al. (2010) Extracellular microbial synthesis of biocompatible CdTe quantum dots. Acta Biomaterialia 6: 3534-3541.
[18] Krizkova S, Dostalova S, Michalek P, Nejdl L, Kominkova M, et al. (2015) SDS-PAGE as a Tool for Hydrodynamic Diameter-Dependent Separation of Quantum Dots. Chromatographia 78: 785-793.

ELECTROCHEMICAL DETECTION OF ZINC IONS USING GLASSY CARBON ELECTRODE MODIFIED WITH ELECTROCHEMICALLY REDUCED GRAPHENE OXIDES

Jiri KUDR[1], Ondrej ZITKA[1,2], Vojtech ADAM[1,2*]

[1] *Department of Chemistry and Biochemistry, Faculty of Agronomy, Mendel University in Brno, Zemedelska 1, 613 00 Brno, Czech Republic*

[2] *Central European Institute of Technology, Brno University of Technology, Technicka 3058/10, 616 00 Brno, Czech Republic*

**vojtech.adam@mendelu.cz*

Abstract

Industrialization and urbanization resulted in increasing concentrations of metals in biosphere, which nowadays represent serious issue for public health. In this contribution, direct electrochemical reduction of Zn(II) on glassy carbon electrode (GCE) modified with electrochemically reduced graphene oxide (ERGO) is reported. Graphene oxide (GO) fabricated using Hummers method was electrodeposited on the surface of GCE at +1.0 V *vs.* Ag/AgCl/3M KCl and subsequently reduced by performing cyclic voltammograms from 0 to −1.5 V. The modification of electrode was optimized and properties of GCE/ERGO were determined. Although the surface of GCE increased after modification with ERGO by 9.4 %, the electrocatalytic activity towards Zn(II) increased three times and detection limit 5 ng·L^{-1} was obtained.

1. INTRODUCTION

Heavy metal pollution has become a major concern all over the world. The only way to meet the legislative demands is to steadily monitor the levels of metals in biosphere compartments. Zinc belong to group of essential micronutrients hence pose health risk in high supplementation only. However, zinc monitoring is also needed [1-3].

Atomic absorption spectrometry (AAS) and inductively coupled plasma mass spectrometry are considered as a golden standard in metal *analysis*. Nevertheless in this field electrochemistry provides several superior features like low cost analysis, portability, possibility of miniaturization, easy-to-use and high sensitivity and several time was proved to be suitable analytical method for metal analysis [4-7].

In this study GCE was modified with GO using potentiostatic deposition. Deposited GO was subsequently electrochemically reduced using cyclic voltammetry at negative potentials. Performance of as prepared electrode was tested towards Zn(II) ions.

2. MATERIAL AND METHODS

Glassy carbon modification with reduced graphene oxide

GCE was mechanically polished by the 1.0 and 0.3 μm alumina suspension. As prepared, the electrode was rinsed with water solution of GO (0.5 $mg \cdot mL^{-1}$) and potential +1.0 V was applied on working electrode *vs.* Ag/AgCl/3M KCl. The deposited film of GO was reduced by performing CV from 0.0 V to −1.5 V in acetate buffer (0.2 $mol \cdot L^{-1}$ CH_3COONa and CH_3COOH, pH 5) to produce ERGO.

Zinc ions determination

Determination of Zn(II) by differential pulse voltammetry was performed using PGSTAT302N (Metrohm, Herisau, Switzerland) using a three electrode system. A 3 mm diameter GCE (CH Instruments, Austin, USA) was employed as the working electrode. An Ag/AgCl/3M KCl electrode was used as the reference and platinum wire served as auxiliary. Acetate buffer was used as a supporting electrolyte. The parameters of the measurement by DPV were as it follows: initial potential −1.3 V, end potential −1.0 V, deposition time 60 s, time interval 0.03 s, step potential 5 mV, scan rate 50 $mV \cdot s^{-1}$.

Determination of electrode active surface area

In order to determine electroactive area of GCE and to compare it with GCE/ERGO CV of 2 mM $[Fe(CN)_6]^{3-}/[Fe(CN)_6]^{4-}$ in 0.1 M KCl were recorded using mentioned electrodes. Electroactive surface was calculated according to Randles-Sevcik equation [8].

3. RESULTS AND DISCUSSION

The GCE/ERGO was fabricated by immersion of clean GCE within sonicated GO solution (0.5 $mg \cdot mL^{-1}$) and application of constant potential +1.0 V *vs.* Ag/AgCl/3M KCl reference electrode. GO possess negative net charge due to the presence of oxygen-containing moieties and was electrostatically attracted to positively charged working electrode. Subsequently working electrode was gently rinsed within water and transferred within acetate buffer where several CV from 0 to −1.5 V were performed. Irreversible reduction peaks at −1.05 V and −0.85 V were observed (data not shown). Previously, reduction of GO at −1.10 V was

reported [9]. Further, deposition time of GO (0–480 s) on electrode was optimized using detection of 20 µmol·L^{-1} Zn(II) signal and the deposition for 60 s was found as an optimal (Figure 1A). Using deposition at potential −1.25 V for 60 s Zn(II) were measured using GCE/ERGO and calibration curve was determined and compared with performance of bare GCE (Figure 1B). Analytical parameters of detection are displayed in Table 1. The modification of GCE with ERGO improved the detection of zinc ions (35 µmol·L^{-1}) four-fold in comparison with bare GCE and slightly shifted peak potential from −1.18 V to −1.2 V (Figure 1C). Using GCE/ERGO, we obtained limit of detection (LOD) 0.1 µmol·L^{-1} Zn(II) (~5 ng·mL^{-1}).

4. CONCLUSION

The electrode surface is place where redox processes take place. Hence its modifications represent suitable way to improve electrodes performance. As is evident from out experiments, modification of electrodes with GO could significantly improve sensitivity of GCE towards Zn(II). Although the surface increased after GCE modification with ERGO by 9.4 %, sensitivity increased three times.

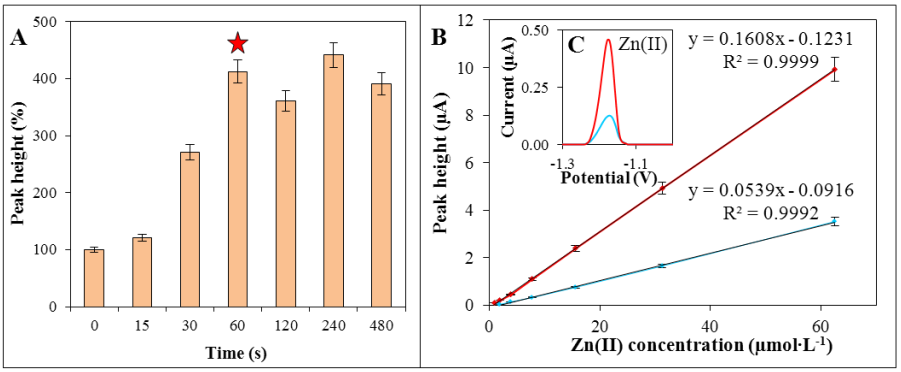

Figure 1.: (A) Dependence of Zn(II) reduction signal obtained using GCE/ERGO on deposition time of GO (0.5 mg·mL^{-1}) on the electrode (deposition time selected as optimal is marked with star); (B) Dependence of electrochemical signal on Zn(II) concentration (1.0–62.5 µmol·L^{-1}) and comparison of DPV reduction signals of Zn(II) (4 µmol·L^{-1}) (D) obtained using GCE/ERGO (red line) and bare GCE (blue line).

Table 1.: Analytical parameters of electrochemical detection of Zn(II).

Substance	Working electrode	Regression equation	Linear dynamic range ($\mu mol \cdot L^{-1}$)	$R^{2\,a}$	LOD [b] ($\mu mol \cdot L^{-1}$)	LOQ [c] ($\mu mol \cdot L^{-1}$)	RSD (%)
Zn(II)	GCE/ERGO	y = 0.1608x − 0.1231	62.5 - 1.0	0.9999	0.1	0.4	4.8
Zn(II)	GCE	y = 0.0539x − 0.0916	500.0 - 2.0	0.9992	0.5	2.0	5.2

5. ACKNOWLEDGEMENT

The work has been financially supported by the Ministry of Education, Youth and Sports of the Czech Republic under the project CEITEC 2020 (LQ1601).

6. REFERENCES

[1] Haider S, Anis L, Batool Z, et al.: Metabolomic Brain Disease, 30 (2015), 83-92
[2] Blazovics A, Szentmihalyi K, Vinkler P, et al.: Trace Elements and Electrolytes, 21 (2004), 240-247
[3] Krystofova O, Trnkova L, Adam V, et al.: Sensors, 10 (2010), 5308-5328
[4] Mazzei V, Longo G, Brundo MV, et al.: Ecotoxicology and Environmental Safety, 110 (2014), 269-279
[5] Nejdl L, Ruttkay-Nedecky B, Kudr J, et al.: Sensors, 13 (2013), 14417-14437
[6] Nejdl L, Kudr J, Cihalova K, et al.: Electrophoresis, 35 (2014), 2333-2345
[7] Prasek J, Adamek M, Hubalek J, et al.: Sensors, 6 (2006), 1498-1512
[8] Prathish KP, Barsan MM, Geng DS, et al.: Electrochimica Acta, 114 (2013), 533-542
[9] Zhang ZP, Yan J, Jin HZ, et al.: Electrochimica Acta, 139 (2014), 232-237

GOLD NANOSTRUCTURED SURFACES BASED ON ALUMINA TEMPLATE

Hana KYNCLOVÁ[1*], Tomáš LEDNICKÝ [2], Radim HRDÝ[1], Jan PRÁŠEK[1, 2], Jaromír HUBÁLEK [1, 2]

[1] *Department of Microelectronics, Faculty of Electrical Engineering and Communication, Brno University of Technology, Technická 3058/10, 616 00 Brno, Czech Republic*

[2] *Central European Institute of Technology, Technická 3058/10, 616 00 Brno, Czech Republic Brno, Czech Republic*

**xkyncl02@stud.feec.vutbr.cz*

Abstract

Nanostructured surfaces are promising approach to improve properties of electrochemical sensors and biosensors. Their biggest advantage is possibility to considerably increase and control electrochemical area while small geometrical area of sensor is preserved. This fact can provide more sensitive nanostructured electrodes and opportunity to involved nanostructured surfaces into electrochemical sensors and biosensors devices. In this work, we prepared nanostructured surfaces by electrochemical anodization of thin aluminium layer and subsequent electrodeposition of gold material to the obtained template. These nanostructured electrodes were electrochemically characterized by cyclic voltammetry using $K_3[Fe(CN)_6]/K_4[Fe(CN)_6]$ probe and compared with the results measured on a flat gold electrode. Gold nanostructured surfaces are planned to be involved in biosensor devices.

1. INTRODUCTION

In recent years, fabrication of various nanostructured surfaces has become very actual topic. The main goal is prepare them easy and cheap. Great interest is especially about self-assembled arrays of nanocolumns because of their possible usage in many applications eg. photocatalysis, fuel cells, electrochemical sensors and biosensors [1]. In sensing applications of nanostructured surfaces could increase an active electrochemical area significantly while a small geometrical area is maintained and thereby improve sensitivity of sensors [2]. Electrochemical anodization of aluminium film combined with electrochemical deposition into nanoporous templates is well-established method for fabrication of nanostructured surfaces [3]. Self–ordered anodic alumina oxide (AAO) offers highly ordered and vertically aligned nanoporous templates which are suitable for various material synthesis

and alignment of nanosized structures [4-7]. This method also provides relatively cheap fabrication in comparison with lithographic and others methods.

2. MATERIAL AND METHODS

Electrodes

Self-assembled gold nanostructured surfaces were produced by pulse galvanic deposition of gold material into AAO nanoporous template fabricated via electrochemical anodic oxidation method of thin aluminium layer. Firstly, the titanium, tungsten and aluminium layers were successively sputtered on silicon wafer covered by SiO_2. Upper aluminium layer was anodically oxidized in 0.3 M oxalic acid under the constant voltage of 50 V. During this process, upper aluminium layer was transformed to nanoporous alumina (Al_2O_3) with hexagonally ordered nanopores perpendicular to the surface. Whereas the anodization was being finished, tungsten oxide nanostructures were created on the bottom as a result of oxidation of tungsten layer below. Then these WO_3 nanostructures were etched away which created tungsten nanodimpled surface with AAO above. These nanodimples enable to strongly anchor the gold nanostructures below the ambient surface and thus improve their stability. Pulse deposition of gold into such AAO with nanodimpled bottom was performed from dicyanoaurate and boric acid solution. The number of pulses controlled the length of obtained gold nanocolumns in the AAO template. The last step of production is dissolving of alumina template. Gold layer was also prepared for comparison of gold nanostructures impact on the enhancement of electrode active surface area.

Electrochemical characterization

All electrochemical measurements were performed using μAUTOLAB III/FRA2. Two-electrode arrangement with Pt pseudoreference electrode was used for all experiments. The measurement was performed in a droplet of 20 μl volume of solution. The geometrical area of electrodes was determined by circle in parafilm with 3 mm in diameter. All fabricated electrodes were electrochemically cleaned by cyclic voltammetry methods performed in 0.1 M sulphuric acid before each measurement. The measurements were proceeded in 0.1 M potassium chloride with additions of 6 mM potassium ferricyanide and 6 mM ferrocyanide.

3. RESULTS AND DISCUSSION

The tungsten film electrodes modified by gold nanocolumns were successfully prepared by anodization method with subsequent electrochemical deposition of gold material to the prepared alumina templates. The nanocolumns have about 60 nm in diameter and about 200 nm high. Fabricated nanostructured surfaces were electrochemically characterized by cyclic voltammetry. It has been found, key role in electrochemical characterization is electrochemical cleaning which influences the resulted data significantly. Generally, cyclic voltammetry performed in redox electrochemical system is useful for evaluation and comparison of electrochemically active surfaces of working electrodes [7]. It is obvious that the electroactive electrode area is often very different than geometrical electrode area due to roughness of electrode surface or a result of surface modifications. Evaluation of CV results also can reveal a real penetration of electrolytic solution into the spaces among the gold nanostructures. The higher current response of CV voltammogram means the higher electroactive area involved in reaction. The peak height is dependent on the electrolyte concentration as well. CV voltammograms for flat gold electrode without any modification and for nanostructured surface with gold nanostructures are shown in Figure 1. We can observe that flat gold electrode exhibits higher peaks at low scan rates (< 25 $mV.s^{-1}$) and nanostructured surface shows higher peaks at higher scan rates (≥ 50 $mV.s^{-1}$). It is obvious; electroactive area of nanostructured electrode is changed with scan rate. Higher scan rate means higher electroactive area than electroactive area for flat gold electrode and vice versa.

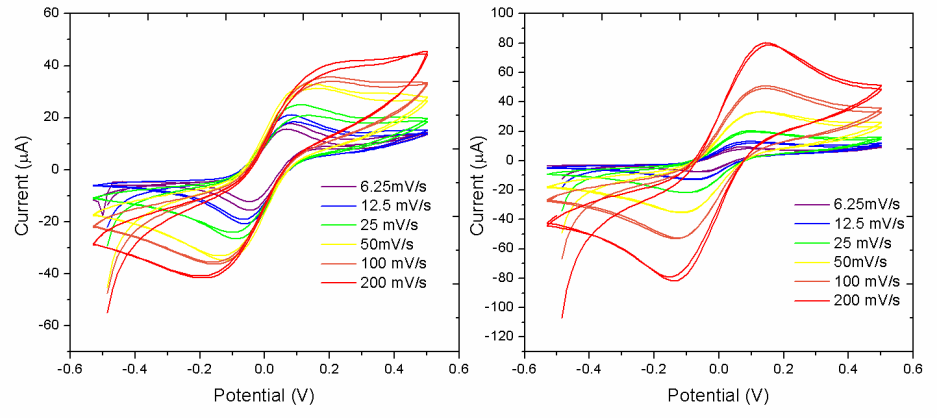

Figure 1.: Cyclic voltammograms measured in 6 mM ferro-ferricyanide in 0.1M KCl for flat gold electrode (on the left) and electrode modified with gold nanocolumns (on the right)

Nevertheless, the electroactive area of electrodes is also evaluated as a ratio of the slopes of dependencies of peak heights on square roots of scan rates. According to this fact,

nanostuctured electrode exhibits approximately 2.5 times higher electroactive area. The change of the electroactive area depending on the scan rate is probably related to difficult penetration of electrolyte to the gaps between nanostructures at lower scan rates because the kinetics of mass transport near the interface between electrode and electrolyte plays an important role influencing the current responses of electrochemical sensors.

4. CONCLUSION

The tungsten electrodes modified with gold nanocolumns were prepared and electrochemically studied by CV in the presence of potassium ferro-ferricyanide probe and compared with flat gold electrode. It was found, the electroactive area is changing with scan rate. Nanostructured surfaces showed impact at higher scan rates. This fact is probably caused by difficult penetration of electrolyte to the spaces between nanostructures at lower scan rates.

5. ACKNOWLEDGEMENT

The work has been supported by project no. FEKT-S-14-2300 A new types of electronic circuits and sensors for specific applications. Research described in this paper was financed by Czech Ministry of Education in frame of National Sustainability Program under grant LO1401. For research, infrastructure of the SIX Center was used.

6. REFERENCES

[1] Anandan V, Rao Y L and Zhang G. (2005). Nanopillar arrays with superior mechanical strength and optimal spacing for high sensitivity biosensors. 2005 NSTI Nanotechnology Conference and Trade Show pp. 217-220.
[2] Lee S J, Anandan V and Zhang G: Biosensors and Bioelectronics, 23 (2008), 7, 1117-1124
[3] Bharath Bhushan, Dan Luo, Scott R. Schricker, et al. (2014), Handbook of Nanomaterials Properties, Springer Verlag, Heidelberg.
[4] Drbohlavova J, Kynclova H, Hrdy R, et al.: Analytical Letters, 49 (2016), 1, 135-151
[5] Noh K, Brammer K S, Seong T Y, et al.: Nano, 6 (2011), 6, 541-555
[6] Anandan V, Rao Y L and Zhang G: International Journal of Nanomedicine, 1 (2006), 1, 73-79
[7] Anandan V, Yang X, Kim E, et al.: Journal of Biological Engineering, 1 (2007)

SOLID-STATE SYNTHESIS OF GOLD NANOPARTICLES FILMS FOR SPECTROSCOPIC MEASUREMENT ENHANCEMENT

Tomáš LEDNICKÝ

[1] *CEITEC – Central European Institute of Technology, Brno University of technology, Brno, Czech Republic*
tomas.lednicky@ceitec.vutbr.cz

Abstract

In this work, it is proposed a novel fabrication method of gold nanoparticle films. The method involves a fabrication of templated aluminium substrate by porous-type anodic oxidation of aluminium foils. Furthermore, a thin deposited gold layer is annealed resulting into the gold nanoparticles formation. Additionally, the transfer onto transparent substrates such as PDMS is demonstrated. The aim of this research is to develop a cost-effective method of nanoparticles films production for localized surface plasmon resonance (LSPR) sensor element with a high performance.

1. INTRODUCTION

In recent years, much attention was given to noble metal nanoparticles (NPs) with sizes well below 100 nm, being the active localized surface plasmon (LSP) element. This size parameter of the NPs is critical for LSPR detection in near infrared or even visible region. However, nowadays, several technologies for fabrication of NPs are capable of developing extremely sensitive sensors, but the costs are unacceptably high, while simpler technologies result in sensors having poor sensitivity [1]. Therefore, the urgent challenge is to find optimal fabrication technologies combining realistic manufacture costs with high sensor sensitivities.

In this work is present the technological approach for synthesis of gold NP surfaces. The fundamental advantage is that it is versatile, could be performed in large-scale, and is of low-cost, being favorable as compared to other methods. The prepared NPs films are well ordered, with high density of NPs as well as organic-free.

2. METHODS

The essential starting point is the fabrication of nanostructured substrate. In this work, we present the use of dimpled aluminium substrate, being a secondary product of anodic oxidation of aluminium into porous anodic alumina (PAA). By controlling the electrochemical conditions a variety of PAA parameters can be tailored [2]. Since the

aluminium template inversely replicates the PAA bottom structure, these parameters play a crucial role for the final size, alignment, and homogeneity of gold NP films. These processes of Al template fabrication are shown schematically in Figure 1.

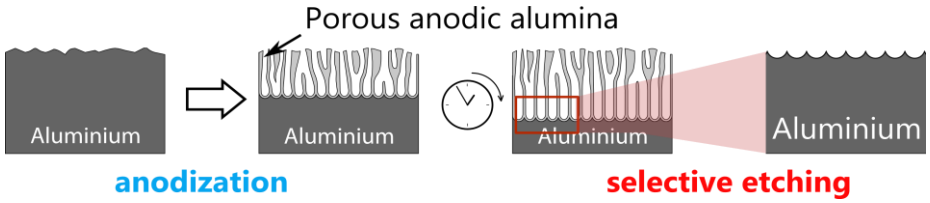

Figure 1.: Scheme of aluminium template fabrication by formation and etching of PAA layer.

The gold NP film is obtained by deposition of a thin gold layer over the Al template, followed by an annealing in a vacuum or even ambient atmosphere. This technique, called controlled dewetting, is well studied especially in the case of gold layers [3]. After the NP layer is created, it can be transferred to a more suitable (transparent) substrate by its application over the layer and subsequent Al dissolution. This process is illustrated in Figure 2.

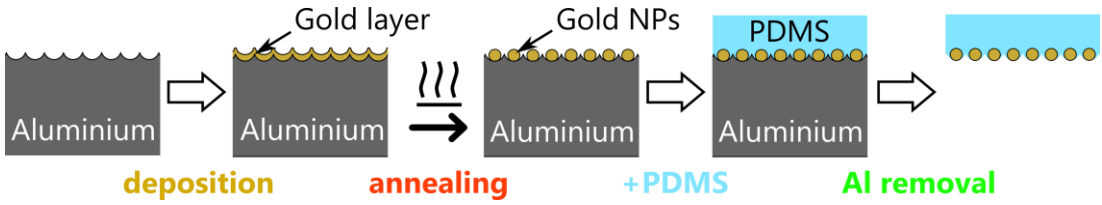

Figure 2.: Schematic illustration of gold NP layer preparation on the structured aluminium template and their transfer to another substrate.

3. EXPERIMENTAL AND RESULTS

An aluminium foil of 99.999 % purity and 250 μm thickness (Goodfellow) was used as the starting material. The aluminium foil was annealed in a vacuum at 550 °C for 5 h to allow the material to relax and recrystallize. Subsequently, the foil was mechanically and electrochemically polished. The mechanical polishing was done under ethanol by an ultra-fine P3000 sandpaper. The electrochemical polishing was performed in 1:4 (*v*:*v*) perchloric acid ($HClO_4$) and ethanol solution at 3 °C for 1 min at 20 V (about 100 mA/cm^2). The Al foil was set as the anode and a stainless steel mesh was used as the cathode.

After polishing the foil was anodized in galvanostatic mode at 40 V in 0.3 M oxalic acid ($H_2C_2O_4$) at 7 °C for 18 hours. The long anodizing was set to obtain the best order of pores at the aluminium/alumina interface [4]. The nanostructured aluminium surface was revealed by

selective etching of PAA in 0.42 M phosphoric acid (H_3PO_4) and 0.2 M chromium trioxide (CrO_3) solution at 60 °C for 1h. Furthermore, over the template was deposited by sputtering 7 nm thin gold layer. This sample was further annealed in the ambient atmosphere at 350 °C for 2 h. Resulting NP surface is shown in Figure 3A.

The NPs were transferred to a PDMS substrate by standard casting method in a specially prepared mold. The PDMS was pour into mold over NPs on the Al substrate. After hardening on a hotplate at 60 °C for 2 h, the Al substrate was dissolved in 5 M hydrochloric acid (HCl)

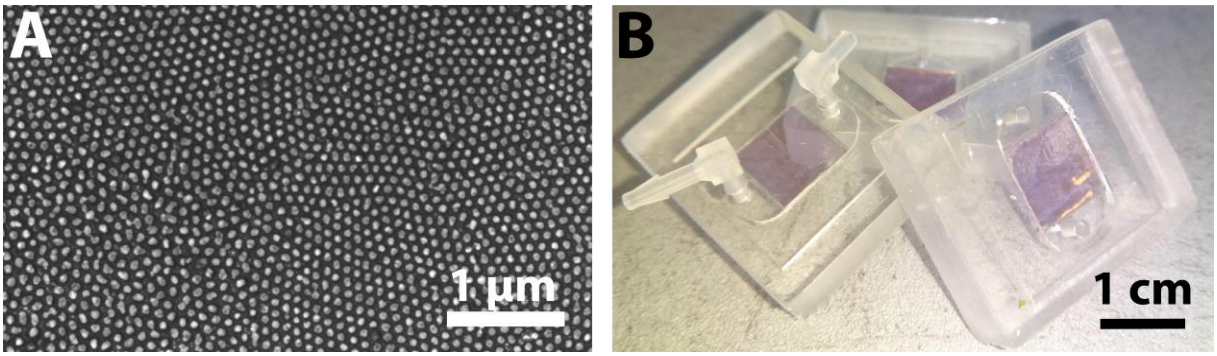

Figure 3.: SEM image of dimpled aluminium surface after removal of PAA with gold NPs formed over the surface (A) and the samples of PDMS microfluidic cell modified with NPs (B). The mean size of NPs is 75 nm.

and 2 M copper (II) chloride ($CuCl_2$). The removal of Al substrate results into final PDMS cell with a simple channel modified by NPs (shown in Figure 3B).

4. CONCLUSION

In this work, we have developed and demonstrated an interesting technological approach for synthesis of ordered gold nanoparticle layers. We have demonstrated that this technique could be performed in large-scale, and thus it can be unpredictably economical. Additionally, this technique compared to others, produce NPs which are well align, with a high density distribution and organic-free composition. Furthermore, this technique can be reasonably versatile since NPs' sizes and distribution depends mainly on the template and the thickness of deposited layer, where both are undeniably tuneable.

In the last decade, the demand for NPs, especially for layers with a high density, has increased immensely due to rapid progress in fields of optics, especially the plasmonics. Nowadays, there are a vast number of scientific ideas as well as commercial devices utilizing SPR or LSPR for detection and recognition of various bio-molecules [5-7]. Therefore, it is greatly encourage to further develop and optimize NPs fabrication techniques such as this.

5. ACKNOWLEDGEMENT

This research has been financially supported by the Ministry of Education, Youth and Sports of the Czech Republic under the project CEITEC 2020 (LQ1601).

6. REFERENCES

[1] Mayer K. M, Hafner J. H.: Chemical Reviews, 111 (2011), 6, 3828-3857
[2] Sulka G. D.: Highly Ordered Anodic Porous Alumina Formation by Self-Organized Anodizing, Wiley-VCH Verlag GmbH & Co. KGaA (2008), 1-116
[3] Müller M. C, Filippo F. C, Spolenak R.: Nanotechnology, 19 (2008), 48, 485306
[4] Masuda H.: Ordered Porous Nanostructures and Applications, Springer US, Boston (2005), 37-55
[5] Petryayeva E, Krull U. J.: Analytica Chimica Acta, 706 (2011), 8-24
[6] Homola J, Piliarik M.: Surface Plasmon Resonance Based Sensors, Springer Berlin Heidelberg (2006), 45-67
[7] Jatschka J. et al.: Sensing and Bio-Sensing Research, 7 (2016), 62-70

ZINC-SCHIFF BASE-NOVICIDIN COMPLEX AS A POTENTIAL ANTITUMOR DRUG FOR PROSTATE CANCER THERAPY

Vedran MILOSAVLJEVIC[1], Yazan HADDAD[1], Miguel Angel MERLOS RODRIGO[1,2], Amitava MOULICK[2], Hana POLANSKA[3], David HYNEK[1,2], Zbynek HEGER[1,2], Pavel KOPEL[1,2] and Vojtech ADAM[1,2]*

[1] *Department of Chemistry and Biochemistry, Faculty of Agronomy, Mendel University in Brno, Zemedelska 1, 613 00 Brno, Czech Republic*

[2] *Central European Institute of Technology, Brno University of Technology, Technicka 3058/10, 616 00 Brno, Czech Republic*

[3] *Department of Physiology, Faculty of Medicine, Masaryk University, Kamenice 5, CZ-625 00 Brno, Czech Republic, European Union.*

**vojtech.adam@mendelu.cz*

Abstract

Prostate cancer cells control energy metabolism by chelating intracellular zinc, thus zinc delivery has been a highly recommended therapeutic approach to prostate cancer. Here, we propose the usage of membrane penetrating peptide Novicidin connected with zinc-Schiff base as carrier vehicle of zinc to prostate cells. Mass spectrometry, electrochemistry and spectrophotometry confirmed the formation/stability of this complex and gave insight to the availability of zinc to interact within complex. This delivery system showed minor toxicity in normal PNT1A cells and high potency towards PC3 tumor cells. The complex showed preference to penetrate PC3 tumor cells in contrast to confinement to membranes of PNT1A. Further, the zinc uptake was confirmed in both cell lines. Molecular analysis was used to confirm the activation of zinc stress (e.g. *ZnT-1*) and apoptosis (e.g. *CASP-1*). Our results strongly suggest that zinc-Schiff base-Novicidin complex have great potential to be developed into novel anticancer drug.

1. INTRODUCTION

Detection of PCa in early stage with curative treatment modalities including surgical and radiation therapies is required. However, hormonal ablation of metastatic cells can lead PCa cells to lose androgen-dependency and become hormone-independent tumor with very low survival rate [1-3]. Glandular epithelial cells of the human prostate gland have ability to accumulate high level of zinc; two- to five-fold greater than the zinc level found in other tissues [4]. Prostate cells have the ability to accumulate high level of citrate to chelate

intracellular zinc, whereas other cells, in which 95% of zinc is mostly bound with macromolecules is in immobile form such as metalloenzymes, metalloproteins (such as Metallothioneins), nucleoproteins, and nucleic acids [5-8]. The accumulation of zinc causes inhibition of mitochondrial aconitase activity leading to inability of cells to oxidize citrate [9]. The problem of zinc deficiency in malignant cells can be treated using various delivery systems. In the search for new delivery systems, cell penetrating peptides (CPP) attracted attention due to their abilities for intracellular delivery of a wide range of molecules [10-12]. Novicidin (NVC) peptide is a promising delivery system candidate due to several properties such as cell penetrating abilities, low hemolytic effect, highly amphipathic alpha helix structure and high affinity to anionic lipids which are characteristic for cancer cells [13]. To carry the metal ion cargo, Schiff bases are organic compounds that have versatile biological properties. The type of metal and the complexity of Schiff base play a major role in the potency of these compounds as chemotherapeutic agents. Schiff bases bounded with metal ions interact directly with cellular membrane and cause oxidative stress damage. Binding of Schiff base-metal ion complex with other compound can neutralize this oxidative capability and allow delivery within the biological system [14,15].

Here we attempted to synthesize zinc delivery system that can increase the availability of zinc in PCa cells and to investigate the molecular changes that take place after the delivery of zinc complex system by studying genes involved in a zinc stress. This delivery system showed minor toxicity in normal PNT1A cells and high potency towards PC3 tumor cells shown by preference to penetrate PC3 cells in contrast to localized confinement to membranes of PNT1A. Further, the zinc uptake was confirmed in both cell lines. Molecular analysis was used to confirm the activation of zinc stress (e.g. ZnT-1) and apoptosis (e.g. CASP-1).

2. MATERIAL AND METHODS

Preparation of Schiff base (S)

(2-[(E)-2-pyridylmethyleneamino]-N-[2-[(E)-2-pyridylmethylene-amino]ethyl]ethanamine)

2-pyridinecarboxaldehyde (1902 μL) and diethylenetriamine (1080 μL) were stirred and heated under reflux in methanol (35 mL) for 6 h. Color turned to orange. After cooling, methanol was added to 50 mL.

Synthesis of Schiff base complex Zn-S

Zinc perchlorate hexahydrate (0.372 g) was dissolved in 50 mL of water and Schiff base S (5 mL) was added with stirring. Light orange solution was heated at 80 °C for 2 h. Solution was than filtrated and water was added to reach 100 mL.

Synthesis of NVC peptide

For synthesis, Liberty Blue peptide synthesizer was used (CEM, Matthews, NC, USA). The sequences and monoisotopic molecular weight of synthesized peptide were as follows: KNLRRIIRKGIHIIKKYF - 2296 Da.

Preparation of Zn-S-NVC

A stock solution of NVC peptide (1 mM) was mixed with Zn-S (1 mM) in 1:1 ratio. Final concentration of complex in PBS buffer was 1 mM. The sample was incubated for 60 min at 25 °C. After incubation, unbound Zn-S was removed using FPLC purification. For fractionation of complex, fluorescein fast protein liquid chromatography (FPLC) system Biologic DuoFlow (Bio-Rad, Philadelphia, PA, USA) was used.

3. RESULTS AND DISCUSSION

Several studies reported changes in the regulation of that MTs isoforms, zinc transport (ZnT), and tumor protein 53 (p53) in human prostate cells and tissues [16-19]. Western blot analysis showed absence of *p53* protein in PC3 cells. However, no visible differences were observed in *p53* protein expression in PNT1A (Figure 1 (A1)). In order to evaluate the effect of Zn-S-NVC complex delivery on prostate cancer cells, the gene expression in PC3 and PNT1A cells lines was assessed by quantitative RT-PCR method. Three independent experiments were carried out on 5 genes after treatment with Zn-S-NVC complex: *SP1, p53, MT-1X, MT-2A and ZnT-1*, as shown in Figure 1 (A2).

As shown in Figure 1 (A2), *p53* expression levels were increased by two folds in PNT1A cells after treatment and by five folds in PC3 cells after treatment. *SP1* transcription factor expression levels were relatively unchanged after treatment in both normal and tumor cells. Two MTs isoforms genes (*MT-1X and MT-2A*) showed variable expression levels with *MT-2A* expression levels of 2.2 folds more in treated PC3 cells when compared to treated PNT1A cells. Interestingly, the expression of zinc transporter *ZnT-1* was nearly two folds increased after treatment of both PNT1A and PC3 cells. Our results also show that p53 and not SP1 gene was activated by more than two folds, respectively, within 40 min of exposure to Zn-S-

NVC. PC3 cells have mutant p53 gene with 1bp deletion at codon 138 that produces a truncated protein due to formation of stop codon at position 169 via frame shift, which was undetected by the antibody we used (clone sc-126). As for PNT1A cells, no visible change in p53 protein level was observed after treatment with Zn-S-NVC. *p53* protein expression did not change in PNT1A cells and thus did not lead to apoptosis. Even though *p53* gene was activated at the mRNA level in our experiment, the activation of *p53* at the protein level is multistep post-translational modifications, where DNA binding and protein-protein interactions comprise stabilization, anti-repression and promoter specific transcriptional activation. Our results showed increased expression levels of ZnT-1 in both cell lines upon treatment. Unfortunately, the regulation mechanism of ZnT-1 is unclear, e.g. it is unclear whether this protein is hormone-responsive as ZIP1 transporter or not.

The employed DNA microarray consists of several oligonucleotide probes that have been immobilized on a solid glass support, and the technique used has great potential for the identification of closely related biomarker of cancer by employing oligonucleotides specific for each type of cancer. We used for this study a commercial chip (Human Cancer 3711 ElectraSense 4×2k array slides) from CombiMatrix (Custom Array, Bothell, WA, USA) to identify which cancer biomarkers are expressed in PC3 cells when they are treated with the Zn-S-NVC complex. In the present study, we show four different treatments: PNT1A (PNT1A cell line before treatment with Zn-S-NVC complex), PNT1A-Zn-S-NVC (PNT1A cell line after treatment with Zn-S-NVC complex), PC3 (PC3 cell line before treatment with Zn-S-NVC complex) and PC3-Zn-S-NVC (PC3 cell line after treatment with Zn-S-NVC complex). To understand the results, we show the fold ratio or relative expression of genes in all possible combination between treatments: Effect of Zn-S-NVC complex in PC3 cells (PC3-Zn-S-NVC vs PC3) and PNT1A cells (PNT1A-Zn-S-NVC vs PNT1A) and the global effect between PC3 and PNT1A cells after treatment with Zn-S-NVC complex (PC3-Zn-S-NVC vs PNT1A-Zn-S-NVC). Our control was variant PC3 vs PNT1A (before treatment with Zn-S-NVC) as verification of the cancer general genes expression and specific genes related to prostate cancer in our samples: The Figure 1B shows the specific genes up-regulation in PC3 cells when compared with PNT1A cells before treatment with Zn-S-NVC complex. Among them were shown: ADAM17 (ADAM metallopeptidase domain 17) gene, KLK13 (kallikrein-related peptidase 13) gene, BIRC5 (effector cell peptidase receptor 1, as an inhibitor of apoptosis) gene, CDKN1B (the cyclin-dependent kinase inhibitor p27Kip1) and CD47 (also known as integrin associated protein) gene. The most important and interesting comparison

was the global effect between PC3 and PNT1A cells after treatment with complex (PC3-Zn-S-NVC vs PNT1A-Zn-S-NVC). Moreover, this comparison showed over-expression in different genes with biological pathway on cell proliferation and cell differentiation (Figure 1C): GLS (glutaminase) gene and FGF3 (fibroblast growth factor 3) gene. Many genes responsible for negative regulation of cellular metabolic process and positive regulation of programed cell death were up-regulated (CASP1, NR4A3 and DNAJA1). These results give us an idea about the activation of genes that induce cell death or apoptosis in PC3 cell line after applying the Zn-S-NVC complex (Figure 1D). In our study it was obvious that PC3 cells after treatment with Zn-S-NVC complex (PC3-Zn-S-NVC vs PC3) and the global effect between PC3 and PNT1A after treatment with Zn-S-NVC complex (PC3-Zn-S-NVC vs PNT1A-Zn-S-NVC) suppressed cell proliferation. These results may be due to increasing gene expressions of CASP1 as shown in the Figure 1C. The up-regulation of CASP1 can be inducing for increasing of intracellular zinc in PC3 cells after treatment with Zn-S-NVC complex. Their activation during apoptosis is an important underlying theme in prostate cancer therapy and the importance of recent therapeutic strategies aimed at specifically targeting these proteases in relation to prostate cancer.

In addition, NR4A3 gene showed up-regulation in the global effect between PC3 and PNT1A cell lines after treatment with Zn-S-NVC complex (PC3-Zn-S-NVC vs PNT1A-Zn-S-NVC) (Figure 1C). Therefore, this over-expression of NR4A3 gene can be activated by the Zn-S-NVC complex in our PC3 cells. Also, the results from microarray in our samples showed over-expression of DNAJA1 gene in the global effect between PC3 and PNT1A cell lines after treatment with Zn-S-NVC (PC3-Zn-S-NVC vs PNT1A-Zn-S-NVC). DNAJA1 gene is important in the program of death cells. Therefore, we report the first information about the over-expression of this gene in PC3 cell line after treatment with the Zn-S-NVC complex. We also can assume that this gene induces apoptosis in prostate cancer cells. These microarrays results could shed some light on the genes and biomarkers involved in inducing cellular death in PC3 cell line after applying the Zn-S-NVC complex. The data strongly suggest that Zn-S-NVC complex can be used as potent inducer of apoptosis in prostate cancer cells, which have great potential to be developed into novel anticancer therapy.

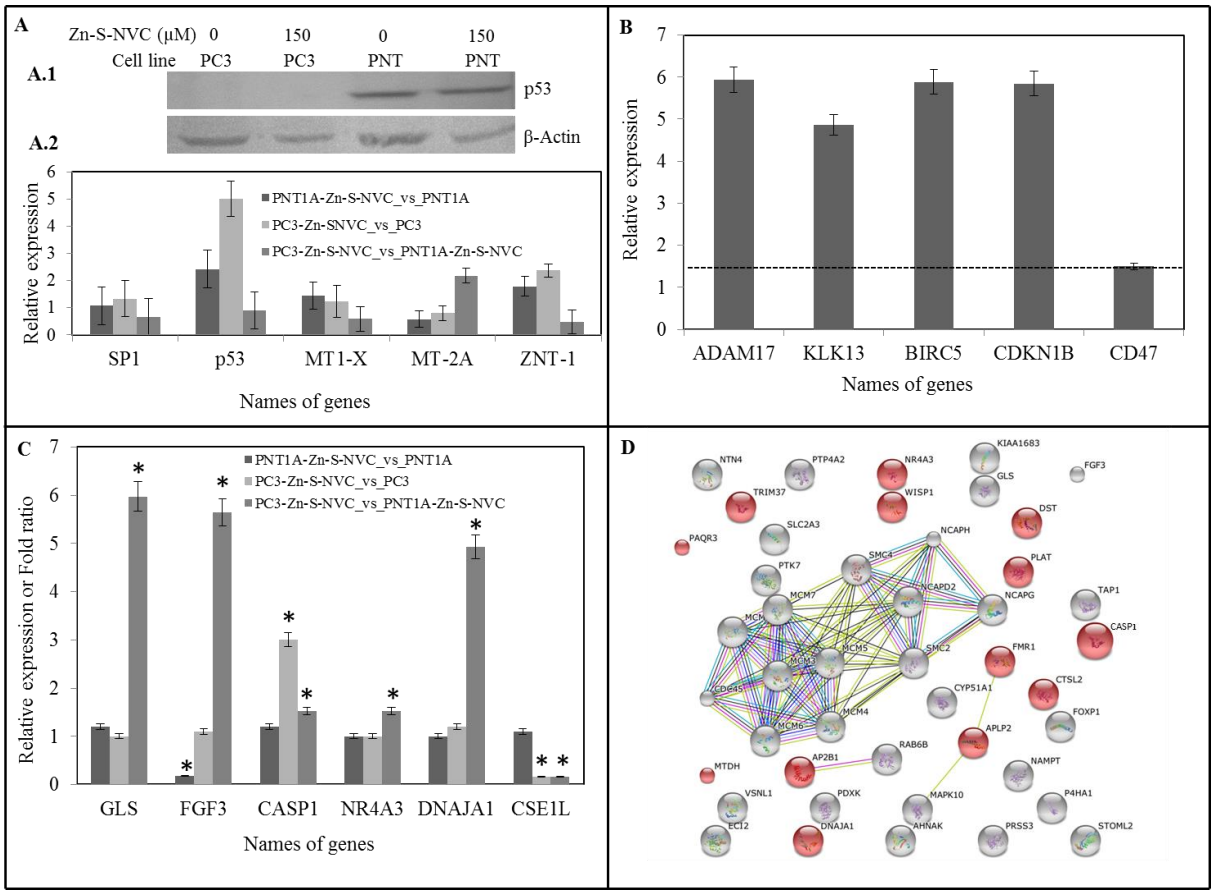

Figure 1.: A.1) Western blot of p53 protein expression is null in PC3 cells and unaffected in PNT1A cells line. Western blot analysis using anti-p53 (sc-126) after treatment with 150uM Zn-S-NVC complex for 40 min. Anti β-Actin (sc-130657) was used as internal control. A.2) Gene expression change in PC3 and PNT1A cells assessed by qRT-PCR. B) Relative expression genes or fold change in different treatments after appliqued Zn-S5-NVC complex in PC3 and PNT1A cells lines by ElectreSense CombiMatrix microarray. D) Diagram of up-regulation genes in the global effect between PC3 and PNT1A cells lines after treated with Zn-S-NVC complex by KEGG 10 software (Known and Predicted Protein-Protein Interactions). The red genes are genes inside of negative regulation of cellular processes (metabolic, cell death or apoptotic processes). Different line colors represent the types of evidence for the association (neighborhood, gene fusion, co-occurrence and co-expression).

4. CONCLUSION

Targeting the zinc metabolic pathway to induce apoptosis is a progressive field in prostate cancer therapy. Here, we investigated a novel drug delivery system composed of membrane penetrating peptide and Schiff base carrier of zinc. Targeting the zinc pathway in treatment of prostate cancer has been the interest of many researchers for the past decade. We believe that developing zinc delivery systems should be the next step for prostate cancer treatment. The versatility of cell penetrating peptides and Schiff bases allow for the development of highly selective and potent therapeutic compounds in the future. In the current study, a Novicidin

(NVC) conjugate with Schiff base zinc complex has been synthesized and evaluated for its apoptosis-inducing activities in human prostate cancer cells. We reported that this zinc complex can potently induce apoptosis in a dose- and time-dependent manner. Our study reinforces the idea that peptide carrying zinc compounds have great potential to be developed into novel anticancer drugs. This new complex was successfully tested for stability, biocompatibility, cancer specificity, potency and mechanism of action in PC3 cell line.

5. ACKNOWLEDGEMENT

The financial support from CEITEC CZ.1.05/1.1.00/02.0068 and GACR 16-18917S is highly acknowledged.

6. REFERENCES

[1] E. Francini, A. I. Fiaschi, R. Petrioli, L. Laera, V. Bianco, R. Ponchietti and G. Roviello, Anti-Cancer Drugs, 26 (2015) 884.
[2] J. S. de Bono, S. Oudard, M. Ozguroglu, S. Hansen, J.-P. Machiels, I. Kocak, G. Gravis, I. Bodrogi, M. J. Mackenzie, L. Shen, M. Roessner, S. Gupta, A. O. Sartor and T. Investigators, Lancet, 376 (2010) 1147.
[3] B. G. Redman and K. J. Pienta, Seminars in urology, 13 (1995) 164.
[4] M. F. Biancardi, F. C. A. Santos, L. Madi-Ravazzi, R. M. Goes, P. S. L. Vilamaior, S. L. Felisbino and S. R. Taboga, Anatomical Record-Advances in Integrative Anatomy and Evolutionary Biology, 293 (2010) 2163.
[5] D. J. Eide, Pflugers Archiv-European Journal of Physiology, 447 (2004) 796.
[6] N. Thi Hoa, U. Thi Dieu Thuy, V. Thi Hien, T. Thi Kim Chi, D. Van Quyen, D. Duy Khang and N. Quang Liem, Advances in Natural Sciences: Nanoscience and Nanotechnology, 3 (2012) 035014.
[7] S. R. Lee, S. J. Noh, J. R. Pronto, Y. J. Jeong, H. K. Kim, I. S. Song, Z. L. Xu, H. Y. Kwon, S. C. Kang, E. H. Sohn, K. S. Ko, B. D. Rhee, N. Kim and J. Han, Korean Journal of Physiology & Pharmacology, 19 (2015) 389.
[8] T. Kambe, A. Hashimoto and S. Fujimoto, Cellular and Molecular Life Sciences, 71 (2014) 3281.
[9] L. C. Costello and R. B. Franklin, Prostate, 35 (1998) 285.
[10] A. Floren, I. Maeger and U. Langel, in U. Langel (Editor), Cell-Penetrating Peptides: Methods and Protocols, 2011, p. 117.
[11] L. N. Johnson, S. M. Cashman and R. Kumar-Singh, Molecular Therapy, 16 (2008) 107.
[12] J. J. Turner, G. D. Ivanova, B. Verbeure, D. Williams, A. A. Arzumanov, S. Abes, B. Lebleu and M. J. Gait, Nucleic Acids Research, 33 (2005) 6837.
[13] J. Dorosz, Y. Gofman, S. Kolusheva, D. Otzen, N. Ben-Tal, N. C. Nielsen and R. Jelinek, Journal of Physical Chemistry B, 114 (2010) 11053.
[14] A. A. Osowole, G. A. Kolawole and O. E. Fagade, Journal of Coordination Chemistry, 61 (2008) 1046.
[15] N. M. Agh-Atabay, B. Dulger and F. Gucin, European Journal of Medicinal Chemistry, 40 (2005) 1096.
[16] M. Hasumi, K. Suzuki, H. Matsui, H. Koike, K. Ito and H. Yamanaka, Cancer Letters, 200 (2003) 187.
[17] N. Rivlin, R. Brosh, M. Oren and V. Rotter, Genes & cancer, 2 (2011) 466.
[18] S. Stelloo, E. Nevedomskaya, H. G. van der Poel, J. de Jong, G. van Leenders, G. Jenster, L. F. A. Wessels, A. M. Bergman and W. Zwart, Embo Molecular Medicine, 7 (2015) 1450.
[19] S. Krizkova, M. Ryvolova, J. Hrabeta, V. Adam, M. Stiborova, T. Eckschlager and R. Kizek, Drug Metabolism Reviews, 44 (2012) 287.

STUDDING OF QDS FLUORSCENCE QUENCHING EFFECT CAUSED BY COVALENT CONJUGATION WITH BSA

Jelena PEJOVIĆ [2*], Jana PEKÁRKOVÁ[1], Jaromír HUBÁLEK[1,2]

[1] *Department of Microelectronics, Brno University of Technology in Brno Technicka 3058/10, 616 Brno, Czech Republic*

[2] *Central European Institute of Technology, Brno University of Technology, Purkynova 123, 612 00 Brno, Czech Republic*

**jelena.pejovic@ceitec.vutbr.cz*

Abstract

Semiconductor nanocrystal, quantum dots (QDs), are nanoscale particles that have been attract a lot of attention due to their unique optic and electronic properties. One of the most important properties of QDs is their bioconjugation with different biological molecules such as a protein, peptides and nucleic acids. In this study, quenching effect of different concentration of BSA (bovine serum albumin) on fluorescence intensity of QDs was monitored. It was found that with increasing concentration of BSA fluorescence intensity of QDs is decreasing. This research can lead to a better understanding of interaction between different size QDs and biomolecules.

1. INTRODUCTION

QDs belong to family of inorganic nanoparticles and they are defined as semiconductors nanocrystals [1]. Their unique optical and electronic properties can be placed between those of bulk materials and isolated molecules of atoms [2]. QDs modified by BSA have been applied as ion sensors, fluorescence resonance energy transfer and chemiluminescence resonance energy transfer [3]. In last decade QDs find great application in medicine and biology usage, due to their photostability and resistance to chemical degradation [4]. However, the core of QDs created with inorganic elements is toxic for living systems and cells. Nowadays, concerning environment issues and toxic of QDs lot of improve environment- friendly technologies are used for synthesis of QDs as well as modification of their surface to make it less toxic for usage in medicine [5]. Even, these modified QDs bring doubts [6], and more research need to be done to investigate QDs and their bioconjugation.

Taking in consideration everything above, aim of this work is to use fast and simple method for investigate bonding between QDs and biomolecules. In this work conjugation of QDs with bovine serum albumin (BSA) was achieved via covalent coupling using different cross-linkers: carbolyldiimidazole (CDI), 1-ethyl-3-(3-dimethylaminopropyl), carboiimide hydrochloride (EDC), N-hydroxysulfosuccinimide (NHS/EDC). Fluorescence detection was used to study quenching effect of protein and QDs. It was found out that higher concentration of BSA led to a stronger quenching of fluorescence emission, which could be explained by the covalent interaction between the protein and QDs. In this work detection and separation of bioconjugated QDs was done in microfluidic system, using on chip electrophoresis and optical detection. By investigating interaction between different sized QDs and biomolecules this research can lead to a better understanding of how QDs behave in cell environment, which is extremely important for their biological application.

2. MATERIAL AND METHODS

Synthesis of CdTe QDs capped with MPA

To obtain CdTe-MPA QDs, $CdCl_2$ solution (91.6 mg) was diluted to 50 ml in one-necked flask and sodium citrate dihydrate (200 mg) was added followed by addition of MPA (52 µl). The pH of the solution was adjusted to 10.5 using NaOH (1 mol/l), followed by addition of Na_2TeO_3 (22.15 mg) and $NaBH_4$ (50 mg) under vigorous stirring. Solution was then refluxed at 95°C for 4 h [7].

Equipment

Capillary electrophoresis of QDs and QDs-protein conjugates was carried out using home built system “black box. The black box consists of the three parts: light source, sample holder and light detector. Excitation light is generated by ultraviolet light-emitting diode (UV LEDs) and filtered by optical 380 nm low pass filter. This light excites fluorescence of the sample and emitted light is selected by 560 nm high pass optical filter. This emitted light is detected by photodetector including photomultiplier.

3. RESULTS AND DISCUSSION

QDs and BSA were conjugated via covalent coupling using carboxyl groups of cross-linkers (CDI, EDC, and EDC/NHS). With increasing of concentration of BSA, fluorescence intensity

of QDs is decreasing. The fluorescence quenching of QDs by BSA can be described by the linear Stern-Volmer equation:

$$I_0/I = 1 + K_{sv}[Q] \quad (1)$$

where I_0 and I are the steady-state fluorescence intensities of QDs in the absence and presence of BSA, respectively. K_{SV} is the Stern-Volmer quenching constant, and [Q] is the concentration of BSA. The I_0/I ratio was calculated and plotted against BSA concentration as described in (1).

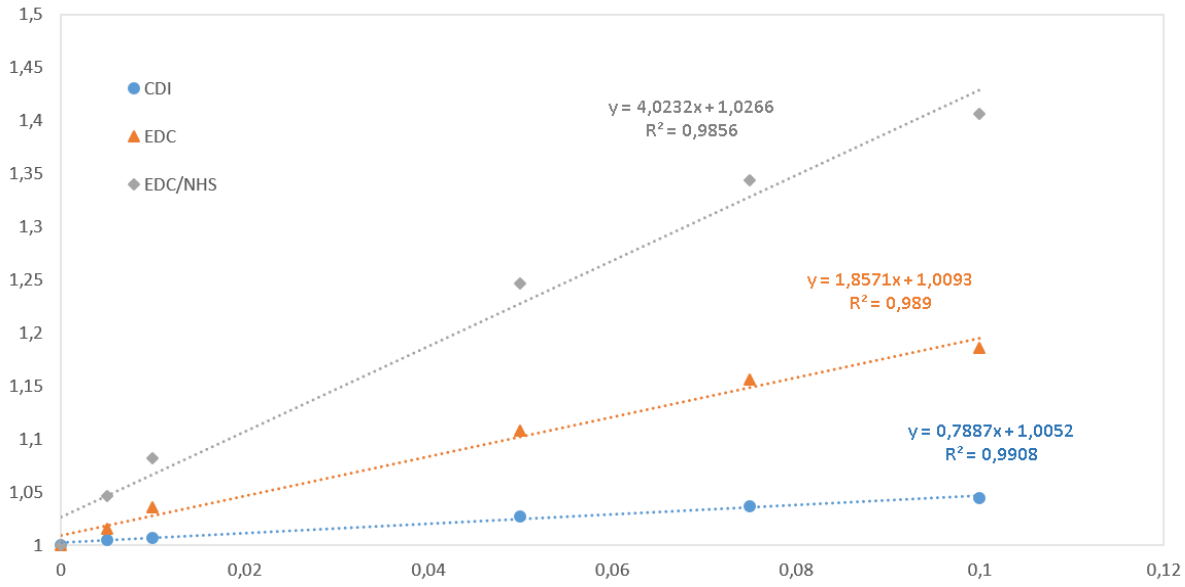

Figure 1.**:** Stern- Volmer plot of QDs quenching effect caused by CdTe QDs electrostatic conjugation with BSA

The slope of the curve represents the Stren-Volmer quenching constant (K_{sv}) and the higher K_{sv}, the higher the quenching effect is [8]. Stern- Volmer plot of all three cross-linkers quenching properties shown exhibiting linear trend. The results show that the quenching constant is different for different types of bioconjugated QDs. From Figure 1 it is obvious that in case where EDC/NHS is used as a cross-linker the fluorescence intensity is decreasing significantly, so the highest quenching effect was notable.

4. CONCLUSION

Water soluble CdTe QDs were prepared using a simple one step method. The present of BSA is leading to a strong quenching effect of fluorescence emission of QDs. Quenching effect depends of a cross linker we are using to conjugate protein and it was shown to be the highest

when using EDC/NHS. Overall, this simple, fast and not expensive method can be used as powerful tool to better understand interaction between biomolecules and QDs.

5. ACKNOWLEDGEMENT

The work has been supported by the SIX project; the registration number CZ.1.05/2.1.00/03.0072, the operational program Research and Development for Innovation and by Grant Agency of the Czech Republic under the contract GACR 102/13-20303P.

6. REFERENCES

[1] Mattoussi, H., G. Palui, and H.B. Na, Luminescent quantum dots as platforms for probing in vitro and in vivo biological processes. Advanced Drug Delivery Reviews, 2012. 64(2): p. 138-166.
[2] Tomczak, N., et al., Designer polymer-quantum dot architectures. Progress in Polymer Science, 2009. 34(5): p. 393-430.
[3] Liang, J., Y. Cheng, and H. Han, Study on the interaction between bovine serum albumin and CdTe quantum dots with spectroscopic techniques. Journal of Molecular Structure, 2008. 892(1–3): p. 116-120.
[4] Byers, R.J. and E.R. Hitchman, Quantum Dots Brighten Biological Imaging. Progress in Histochemistry and Cytochemistry, 2011. 45(4): p. 201-237.
[5] Jha, R.K., et al., An emerging interface between life science and nanotechnology: present status and prospects of reproductive healthcare aided by nano-biotechnology. 2014, 2014.
[6] Morelli, E., et al., Chemical stability of CdSe quantum dots in seawater and their effects on a marine microalga. Aquatic Toxicology, 2012. 122: p. 153-162.
[7] Mihajlovic, A., Synthesis of core/shell quantum dots for diagnostics. Brno: Brno University of Technology, The Faculty of Electrical Engineering and Com-munication, 2014: p. 88.
[8] Ryvolova, M., et al., Glutathione modified CdTe quantum dots as a label for studying DNA interactions with platinum based cytostatics. Electrophoresis, 2013. 34(6): p. 801-808.

SYNTHESIS OF SILVER NANOPARTICLES AS ANTIMICROBIAL COATING FOR ION EXCHANGE MEMBRANE

Evelína POLIEVKOVÁ[1], Jana DRBOHLAVOVÁ[1*], Jaromír HUBÁLEK[1,]

[1] *Central European Institute of Technology, Brno University of Technology, Technická 3058/10, 616 00 Brno, Czech Republic*

**jana.drbohlavova@ceitec.vutbr.cz*

Abstract

This paper deals with synthesis of antimicrobial silver nanoparticles which will be immobilized onto commercial polymeric membrane utilized in food industry. This work summarizes the fundamental part of research: the synthesis of silver nanoparticles employing UV radiation with three different wavelengths. It was investigated how different wavelengths can affect the final properties of Ag NPs, mostly their size, shape and stability.

1. INTRODUCTION

Silver nanoparticles (further denoted as Ag NPs) recently have been used for antimicrobial purposes not just in science or medicine but also in commercial sphere [1]. Silver-based materials are significantly toxic to microorganisms; exactly to 16 major species of bacteria including *E.coli*. Silver is usually used in its nitrate form to originate antimicrobial effect but in the case of using Ag NPs the available surface area exposed to microbes increases very rapidly [2, 3]. This antibacterial effect is very closely related with Ag NPs size; general postulate is that the smaller is the silver nuclei, the higher is antibacterial activity, see Figure 1 which shows the mechanism of antibacterial activity [4].

UV-induced synthesis seems to be very efficient route how to prepare Ag NPs with exact physical properties for concrete application. This paper presents an innovative synthesis of Ag NPs via UV-assisted chemical reduction. Utilization of different wavelengths can significantly affect size and shape distribution of colloidal Ag NPs. These Ag NPs will be used as antimicrobial substances for commercial polymeric membranes used in food industry for desalination of milk and whey in cooperation with company MemBrain, ltd. These membranes suffer during desalination process from contamination with bacteria, namely above mentioned strain *E.coli*, which damage and congest membrane pores and subsequently debase not only membranes but also desalination process.

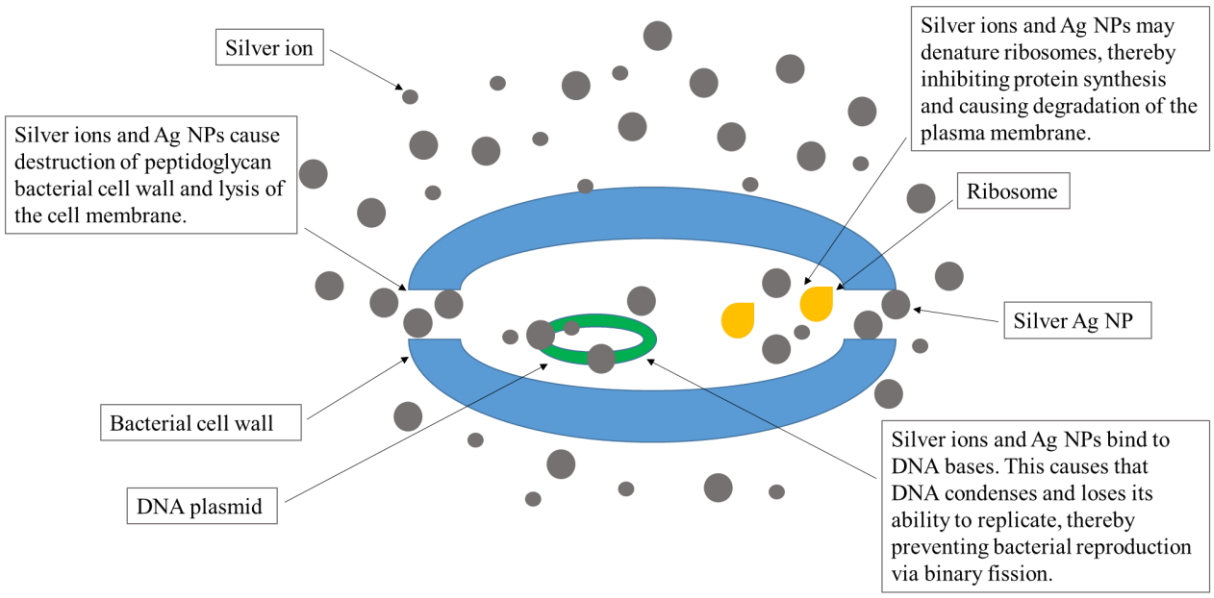

Figure 1.: Mechanism of antibacterial activity of Ag NPs

2. MATERIAL AND METHODS

Materials:

- silver nitrate (p.a.) – precursor of silver ions (Penta),
- sodium citrate dihydrate (p.a.) – reducing and stabilizing agent (Sigma-Aldrich),
- hydrazine hydrate (p.a.) – reducing agent (Aldrich),
- deionized water (resistivity of 18.2 MΩ·cm) was used to prepare all aqueous substances of reaction.

Ag NPs were prepared via chemical reduction according to Guzmán et al. with modified vol-umes of reagents and conditions [5]. Scheme of this process is shown in Figure 2. Reaction time was 1 h and preparation process was carried out at temperature of 22–24 °C. UV lamp was placed above a beaker in the distance of 1.5 cm from the top of the beaker. The beaker with aqueous solution of silver nitrate was placed on magnetic stirrer under 200 rpm. After that the aqueous

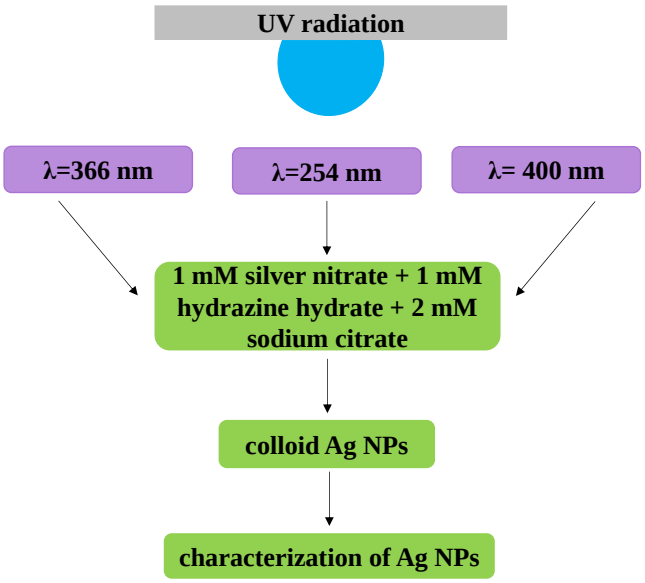

Figure 2.: Preparation process of Ag NPs

solutions of reducing agents were added to silver nitrate at the same time. The colour of reaction solution changed after 1 min after adding reducing substances into light orange which indicates the formation of Ag NPs in solution.

Colloid samples of Ag NPs were purified 3 times with deionized water via centrifugation at 14 500 rpm for 30 min. Ag NPs were dispersed in ultrasound water bath (power of 100%, temperature of 24 °C) for 5 min after purification process. Colloidal Ag NPs were stored in dark bottles in fridge.

3. RESULTS AND DISCUSSION

As prepared Ag NPs were characterized by scanning electron microscopy (SEM) on Lyra3 XMH to determine their morphology (shape, size, aggregation). UV-VIS spectroscopy (absorbance) was provided on Spectronic Helios Alfa spectrophotometer.

Figure 3 shows SEM analysis of samples A (λ_1 = 366 nm), B (λ_2 = 254 nm) and C (λ_3 = 400 nm). Sample A shows bigger Ag NPs with anisotropic shape and smaller nearly spherical Ag NPs. Sample B shows smaller Ag NPs than in previous case with mostly rounded shape. Ag NPs of sample C show smaller spherical and bigger rounded Ag NPs. It is probably due to the temperature. Intensity of UV radiation with wavelength of 400 nm was much higher than in case of samples A and B. It could cause some resonance which increased the temperature and affected shape of Ag NPs.

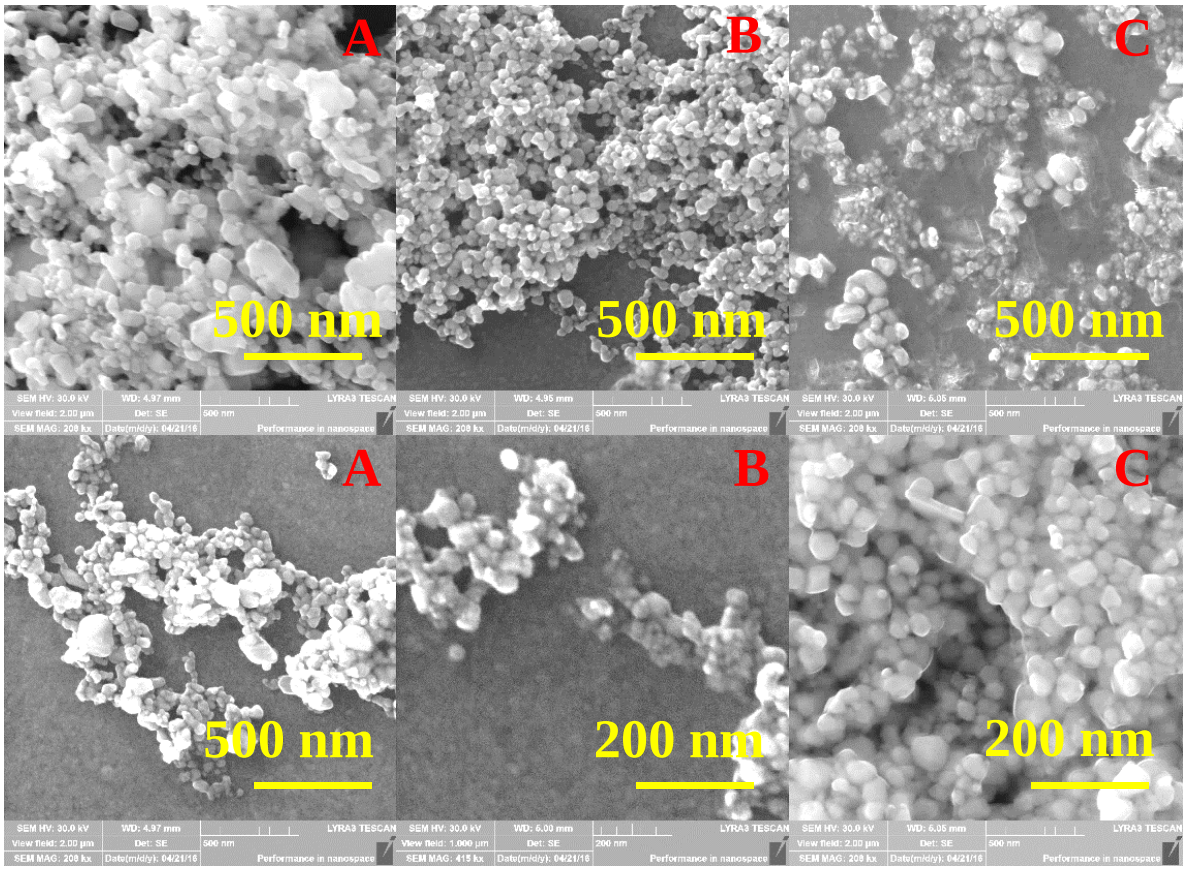

Figure 3.: SEM images of Ag NPs- samples A, B and C

Absorption spectra of samples A, B and C are shown in Figure 4. All samples have typical absorption maximum of SPR at wavelength of 420 nm. The stability was 3 weeks for each sample. The absorption spectra of samples A and B are very similar with little difference that sample A shows higher intensity of SPR. Absorption spectrum of sample C has the highest intensity and exhibit also second absorption peak at longer wavelengths which is probably caused by aggregates or bigger Ag NPs.

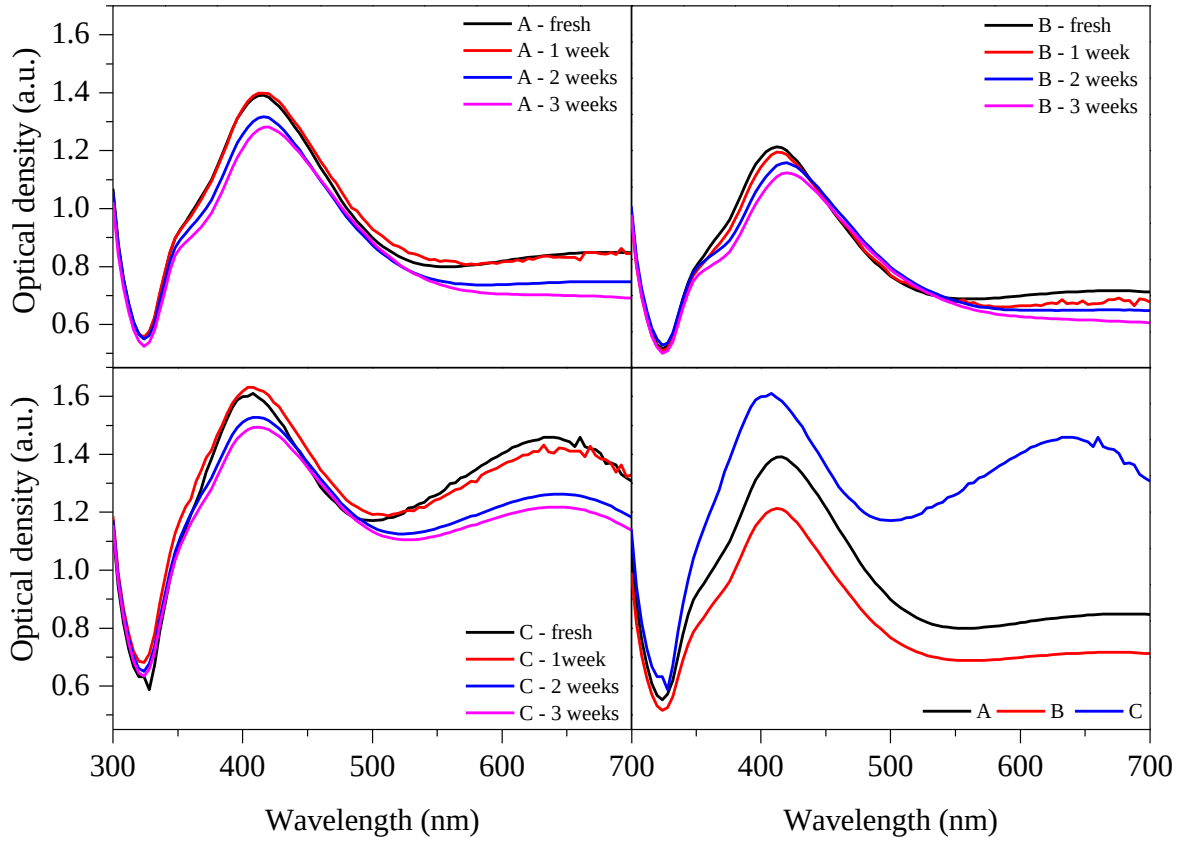

Figure 4.: Absorption spectra of Ag NPs-samples A, B, C and their comparison

4. CONCLUSION

Ag NPs were prepared via UV-assisted chemical reduction. It was demonstrated that different wavelengths of UV radiation significantly affected both the shape and the size of final Ag NPs in colloidal solution. General postulate is that the shorter is the wavelength, the more spherical shape of nanoparticles can be obtained. The longer is the wavelength, the more anisotropic shape of nanoparticles can be observed. Photoinduced synthesis of Ag NPs seems to be very easy and efficient way how to tune the size and the shape of Ag NPs in colloidal solution according to desired application.

5. ACKNOWLEDGEMENT

This paper was supported by IGA FEKT/STI-J-16-3625 research grant.

6. REFERENCES

[1] Tran QH, Le A-T: Advances in Natural Sciences: Nanoscience and Nanotechnology, 4 (2013), 3, 033001
[2] Sharma VK, Yngard RA, Lin Y: Advances in Colloid and Interface Science, 145 (2009), 1-2, 83-96
[3] Zain NM, Stapley AGF, Shama G: Carbohydrate Polymers, 112 (2014), 0, 195-202
[4] Kim JS, Kuk E, Yu KN, et al.: Nanomedicine-Nanotechnology Biology and Medicine, 10 (2014), 5, 1119-1119
[5] Guzmán MG, Dille J, Godet S: Int J Chem Biomol Eng, 2 (2009), 3, 104-111

STRUCTURAL AND THERMODYNAMIC PROPERTIES OF THE QUADRUPLEX IN THE PROMOTER OF THE POU5F1 GENE

Daniel RENČIUK[1], Iva KEJNOVSKÁ[1], Lukáš TRANTÍREK[2], Michaela VORLÍČKOVÁ[1*]

[1] *Department of CD spectroscopy of nucleic acids, Institute of Biophysics, v.v.i., Academy of Sciences of the Czech Republic, Kralovoplska 135, 612 65 Brno, Czech Republic*

[2] *CEITEC – Central European Institute of Technology, Masaryk University, Kamenice 5, 625 00 Brno, Czech Republic*

**mifi@ibp.cz*

Abstract

The pou5f1 gene codes the key regulator of cellular pluripotency, the POU5F1 protein. In close proximity to the transcription start site, the pou5f1 gene has in its promoter, a very strong potential quadruplex-forming site (PQS). This site is highly conserved in all mammalian species. We found that this motif forms a stable parallel-stranded quadruplex in physiological buffer; the structural and thermodynamic properties of the quadruplex are presented, as well as the effect of buffer composition, single- and double-stranded overhangs, point mutations and the effect of quadruplex-specific ligand N-methyl mesoporphyrin IX.

1. INTRODUCTION

The POU5F1 protein (also called Oct4) is a member of the POU family of transcription factors. It plays a major role in the formation and regulation of pluripotent embryonic stem (ES) cells (1). Pou5f1 gene is active during early embryogenesis but during gastrulation, its expression is irreversibly silenced in all cells except the germ line (2). Owing to its function, the expression of pou5f1 has to be tightly regulated. In humans, the pou5f1 gene is located on chromosome 6. The gene expression depends on a promoter region, proximal and distal enhancer and the activity of the enhancers is tissue specific. Comparative analysis of the pou5f1 gene promoter sequences in humans, mouse and cow showed that there are four conserved guanine-rich regions (3). The first region contains a guanine rich sequence with characteristics of a potential guanine quadruplex forming site (PQS) close to the transcription start site (TSS).

Guanine quadruplexes are DNA secondary structures formed by guanine rich DNA. They are based on the so-called guanine tetrad, formed by four guanines arranged in a square by eight Hoogsteen bonds with a central hole. Such tetrads tend to stack over each other to form a

quadruplex core (4). The central hole usually accommodates a monovalent cation, typically potassium, which electrostatically compensates the negative charges of guanine oxygen atoms. It was shown that the PQSs are frequently located all over the genome (5), with accumulation at specific positions in genes, especially in promoters upstream of TSS (6). Many genes, preferentially transcription factors, have been described as having a PQS in their promoter regions (7). The mechanisms of quadruplex-mediated transcription regulation are still unclear.

2. MATERIAL AND METHODS

CD spectra were taken on a J-815 dichrograph (Jasco, Japan) between 330 and 210 nm with data pitch 0.5 nm and D.I.T. 0.25 s at 200 $nm.min^{-1}$ scan speed averaging four accumulations.

UV absorption spectra and melting experiments were conducted on a Varian Cary 4000 UV/Vis spectrophotometer, where two temperature ramps ranging from 98°C to 8°C and 8°C to 98°C, respectively, in 1°C steps at scan rate around $0.25°C.min^{-1}$ were taken.

Non-denaturing PAGE electrophoresis was performed in a 16 % PAA gels containing the proper salt concentration and run at 40 V and 23 °C for 16 hours.

Chemical and enzymatic probing was performed using dimethyl sulphate and P1 nuclease, respectively, in selected buffers, using 5'-terminally radio-labelled oligonucleotides.

The 1D 1H NMR spectra were measured at 700 MHz Bruker Avance III NMR spectrometer equipped with a room temperature probe using the WATERGATE pulse sequence.

3. RESULTS AND DISCUSSION

Based on electronic circular dichroism (CD), 1H NMR and UV absorption spectroscopy, we found that this motif, represented by short synthetic oligonucleotides, forms in potassium-containing buffer a parallel-stranded quadruplex of a substantial thermal stability.

Chemical and enzymatic footprinting revealed that the quadruplex is formed in the same place even when the oligonucleotide is embedded in long single- or double-stranded DNA; neither the structure nor the stability of the quadruplex are significantly affected by neighbouring sequences.

Mutational analysis revealed that single G/A point mutation in the central G of any G_n block within the PQS cannot prevent the formation of the quadruplex; the resulting quadruplex structure is altered and the thermodynamic stability is lower, but still relevant under physiological conditions.

The known quadruplex-stabilizing ligand N-methyl mesoporphyrin IX increases the Tm of the wild-type quadruplex, as well as of the single G/A mutants by around 13°C.

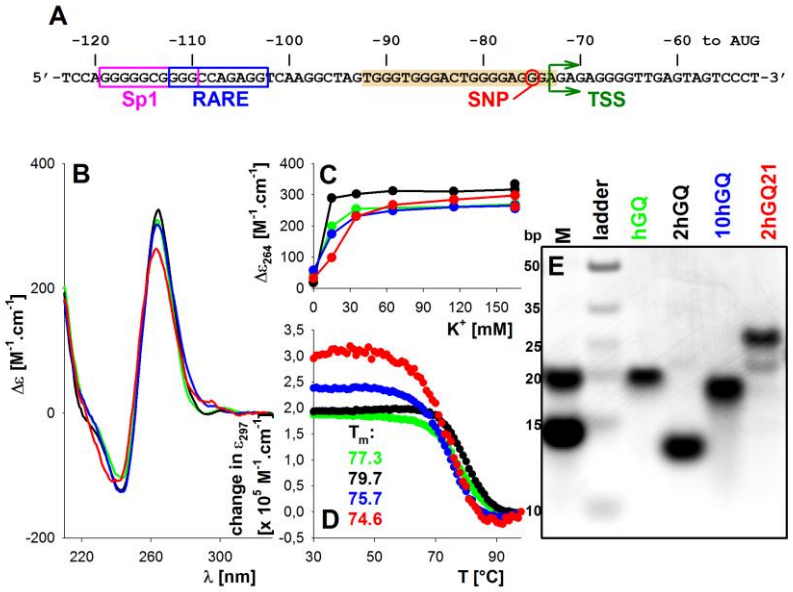

Figure 1.: Sequence of the PQS motif in the pou5f1 promoter (A), CD spectra (B), Δε264 vs K^+ conc. plot (C), UV melting curves recorded at 297 nm (D) and native PAGE (E) of various quadruplex-forming fragments.

4. CONCLUSION

We characterized the quadruplex in the promoter of the pou5f1 gene: the respective sequence forms very stable parallel-type quadruplex, which is not affected by the surrounding sequences independently of their nature. We also showed that the quadruplex is highly resistant towards destabilization by point mutations.

5. ACKNOWLEDGEMENT

The study was supported by Grant Agency of the Czech Republic grants 14-33947P, P205/12/0466, 13-28310S, European Social Fund and the state budget of the Czech Republic, under project Postdoc II [CZ.1.07/2.3.00/30.0037].

6. REFERENCES

[1] Nichols, J., Zevnik, B., Anastassiadis, K.,et al.: Cell, 95 (1998), 379-391
[2] Hattori, N., Nishino, K., Ko, Y. G., et al.: J. Biol. Chem., 279 (2004), 17063-17069
[3] Nordhoff, V., Hubner, K., Bauer, A., et al.: Mamm. Genome, 12 (2001), 309-317
[4] Neidle, S., and Balasubramanian, S. (2006) Quadruplex Nucleic Acids, London, Cambridge
[5] Todd, A. K., Johnston, M., and Neidle, S.: Nucleic Acids Res., 33 (2005), 2901-2907
[6] Maizels, N., and Gray, L. T.: PloS Genetics, (2013), 10.1371/journal.pgen.1003468
[7] Brooks, T. A., Kendrick, S., and Hurley, L.: FEBS J., 277 (2010), 3459-3469

ELECTROCHEMICAL DEPOSITION OF GOLD NANORODS FOR VOCS SENSING

Milena ŠETKA[1], Jana DRBOHLAVOVÁ[1*,2], Radim HRDÝ[1,2]

[1] *Central European Institute of Technology, Brno University of Technology, Purkyňova 123, 612 00 Brno, Czech Republic*

[2] *Department of Microelectronics, Faculty of Electrical Engineering and Communication, Brno University of Technology, Technická 3058/10, 616 00 Brno, Czech Republic*

** jana.drbohlavova@ceitec.vutbr.cz*

Abstract

Gold nanostructures have attracted great attention due to their potential application in chemical and biochemical sensing, such as detection of volatile organic compounds (VOCs), medical diagnostics and therapeutics, and biological imaging because of their unique optical and electrical properties [1]. This work describes a developing of gold nanorods by electrochemical anodization and electrochemical deposition. The anodization voltage together with the current density and the electrolyte type are recognized as the most critical parameters to control the pore geometry [2].

1. INTRODUCTION

Gas sensors based on gold nanostructures have high sensitivity and selectivity, good reproducibility and long-term stability [3]. Gold nanoparticles covered with thiols are used like sensitive layer in chemiresistive sensors for detection of VOCs. VOCs have been found as significant biomarkers in exhaled breath, which reflect the biochemical alterations related to metabolic changes, which are helpful in diagnosis and monitoring of various diseases [4]. Those kind of sensors have a very high sensitivity, from tens of ppb to hundreds of ppm, with a detection limit of 1–5 ppb. They show a low sensitivity to water and it is particularly suitable for breath testing, which is an advantage since the exhaled breath contains ~ 80% relative humidity [5]. Lee et al. developed VOCs gas sensors based on metal-organic framework of gold–polypyrrole (Au–Ppy) nanorods via an electrochemical deposition. This gas sensor operates on the principle of localized surface plasmon resonance and it shows a good stability and high sensitivity up to 10 ppm of target VOCs gases [6]. Nanostructures can be synthesized by wet-chemical synthesis or fabricated by templates such as nanoporous alumina template. It can be prepared by electrochemical anodization of aluminium, which

allows to produce uniform pores with the diameter as small as 5 nm [7]. An electrochemical deposition of metal into pores leads to the growth of metal nanorods and nanowires [8].

2. MATERIAL AND METHODS

Electrochemical preparation of nanostructured surface

The silicon wafer was covered by layers of: SiO_2 (thickness of 1 μm), titanium (20 nm), tungsten (150 nm), and aluminium (300 nm). The aluminium layer was transformed by anodic oxidation to nanoporous alumina template (Al_2O_3). The anodization process was done as described in the following paper [9], under constant voltage, either at 53 V in 0.3 M oxalic acid or at 20 V in 2 M sulphuric acid. The gold was electrodeposited from potassium dicyanoaurate solution into the alumina oxide template with the nanodimpled bottom. The conditions were set up during this process as follows: the constant current of 1 mA, the pulse length of 400 ms, the period between pulses of 2 s, the amplitude of 5 V, and the number of pulses 45. The etching of WO_3 nanstructures was done in the phosphate buffer solution at pH= 7. The alumina template was selectively dissolved in the mixture of chromium trioxide and phosphoric acid.

3. RESULTS AND DISCUSSION

In 0.3 M oxalic acid and at applied voltage of 53 V was obtained the nanopores with the pore diameter of about 50–60 nm. In 2 M sulphuric acid and at applied voltage of 20 V, the nanopores have the size of pores of around 25 nm, see Figure 1. These results confirmed the very well–known theory, the anodization voltage and the electrolyte type are the most important parameters to control the pore geometry of the alumina nanoporous template.

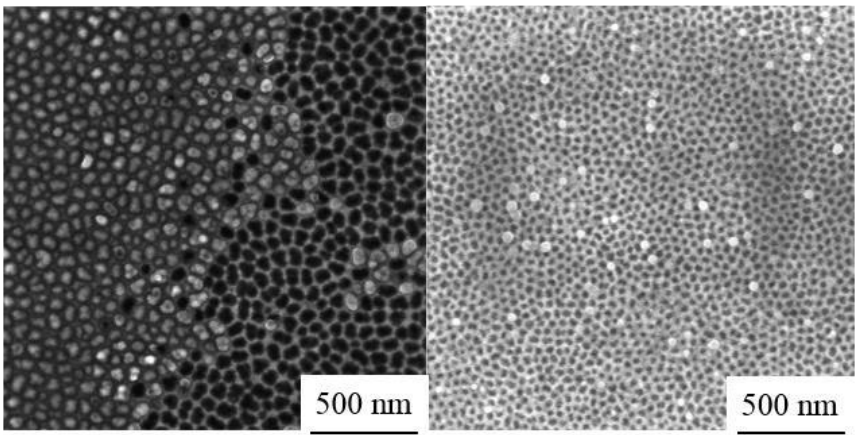

Figure 1.: SEM images of template after etching of WO3 and Al2O3 nanostructures, anodized in: 3 M oxalic acid at applied voltage of 53 V (left) and 2 M sulphuric acid at applied voltage of 20 V (right).

The electrochemical deposition of gold into nanoporous alumina template was successfully done under above mentioned conditions. It was possible to obtain gold nanorods with the uniform size, the diameter of ~ 50–60 nm, see Figure 2.

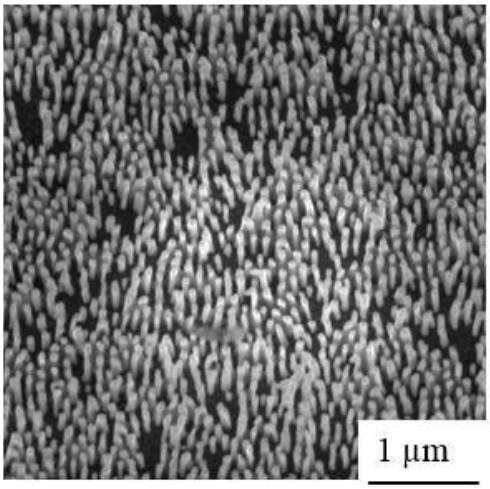

Figure 2.: SEM image of gold nanorods prepared via electrochemical deposition.

4. CONCLUSION

In summary, this work has demonstrated the preparation of nanoporous alumina template via electrochemical anodization of aluminium, and successfully synthesized gold nanorods via gold pulse deposition into the template. Sulphuric acid comparing to oxalic acid greatly decreased the pore diameter of nanoporous alumina template. With the rapid developments in nanorods preparation, surface modification, and assembly, the emergence of novel applications of gold nanorods are likely to impact the areas of VOCs sensing.

5. REFERENCES

[1] Lee K-S, El-Sayed MA: Journal of Physical Chemistry B, 110 (2006), 39, 19220-19225
[2] Drake C, Deshpande S, Bera D, et al.: Int. Mater. Rev., 52 (2007), 5, 289-317
[3] Zanoli LM, D'Agata R, Spoto G: Analytical and Bioanalytical Chemistry, 402 (2012), 5, 1759-1771
[4] Mazzatenta A, Pokorski M, Sartucci F, et al.: Respiratory Physiology & Neurobiology, 209 (2015), 81-84
[5] Peng G, Tisch U, Adams O, et al.: Nat Nano, 4 (2009), 10, 669-673
[6] Lee J-S, Yoon N-R, Kang B-H, et al.: Journal of Nanoscience and Nanotechnology, 15 (2015), 10, 7738-7742
[7] Martin CR: Chemistry of Materials, 8 (1996), 8, 1739-1746
[8] Vigderman L, Khanal BP, Zubarev ER: Advanced Materials, 24 (2012), 36, 4811-4841
[9] Hrdy R, Kynclova H, Drbohlavova J, et al.: International Journal of Electrochemical Science, 8 (2013), 4, 4384-4396

THE EFFECT OF WATER CONTAMINATED BY HEAVY METALS ON *TRAMETES VERSICOLOR*

Martina VRSANSKA[1*], Stanislava VOBERKOVA[1], Zuzana KOUDELKOVA[1], Vojtech ADAM[1]

[1] *Department of Chemistry and Biochemistry, Faculty of Agronomy, Mendel University in Brno, Zemedelska 1, 613 00 Brno, Czech Republic*

**martina.vrsanska@.mendelu.cz*

Abstract

The present study investigated the effect of two different types of water contaminated by the heavy metals on white-rot basidiomycetous fungus *Trametes versicolor*. This fungus is useful due to efficient and complex ligninolytic enzyme system, which is able to degrade wide variety of recalcitrant compounds (heavy metals), which cause environmental problems. Electrochemical *pulse voltammetry* at a hanging-*mercury-drop* electrode (HMDE) was used for the determination of metals in various types of water and laccase activity using ABTS as substrate was measured. The results collectively suggest that *T. versicolor* can be use as suitable candidate in the processes of bioremediation and detoxification.

1. INTRODUCTION

Fungi are known as biosorbents of heavy metals, which can be useful for the processes of bioremediation and detoxification of heavy metal from wastewater. Recently, there has been much interest in white-rot fungi (WRF) due to their unique capacity to degrade wastewater pollutants [1].

The white-rot fungus *Trametes sp.* is able to degrade recalcitrant biopolymers and wide range of pollutants due to their extracellular ligninolytic enzyme system [2]. Laccase (Lac, E.C. 1.10.3.2) has become important, industrially relevant ligninolytic enzyme that can be used for a number of diverse applications, including biocatalytic purposes or bioremediation applications [3]. Heavy metals in general are potent inhibitors of enzymatic reactions and from this point of view their concentration plays very important role. Usually the metals start to be toxic in concentration only a few times greater than those required [4].

Accumulation of metals by fungi has been known for a few decades and a number of works describing metal content in fruit bodies collected in different areas have been published. Some

WRF are known to have the ability to accumulate toxic elements such arsenic, cadmium or lead from the environment [5].

2. MATERIAL AND METHODS

Wastewater characterisation and determination of heavy metals

Two types of water were used for this experiment. Water 1 is chemically pre-treated water containing Cu (0.256 mg / l) and Ni (1.248 mg / l) and Water 2 is mine water from shaft from site Dolní Rožínka (water with increased content of P, Sr and Te).

Determination of nickel and cooper by differential pulse voltammetry were performed with 797 VA Computrace instrument connected to 813 Compact Autosampler (Metrohm, Switzerland), using a standard cell with three electrodes. 797 VA Computrace software by Metrohm was employed for data processing.

Fungal strain and culture conditions

Fungal strain *T. versicolor* obtained from the Culture Collection of the Faculty of Forestry and Wood Technology of the Mendel University in Brno (Czech Republic) was used in this study. This strain was cultivated on the growth medium consisted of 25 ml tested water, 75 ml distilled water and 25 ml potato dextrose agar (PDA) for 10 days at 22°C. Three agar plugs were used to inoculate static liquid cultures (25 ml tested water, 75 ml distilled water and 25 ml Potato Dextrose Broth (PDB)) and cultures were incubated at 22°C in dark. Laccase activity was determined periodically.

Enzyme assay

The enzyme activity was determined spectrophotometrically using a UV/VIS Lambda 25 Spectrophotometer (Perkin-Elmer) at 415 nm by detecting the oxidation of 2,2-azino-bis-[3-ethyltiazoline-6-sulfonate] (ABTS).

3. RESULTS AND DISCUSSION

The effect of heavy metals from wastewater on the fungal growth and laccase activity

Many studies regarding *Trametes* strains and their enzyme activity have been extensively conducted [4-7] and genus *Trametes* is assumed to be one of the main producer of laccase. Therefore this strain appears to be a suitable candidate for testing the effects of heavy metals on fungal growth and enzyme activity. Laccase activity of *T. versicolor* cultivated in PDB

medium without tested water was measured in this study and results showed that the highest activity was observed after 4 days of cultivation (Figure 1).

To establish the toxicity of different metal ions, the wood-rotting basidiomycete *T. versicolor* was cultivated in the presence of heavy metals contained in water. We found that high concentration of mercury, cadmium and cobalt in Water 1 is the most toxic for *T. versicolor*. These elements probably caused inhibition of growth and laccase activity. These results are comparable with the study of Sanglimsuwan et al. [6]. It also agrees with work of Baldrian and Gabriel [7], who also studied effect of heavy metals on white rot fungi and mercury seemed to be inhibitor of growth. In other hand, low concentration of mercury, cobalt and cadmium and higher concentration of copper and manganese, known as inducers of laccase activity [4], which contains Water 2, caused the growth and higher activity of fungus and minor inhibition effect.

Our results indicated that *Trametes sp.* seems to be potential biosorbent of heavy metals from wastewater. The different concentration of heavy metals (Table 1) plays important role on laccase activity.

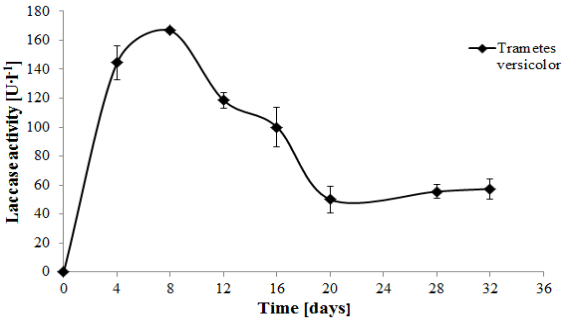

Figure 1.: Laccase activity of *T. versicolor* in PDB medium

Table 1.: Element composition of wastewater 1 and 2

Elements [%]	Mg	Al	Si	P	S	Cl	K	Ca	Ti	V	Cr	Mn	Fe	Co	Ni	Cu	Zn
Water 1	7	2.13	0.007	0.7859	52.96	20.5	1.66	14.6	0.002	0.0026	0.004	0.008	0.032	0.0015	0.004	0.0007	0.0001
Water 2	7.25	1.65	0.007	0.9999	56.8	3.6	2.54	26.3	0.003	0.0018	0.004	0.026	0.593	0.0015	0.006	0.0017	0.0089

Ga	Ge	As	Se	Br	Rb	Sr	Y	Zr	Nb	Mo	Ag	Cd	In	Sn
0.0002	0.00015	0.0001	0.0001	0.0476	0.0003	0.0852	0.0001	0.11	0.0008	0.005	0.004	0.0011	0.0007	0.00079
0.0002	0.00014	0.0024	0.0001	0.0007	0.0009	0.1065	0.0004	0.06	0.0013	0.004	0.003	0.0006	0.0006	0.00061

Te	I	Cs	Ba	La	Ce	Hf	Ta	W	Hg	Tl	Pb	Bi	Th	U
0.0158	0.0028	0.0034	0.005	0.0045	0.0096	0.0006	0.0048	0.00041	0.006	0.00021	0.0002	0.0003	0.0004	0.0007
0.0099	0.002	0.0024	0.004	0.0026	0.0059	0.00059	0.00255	0.00093	0.0002	0.00023	0.0002	0.0002	0.0003	0.0076

4. CONCLUSION

Monitoring of heavy metals content in different types of water and observation of their effect on fungal strain is presented in this paper. Using *T. versicolor* as biosorbent of heavy metals is an attractive alternative to existing methods due to good performance and low cost of biosorbent material, because the removal of heavy metals from wastewater through environment friendly low cost technology before its use in agriculture or discharge into water bodies is necessary.

5. ACKNOWLEDGEMENT

This work was particularly supported by the Specific Research program at the Mendel University in Brno.

6. REFERENCES

[1] Rodríguez-Rodrígueza CE, Jelic A, Llorca M, et all.: Bioresource Technology, 102 (2011), 10, 5602-5608
[2] Tisma M, Zelic B, Vasic-Racki D.: Croatian Journal Food Science and Technology, (2010), 34-47.
[3] Gianfreda L, Xu F, Bollag JM: Journal of Environmental Quality, 32 (1999), 1, 63-69
[4] Baldrian P: Enzyme and Microbial Technology, 32 (2003), 78-91
[5] Stijve T, Bourqui B: Deutsche Lebensmittel-Rundschau, 87 (1991), 307-310
[6] Sanglimsuwan S, Naoto Y, Tsutomu M, Yoshikatsu M: Journal of Fermentation and Bioengineering, 75 (1993), 2, 112-114
[7] Baldrian P, Gabriel J, et all.: Environmental Contamination and Toxicology, 59 (1997), 595-602

EFFECT OF HYALURONAN ON DIFFUSION PROPERTIES OF ARTIFICIAL CELL MEMBRANE STUDIED BY FLUORESCENCE CORRELATION SPECTROSCOPY

Zuzana ADAMCOVÁ[1*], Filip MRAVEC[1], Miloslav PEKAŘ[1]

[1] *Institute of Physical and Applied Chemistry, Faculty of Chemistry, Brno University of Technology, Purkyňova 464/118, 612 00 Brno, Czech Republic*

**xccervenkova@fch.vut.cz*

Abstract

Supported lipid bilayers were used as simplified models of cell membranes to study the effect of hyaluronan solution on their diffusion properties. The bilayers were prepared from lecithin liposomes in phosphate buffer using the vesicle fusion method. Hydrophilized cover glass slides were chosen as the supporting substrate. Two fluorescence probes – Nile Red and DiO were utilized to quantify the diffusion properties of the bilayer with and without addition of hyaluronan. For this purpose Z-scan Fluorescence Correlation Spectroscopy, which is a method developed specially for planar samples, was used. It was found out, that addition of this biopolymer causes slowing of the fluorescence probe diffusion within the bilayer.

1. INTRODUCTION

The cell – so small and yet so important. In order to understand various processes in (human) body, it is necessary to understand processes in the scale of single cell. As the plasmatic membrane is the first cellular structure, which communicates with the extracellular environment, it is desirable to know as much as possible about various interactions that can occur between the cell membrane and miscellaneous substances. For the purpose of fundamental research supported lipid bilayers as form of simplified cell membrane models are often used [1]. Fluorescence correlation spectroscopy is an appropriate method to study changes of membrane dynamics and evaluate influence of tested substances on artificial membranes [2].

2. MATERIAL AND METHODS

The artificial membranes were prepared using lecithin (Egg, Chicken), purchased from Avanti Polar Lipids. Nile Red (purchased from BioReagent®) and DiO (3,3´-Dioktadecykloxakarbo-cyanin perchlorate, purchased from Sigma Aldrich) were used as membrane fluorescence

probes. Other common chemical were purchased from Lachner. To prepare liposome solution (0,5 $g \cdot L^{-1}$), appropriate amount of the lecithin stock solution was pipetted into a glass vial and given amount of acetone stock solution of chosen fluorescence probe (to achieve final concentration of 10^{-9} M) was added. The volatile solvents were evaporated under reduced pressure and the thin lipid film was rehydrated in phosphate buffer (10 mM phosphate buffer in 150 mM NaCl, ionic strength 25,484 mM, pH 7,4). The system was vortexed and the size of liposomes was reduced using ultrasound. In order to get supported lipid bilayers, plasma pre-treated (hydophilized) cover slip glass was used and liposomes were left to spontaneously reorganize and form bilayer structure deposited on glass surface (method known as vesicle fusion). Measurement was performed immediately after bilayer preparation and then repeated with addition of hyaluronan solution. Sodium hyaluronate (Hya), molecular weight 300-500 kDa, was purchased from Contipro Biotech. Hyaluronan was stirred overnight in water (1 $g \cdot L^{-1}$) and 1 mL of such solution was then added to the solution surrounding the artificial membrane and Z-scan measurement was performed.

Measurement of model membranes' diffusion properties was performed on time-resolved confocal microscope MicroTime 200 equipped with water immersion objective Olympus, UPLSAPO 60XW. Special technique allowing measurement of plane samples – Z-scan FCS [3] was utilized. The principle of this method is to measure several autocorrelation curves along the *z* axis and extract the diffusion coefficient from diffusion time on Δz dependency.

3. RESULTS AND DISCUSSION

Prior to investigating effects of hyaluronan on lecithin bilayer, the integrity of the bilayer and homogeneity of probe distribution was studied. The scan of fluorescence intensity (80×80 µm, 300×300 pixels) was measured in the axial position corresponding to the position of the bilayer. The results are shown in the Figure 1. Both bilayers were found to be compact and used probes Nile Red and DiO were uniformly distributed.

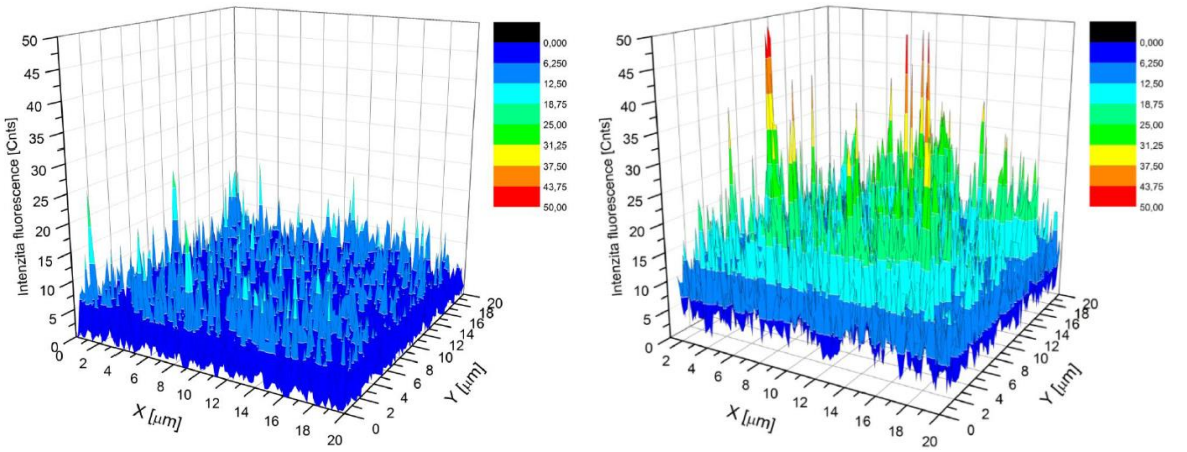

Figure 1.: Verification of homogenous distribution of Nile Red (left) and DiO (right) within the membrane.

To obtain reference values, diffusion coefficients of Nile Red and DiO were measured without presence of hyaluronan. Diffusion coefficient of Nile Red was determined to be **6,04 ± 0,46 µm^2·s^{-1}** and for DiO the obtained value was **6,06 ± 0,87 µm^2·s^{-1}**. After addition of hyaluronan solution, decrease of diffusion coefficients for both probes was observed. The presence of biopolymer caused lowering of the diffusion coefficients to one half of their original value: **3,30 ± 0,31 µm^2·s^{-1}** for Nile Red and **2,95 ± 0,35 µm^2·s^{-1}** in case of DiO. One part of DiO molecule is in contact with the solution surrounding the artificial membrane, which means that the effect of slowing DiO diffusion could be caused by interactions of the probe with HyA. DiO in form of perchlorate (salt) is positively charged in water and hyaluronan is a polyanion, which means that electrostatic interactions are possible. On the other hand, considering Nile Red to be solubilized in the middle of the phospholipid bilayer, the decrease of its diffusion coefficient must be due to slowing lateral diffusion of phospholipid molecules, whose acyl chains form the environment surrounding Nile Red. This explanation is based on presumption that the diffusion of Nile Red within the bilayer is given by combination of her own movement and movement of its surroundings and would denote interaction of hyaluronan with model cell membrane.

4. CONCLUSION

Supported lipid bilayers were created from lecithin liposomes utilizing the vesicle fusion method. Integrity of the bilayer and homogeneity of fluorescence probe distribution were checked by performing *xy* scan. Addition of hyaluronan solution to environment surrounding lecithin bilayer caused decrease of fluorescence probes' diffusion coefficient to one half of the original value. The effect is believed to be caused by certain interactions between hydrophilic

heads of phospholipid molecules with hyaluronan chains. Such interpretation was supported by comparing two fluorescence probes with different way of labelling the lecithin bilayer.

5. ACKNOWLEDGEMENT

The work has been supported by Materials Research Centre at FCH BUT – Sustainability and Development, REG LO1211, with financial support from National Programme for Sustainability I (Ministry of Education, Youth and Sports).

6. REFERENCES

[1] Hardy G J, Nayak R, Zauscher S: Current Opinion in Colloid, 16 (2013), 5, 448-458
[2] Macháň R, Hof M: BBA – Biomembranes, 1798 (2010), 7, 1377-1391
[3] Steinberger T, Macháň R, Hof M: Fluorescence Spectroscopy and Microscopy: Methods and Protocols (2014), 617-634

EXPOSURE OF RATS TO A MIXTURE OF ARISTOLOCHIC ACID I AND II INFLUENCES GENOTOXICITY OF THESE PLANT ALKALOIDS

Frantisek BARTA[1], Alena HUDECOVA[1], Petr HODEK[1], Michaela BALOGOVA[1], Jaroslav MRAZ[2], Sarka DUSKOVA[2], Eva FREI[1], Heinz H. SCHMEISER[3], Volker M. ARLT[4], Marie STIBOROVA[1*]

[1] *Department of Biochemistry, Faculty of Science, Charles University, Albertov 2030, 128 40 Prague 2, Czech Republic*

[2] *Centre of Occupational Health, The National Institute of Public Health, Srobarova 48, 100 42, Prague 10, Czech Republic*

[3] *Division of Radiopharmaceutical Chemistry, German Cancer Research Center (DKFZ), Im Neuenheimer Feld 280, 69120 Heidelberg, Germany*

[4] *Analytical and Environmental Sciences Division, MRC-PHE Centre for Environment & Health, King's College London, Franklin-Wilkins Building, 150 Stamford Street, London SE1 9NH, UK*

**stiborov@natur.cuni.cz*

Abstract

Aristolochic acid (a plant extract containing a mixture of AAI and AAII) causes Aristolochic acid nephropathy, Balkan endemic nephropathy, and urothelial malignancies. The impact of exposure of both the AAI or AAII alone and the combination of both compounds on genotoxicity of AA and expression and activities of enzymes dictating AA metabolism in rats *in vivo* was investigated. The results suggest that additive effects of treatment of rats with AAI combined with AAII on AA-genotoxicity results not only from an increase in activities of enzymes activating AAI and AAII, but also from the AAs biodistribution in the rat body.

1. INTRODUCTION

The herbal drug aristolochic acid (AA) derived from *Aristolochia* species has been shown to be the cause of so-called Chinese herbs nephropathy (CHN), now termed Aristolochic acid nephropathy (AAN) and Balkan endemic nephropathy (BEN) [1,2]. The plant extract AA is a mixture of structurally related nitrophenanthrene carboxylic acids, the major components being aristolochic acid I (AAI) and aristolochic acid II (AAII) [2].

Exposure to AA was demonstrated by identification of specific AA-DNA adducts in urothelial tissue of AAN and BEN patients [1-3]. The most abundant DNA adduct detected in patients is 7-(deoxyadenosin-N^6-yl)-aristolactam I (dA-AAI) which causes characteristic

AT→TA transversions. Such AT→TA mutations have been observed in the *TP53* tumor suppressor gene in tumors from AAN and BEN patients [2,3], indicating a probable molecular mechanism associated with AA-induced carcinogenesis [2]. More recently, AA exposure was discovered to contribute to the high incidence of upper urinary tract urothelial carcinoma (UUC) in Taiwan, where medicinal use of *Aristolochia* plants is widespread [4]; again, the *TP53* mutational signature in patients with UUC was predominant among otherwise rare AT→TA transversions. AA has been classified as a Group I carcinogen in humans by the International Agency for Research on Cancer.

Nitro-reduction of AAI, the compound which is considered as the major cause for AA-mediated development of AAN and BEN, is required to exert its carcinogenic properties (*i.e.* UUC development) [5-7]. One of the most efficient enzymes reductively activating AAI to species forming AAI-DNA adducts is NAD(P)H:quinone oxidoreductase 1 (NQO1) [7]. AAI is also either reductively activated or oxidatively detoxified to 8-hydroxyaristolochic acid (AAIa) by cytochrome P450 (CYP) 1A1 and 1A2 [8,9]. Beside CYP1A/2, rat CYPs of the 2C subfamily also oxidize AAI [8]. A balance between activation and detoxification reactions is considered to dictate the development of AAN and BEN.

However, information is still lacking how drug-drug interaction between the AA components, AAI and AAII, influences the AA-induced BEN/UUC development. Hence, the aim of this study was to evaluate the impact of exposure of AAI alone, AAII alone and combination of both compounds in their ratio of 1:1 on genotoxicity of AA (the AA-DNA adduct formation) in rats *in vivo*. Therefore, the target of this study was to evaluate the impact of exposure of both the AAI or AAII alone and the combination of both compounds (in ratio of 1:1) on genotoxicity of AA (the AA-DNA adduct formation) in rats *in vivo*. The effect of exposure of both the AAI or AAII alone and the combination of both compounds on expression and activities of enzymes dictating AA metabolism in rats *in vivo* was also investigated.

2. MATERIAL AND METHODS

Immunoquantitation of CYP1A enzymes and NQO1 expressed in liver, kidney and lung of Wistar rats was carried out by Western blots. CYP1A/2C and NQO1 activities were measured essentially as described [8-10]. DNA adducts were analyzed by ^{32}P-postlabeling as shown previously [2,5-7].

3. RESULTS AND DISCUSSION

The AA-DNA adducts were formed in liver, kidney and lung of rats treated with AAI, AAII and both compounds in combination in rats treated with these compounds. Up to 2.2-, 5.1- and 3.1-fold higher levels of AAII- than AAI-derived DNA adducts were formed in liver, kidney and lung of rats treated with either compound, respectively. Compared to rats treated with AAI or AAII alone, the sum of total levels of AA-DNA adducts were 1.5- and 2.9-fold higher in liver and kidney, respectively, but not in lung of rats treated with both AA components in combination than the levels of AAI- and AAII-DNA adducts formed after exposure of these compounds individually.

Strong induction of NOQ1 activity in liver, up to more than 10-fold, was caused by exposure of rats to AAs, mainly by exposure to the combination of both compounds. However, the combined treatment leads to higher NQO1 activity only in the liver, but not in kidney. Compared to control (untreated) rats, oxidation of Sudan I, 7-ethoxyresorufin-*O*-deethylase and 7-methoxyresorfin-*O*-demethylase, marker activities of CYP1A1, 1A1/2 and 1A2, respectively, were increased in livers of exposed animals, while they were almost not influenced in kidney. The diclofenac 4'-hydroxylation reaction, a marker for CYP2C6, catalyzed by hepatic microsomes was also elevated by treatment of rats with AAs, while 16α-hydroxylation of testosterone, a marker for CYP2C11, decreased by this treatment. Elevated activities of CYP1A1/2 and 2C6 correlated with an increase in oxidation of AAI to its detoxification metabolite, AAIa. The results demonstrate that induction of CYP enzyme activities by treatment of rats with AAI combined with AAII decreases the toxic effect of AAI, but induction of NQO1 potentiates its genotoxicity.

The results suggest that additive effects of treatment of rats with AAI combined with AAII on AA-genotoxicity (the AA-DNA adduct formation) results not only from an increase in activities of enzymes activating AAI and AAII, but also from the AAI and/or AAII biodistribution in the rat body.

4. ACKNOWLEDGEMENT

Supported by GACR (14-18344S) and Charles University (UNCE 204025/2012).

5. REFERENCES

[1] Gökmen MR, Cosyns JP, Arlt VM, et al.: Annals of Internal Medicine, 158 (2013), 469-477
[2] Arlt VM, Stiborova M, vom Brocke J, et al.: Carcinogenesis 28 (2007), 2253-2261
[3] Grollman A.P., Shibutani S., Moriya M., et al.: Proceedings of American Chemical Society U.S.A., 104 (2007), 12129-12134
[4] Chen CH, Dickman KG, Moriya M, et al.: Proceedings of American Chemical Society U.S.A., 109 (2012), 8241-8246
[5] Stiborova M, Frei E, Arlt VM, et al.: Mutation Research, 658 (2008), 55-67
[6] Stiborová M, Frei E, Schmeiser HH: Kidney International, 73 (2008), 1209-1211
[7] Stiborová M, Levová K, Bárta F, et al.: Mutagenesis 29 (2014), 189-200
[8] Stiborová M. Barta F, Levova K, et al.: International Journal of Mololecular Sciences, 16, (2015), 27561-27575
[9] Dracinska H, Barta F, Levova K, et al.: Toxicology 344 (2016), 7-18

NATURALLY OCCURRING BASE LESIONS EFFECT THE FOLDING AND THE STABILITY OF THE HUMAN TELOMERE G-QUADRUPLEX

Klára BEDNÁŘOVÁ[1], Helena KAŠPAROVÁ[1], Zuzana DVOŘÁKOVÁ[1], Iva KEJNOVSKÁ[1], Daniel RENČIUK[1], Petra ŠKOLÁKOVÁ[1], Michaela VORLÍČKOVÁ[1*]

[1] *Institute of Biophysics, Academy of Sciences of the Czech Republic, v.v.i., Královopolská 135, 612 65 Brno, Czech Republic*

**mifi@ibp.cz*

Abstract

Various base lesions continuously form in cellular nucleic acids and the unrepaired lesions are promutagenic and procarcinogenic. We studied the effects of various naturally occurring lesions to a human telomere (htel) DNA quadruplex, which is a critical formation in the genome.

1. INTRODUCTION

Nucleic acids in living organisms are continuously attacked by exogenous and endogenous agents including UV light, ionizing radiation, and reactive compounds. DNA bases are susceptible to chemical modification via different type of damage, such as oxidation, alkylation, radiation damage, and hydrolysis. These modifications are widespread and play important roles in altering physiological states and they can lead to disease. The majority of genetic impairments are widely believed to originate in oxidative processes that can be the basis of mutation, aging, cell death and carcinogenesis.

2. MATERIAL AND METHODS

Using circular dichroism (CD) and UV absorption spectroscopy and polyacrylamide gel electrophoresis, we probed conformational properties of the htel quadruplexes formed by $G_3(TTAG_3)_3$ or $AG_3(TTAG_3)_3$. The thermodynamics parameters were determined from thermal melting dependences.

3. RESULTS AND DISCUSSION

We studied conformational properties of the quadruplexes formed by $G_3(TTAG_3)_3$ or $AG_3(TTAG_3)_3$, in which each guanine was replaced by an adenine, an abasic site or 8-oxo

guanine [1-3]. None of these single base substitutions hindered the formation of antiparallel quadruplexes in NaCl solutions, but their thermal stabilities were substantially decreased. Unlike the parent wild-type quadruplex, no structural transitions were observed with the substituted sequences when sodium ions were replaced by potassium ions. The effect of substitutions differed depending on the position of the substituted base but hardly depended on the lesion type.

In addition to the lesions of the quadruplex core, we have further studied the effect of the abasic site and 8-oxoadenine replacing adenine and the 5-hydroxymethyluracil substituting for thymine in the TTA loops [4,5]. These lesions hindered neither the formation of the quadruplexes in Na^+ or K^+ solution nor their transition to a parallel quadruplex form. However, the three lesions impacted the stability and quadruplex folding in markedly different ways. The effect of the substitution in this case depended on its position in the htel sequence and mainly on the type of the lesion. We have found that the loss of adenine in individual loops of the quadruplex changes specifically its folding. In view of the critical functions of the telomeres, the changes in their quadruplex structures may have significant biological consequences.

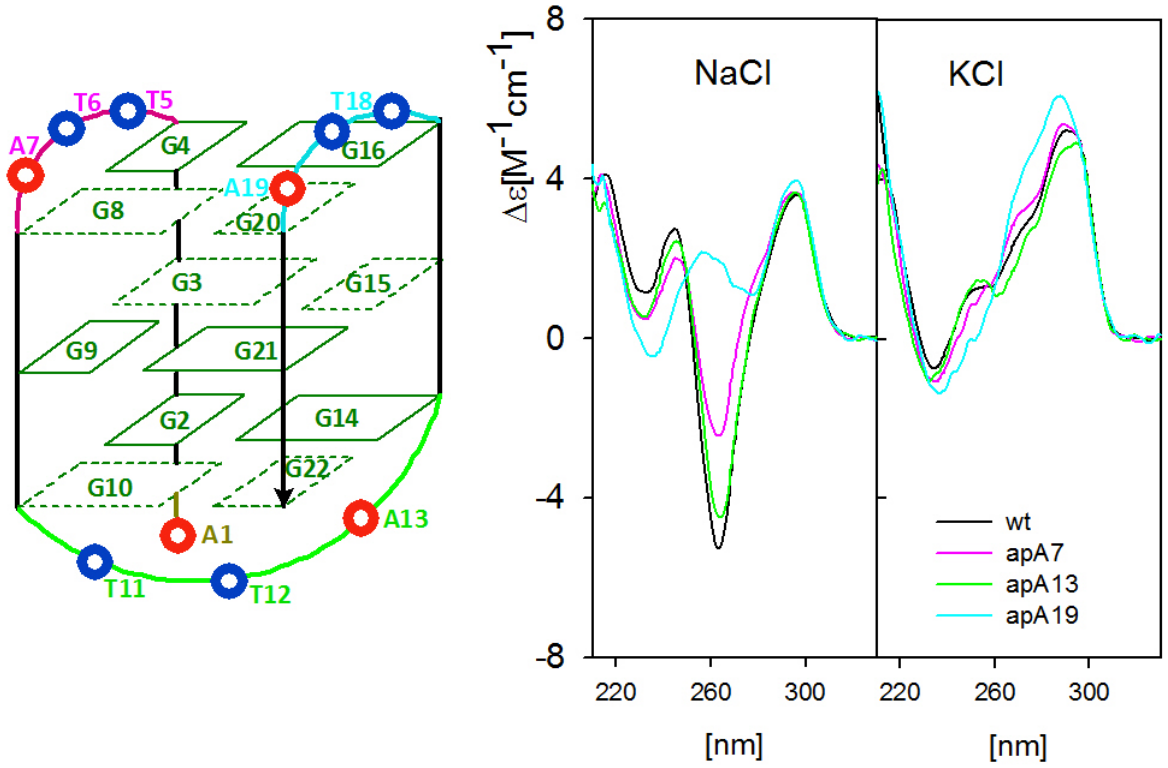

Figure 1.: Left: Schematic structure of $AG_3(TTAG_3)_3$ quadruplex with numbering and loop colours used in the figure. Right: CD spectra of the wild type $AG_3(TTAG_3)_3$, and of its analogs containing abasic site (ap) for adenine in loop.

4. CONCLUSION

The studied naturally occurring lesions in the loops of the human telomeric DNA sequence influence the stability and even the type of folding of its quadruplex structure. The lesion impact depends on the modification nature and on the modification position. Given an important role of quadruplex in the natural aging of cells and their cancer transformation, it is obvious that unrepaired lesions can have serious biological consequences.

5. ACKNOWLEDGEMENT

The work has been supported by The Grant Agency of the Czech Republic grants P205/12/0466.

6. REFERENCES

[1] Tomaško M., Vorlíčková M., Sagi J.: Biochimie, 91 (2009) 171-179
[2] Školáková P., Bednářová K., Vorlíčková M., Sagi J.: BBRC, 399 (2010) 203-208
[3] Vorlíčková M., Tomaško M., Sagi AJ., et all.: FEBS J., 279 (2012) 29-39
[4] Babinsky M., Fiala R., Kejnovská I., et all.: NAR, 42 (2014) 14031-14041
[5] Konvalinová H, Dvořáková Z, Renčiuk D, et all.: Biochimie 118 (2015) 15-25

FLUORESCENCE CHEMOSENSORS FOR GAS PHASE DETECTION BASED ON NAPHTHALIMIDE DERIVATIVES

Juraj DIAN[1*], Jindřich JINDŘICH[2], Ivan JELÍNEK[3]

[1] *Department of Chemical Physics and Optics, Faculty of Mathematics and Physic, Charles University in Prague, Ke Karlovu 3, 121 16 Prague, Czech Republic*

[2] *Department of Organic Chemistry, Faculty of Science, Charles University in Prague, Albertov 2030, 128 43 Prague, Czech Republic*

[3] *Department of Analytical Chemistry, Faculty of Science, Charles University in Prague, Albertov 2030, 128 43 Prague 2, Czech Republic*

**Juraj.Dian@mff.cuni.cz*

Abstract

We present a fluorescence based sensor system for detection of chemical compounds in gas phase that can be easily integrated into detection parts of present chromatographic devices. Fluorescence sensor is based on 1,8-naphalimide based dye attached to a 75 μm glass beads and placed in a capillary. We have measured changes in fluorescence spectra in the presence of various organic vapors. Spectral changes at various concentrations of studied organic compounds are presented and possible mechanisms of sensor response are presented.

1. INTRODUCTION

Gas sensors are a subset of the broader field of chemical sensors and allow inferring on the chemical species in the surrounding environment [1]. Detection of chemical species in gas phase using simple systems simplifies their applicability in commercial devices. Combination of simple sensor elements of different chemistry and surface properties enables construction of electronic noses that are needed for food industry, cosmetic, biomedical industries and environmental studies. Understanding main features of interaction between sensor material and detected analyte represents the essential condition for their successful application.

2. MATERIAL AND METHODS

Synthesis of PHIAHA and attachment to the glass beads

4-(2-Aminohexyl)amino-N-propyl-1,8-naphthalimide (PNIAHA) was synthetized, in a similar way as its recently published analog [2] from 4-bromo-1,8-naphthalimide by refluxing with 1,6-hexanediamine in ethylene glycol monomethyl ether for 6 h and purified by

chromatography on silica gel column using hexane/ethyl acetate elution mixture. The surface of 75 μm glass beads (purified by 2 h refluxing in 6 M HCl) was modified by reaction with neat 3-(glycidyloxypropyl)trimethoxysilane for 6 h at 80°C. The PNIAHA was then covalently bound to the surface by heating the pretreated glass beads with 20 mM solution of PNIAHA in methanol for 6 h at 80 °C (Figure 1).

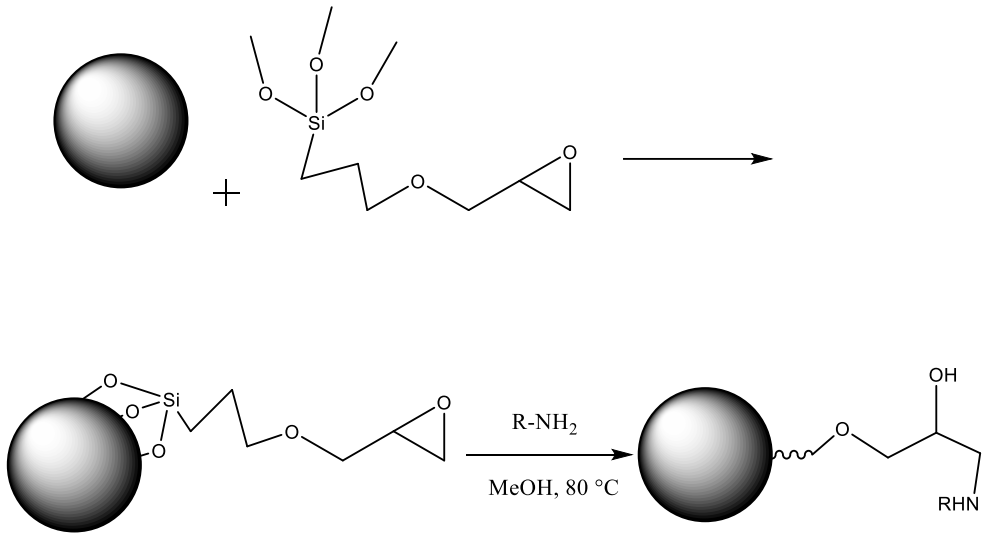

Figure 1.: Silanization of glass beads and attachment of fluorophore to the surface

Fluorescence setup

Fluorescence from PHIAHA modified glass beads embedded in a capillary was measured with an Avantes AvaSpec ULS3648TEC optical fiber spectrometer (resolution ~2 nm). Capillary with glass beads was placed in a home-build holder that fixes the optical paths of a fiber with an excitation of 405 nm laser (Flexpoint, excitation power 5 mW) and a fiber guiding the fluorescence to the spectrometer. The capillary with fluorophores was connected to a closed-cycle system (internal volume of the system 1.1 dm^3) that enables to realize precise concentrations of studied analytes in gas phase (nitrogen was used as a carrier gas).

3. RESULTS AND DISCUSSION

Fluorescence of glass beads modified with PHIAHA fluorophore changes in the presence of various organic compounds in gas phase. We tested gas phase sensor response for various organic compounds and various concentrations. In most cases we observed fluorescence quenching except for n-hexane. After purge of nitrogen the fluorescence intensity was only partly recovered. In Figure 2 there are fluorescence spectra for various concentrations of

ethanol and n-hexane. Peak at about 430 nm represents reflected laser radiation after passing the GG3 edge filter.

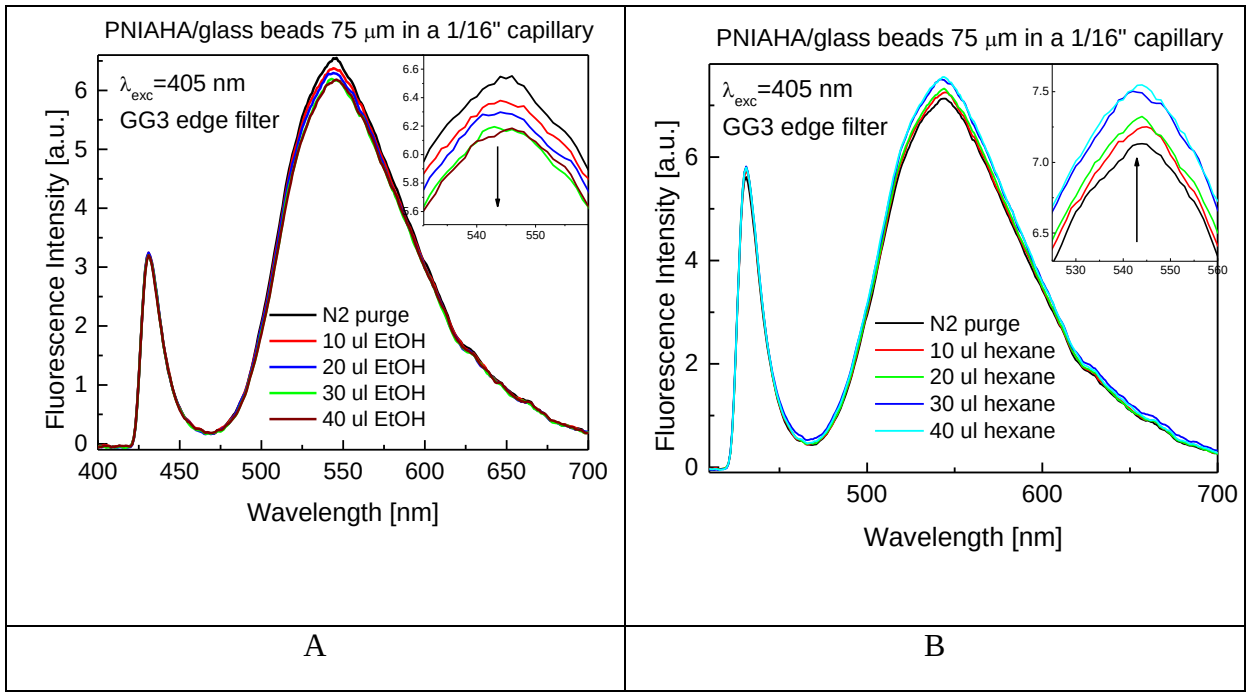

Figure 2.: Dependence of fluorescence sensor response to various concentrations of ethanol (A) and hexane (B)

The fluorescence response of sensor to toluene was more complicated – after initial increase of the intensity (first injection of toluene after purging the system with nitrogen) – a fluorescence quenching with increasing toluene concentration was observed. Simultaneously, fluorescence recovery after toluene removal was very slow as compared to other analytes. This indicates a very strong binding of toluene to the fluorophore and the important role of π-π interaction between aromatic rings of toluene and naphtalimide derivative in the mechanism of fluorescence response [3].

4. CONCLUSION

Fluorescence-based sensor of organic compounds in the gas phase is presented in this paper. Observed fluorescence changes in the presence of various concentrations of studied analytes revealed various interactions of different organic compounds with the studied fluorophore.

5. REFERENCES

[1] Korotcenkov G, Handbook of Gas Sensor Materials, Vol.1: Conventional Approaches, Springer 2013.
[2] Zhang L M, Guo L E, Li X M, et all: Tetrahedron Letters 55 (2014), 44, 6131–6136
[3] Hunter C A, Sanders J K M,: J. Am. Chem. Soc. 112 (1990) 5525-5534

A NEW APPROACH TO PRETREATMENT OF A PENCIL GRAPHITE ELECTRODE SURFACE FOR 3N-METHYLADENINE DETERMINATION

Libor GURECKÝ[1], Libuše TRNKOVÁ[1], Iveta TŘÍSKOVÁ[1]

[1] *Department of Chemistry, Faculty of Science, Masaryk University in Brno, Kamenice 5, 62500 Brno, Czech Republic*

**libuse@chemi.muni.cz*

Abstract

Purine derivatives are important molecules in human metabolism. DNA is constantly attacked by many species forming different products such as oxidized forms. Methyl groups have been commonly observed in the case of DNA damage. The purine ring of adenine can be methylated at different positions. So far there have been only few studies of electrochemical behavior aimed at oxidation processes of N-methyladenines. We found out the possibility of measuring 3N-methyladenine (3N-mAde) on a pencil graphite electrode (PeGE) whose surface requires a surface pretreatment. The unique surface morphology of the PeGE, together with adsorption stripping, gives us the opportunity to study 3N-mAde signals. It is noteworthy that there were no 3N-mAde signals at a glassy carbon (GC) electrode at the same experimental conditions.

1. INTRODUCTION

DNA is under constant attack of many factors, and oxidative lesions are the primary risk factor for genetic mutations, leading to carcinogenetic and faster aging[1]. DNA can be modified in several ways, and a typical representative is methylation, a substance widely used for gene control and cell processes. Methylation is formed by the cell mechanism or an external factor causing the addition of information into DNA[2,3]. The methylation process is limited to adenine and cytosine and simplifies or affects DNA-protein interactions, which is related to gene expressions, DNA restriction, mismatch repairing, and chromosome replications[4,5,6].

The methylation of adenine on the 3N position could be induced by antineoplastic drugs, natural or endogenous compounds. The recent discovery of 3N-methyladenine toxicity via

strong blocking of DNA polymerization could be used as a new pharmacological procedure for resistant tumor treatment[7].

There are no features of the electrochemistry of methylated adenine derivatives, and relevant literature states that solid electrodes exhibit very low or zero oxidation. This paper discusses the electrochemical properties of methylated adenines compared to adenine behavior on a PeGE, using cyclic voltammetry (CV) and square wave voltammetry (SWV). For the electrochemical experiment, we used 3N-mAde as a model derivative.

The aim of this article was to set experimental conditions for the clear detection of methyl derivatives or their oxidation products on a PeGE. We expect their high adsorptive properties? The fact that the toxicity of 3N-mAde is linked with DNA could be used in the field of tumor treatment. However, there still remains the question of how important the role of 3N-mAde in therapy will be; thus, it is important to study not only the structure but also the properties of 3N-mAde.

2. MATERIAL AND METHODS

Chemicals

The adenine and 3N-methyladenine were purchased from Sigma Aldrich (St. Louis, USA). The concentration was $2 \cdot 10^{-5}$ M, confirmed by spectrophotometry. The phosphoric acid (85 %) was purchased from Penta Chrudim. The acetic acid glacial (100 %) was purchased from Sigma Aldrich (St. Louis, USA). The sodium hydroxide (100 %) was purchased from Sigma Aldrich (St. Louis, USA) ASC ≥ 99.0 % MILIPORE (MiliQ) water (18.2 MΩ.cm).

Equipment and procedures

The voltammetric experiments were performed on an Autolab potentiostat PGSTAT30 (Metrohm Czech Republic) connected with a PC with the NOVA 1.11 software at room temperature (23º). Solutions were bubbled by argon before each experiment, and the argon atmosphere was maintained during the whole experiment in a measuring cell. The three-electrode system consisted of a working PeGE electrode with the effective area of 16 mm^2 (Tombow, Japan) or a glassy carbon electrode (GCE) with the effective area of 12 $mm^{2,}$ an Ag/AgCl/KCl reference electrode, and a platinum wire as the auxiliary electrode. The measurement conditions for the cyclic voltammetric (CV) pretreatment were as follows: the start potential was 0 V; the higher and lower vertex potentials corresponded to 1.5 V and -0.1

V, respectively; the reference scan rate was 400 mV/s; the number of cycles was 2; and the waiting time on the 0 V potential between the scans equalled to 120 s. SWV was performed with the scan rate of 400 mV/s. The pH of the phosphate-acetic buffer was determined on a Hamilton Single Pore Glass electrode connected with a pH CyberScan PC5500 (Eutech Instruments). Hamilton duracal buffers (4.01 ± 0.01 and 7.00 ± 0.01; Hamilton Bonaduz AG, Switzerland) were used for the calibration of the pH electrode.

3. RESULTS AND DISCUSSION

To find the oxidation peak of 3N-mAde on the PeGE, we perform experiments to confirm the urgency of electrochemical electrode pretreatment. The pretreatment, successful for the PeGE but not for the glassy carbon electrode (GCE), consists in activating the electrode surface by one CV cycle followed by the adsorption of methyladenine (120 seconds at 0 V). To be sure that the measured peak is that of 3N-mAde, the pretreatment was performed in solutions with and without the presence of 3N-mAde. For both cases, the oxidation 3N-mAde peak occurs in the second cycle at 1.21 V. The same pretreatment was applied in the square wave voltammetric (SWV) experiment, and the results confirmed that the electrode activation is performed by changing the potential from lower values to higher ones. The best results of the Tombow PeGEs can be supported by a unique surface morphology, such as high sp^3 hybridized carbon together with silicon monooxide (SiO). The unwillingness of 3N-mAde to oxidize was discussed with respect to not only the electrode surface morphology but also the methyl group and its position on the purine skeleton. We assume that the above-mentioned electrode surface pretreatment changes the electrode surface, which then ensures the detection of 3N-mAde. Interestingly, the GCE is not capable of providing such an effect.

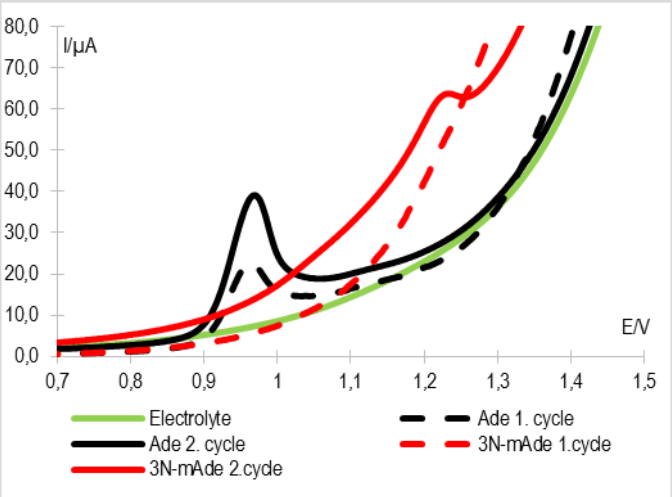

Figure 1.: Comparison of the 1st and 2nd cycles of adenine voltammograms and 3N-mAde with the scan rate of 400 mV/s

4. CONCLUSION

We found that, for the determination of methyladenines on a PeGE, the pretreatment of the electrode surface by CV cycling is necessary. We assume that the pretreatment changes the morphology of the electrode surface; this change then enables, after 120 seconds of adsorption at 0 V, a better "fitting" of 3N-mAde molecules into the electrode double layer. Our study shows the possibility of detecting not only 3N-mAde but also other purine derivatives and their mixtures. In conclusion, the results of this study a) help us to acquire better understanding of the different behavior of methyladenines on a charged electrode/electrolyte interface; b) give suggestions for studying methyladenine together with other purine derivatives; c) provide new knowledge about the fast pretreatment of PeGE surfaces for the electroanalysis of purine derivatives.

5. ACKNOWLEDGEMENT

This research was supported by the following projects: MUNI/A/0972/2013 and MUNI/A/1500/2015.

6. REFERENCES

[1] Alvarez N.: Electrochem. Com. 9 (2007).
[2] Low D. A., Weyand N. J., Mahan M. J.: Infect. Immun. 69, 12 (2001).
[3] https://www.plosgenetics.org, downloaded October 20th 2015
[4] Low D. A.: Curr. Opin. Microbiol. 11 (2008).
[5] Lwbner-Olesen A: Curr. Opin. Microbiol. 8 (2005).
[6] Casadesus J. Low D.: Microbiol. Mol. Biol. Rev. 70 (2006).
[7] Tentori L., Forini O., Fossile E., Muzi A., Vergati M., Portarena I., Amici C., Gold B., Graziani G.: Mol. Pharmacol. 67, 572 (2005).

FLUORESCENCE PROBE STUDY OF INTERACTIONS BETWEEN CATIONIC MICELLES AND NEGATIVELY CHARGED POLYELECTROLYTE

Petra HOLÍNKOVÁ[1*], Miloslav PEKAŘ[1]

[1] *Institute of Physical and Applied Chemistry, Faculty of Chemistry, Brno University of Technology, Purkyňova 464/118, 612 00 Brno, Czech Republic*

**xcucekajova@fch.vut.cz*

Abstract

This paper deals with fluorescence study of cetyltrimethylammonium bromide (CTAB) micellar solution after an addition of oppositely charged polyelectrolyte - hyaluronan. Two fluorescence probes solubilized in different region of micelles were used. The excitation and emission spectra, fluorescence intensity, steady-state fluorescence anisotropy and lifetime of probes in the samples were measured. It was observed that the interactions between cationic micelles and hyaluronan probably lead to binding micelles on hyaluronan chains and reduction of their size.

1. INTRODUCTION

The hyaluronan can interact with cationic micelles via electrostatic interactions to form some aggregates, which could be potential used for targeted drug delivery [1]. For fluorescence study of these aggregates, two fluorescence probes were used – hydrophilic fluorescein, which is located in the inner part of Stern layer [2] and perylene, which is solubilized in micellar core due to its hydrophobic character [3].

The main method – fluorescence anisotropy can be used for determining the viscosity in the nearby area of the molecule fluorescent probes. This method characterizes the extent of linear polarization of fluorescence emission, resulting from photoselection from an optically isotropic sample.

2. MATERIAL AND METHODS

Stock solution of perylene (Fluka) and fluorescein (Sigma-Aldrich) were prepared in acetone and methanol, respectively. Stock solution of cetyltrimethylammonium bromide (Sigma-Aldrich) and low molecular weight hyaluronan (90–130 kDa, Contipro Biotech s. r. o.) were prepared in mili-Q water.

The stock solution of one probe was added to the glass vials and then the volatile solvent was evaporated. Then, the solutions of CTAB and hyaluronan were added in corresponding quantities. The samples were left on a shaker for 24 hours at room temperature. Individual samples were blended three times.

The steady-state measurements of fluorescence (excitation and emission spectra, fluorescence anisotropy) were carried out on a luminescence spectrophotometer Fluorolog (HORIBA Jobin Yvon) with 150-W xenon lamp as the excitation. Anisotropy measurements were realized in L-format instrumental configuration and an automatic interchangeable wheel with Glan-Thompson polarizers. The lifetime was measured on TCSPC lifetime spectrofluorometer Fluorocube from HORIBA Jobin Yvon with Nano LED diod as the excitation.

3. RESULTS AND DISCUSSION

Comparison of normalized excitation and emission spectra of both fluorescence probes in CTAB micellar solutions without hyaluronan and with concentration of hyaluronan 0,15 g l^{-1} showed the hyaluronan presence did not affected the shape of these spectra. Also the lifetime of fluorescein/perylene has the same value in all samples, respectively.

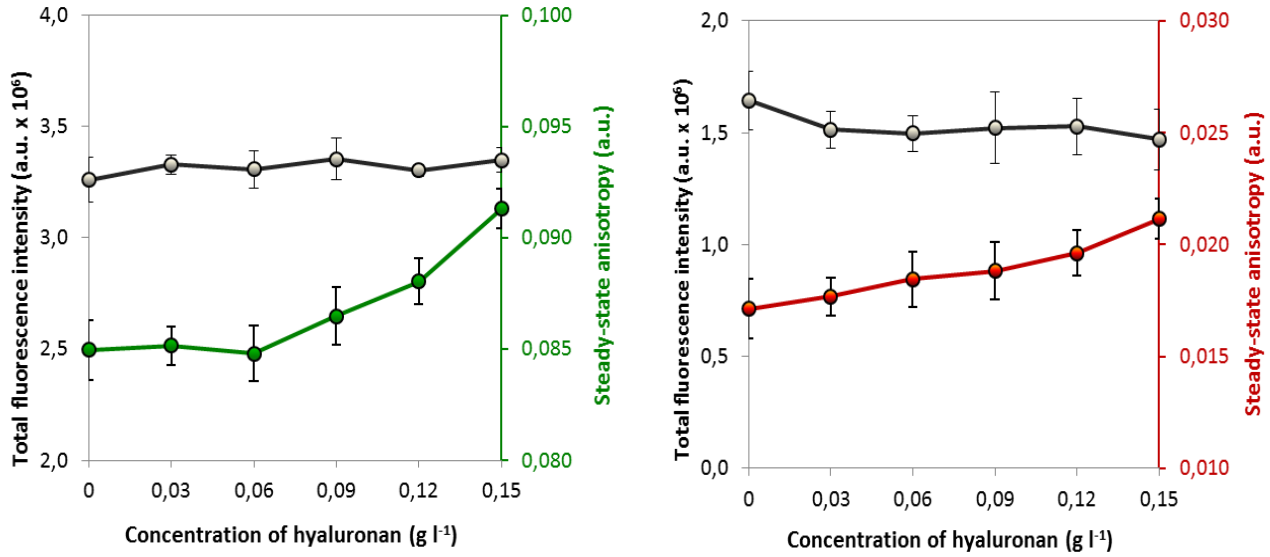

Figure 1.: Steady-state fluorescence anisotropy and total intensity of fluorescence of fluorescein (left) and perylene (right) in CTAB micellar solution as a function of hyaluronan concentration in the sample.

Figure 1 shows the results obtained for fluorescence anisotropy and total fluorescence intensity of fluorescein (left) and perylene (right) in CTAB micellar solution as s function of hyaluronan concentration in the sample. In case of fluorescein, the total fluorescence intensity

is roughly constant and fluorescence anisotropy significantly increased from hyaluronan concentration 0,06 g l^{-1}, which indicates that the micellar surface is affected by hyaluronan addition – microenvironment near the molecules of fluorescein has higher and higher viscosity. As we can see, also results from measurement with perylene have a very similar trend, fluorescence intensity in the samples with hyaluronan are roughly constant and it is little bit smaller than clear CTAB solution. The anisotropy of fluorescence slightly increasing, this fact is probably caused by reduction of micellar size. Interaction between hyaluronan and CTAB probably lead to binding micelles on hyaluronan chains and reduction of their size.

4. CONCLUSION

Through analysis of photophysical response of perylene and fluorescein, which are solubilized in different region of CTAB micelles, we have obtained information about structural changes of this micelles induced by presence of hyaluronan.

It was observed, that the hyaluronan addition to micellar solution affected structural changes of entire micelle, i.e. hydrophobic region and micellar surface and interaction between hyaluronan and CTAB micelles probably lead to binding micelles on hyaluronan chain and reduction of their size.

5. ACKNOWLEDGEMENT

This work was supported by Materials Research Centre at FCH BUT- Sustainability and Development, REG LO1211, with financial support from National Programme for Sustainability I (Ministry of Education, Youth and Sports).

6. REFERENCES

[1] HALASOVÁ, T., J. KROUSKÁ, F. MRAVEC a M. PEKAŘ. Hyaluronan-surfactant interactions in physiological solution studied by tensiometry and fluorescence probe techniques. Colloids and Surfaces A: Physicochemical and Engineering Aspects. 2011, 391(1-3), 25-31. DOI: 10.1016/j.colsurfa.2011.05.035. ISSN 09277757.

[2] SÁNCHEZ, F.García a C.Carnero RUIZ. Intramicellar energy transfer in aqueous CTAB solutions. Journal of Luminescence. 1996, 69(4), 179-186. DOI: 10.1016/S0022-2313(96)00116-0. ISSN 00222313.

[3] RUIZ, Cristóbal Carnero. Fluorescence Anisotropy of Probes Solubilized in Micelles of Tetradecyltrymethylammonium Bromide: Effect of Ethylene Glycol Added. Journal of Colloid and Interface Science. 2000, 221(2), 262-267. DOI: 10.1006/jcis.1999.6555. ISSN 00219797.

PREPARATION OF SILVER NANORODS VIA TEMPLATE BASED METHOD

Radim HRDY[1], Katerina PRIKRYLOVA[1], Hana KYNCLOVA[1]

[1] *Department of Microelectronic, Faculty of electrotechnology and comunication, Brno University of Technology, Technicka 10, 616 00 Brno, Czech Republic*

**hrdy@feec.vutbr.cz*

Abstract

We present the fabrication process of various silver nanostructured surfaces which can have widespread utilization in electrochemistry. Silver nanorods surface has been prepared by controlled electrochemical deposition in anodic alumina oxide template. We fabricated the silver nanorods with length 50-100 nm, the nanowires with length more than 500 nm and silver nanodots.

1. INTRODUCTION

The advantages of sensing interfaces that contain Ag nanostructures (Ns) networks are the increased surface area for sensing, improved electrical connectivity through the AgNs network and chemical accessibility to the analyst through these networks compared to sensing interfaces based on flat surfaces [1]. The Ag nanostructured surfaces can be used as reference electrode, as well. The next advantages are electrocatalysis, utilization in separation technique and biosensors fabrication [2]. Biosensor is an analytical tool that fulfills two functions, capturing biological targets and transducing target binding events to measurable signals, determination of heavy metals [3].

2. MATERIAL AND METHODS

The fabrication process is composed of two steps. The first step is the alumina template creation. The silicon wafer was coated with metalic layer with the thickness of 250 nm and subsequently with a high-purity (99.99+ %) thin aluminum layer with the thickness of 500 nm by thermal evaporation (PVD). The thin porous anodic alumina oxide (AAO) templates were prepared by using equipment consisting of a flow-system controlled by membrane pump, power source, thermostat and personal computer providing automatic driving of all processes. The AAO templates were prepared by one-step anodic oxidation of aluminum thin film under constant voltage of 53 V in 0.3 mol/L oxalic acid solution in conventional two electrode

system at 10 °C for 360 sec. The gold wire was used as counter electrode. Vertically aligned pores formed the honeycomb structure in alumina layer. After the high current droop was detected, the Al layer was completely transformed to AAO and AAO interface below each pore. Thereafter it was washed by distilled water and dried. That technique of AAO fabrication has been described in more details in recent papers [4].

The second step is electrochemical pulsed deposition of AgNs. The controlled pulse deposition was used to obtain the homogenous silver nanostructures into the AAO template. Deposition was performed from 0.2 mol/dm^3 $AgNO_3$ (pH 2.5) at 60°C consisting of pulses with current intensity of 1 mA and duration of 2 s. The electrolyte was circulated on the AAO template surface for 10 minutes before deposition to fill the pores of membrane. The current pulses were applied using an Autolab PGSTAT 302N potentiostat with the standard two-electrode setup. Finally the surface was etched in aqueous solution containing 5 ml of 85% H_3PO_4 and 3 g CrO_3 for 360 seconds at temperature 45°C to remove AAO.

3. RESULTS AND DISCUSSION

Three ring types of silver electrodes with diameter of 5 mm have been fabricated. One type of nanostructured electrode was obtained by 3 pulses resulting in reduced nanowires length. The second type was fabricated under 20 pulses, see Figure 1a, where the deposition time was determined by full filing of alumina template and obtaining nanowires with length close to 500 nm of nanometers see Figure 1b. The same time was applied under lower current deposition, where the nanowires, in this case rather nanorods, have the height up to one hundred of nanometers. Nano-sized structure consists of nanorods with the diameter 50 nm and height 100, 500 nm and nanodots with length 50 nm as well, Figures 2.

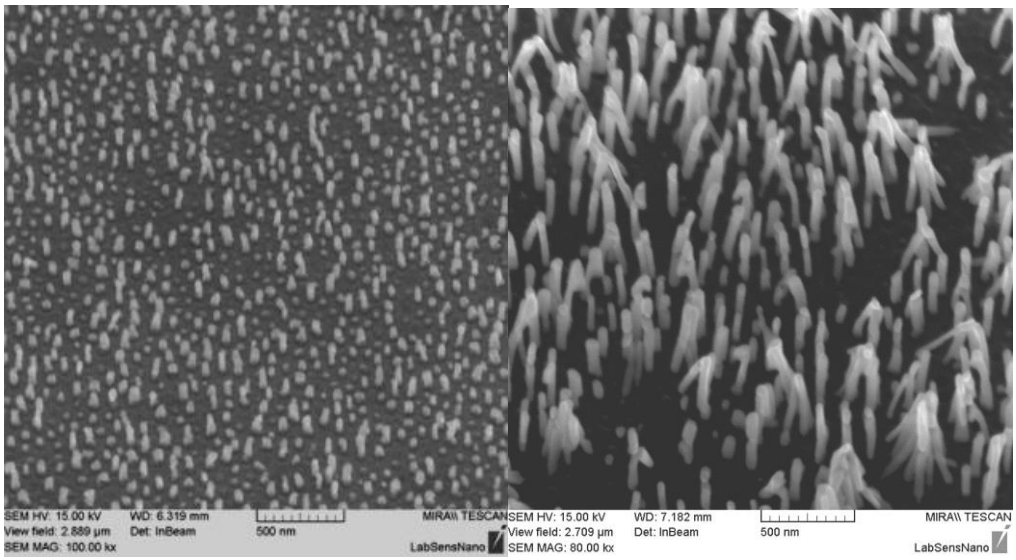

Figure 1a, 1b.: Short Ag nanorods (left), long nanowires (right) deposited on metallic surface.

As it can be seen in Figures 1 and 2, all surfaces have the same nanowires distributions. According to recent works, the time of deposition was the only factor, which affected the length of nanowires without any effect on distributions. We also tested the stability in aqueous solution. We observed the perfect stability of structures. However, the nanowires with length 500 nm have been formed to clusters. This phenomenon was described in recent work and it relates with the ratio of diameter and length of nanowires [4].

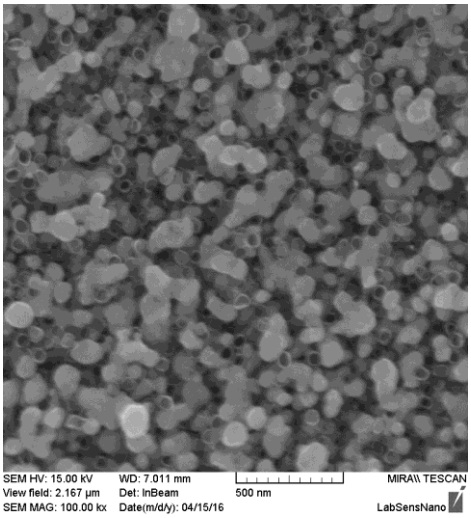

Figure 2.: Ag nanodots prepared on conductive metallic oxide

4. CONCLUSION

Surface functionalization and control over nanostructured interfaces represent a key aspect in nanoscale functionality. We presented the highly controlled process of Ag nanowires fabrication.

5. ACKNOWLEDGEMENT

The work has been supported by SIX centrum, IGA FEKT/STI-J-16-3625 and IGA FEKT-S-14-2300 research grants.

6. REFERENCES

[1] Archer-Hartman A., Holland L.A, Majors, R.E., et all.: LC-GC International, May 1(2011), 1-7
[2] Kist, T.B.L, Mandaji M., et all.: Electrophoresis, 25 (2004) 3492-3497
[3] Doria G, conde J, et all.: Sensors, (2012), 12, 1657-1687
[4] Hrdy R, Kynclova H, Drbohlavova J, et al.: Int. J. Electrochem. Sci., 8 (2013), 4, 4384-4396

CYTOCHROME B_5 PLAYS A DUAL ROLE IN THE REACTION CYCLE OF CYTOCHROME P450 3A4 DURING OXIDATION OF AN ANTICANCER DRUG ELLIPTICINE

Radek INDRA, Eva FREI, Václav MARTÍNEK, Marie STIBOROVÁ*

[1] *Department of Biochemistry, Faculty of Science, Charles University, Albertov 6, 128 43 Prague 2, Czech Republic*

**stiborov@natur.cuni.cz*

Abstract

Ellipticine is an anticancer agent that forms covalent DNA adducts after its enzymatic activation by cytochromes P450 (CYP), mainly by CYP3A4 in the presence of cytochrome b_5. We found that cytochrome b_5 plays a dual role in the CYP3A4-catalyzed oxidation of ellipticine; it mediates the CYP3A4 catalytic activities by donating the first and second electron to this enzyme in its catalytic cycle and it acts as an allosteric modifier of the CYP3A4 oxygenase.

1. INTRODUCTION

Ellipticine is an efficient anticancer agent that functions through multiple mechanisms participating in cell cycle arrest and initiation of apoptosis. This drug forms covalent DNA adducts after its enzymatic activation by cytochromes P450 (CYP), predominantly by CYP3A4, the process that is one of the most important ellipticine DNA-damaging mechanisms of its antitumor action [1].

The CYP enzymes are components of a mixed-function oxidase (MFO) system located in the membrane of endoplasmic reticulum. This enzymatic system also contains other enzymes, the multidomain flavoprotein NADPH:cytochrome P450 oxidoreductase (POR) and cytochrome b_5 accompanied by its NADH:cytochrome b_5 reductase (CBR). Microsomal CYPs function by catalyzing the insertion of one atom of molecular oxygen into a variety of xenobiotics, while reducing the other atom to water, a reaction that requires two electrons. It is generally accepted that POR with NADPH serves as donor of electrons for both reductions of CYP in the MFO reaction cycle. But, the second electron may also be provided by CBR with cytochrome b_5 and NADH, but cytochrome b_5 has also additional roles in the CYP system. Although POR is considered an essential constituent of the electron transport chain towards CYP, its exact role in the CYP-mediated reaction cycle is still not clearly established

[2,3]. Therefore, here we investigated whether CBR in the presence of cytochrome b_5 can act as sole electron donor to human CYP3A4 during oxidation of ellipticine and replace the POR system.

2. MATERIAL AND METHODS

Human CYP3A4 expressed in the eukaryotic system (microsomes of insect cells transfected with human CYP3A4 and NADPH:CYP reductase, POR - Supersomes™) with or without cytochome b_5 was used. HPLC was used to separate and identify ellipticine metabolites and ^{32}P-postlabeling to detect and quantify ellipticine-derived DNA adducts [1,3].

3. RESULTS AND DISCUSSION

Human recombinant CYP3A4 expressed with POR, CBR, epoxide hydrolase and cytochrome b_5 in Supersomes™ oxidized ellipticine to 9-hydroxy-, 12-hydroxy and 13-hydroxyellipticine as the major metabolites, both in the presence of NADPH (a cofactor of POR) and NADH (a cofactor of CBR), and formed two adducts with DNA generated by two of these metabolites, 12-hydroxy and 13-hydroxyellipticine. Even though NADH was less efficient than NADPH to mediate the ellipticine oxidation, this finding indicates that the NADH/cytochrome b_5/CBR system can act as the sole electron donor both for the first and second reduction of CYP3A4 during the oxidation of ellipticine. However, because cytochrome b_5 stimulated not only the NADH-dependent ellipticine oxidation, where NADH is necessary for reduction catalyzed by the NADH-dependent reductase CBR, but also the oxidation mediated by NADPH, this protein plays also another role in the CYP3A4 reaction cycle. The CYP3A4-mediated oxidation of ellipticine in the presence of NADPH was significantly changed only by holo-cytochrome b_5, while apo-cytochrome b_5 without heme or Mn-cytochrome b_5 had no such effect. These findings indicate a high specificity of interaction of CYP3A4 with holo-cytochrome b_5 containing heme, which is necessary not only for electron transfer, but also for the natural conformation of the cytochrome b_5 protein [3]. The lack of effect of apo-cytochrome b_5 on CYP3A4 catalysis might hence be the result of not only the loss of the electron transfer activity, but may also result from changes in 3D structure of its protein. The results found demonstrate that cytochrome b_5 plays a dual role in the CYP3A4-catalyzed oxidation of ellipticine; it mediates the CYP3A4 catalytic activities by (*i*) donating the first and second electron to this enzyme in its catalytic cycle and by (*ii*) acting as an allosteric modifier of the CYP3A4 oxygenase.

4. ACKNOWLEDGEMENT

Supported by GACR (14-18344S) and Charles University (UNCE 204025/2012)

5. REFERENCES

[1] Stiborová M, Frei E: Curr Med Chem, 21 (2014) 575-591
[2] Stiborová M, Indra R, Moserová M., et al.: Monatsh. Chem. 147 (2016) 847-855
[3] Stiborová M, Indra R, Moserová M., et al.: Chem Res Toxicol 25 (2012) 1075-1085

SPECTROELECTROCHEMISTRY OF RHENIUM-CATECHOL COMPLEX

Martin ŠTÍCHA[1], David KALIBA[2], Ivan JELÍNEK[2*], Juraj DIAN[3]

[1] *Department of Chemistry, Faculty of Science, Charles University in Prague, Albertov 2030, 128 43 Prague 2, Czech Republic*

[2] *Department of Analytical Chemistry, Faculty of Science, Charles University in Prague, Albertov 2030, 128 43 Prague 2, Czech Republic*

[3] *Department of Chemical Physics and Optics, Faculty of Mathematics and Physics, Charles University in Prague, Ke Karlovu 3,121 16 Prague 2, Czech Republic*

*ijelinek@natur.cuni.cz

Abstract

Rhenium complexes vith suitable organic ligands play important role in medicine, catalysis and the development of novel sources of energy. We synthetized and chromatographically purified Re^{VII}–catechol complex and studied its properties by means of UV/Vis absorption and spectroelectrochemical experiment. We observed complex redox behaviour involving reversible and irreversible electrochemical processes. Based on comparison of absorption spectra of rhenium complexes obtained via controlled chemical oxidation of Re^{V} complexes and the absorption spectra provided by spectroelectrochemistry, we ascribed electron transition between Re^{VII} and Re^{V} species.

1. INTRODUCTION

Rhenium is able to form numerous coordination complexes with inorganic and organic ligands, the stability of whose depend on individual redox states of central metal ion and coordinated ligands. Rhenium complexes play important role in radiodiagnostics [1,2]. Re^{V} complexes possess promising catalytic activity [3,4] and play important role in modern organic chemistry, Re^{I} complexes were successfully tested as selective transducers in optical chemical sensors [5]. Detailed knowledge of overall chemical properties of rhenium complexes, namely their exact structures, chemical stabilities and possible transformation pathways are essential pre-requisites for their application.

2. MATERIAL AND METHODS

Preparation of $[Re^{VII}(O)_2Cat)_2]^-$ complex

1.76 mg of tetrabutylammonium tetrachlorooxorhenate [(n-Bu_4N)($ReOCl_4$)] (1.0 µmol) with 0.66 mg of catechol (Cat) (2.0 µmol) were dissolved in in 3 ml of acetonitrile. After complete dissolution, 8 equivalents of triethylamine (TEA) (33.5 µl of 10% TEA solution in acetonitrile) were added and the reaction mixture kept at a laboratory temperature for 6 hours. Desired reaction product was chromatographically purified on a Phenomenex Luna 5 semi-preparative column 100 x 10 mm (3 µm) and recrystalized from acetonitrile:water (90:10 v/v) solution. Before spectroelectrochemical (SE) measurements the samples were dried under vacuum, dissolved in 0.1 M solution of tetrabutylammonium hexafluorophosphate ($TBAPF_6$) in dried acetonitrile to concentration of about 1 mmol/l. Solution was bubbled for 15 minutes with argon prior to SE measurements.

Spectroelectrochemical setup

SE measurements were performed using optical thin-layer electrochemical cell with Pt mesh electrode and Ag pseudoreference electrode. The optical path was about 0.2 mm. Cyclic voltammetry experiment was performed by Autolab PGSTAT101 potentiostat with NOVA software, absorption experiment by Avantes AvaSpec ULS3648TEC optical fiber spectrometer (resolution ~2 nm) with AvaLight DHc deuterium halogen lamp.

3. RESULTS AND DISCUSSION

Cyclic voltammogram of $[Re^{VII}(O)_2Cat)_2]^-$ complex in 0.1 M TBAPF6 in acetonitrile is presented in Figure 1A.

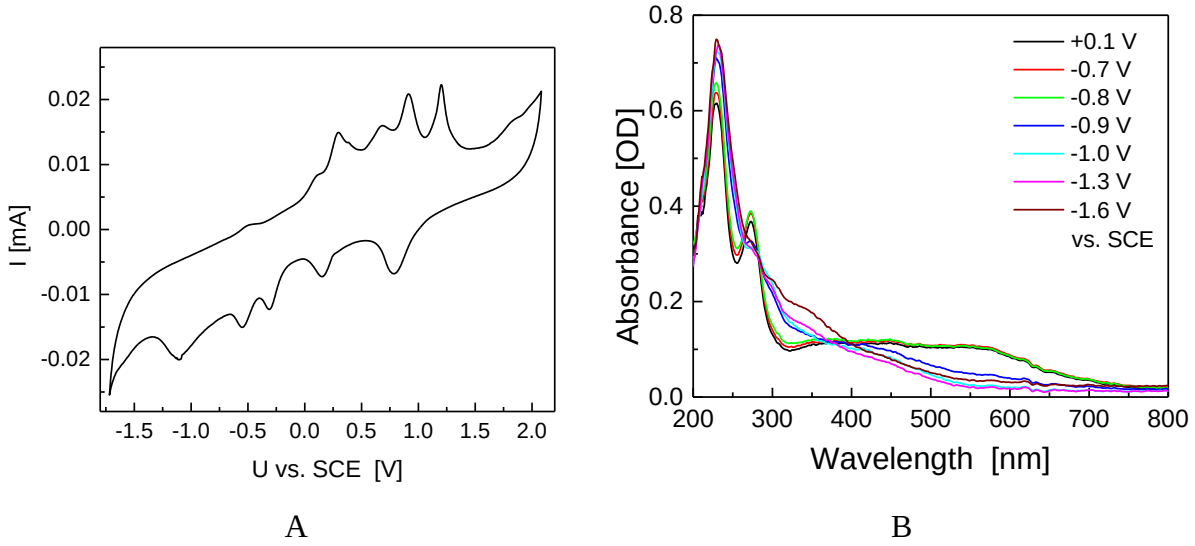

A B

Figure 1.: (A) – Cyclic voltammogram of $[Re^{VII}(O)_2Cat)_2]^-$ complex in 0.1 M TBAPF6 in acetonitrile. (B) – Absorption spectra depicting $[Re^{VII}(O)_2Cat)_2]^-$ reduction to $[Re^{V}(O)Cat)_2]^-$ in 0.1 M TBAPF6 in acetonitrile (cathodic region, first cycle).

We observed a complicated redox behavior due to complex chemistry of Re redox states. Spectroelectrochemical data from UV/VIS absorption enables us to determine origin of CV peaks in the cathodic region. In Figure 1B there are absorption spectra of the studied Re^{VII} complex under lowering the potential. We observed a decrease of a broad absorption band consisting of three peaks at about 370 nm, 460 nm and 550 nm. This spectral transition corresponds to the one between the $[Re^{VII}(O)_2Cat)_2]^-$ and $[Re^{V}(O)Cat)_2]^-$ [6] and occurred between -0.8 V and -0.9 V vs SCE. The corresponding CV peak was irreversible and we observed only $E_{p,c}$ peak at about -1.1 V (Figure 1A). Further study is in progress.

4. CONCLUSION

Study of relation between electrochemical and spectral properties is a key factor for the characterization of transition metal complexes used as catalysts and active components in novel sources of energy. As it follows from presented cyclic voltammogram, rhenium-catechol complex undergoes numerous redox transitions involving reversible and irreversible electrochemical processes. Based on comparison of absorption spectra of rhenium complex species and the spectra provided by SE measurement, we identified a transition between Re^{VII} and Re^{V} complex species.

5. ACKNOWLEDGEMENT

This research was carried out within the framework of the project of the Specific University Research (SVV). The Norwegian Financial Mechanism project CZ01116 is gratefully acknowledged.

6. REFERENCES

[1] Blower PJ, Singh J, Clarke SE, Bisundan MM, Went MJ (1990) J. Nucl. Med. 31:212
[2] Volkert WA, Deutsch EA (1993) Advances in metals in medicine. State College, PA: JAI Press.
[3] Gable KP, Brown EC (2003) J Am Chem Soc 125:11018
[4] Vikuturi S, Chapman G, Ahmad I, Nicholas KM (2010) Inorg Chem 49:4744
[5] Xia H, Liu X, Wu Q, Zhang Y, Gao W, MU Y (2012) J. Coord. Ch. 65:1266
[6] Štícha M, Kaliba D, Jelínek I, Poláková J, Ch. Lett., Submitted for publication

EFFECT OF ANTI-PAIIL ANTIBODY ON *PSEUDOMONAS AERUGINOSA* INFECTION IN CELLULAR AND ANIMAL MODELS

Božena KUBÍČKOVÁ[1*], Jana HADRABOVÁ[1], Lucie VAŠKOVÁ[1], Michaela WIMMEROVÁ[2], Marie STIBOROVÁ[1], Petr HODEK[1]

[1] *Department of Biochemistry, Faculty of Science, Charles University in Prague, Hlavova 8, 128 40 Prague 2, Czech Republic*

[2] *Department of Biochemistry, Faculty of Science, Masaryk University, Kamenice 753/5, 625 00 Brno, Czech Republic*

[*] *bojkaku@gmail.com*

Abstract

We have prepared hen yolks antibodies (IgYs) against *Pseudomonas aeruginosa* (PA) lectin, anti-PAIIL IgY and tested them as a possible prophylaxis of PA bacterial infection. Using a luminescent (lux) strain of PA the anti-PAIIL antibody protective effect against adhesion of this bacterium on epithelium cell lines derived from normal or cystic fibrosis (CF) human lungs was examined. The antibody was also applied to mice infected with PA. While the anti-PAIIL antibodies almost equally prevented PA bacteria adhesion in both cell lines, they did not protect mice from PA infection.

1. INTRODUCTION

Cystic fibrosis (CF) is an autosomal recessive disorder caused by mutations in the gene coding for CF transmembrane conductance regulator. Pathophysiology changes of lungs are associated with increased susceptibility of CF patients towards microbial infections, namely with *Pseudomonas aeruginosa* (PA), which leads to chronic lung disease resulting in life-threatening conditions. Antibiotics are currently the first-line therapy of this condition. Nevertheless, due to PA antibiotics resistance there is an urgent need to develop alternative therapeutics. The passive immunization by specific hen egg-yolk antibodies (IgY) against *P. aeruginosa* is promising tool for prevention of this infection. The most significant advantage of IgY, in contrast to mammalian IgG, consists in IgY inability to induce inflammatory reaction when antigen is bound. The application of specific hen antibodies for passive immunization of CF patients against PA infections is suggested to be a plausible option. As the PA bacterium binds to the sugar moiety (D-galactose and L-fucose) on the cell surface of respiratory epithelium *via* its PAIIL lectin (major virulence factor of this pathogen), the

antibodies against this lectin might prevent the PA infection by interfering with the recognition process between host cells and bacteria, and thus affect the PA adhesion [1].

2. MATERIALS AND METHODS

Preparation of antibody

Antibodies were prepared from egg yolks laid by hens immunized with recombinant PA lectin, PAIIL, as described elsewhere [2]. Pre-immune IgY sample (control) was purified from eggs collected a week prior to the immunization. The presence of anti-PAIIL IgY was determined on ELISA and Western blots using a recombinant PAIIL and PA lysate as antigens, respectively.

Assay of bacterial adhesion on epithelial cells

The assay was performed according to Noskova et al. [3] with minor modifications. In brief, immortalized epithelium cell lines derived from normal (NuLi) or CF (CuFi) human lungs (ATCC) were stained with a fluorescent dye PKH67, seeded onto well plates (24 wells) and incubated for 24 h at 37°C, 5% CO_2 to form a confluent layer. Bioluminescent strain PAO1 (ST 549) containing a luxCDABE cassette (generous gift of Dr. Robert E. W. Hancock, University of British Columbia, Vancouver, Canada) was used in the assay. The bacterial suspension with anti-PAIIL or control IgYs (1 mg/ml), or PBS, was applied onto epithelium cells in well plates. After 2 hrs incubation non-adhered bacteria were removed by extensive washing with PBS. The luminescence of adhered PA on epithelial cells was quantified using spectrofluorometer (Tecan Infinite M200 Pro). Results were expressed as a ratio of the PA luminescence/epithelium cell fluorescence.

IgY inhalation and monitoring of the level of airway infection in model animals

The antibody prophylaxy was tested *in vivo* in model animals. Mice (strain ICR CD1, males) inhaled nebulized anti-PAIIL antibodies (for 4 days, 10 minutes per day). Two hours after the last inhalation animals (in anesthesia) were infected with optimized dose of bacterial suspension of PA (5×10^5 CFU/30 μl) by intratracheal instillation. The use of luminescent PA strain allowed a non-invasive monitoring of the PA infection during the experiment using IVIS imaging system Lumia XR. PA infection loads in lung were quantified as a luminescence intensity per area of lungs (photon x $sec.^{-1}$ x cm^{-1}).

3. RESULTS AND DISCUSSION

The adherence of bacteria to epithelial cells is an essential process in PA pathogenesis. The bacterium possesses several specific adhesins, which significantly contribute to its virulence. It is thought that airway surfaces of CF patients are lacking the sialylation of glycoconjugates such as GM1, which enables the binding of PA *via* saccharide specific lectins, e.g. PAIIL [4]. To prevent the bacteria adhesion on host cells hen yolk antibodies against the recombinant PAIIL were prepared and tested. Their prophylactic properties against the PA colonization of lung epithelial cells derived from normal (NuLi) or CF-patient (CuFi) lung tissues has been already proven using an adhesion assay based on a dual fluorescence determination of PA and epithelial cells [3].

In our study, we used two experimental models to evaluate prophylactic effect of anti-PAIIL antibodies. Firstly, the potency of the lectin PAIIL antibodies to prevent the adhesion of bacteria PA was tested *ex vivo* in epithelium cell lines NuLi and CuFi. Next, the antibody prophylaxis was tested *in vivo* in model animals – experimental mice. The obtained results showed that hen antibodies against the bacterial lectin PA-IIL were clearly able to prevent the adhesion of PA to human lung cells. The antibody treatment reduced the amounts of adhered bacteria on the NuLi and CuFi cells by approximately 35 % and 30 %, respectively, relative to PBS-treated control. On the other hand, the animal treatment with nebulized anti-PAIIL antibodies showed an opposite tendency. The PA colonization was more pronounced in the antibody-inhaled mice than in PBS controls. This unexpected result most probably reflects the lack of specific anti-PAIIL antibodies in lungs to neutralize lectin binding ability. Under these conditions bacterial lectin PAIIL binds to carbohydrates of IgY antibodies, which causes bacteria agglutination and thus impaired bacteria clearance from the lungs. Such phenomenon has been noticed in experiments with human lung cells, when control hen antibody was used in PA adhesion assay.

4. CONCLUSION

Hen yolk antibodies against *P. aeruginosa* lectin PAIIL repeatedly proved their ability to reduce PA bacteria adhesion on human airway epithelia cells under experimental condition used. On the other hand, *in vivo* in animal model, we found that the antibodies inhaled before the application of the bacteria do increase the development of bacterial infection. Such result reflects the conditions when lectin PAIIL is not inhibited by antibody, but binds antibody via its saccharides.

5. ACKNOWLEDGEMENT

The work has been supported by GAUK 1584814 and UNCE 204025/2012.

6. REFERENCES

[1] Imberty A, Wimmerova M, Mitchell E P, Gilboa-Garber N.: Microb. Infect, 6 (2004), 222-229
[2] Hodek P, Trefil P, Šimůnek J, et al.: International Journal of Electrochemical Science, 5 (2013), 113-124
[3] Nosková L, Kubíčková B, Vašková L, et al.: Sensors (Basel), 16 (2015), 1945-1953
[4] Bryan R, Kube D, Perez A, et al.: American Journal of Respiratory Cell and Molecular Biology, 19 (1998), 269-277

EFFECT OF LIPOPHILIC MEMBRANE ON PENETRATION OF POTASSIUM LIGNOHUMATE

Marcela LASTUVKOVA[1*], Jiri SMILEK, Petr SEDLACEK[1], Martina KLUCAKOVA[1]

[1] *Materials Research Centre, Department of Physical and Applied Chemistry, Faculty of Chemistry, Brno University of Technology, Purkynova 464/118, 612 00 Brno, Czech Republic*

**xclastuvkova@fch.vut.cz*

Abstract

By the term foliar fertilization it is meant applications of nutrients, pesticides, herbicides, active materials and plant-growth preparations on the field. The era of foliar uptake began 65 years ago and nowadays it belongs to widespread fertilizers applications in the world. The main limiting barrier is cuticle, which formed the surface of plant and it has effect on the application materials. For study of foliar uptake cuticles were used from *Prunus laurocerasus*, because its cuticle is strong and it is possible the simple manipulation. Our research is focused on simple ultra-violet spectroscopy and the studying materials are humic acids respectively potassium lignohumate.

1. INTRODUCTION

Despite the negative perception of the community, pesticides are still going to be used for many decades to ensure the food supply for the ever growing world population. One of the most important ways how to improve the efficiency of pesticides and minimize their impact on off-target living systems is through increasing the penetration of active ingredients into plant foliage [1]. The absorption of minerals by leaves of plants was demonstrated experimentally 100 years ago [2], [3]. The numerous works studied the uptake of mineral ions, fungicides, pesticides, etc. Root absorptions of nutrients were replaced by foliar fertilizers, which became the new method of absorption of the plant beneficial substances. Absorption by living folic cells of any foliar applied chemical (mineral nutrients, growth regulators, pesticides, antibiotics) must be proceeding by transcuticular penetration [4]. For these studies they use top and/or bottom part from the plant leaves – cuticles. It is the first barrier with many important functions (respiration, regulation of water, regulation of ions, penetration of nutrients, etc.). The permeability of the cuticle membrane for ions, herbicides, and pesticides has been discussed in several papers. The foliar uptake of active ingredients is a complex process and depends on the leaf surface of plant, physicochemical properties of the

chemicals structure or properties of cuticles1. An important role for the nutrient absorption plays the concentration of the additives as well as the environmental conditions. Wang and Liu [1] summarized the major progress of the foliar fertilization especially during the last 15 years. They wanted to clarify the pesticide uptake into plant foliage and influence of adjuvants [1].

2. MATERIAL AND METHODS

Isolation methods

The experiments were realized by isolated plant cuticles. The isolation method is based on Solel and Edgington method [5], which used enzymes. Orgel method was used for chemical isolation of cuticles [6], which is based on concentred hydrochloric acid solution 60 wt. % zinc chloride. The isolated plant cuticles were washed and then were used for diffusion experiments.

Diffusion experiments

The diffusion experiments as the simulation of foliar fertilizers were realised by agarose hydrogels. The resource hydrogels were created by 1 wt. % agarose and 1 wt. % potassium lignohumate and the receiving hydrogels were made by only 1 wt. % agarose hydrogels. The plant cuticles were fixed between both of hydrogels. The experiments were realized for 14 days.

3. RESULTS AND DISCUSSION

Measurement of concentration change of potassium lignohumate depending on time of penetration was determined by ultra-violet spectroscopy. It was determinated concentration profile of diffusion (Figure 1).

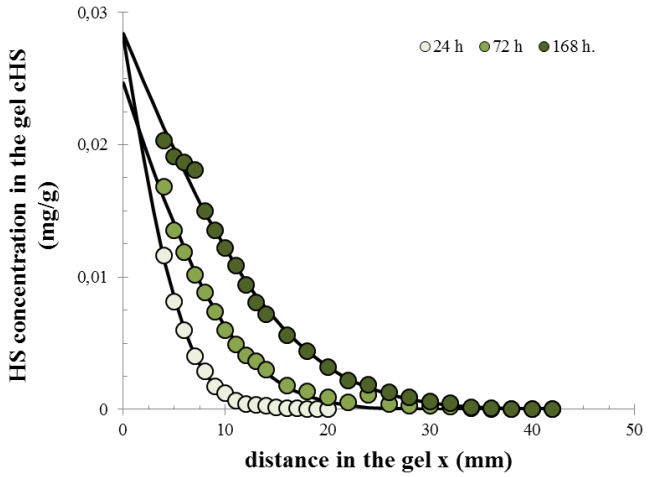

Figure 1.: Concetration profile of potassium lignohumate through plant cuticle.

From the correlation of theoretical and experimental concentration profiles, diffusion coefficient and concentration on the interface were determined, it was used the theoretical diffusion model:

$$c = c_0 \cdot \mathrm{erfc}\sqrt{\frac{x}{4D_{\mathrm{eff}}\, t}},$$

where c is concentration of diffusing solute, c_0 is concentration on the interface, x is distance from the interface hydrogel-solution, D_{eff} is effective diffusion coefficient and t is time of diffusion. Fundamental transport parameters are summarized by Table 1.

Table 1: Transport parameters D_{eff} and c_0.

Bottom plant cuticles			**Top plant cuticles**		
Cuticles	D_{eff} ($\cdot 10^{10}$ m^2/s)	c_0 (mg/g)	**Cuticles**	D_{eff} ($\cdot 10^{10}$ m^2/s)	c_0 (mg/g)
Enzymatically isolated cuticles	1.3 ± 0.1	0.13 ± 0,01	**Enzymatically isolated cuticles**	0.9 ± 0.2	0.047 ± 0.001
Chemically isolated cuticles	1.4 ± 0.1	0.34 ± 0,04	**Chemically isolated cuticles**	0.9 ± 0.3	0.057 ± 0,.001

The work describes simple diffusion techniques which should simulate foliar fertilization under laboratory conditions, where plant cuticles are limiting barriers, because it is formed by lipophilic group. Commercial fertilizers are mainly formed by hydrophilic compounds, while cuticle as the limiting barrier is formed by hydrophobic compounds therefore diffusion solute

may interact with cuticle and the diffusion process can be slowed by these interactions. The studied materials were potassium lignohumates, which have positive behaviours on the plant, too.

4. ACKNOWLEDGEMENT

This work has been supported by Materials Research Centre at Faculty of Chemistry, Brno University of Technology – Sustainability and Development, REG LO1211, with financial support from National Program for Sustainability I (Ministry of Education, Youth and Sports, Czech Republic).

5. REFERENCES

[1] Wang, C. J., Liu Z. Q.: Pesticide Biochemistry and Physiology, 87 (2007), 1, 1-8.
[2] Wittwer, S. H., Teubner, F. G..: Annual Review of Plant Physiology, 10 (1959), 13-30.
[3] Yamada, Y., Wittwer, S. H., Bukovac, J.: Plant Physiology, 39 (1964), 1, 978-82.
[4] Wittwer, S. H.: Plant Science, 8 (1964), 161-82
[5] Solel Z, Edgington L: Phytophatology, 63 (1972), 4, 505-510.
[6] Orgel: Plant Physiology, 30 (1955), 78-80.

FABRICATION AND CHARACTERIZATION OF SELF-ORDERED MERMISTIVE TiO_2 WITH ANODIC OXIDATION

Marian MÁRIK[*1], Jaromír HUBÁLEK[1]

[1] *Central European Institute of Technology, Brno University of Technology, Technicka 3058/10, 616 00 Brno, Czech Republic*

**marian.marik@ceitec.vutbr.cz*

Abstract

Fabrication and characterization of self-ordered mermistive TiO_2 structures was provided. Fabrication was done with anodic oxidation in a water based electrolyte. TiO_2 nanocolumns for electrical characterization were contacted with Ag conductive paste. Electrical characterization was provided with a Semiconductor analyzer system Keithley SMU 4200. Results shown that the TiO_2 nanocolumns has memristive behavior, which is highly influenced by geometrical size.

1. INTRODUCTION

Fabrication and characterization of memristors for non-volatile memory applications with electrochemical processes is a high challenge. Self-ordered TiO_2 nanocolumns with different length prepared and modified with electrochemical processes should be perform as a memristive cells. The self-ordered nanocolumn fields are realized with porous anodic alumina oxide (AAO) mask.

Anodic oxidation of aluminum is a well-known process. This process can produce the porous films possessing high pore density, uniform pore size. The other important advantage is the versatility and low cost. [1] The nanocolumns grown in AAO mask are stable and electrically isolated from each other.

2. MATERIAL AND METHODS

Anodic oxidation process was optimized for the initial surface, which was a sputter-deposited metal bilayer of Ti/Al on the silicon wafer (previously covered with 500 nm of SiO2). Titanium layer with thickness of 300 nm was covered with 550 nm thick Al layer. The anodization was performed at 10 °C with a 0.3 M oxalic acid solution at the circulation speed of 70 mL/min. The apparatus was equipped with polytetrafluor-ethylene (PTFE) head with internal diameter 6.9 mm equipped with a stainless steel electrode. During the anodizing

process, the current was always limited to 5 mA and the potential for the aluminum layer was constantly kept at 40 V. The diameter of the pores in AAO is approximately 40–50 nm. Anodization of the titanium layers were provided at potential of 40 V and 60 V (Figure 1).

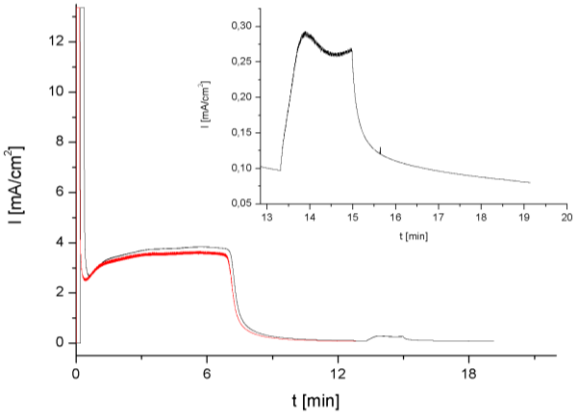

Figure 1.: Anodization curve for Al/Ti bilayer. The first sample was anodized for 13 min including Ti anodizing at 40 V (red curve). The second sample was anodized for 19.25 min and after 13.5 min, the voltage was increased from 40 to 60 V (black curve).

Both potentials are suitable to prepare self-grown TiO_2 nanowires in AAO, the difference is in height of TiO_2 nanowires in the pores (Figure 2). At the potential of 60 V the TiO_2 columns are higher than at 40 V

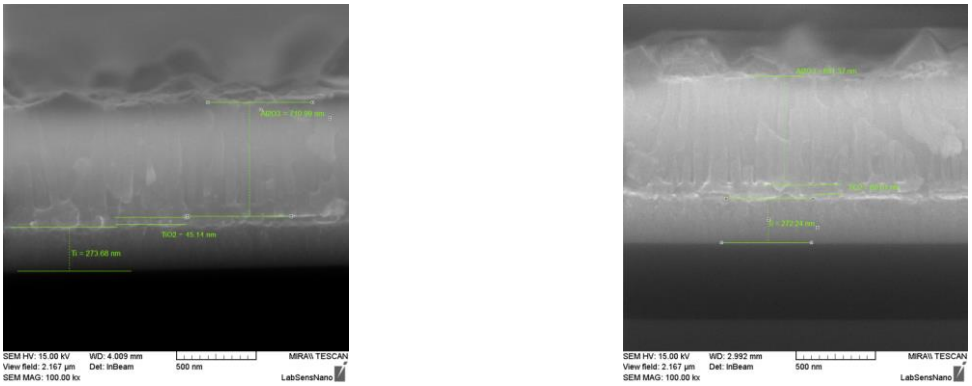

Figure 2.: Cross section of the anodized Ti – Al layers. Anodization of Ti at 40V (a.) and at 60V (b.).

Due to preparation of electrical contacts on the top of TiO_2 columns the AAO was partially etched (Figure 3).

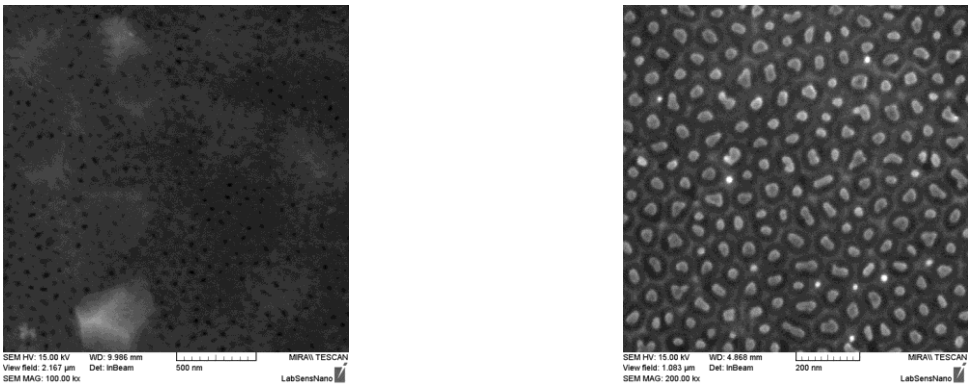

Figure 3.: Surface of the sample Ti at 60V before (left) and after (right) etching of AAO.

3. RESULTS AND DISCUSSION

Electrical characterization of self-ordered TiO_2 columns were provided with Keithley SMU4200 semiconductor analyzer. The electrical contacts were prepared with Ag paste, the Al/Ti layer was used as common.

Nanocolumns anodized at 40 V were tested up to 3V and nanocloumns anodized at 60V were tested up to 5V. The curve *a* in Figure 4 shows voltage sweeping for shorter columns from 0 to -3V and from 0 to 3V. The curve *b* shows IV characterization from 0 to 3V and from 0 to -3V. Similarly as at shorter columns the curve *a* in Figure 5 shows voltage sweeping for longer columns from 0 to -5V and from 0 to 5V. The curve *b* shows IV characterization from 0 to 5V and from 0 to -5V. The hysteresis at both length are not symmetric. The memristic behavior in all cases was depended on the first applied polarity. The characterization in Figure 4*c* and Figure 5*c* was done after forming voltage 3 and 5V for 3sec. The column lost his nonlinear IV character and started to behave as a resistor.

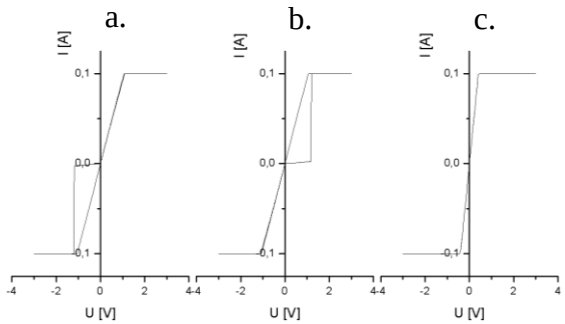

Figure 4.: IV characterization of samples anodized at 40V.

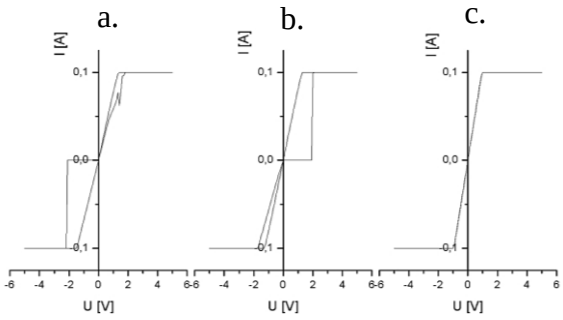

Figure 5.: IV characterization of samples anodized at 60V.

4. CONCLUSION

Comparison of the IV characteristics shown the memristic difference between the samples with 40–45 nm and 60 nm thin TiO_2 layers. The memristic behavior depends on the materials thickness, and this fact was also confirmed by Ref. [2].

5. ACKNOWLEDGEMENT

The work has been supported by the project CEITEC 2020 (LQ1601).

6. REFERENCES

[1] Mozalev, A.; Magaino, S.; Imai, H., Electrochim Acta 2001, 46 (18), 2825-2834.
[2] Strukov, D. B.; Snider, G. S.; Stewart, D. R.; Williams, R. S., Nature 2008, 453 (7191), 80-83.

DIHYDROMYRICETIN AND EXPRESSION OF CYTOCHROMES P450 1A1/2 AND CYTOCHROME B_5 ON TRANSCRIPTIONAL LEVELS IN RATS

Michaela MOSEROVÁ, Kamila KOUCKÁ, Barbara FERIANČIKOVÁ, Tomáš BLECHA, Marie STIBOROVÁ, Petr HODEK*

[1] *Department of Biochemistry, Faculty of Science, Charles University in Prague, Albertov 6, 128 43 Prague 2 Czech Republic*

**hodek@natur.cuni.cz*

Abstract

The chemopreventive compounds might affect the levels of biotransformation proteins such as cytochrome P450 (CYP) of a 1A subfamily and cytochrome b_5 in several rat organs (*i.e.* liver, kidney, lung, small intestine and colon). In this study, we investigate the effect of dihydromyricetin (DHM) on expression of these proteins. The efficiency of DHM to induce these proteins was compared with that of BaP, the compound known to be their strong inducer. DHM slightly affects the expression of studied proteins at the transcriptional level. The results found in this study might be considered as positive in terms of safety of dihydromyricetin usage.

1. INTRODUCTION

Dihydromyricetin, (2R,3R)-3,5,7-trihydroxy-2-(3,4,5-trihydroxyphenyl)-2,3-dihydrochromen-4-one (DHM), is credited with hepatoprotective effects observed in rodents as well as with anti-tumor ability, inhibiting e.g. progression and metastasis of prostate cancer [1]. It is also highly effective in counteracting acute EtOH intoxication, in reducing excessive EtOH consumption *via* antagonizing acute EtOH-induced potentiation of gama-aminobutyric acid receptors and in increasing activity of alcohol and acetaldehyde dehydrogenases [2]. This compound found in Japanese Raisin Tree, *Hovenia dulcis* [3], belongs to numerous groups of flavonoids, which are of a great interest since they provide a wide variety of biological activities [4]. In addition to their powerful anti-oxidant properties, they are suggested to be anti-cancer agents acting at various stages of carcinogenesis. The flavonoids are, because of their natural origin, generally accepted as health-promoting compounds and safe for the human use. Their extensive intake as food supplements may, however, cause potential threats resulting e.g. from altered metabolism of endogenic compounds and from flavonoid pro-

oxidant activity [5]. Much less attention is being paid to flavonoid-drug or flavonoid-carcinogen interactions. These interactions frequently arise from flavonoid abilities to modulate catalytic activity of xenobiotic metabolizing enzymes such as cytochromes P450 (CYPs). Flavonoids are known to be the inhibitors, inducers and even activators of CYPs, the enzymes that participate in metabolism of many exogenous and endogenous hydrophobic substances.

2. MATERIAL AND METHODS

Male Wistar rats were treated by gastric gavages in a single dose (60 mg/kg b.w) with DHM and/or BaP as described previously [6]. The mRNA contents in rat liver and kidney were measured using the real-time polymerase chain reaction (RT-PCR) as described [7-11].

3. RESULTS AND DISCUSSION

In general, the administration of DHM did not significantly increase *CYP1A1, 1A2 or cytochrome* b_5 gene expression in any rat organ examined. In contrast, animals treated with benzo[a]pyrene (BaP) were used as positive control. This carcinogen significantly induces the genes of these proteins in rats under the conditions used. It increases in levels of gene expression of CYP1A, the enzyme whose induction is controlled *via* Ah receptor, and also in levels of gene expression of cytochrome b_5 [8]. More than two-, three- and four-orders of magnitude higher expression of *CYP1A1* mRNA was found in kidney, lung and liver of rats treated with BaP, respectively, than in these organs of control, untreated rats. A lower (up to 100-times), but significant increase in expression of *CYP1A2* mRNA was produced by BaP in the organs of BaP-treated rats. Expression of cytochrome b_5 at the transcriptional levels (mRNA of cytochrome b_5) was also increased by treatment of rats with BaP, in the lung, but not in the liver and kidney. CYP1A1 is known to play an important role in the activation of BaP to reactive metabolites capable of forming covalent adducts with DNA [12], but recent studies, using mice with deleted gene of CYP1A1, showed the higher formation of covalent DNA-BaP adducts in these knock-out animals than in control animals. This indicates that CYP1A1 plays *in vivo* a more important role in BaP detoxification rather than in its activation, and protects the body from its toxicity [12, 13]. The administration of DHM did not significantly affect the gene expression of tested proteins in rat organs. The significant increase in expression of *CYP1A1* gene was observed only in the proximal part of small intestine, whereas the slight decrease was found in the middle part of this tissue and the level

of *CYP1A1* gene expression was unchanged in its distal part and colon. Interestingly, DHM significantly increased the BaP-mediated induction of *CYP1A2* gene in kidney and of *cytochrome* b_5 gene in liver of BaP-treated animals. The present data suggest low potential risk associated with the CYP induction or modulation at systemic concentrations after the DHM ingestion.

4. ACKNOWLEDGEMENT

Supported by GACR (P303/12/G163).

5. REFERENCES

[1] Ni F, Gong Y, Li L, et al.:. PLoS One. 7(2012), e38802
[2] Shen Y, Lindemeyer AK, Gonzalez C, et al.: J Neurosci. 32(2012), 390
[3] Hyun TK, Eom SH, Yu CY, et al.: Planta Med. 76(2010), 943
[4] Hodek P.: Flavonoids in: Metabolism of Drugs and Other Xenobiotics (Anzenbacher P, Zanger UM, eds.) Wiley VCH, Weinheim, Germany 2012, pp. 543
[5] Hodek P, Krizkova J, Burdova K, et al.: Chem. Biol. Interact. 180(2009), 1
[6] Hodek P, Fousova P, Brabencova E, et al..: Neuro Endocrinol Lett. 35 Suppl 2(2014), 158
[7] Vranová I, Moserová M, Hodek P, et al.: International Journal of Electrochemical Science, 8 (2013), 1586.
[8] Arlt VM, Stiborová M, Henderson CJ, et al.: Carcinogenesis, 29 (2008), 656
[9] Kotrbová V., Mrázová B., Moserová M., et al.: Biochemical Pharmacology, 82 (2011), 669
[10] Vranová I, Moserová M, Hodek P, et al.: International Journal of Electrochemical Science, 8 (2013), 1586
[11] Stiborová M, Dračínská H, Martínek V, et al.: Chemical Research in Toxicology, 25 (2013) 290
[12] Uno, S., Dalton, T. P., Derkenne, S., et al..: Molecular Pharmacology 5(2004), 1225
[13] Uno S, Dalton TP, Dragin N, et al.: Molecular Pharmacology 4(2006), 1103.

EFFICIENCIES OF HUMAN CYTOCHROME P450 3A4 ENCAPSULATED IN LIPOSOMAL AND MICROSOMAL NANOPARTICLES TO ACTIVATE ELLIPTICINE TO FORM COVALENT DNA ADDUCTS

Miroslav ŠULC[1], Iveta MRÍZOVÁ[1], Tereza ČERNÁ[1], Eva FREI[1], Tomáš ECKSCHLAGER[2], Vojtech ADAM[3], Marie STIBOROVÁ[1*]

[1] *Department of Biochemistry, Faculty of Science, Charles University, Albertov 2030, 128 40 Prague 2, Czech Republic*

[2] *Department of Pediatric Hematology and Oncology, 2nd Medical Faculty, Charles University and University Hospital Motol, V Uvalu 84, 150 06 Prague 5, Czech Republic*

[3] *Department of Chemistry and Biochemistry, Mendel University in Brno, Zemedelska 1, 61300 Brno, Czech Republic*

**stiborov@natur.cuni.cz*

Abstract

The cytochrome P450 (CYP) 3A4 enzyme both in the liposome and microsome nanoparticle forms was efficient to activate ellipticine to species forming DNA adducts. Two DNA adducts, which are formed from ellipticine metabolites 12-hydroxy- and 13-hydroxyellipticine generated by its oxidation by CYP3A4, were formed by both CYP3A4 nanoparticle systems. A higher effectiveness of CYP3A4 in microsomal than in liposomal nanoparticles to form ellipticine-DNA adducts was found. The results demonstrate the DNA-damaging effects of ellipticine after its activation by CYP3A4 nanoparticle forms and indicate their suitability for active targeting of this enzyme to specific cancer cells.

1. INTRODUCTION

Cancer treatment is one of the most difficult problems in clinic practice. Therefore, many approaches were utilized to develop novel antitumor drugs, which could be applied with other therapeutic modalities. The research in this field has resulted to developing a lot of new substances possessing potent anticancer activity. Ellipticine is an anticancer agent that functions through multiple mechanisms participating in cell cycle arrest and initiation of apoptosis. This drug forms covalent DNA adducts after its enzymatic activation with cytochrome P450 (CYP), which is one of the most important ellipticine DNA-damaging mechanisms of its cytotoxic effects [1]. The improvements of cancer treatment are the major

challenge in oncology research. Nanotransporters (nanoparticles) are promising approaches to target tumor cells, frequently leading to improve drug therapeutic index. Ellipticine has already been prepared in nanoparticle forms [2]. However, since its anticancer efficiency depends on the CYP3A4-mediated metabolism in cancer cells, the aim of our research is to develop nanoparticles containing this enzyme that can be transported to tumor cells, thereby potentiating ellipticine cytotoxicity.

Because the CYP enzymes are the membrane proteins naturally located in a membrane of the endoplasmic reticulum of cells dictating their enzymatic activity [3], the lipid based nanocarriers should be the suitable systems for these membrane enzymes [4,5]. Therefore, the CYP3A4 in the liposomal nanoparticles was prepared, used for evaluation of its catalysis to activate ellipticine and their efficiency was compared with that of CYP3A4 present in a natural nanostructure, microsomes.

2. MATERIAL AND METHODS

The CYP3A4 enzyme encapsulated with NADPH:CYP reductase (POR) into two nanoparticle forms, liposomes and microsomes (Supersomes™, Gentest Corp., Woburn, MI, USA), was tested to activate ellipticine to its reactive species forming covalent DNA adducts. Ellipticine-derived DNA adducts were determined by the ^{32}P-postlabeling method [1,2,4].

3. RESULTS AND DISCUSSION

Liposomes were prepared from 1,2-dilauroyl-sn-glycero-3-phosphocholine, 1,2-dioleoyl-sn-glycero-3-phospho-rac-(1-glycerol), and 1,2-dilauroyl-sn-glycero-3-phosphoserine dissolved in chloroform and mixed in a ratio of 1:1:1. A lipid film was formed by rotary evaporation and nitrogen flushing to remove residual solvent. This lipid film was further dispersed with buffer (pH 7.4) containing CHAPS and reduced glutathione, and ultrasonicated for 5 min at 20 °C. The appropriate amounts of CYP3A4 and POR (in a ratio of 1:1) were added to the prepared dispersion and incubated at 20 °C for 10 min. The liposomes with CYP3A4 and POR were then used in further experiments. The aliquots of the liposomes containing increasing amounts of CYP3A4 were added into the incubation mixtures to reach its final amounts of 50 – 250 pmol and these mixtures were used for activation of ellipticine to species forming ellipticine-derived DNA adducts. The second nanoparticle system used were Supersomes™ that are microsomes isolated from insect cells transfected with a baculovirus construct containing cDNA of human CYP3A4 and its reductase, POR. Besides

overexpressed human CYP3A4 and POR, these microsomes contained a low amount of other enzymes of the monooxygenase system that were present in the membrane of the insect endoplasmic reticulum (*i.e.*, microsomal epoxide hydrolase, cytochrome b_5 and its reductase, NADH:cytochrome b_5 reductase). But their levels were, in comparison to overexpresssed CYP3A4 and POR, negligible.

Both CYP3A4-nanoparticle systems incubated in the presence of a cofactor of POR, NADPH, and DNA activated ellipticine to metabolites forming two ellipticine-derived DNA adducts; one major generated from ellipticine-13-ylium formed by decomposition of 13-hydroxyellipticine and one minor generated from ellipticine-12-ylium formed from 12-hydroxyellipticine These two adducts were analogous to those formed in several and cancer cells *in vitro* and in healthy and tumour cells *in vivo*. An analogous pattern of ellipticine-derived DNA adducts was formed by CYP3A4 present in the second nanoparticle system tested in this work, Supersomes^{TM}. The formation of adduct formed from 13-hydroxyellipticine was dependent on concentrations of human CYP3A4 in the liposomal system present in the incubation mixture, being increased with elevated amounts of CYP3A4 in the system. The levels of this DNA adduct formed in the liposomal and Supersomal systems are of the same order. Nevertheless, the effectiveness of CYP3A4 present in the Supersomal system is higher than that of CYP3A4 in the liposomal nanoparticles. One of the reasons might be the fact that artificially prepared liposomes do not contain all components present in the natural system of the microsomal (Supersomal) particles that can influence the CYP3A4 enzyme activity (*i.e.*, the absence of all spectrum of membrane-making lipids, the absence of proteins of microsomes including those that are components of the monooxygenase system such as cytochrome b_5). The latter suggestion is supported by our recent results, where we found that cytochrome b_5 increases the potency of CYP3A4 to oxidize ellipticine to 13-hydroxyellipticine, thereby increasing the levels of ellipticine-derived DNA adduct [6].

4. ACKNOWLEDGEMENT

Supported by GACR (14-18344S) and Charles University (UNCE 204025/2012)

5. REFERENCES

[1] Stiborová M, Frei E: Curr Med Chem, 21 (2014) 575-591
[2] Stiborova M, Manhartova Z, Hodek P, et al.: Sensors, 14 (2014) 22982-22997
[3] Guengerich FP: Chem Res Toxicol, 14 (2001) 611–650
[4] Stiborova M, Bieler CA, Wiessler M, et al: Biochem Pharmacol, 62 (2001) 1675-1684
[5] Kotrbova V, Mrazova B, Moserova M, et al.: Biochem Pharmacol, 82 (2011) 669-680
[6] Stiborova M, Indra R, Moserova M, et al.: *Chem Res Toxicol* 25 (2012) 1075-1085

STUDY OF EFFECT OF HYALURONAN ADDITION TO SEPTONEX MICELLAR SOLUTION

Tereza PILGROVÁ[1], Miloslav PEKAŘ[1]

[1] *Brno University of Technology, Faculty of Chemistry, Institute of Physical and Applied Chemistry, Purkyňova 464/118, 612 00 Brno, Czech Republic*

**xckrutisova@fch.vut.cz*

Abstract

Association of micelles with hyaluronan could enhance micelles biocompatibility and can lead to target to the specific receptors in a human body. In this report, results of the study of electrostatic association of cationic micelles of Septonex with hyaluronan are reported. The cationic micelle/hyaluronan complexes were studied using turbidimetry and dynamic light scattering method and were evaluated to determine their structure, average size and zeta potential as a function of the amount of the both component in the system. Results of turbidimetry revealed that aggregates formation (turbidity increasing) depends especially on hyaluronan concentration while surfactant concentration (above critical micelle concentration) affects interaction insignificantly. Dynamic light scattering experiments indicate that hyaluronan molecular weight has insignificant effect on isoelectric point of the systems.

1. INTRODUCTION

Micelles can solubilize water-insoluble molecules in their inner thanks to their amphiphilic structure. Over the years aggregates of surfactants have been of interest to the pharmaceutical scientist as drug vehicles carriers. However surfactants may have adverse effects on biological structures. Covering of micelles with suitable bioacceptable molecules (i.e. hyaluronan) may enhance their biocompatibility and perhaps also stability in biological environment and may also provide the micelles with targeting moieties due to physiological roles of hyaluronan in living organism [1, 2, 3].

In this study results of the research on association of cationic surfactant micelles with hyaluronan are reported. Hyaluronan interacts with positively charged micelles by electrostatic interactions mediated by its dissociated carboxyl groups. In our study, these interactions has been studied by turbidimetry and dynamic light scattering method and the effects of concentration of both interacting partners and of the hyaluronan molecular weight

were investigated. These two parameters control the particle size and, consequently, clear to turbid dispersions can be prepared.

2. MATERIAL AND METHODS

Stock solution of hyaluronan (HyA, CPN, Ltd., Czech Republic) at different molecular weights (100 kDa and 1500 kDa) and cationic surfactant Septonex (GBNchem) were prepared in aqueous solution.

Turbidity measurements, reported as absorbance A, were performed at 400 nm using Varian Cary 50 spectrometer. Turbidimetric titrations were carried out by adding hyaluronan solutions (0.3 and 0.5 g/l) to micellar solution at concentration 3 mmol/l.

Interaction between hyaluronan and surfactants were studied using titration experiments by adding hyaluronan at concentration 2 g/l to surfactant solutions at concentration 2 mmol/l. All measurements were carried out by Zetasizer Nano ZS (Malvern Instruments) and Autotitrator MPT 2 (Malvern Instruments). Particle size distributions and zeta potentials were obtained.

3. RESULTS AND DISCUSSION

Turbidimetric titration was chosen as an indicator of the loss of intensity of transmitted light due to the scattering effect of particles associated from hyaluronan and surfactant suspended in it. Hyaluronan was added to the surfactant solution at concentration 3 mmol/l ensuring micelle aggregates presence in the systems [4]. Obtained data (Figure 1 left) indicate that hyaluronan and surfactant interact due to electrostatic attraction forces and that aggregates of these components are formed in the system. In the case of hyaluronan molecular weight 100 kDa, an abrupt increase in turbidity was observed, indicating the onset of macroscopic phase separation when charge ratio of surfactants and hyaluronan carboxyl groups reached 1.8. High molecular weight of hyaluronan causes turbidity gradually increasing from first hyaluronan addition due to aggregation of components.

Interaction between hyaluronan and surfactant were studied using dynamic light scattering method by titration experiments. Figure 1 right shows a way the size and zeta potential change as a function of hyaluronan content. The size of aggregates in the system after adding of hyaluronan into the surfactant solution was in the range of 150 and 400 nm. The size increases in the region of isoneutrality, when the zeta potential curve crosses zero but it could not be measured because the mean size of the complexes increased the values beyond the reliable limit for the equipment. We can clearly observe precipitates in the sample. These data

is not shown because of better display of remaining data. Zeta potential decreases mostly linearly during titration experiments, ending values were about −40 mV indicating high stability of the colloid systems. In addition, it was found that hyaluronan molecular weight has inconsiderable effect on achievement of region of system isoneutrality.

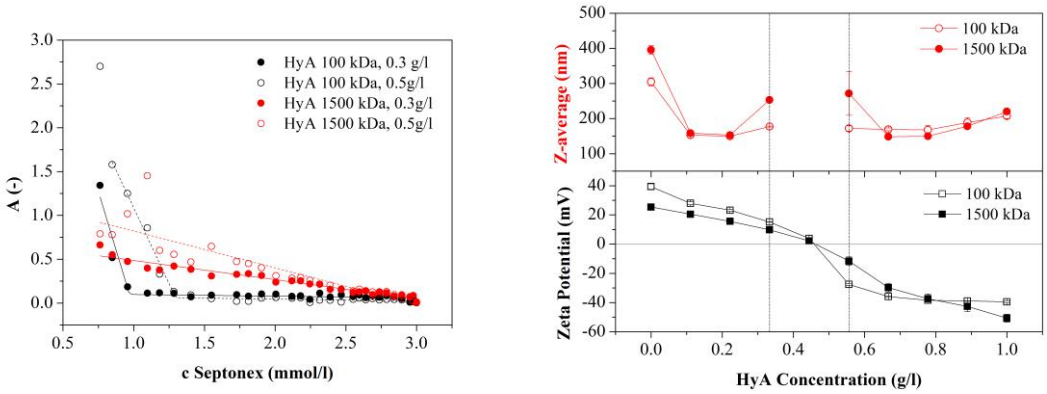

Figure 1.: Left: Turbidimetric titration graph for adding hyaluronan 100 and 1500 kDa (0.3 or 0.5 g/l) to Septonex at initial concentration 3 mmol/l. Right: Additive titration graphs for experiment using hyaluronan (2 g/l) as titrant. Top: zeta potential. Bottom: average hydrodynamic diameter (z-average, intensity-weighted).

4. CONCLUSION

Interactions of micelles with hyaluronan were investigated because of biocompatibility enhancement of this type of surfactant aggregates. There were several combinations of concentration of components compared. Effect of molecular weight of hyaluronan was studied. The result of our experiments showed that these systems are very dynamic and that composition of the system and hyaluronan molecular weight influences the interaction of components, structure of complexes and stability of aggregates. In the following experiments is important focus on all of these parameters.

5. ACKNOWLEDGEMENT

This work is supported by project Materials Research Centre at FCH BUT- Sustainability and Development, REG LO1211, with financial support from National Programme for Sustainability I (Ministry of Education, Youth and Sports).

6. REFERENCES

[1] Dicker K T, et all.: Acta Biomaterialia, 10 (2014), 4, 1558-1570
[2] Girish K S, Kemparaju K, et all.: Life Sciences. 80 (2007), 1921-1943
[3] Balazs E A, et all.: Structural Chemistry, 20 (2009), 341-349
[4] Čermáková L, Rosendorfová J, Malát M, et all.: Collection of Czechoslovak Chemical Communications, 45 (1980), 1, 210-213

AB INITIO STUDY OF SURFACE OF NANOPARTICLES Ag AND Ni

Svatava POLSTEROVÁ[1*], Monika VŠIANSKÁ[2,3], Martin FRIÁK[3,2] and Jiří SOPOUŠEK[4,2]

[1] *Department of Advanced Materials and Nanosciences, Faculty of Science, Masaryk University, Kamenice 753/5, 625 00 Brno, Czech Republic*

[2] *Central European Institute of Technology, CEITEC MU, Masaryk University, Kamenice 753/5, 625 00 Brno, Czech Republic*

[3] *Institute of Physics of Materials, Academy of Sciences of the Czech Republic, v.v.i., Žižkova 22, 616 62 Brno, Czech Republic*

[4] *Department of Chemistry, Faculty of Science, Masaryk University, Kamenice 753/5, 625 00 Brno, Czech Republic*

**svatava.zup@gmail.com*

Abstract

Our research is focused on description of energy contribution of surfaces and morphology of Ag, Ni and Ag-Ni nanoparticles. The first step of our study is to perform *ab initio* calculations of bulk and surfaces of fcc nonmagnetic Ag and ferromagnetic Ni. Here we present the calculation of surface energy and charge density difference at surfaces with different crystallographic orientations, namely (100), (110) and (111).

1. INTRODUCTION

Nanoparticles have a wide range of applications when used as catalysts, indicators, solders and many others. In contrast to bulk materials, they exhibit size-dependent properties due to a high ratio of surface to the volume. Silver [1,2] and nickel [3,4] particles are widely used in many manufacturing processes. Better understanding of phenomena taking place on the surface of particles is critically important in order to develop their yet better applications and to invent new particle-synthesis routes. From this perspective, the surfaces of metals are inseparable part of studies of chemical activity as well as of optical and thermodynamic properties. In recent years, in the field of synthesis, there is an increasing effort to prepare particles with defined surfaces. It is generally known that the particles with specific surface orientation prefer different shapes [5–8].

2. MATERIAL AND METHODS

Our quantum mechanical calculations within the framework of Density Functional Theory (DFT) [9,10] were performed using the Vienna Ab initio Simulation Package (VASP) [11,12].

The exchange and correlation energy was treated in the generalized gradient approximation (GGA) as parametrized by Perdew, Burke, and Ernzerhof (PBE) [13] and we used projector augmented wave pseudopotentials [14]. In order to reduce the forces on atoms under 0.1 meV/Å in all surface slab calculations, we employed the plane-wave energy cut-off of 550 eV and the k-point meshes determined by the smallest allowed spacing between k-points equal to 0.11 $Å^{-1}$.

The surface energies, σ, of (100), (110) and (111) surfaces were calculated as differences between the energies of relaxed surfaces E_{sur} and the energy of relaxed bulk E_{bulk}:

$$\sigma = \frac{E_{sur} - E_{bulk}}{2}$$

with both energies being related to systems with the same number of atoms. In order to analyse the redistribution of charge densities when the atoms interact together and to identify the charge density accumulation as a possible location of chemical bonds, we evaluated charge density differences, $\Delta\rho$:

$$\Delta\rho = \rho_{scf} - \rho_{non-scf}$$

as a difference between the charge densities obtained from non-selfconsistent calculations of superposition of atomic densities, $\rho_{non\text{-}scf}$, and the densities obtained from a self-consistent calculation, ρ_{scf}.

3. RESULTS AND DISCUSSION

The calculated energies of (100), (110) and (111) surfaces for fcc Ag and Ni are summarised in Table 1. This values are in a reasonable agreement with the results obtained by Vitos et al. [15]. For both Ag and Ni, the (111) surface has the lowest energy and it is the energetically most favourable, on the other hand the (110) surface has the highest energy, i.e. the least energetically favourable. This is in good agreement with general trend in fcc solids $\sigma_{(111)} < \sigma_{(100)} < \sigma_{(110)}$.

Table 1: Comparison of *ab initio* calculated surface energy of (100), (110) and (111) surfaces of Ag and Ni.

Surface	**(100)**		**(110)**		**(111)**	
Ag (σ [eV/atom])	0.646	0.653 [15]	0.801	0.953 [15]	0.409	0.553 [15]
Ni (σ [eV/atom])	0.890	0.969 [15]	1.314	1.337 [15]	0.680	0.695 [15]

The difference of surface energy between (100) and (111) surfaces is about 0.2 eV/atom, for both Ag and Ni. On the other side, the difference of surface energies between (110) and (100) is about 0.2 and 0.4 eV/atom for Ag and Ni, respectively.

The studied surfaces affect only two upper layers, the lower layers have bulk-like behaviour. The differences between (100), (110) and (111) surfaces can be seen also from the charge density differences (see Figures 1 and 2).

In the case of (100) surface, the charge density accumulation is located just between the nearest neighbours lying in surface layer. In comparison with (100) surface, (110) surface is less symmetrical and each atom in surface layer has two neighbours. The first (second) nearest neighbours are in the distance of 2.934 (4.147) Å for Ag and 2.479 (3.538) Å for Ni. The charge density accumulation is located only between the first nearest neighbours. On the other hand, the (111) surface is the most symmetrical. The charge density is equally accumulated in interstitial positions between the atoms lying in the surface layer.

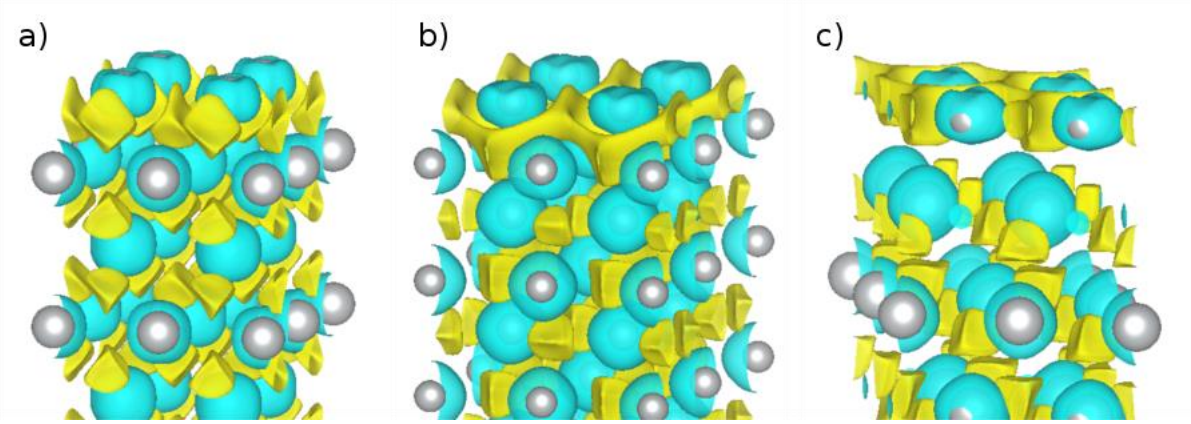

Figure 1.: The charge density differences for a) (100) b) (110) and c) (111) Ag surface. Yellow colour marks a charge accumulation and blue colour a charge depletion (isosurfaces level is 0.0035 $e^-/Å^3$).

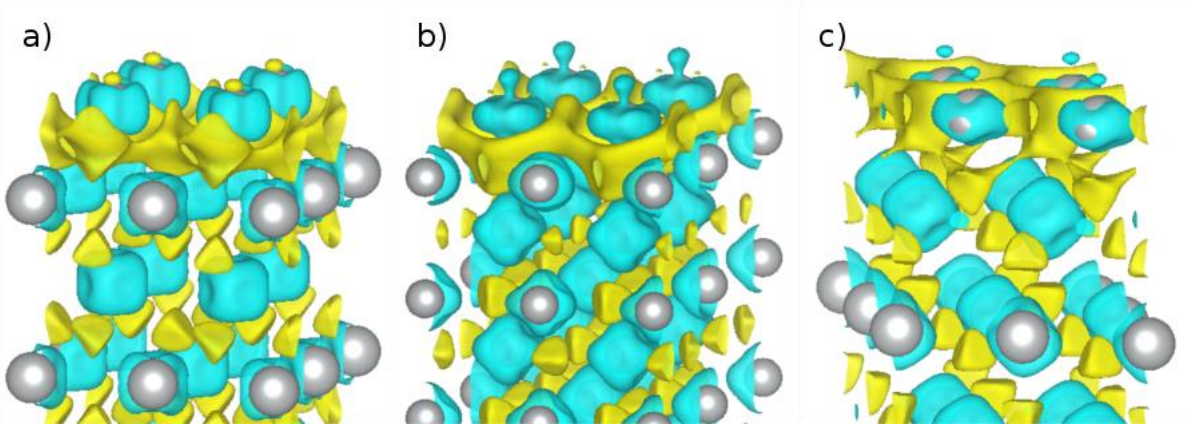

Figure 2.: The charge density differences for a) (100) b) (110) and c) (111) Ni surface. Yellow colour marks a charge accumulation and blue colour a charge depletion (isosurfaces level is 0.007 $e^-/Å^3$).

4. CONCLUSION

We present ab initio study of Ag and Ni surfaces with different crystallographic orientations. For both elements, we found the (111) surface as the most and the (110) surface as the least energetically favourable. The surface energy of Ni is higher than for Ag, it may be supposed that Ag would be energetically more favourable than Ni on surface in Ag-Ni nanoparticles. These results will be used in further theoretical analysis including *ab initio* calculations and thermodynamic modelling, in order to understand the synthesis of nanoparticles.

5. ACKNOWLEDGEMENT

This research has been financially supported by the Ministry of Education, Youth and Sports of the Czech Republic under the Project CEITEC 2020 (Project No. LQ1601) and by the Czech Science Foundation under the Project "Stability and phase equilibria of bimetallic nanoparticles" (Project No. GA14-12653S). Computational resources were provided by the Ministry of Education, Youth and Sports of the Czech Republic under the Project CERIT-Scientific Cloud (Project No. LM2015085) within the program Projects of Large Research, Development and Innovations Infrastructures. We thank Prof. Mojmír Šob (CEITEC MU Brno) for fruitful discussions.

6. REFERENCES

[1] L. Ge, Q. Li, M. Wang, J. Ouyang, X. Li, M.M.Q. Xing, Int. J. Nanomedicine 9 (2014) 2399–407.
[2] R. Janardhanan, M. Karuppaiah, N. Hebalkar, T.N. Rao, Polyhedron 28 (2009) 2522–2530.
[3] S. Chandra, A. Kumar, P.K. Tomar, J. Saudi Chem. Soc. 18 (2014) 437–442.
[4] X. Wu, W. Xing, L. Zhang, S. Zhuo, J. Zhou, G. Wang, S. Qiao, Powder Technol. 224 (2012) 162–167.
[5] N. Lopez, J.K. Nørskov, T.V.W. Janssens, A. Carlsson, A. Puig-Molina, B.S. Clausen, J.D. Grunwaldt, J. Catal. 225 (2004) 86–94.
[6] C. Wang, S. Bai, Y. Xiong, Chinese J. Catal. 36 (2015) 1476–1493.
[7] A.K. Santra, F. Yang, D.W. Goodman, Surf. Sci. 548 (2004) 324–332.
[8] R. Huang, Y.-H. Wen, Z.-Z. Zhu, S.-G. Sun, J. Mater. Chem. 21 (2011) 11578.
[9] P. Hohenberg, W. Kohn, Phys. Rev. 136 (1964) B864.
[10] W. Kohn, L.J. Sham, Phys. Rev. 140 (1965) A1133–A1138.
[11] G. Kresse, J. Hafner, Phys. Rev. B 47 (1993) 558–561.
[12] G. Kresse, J. Furthmüller, Phys. Rev. B 54 (1996) 11169–11186.
[13] J.P. Perdew, K. Burke, M. Ernzerhof, Phys. Rev. Lett. 77 (1996) 3865–3868.
[14] P.E. Blöchl, Phys. Rev. B 50 (1994) 17953–17979.
[15] L. Vitos, A. V. Ruban, H.L. Skriver, J. Kollár, Surf. Sci. 411 (1998) 186–202.

EFFECT OF PREPARATION PARAMETERS ON SHORT TiO_2 NANOTUBES

Kateřina PŘIKRYLOVÁ[1*] and Jana DRBOHLAVOVÁ[1,2]

[1] *Department of Microelectronics, Faculty of Electrical Engineering and Communication, Brno University of Technology, Technická 3058/10, 616 00 Brno, Czech Republic*

[2] *Central European Institute of Technology, Brno University of Technology, Technická 3058/10, 616 00 Brno, Czech Republic*

**xprikr26@stud.feec.vutbr.cz*

Abstract

Titanium dioxide nanotubes (TNTs) were fabricated by anodic oxidation of thin titanium film in organic electrolyte containing ammonium fluoride and water. In this work, the effects of preparation parameters, such as anodization potential, pH, water or ammonium fluoride content, on growth of short TNTs were observed. The chemical etching of initial oxide barrier layer plays a key role in obtaining highly ordered TNTs. The morphology of TNTs was characterized by scanning electron microscopy (SEM) and the photocurrent response of TiO_2 nanostructured electrodes was also evaluated. These surfaces can be used in broad spectrum of application, mainly photocatalysis and solar cells, due to their mechanical, thermal and chemical stability.

1. INTRODUCTION

In the past decade, the considerable attention has been focused on nanostructured TiO_2, because of its unique ionic, electronic behavior and high surface area. TiO_2 nanostructures with different shapes and crystal structures can be created by various methods [1,2]. One of the most sophisticated approach to create TiO_2 layer with large surface area is electrochemical method. Anodic oxidation (AO) of titanium is relatively easy way to control the preparation parameters and dimensions of TiO_2 nanostructures. Many publications provide information about fabrication TNTs from titanium foil [3,4], but only few of them are focused on anodization of thin titanium film (less than 1 μm). In our work, the thickness of titanium film sputter-deposited on silicon substrate with thermal silicon oxide is only 500 nm. The possibility of using even lower Ti layer thickness (about 200 nm) will be also tested. Less material used in anodization makes this process cheaper and faster in comparison with anodization of thick titanium foil while remaining properties of TNTs such as ordering and

homogeneity of surface coverage. In addition, thin layer of TiO_2 is mechanically stable and after thermal treatment completely transparent.

2. MATERIAL AND METHODS

Titanium (99.99%, Porexi, CZ), ethylene glycol p.a. ($C_2H_6O_2$, Penta, CZ) and ammonium fluoride p.a. (NH_4F, Sigma Aldrich, DE) were used as purchased. Deionized water (18.2 MΩ) was obtained from Millipore RG system MilliQ (Millipore Corp., USA).

Titanium thin films with thickness of 500 and 1000 nm were deposited onto 4-inch p-type silicon wafer (100) covered by 1 μm of thermal silicon dioxide. Before AO, the titanium thin film was consecutively immersed into acetone, isopropanol, and deionized water to remove the impurities and then dried by compressed nitrogen stream. The AO was realized in the two-electrode configuration and using power supply controlled by LabView program. The substrate operated as a working electrode and the stainless steel mesh was used as a counter electrode. The potential was kept constant during the whole AO and different values in the range of 10–100 V were tested. The changing current during AO was monitored. The electrolyte solution was prepared from ethylene glycol containing ammonium fluoride (0.3–1.4 wt%) and deionized water (0–2 vol%). The anodized titania was rinsed with deionized water and dried by compressed nitrogen.

3. RESULTS AND DISCUSSION

The present research demonstrates the method for the fabrication of short, vertically aligned open TNTs via anodic oxidation of Ti in organic electrolyte. The influence of electrolyte containing different amount of water and ammonium fluoride together with various applied potential was observed by SEM. The balance between chemical etching and oxidation is the main parameter for successful preparation of TNTs. Due to the thin titanium film, the anodization time is very short. The crucial condition was to slow down the oxidation process in order to prolong the oxidation time and simultaneously to increase the etching power to fully etch the initial oxide barrier layer. The optimization of these two processes led to open self-ordered TNTs. The electrolyte containing 1.2 wt% NH_4F and 1 vol% H_2O in ethylene glycol was found to have the most suitable composition regarding the above mentioned criteria (Figure 1B). If the electrolyte obtained less or more water, the resulting product was disordered porous oxide layer without nanostructures (Figure 1A).

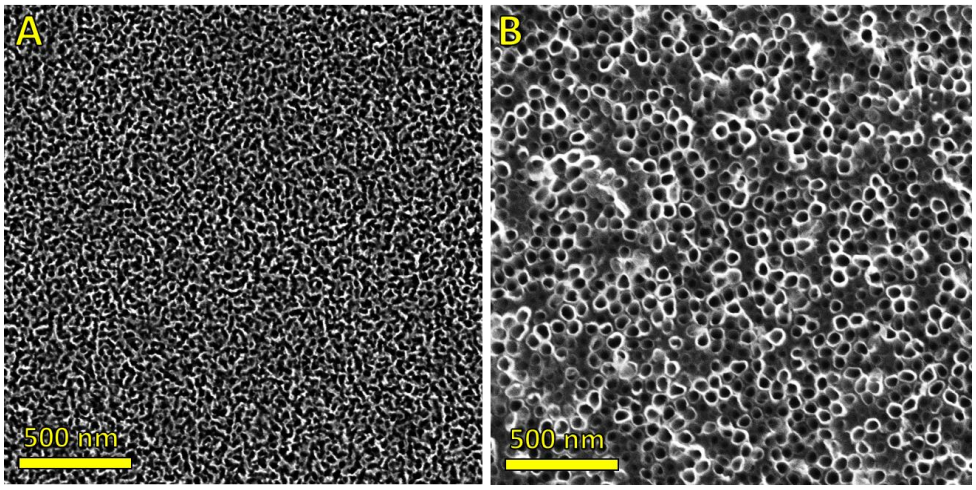

Figure 1.: TNTs created in process A) when anodic oxidation dominates and B) when anodic oxidation is in balance with chemical etching.

4. CONCLUSION

The present work demonstrates a method for direct anodic transformation of Ti thin film into nanotubular TiO_2 array. Simple AO of this substrate in electrolyte containing ethylene glycol, water and NH_4F allows the controlled fabrication of ordered and highly regular TNTs. The influence of different electrolytes on resulting morphology of nanostructures enables us to better understand how the TNTs creation can be controlled. The XPS spectra shows the effect of thermal treatment on the chemical composition of TNTs. The optimization of the anodization process lead to open self-ordered free-standing short TNTs. As fabricated TNTs have a very good potential for future sensing, biomedical and mainly photocatalytic applications, especially in advanced oxidative degradation of persistent organic pollutants in drinking water.

5. ACKNOWLEDGEMENT

The work has been supported by IGA FEKT/STI-J-16-3625 and IGA FEKT-S-14-2300 research grants.

6. REFERENCES

[1] K. Přikrylová et al. "Fabrication of highly ordered short free-standing titania nanotubes". Monatshefte für Chemie - Chemical Monthly, 2016, vol. 147, no. 5, pp. 943-949. ISSN 1434-4475.

[2] Q. Zhang et al. "Anodic Oxidation Synthesis of One-Dimensional TiO2 Nanostructures for Photocatalytic and Field Emission Properties". J. Nanomater., 2014, pp. 14. ISSN 1687-4110.

[3] M. Nischk et al. "Ordered TiO2 nanotubes: The effect of preparation parameters on the photocatalytic activity in air purification process". Appl. Catal. B-Environ., 2014, vol. 144, pp. 674-685. ISSN 0926-3373.

[4] P. Roy et al. "TiO2 Nanotubes: Synthesis and Applications". Angewandte Chemie International Edition, 2011, vol. 50, no. 13, pp. 2904-2939. ISSN 1521-3773.

EFFICIENCIES OF HUMAN CYTOCHROME P450 1A1 EXPRESSED IN EUKARYOTIC AND PROKARYOTIC SYSTEMS IN OXIDATION AND DNA ADDUCT FORMATION BY BENZO[A]PYRENE: A COMPARATIVE STUDY

Marie STIBOROVÁ[1*], Radek INDRA[1], Michaela MOSEROVÁ[1], Eva FREI[1], Heinz H. SCHMEISER[2], Volker M. ARLT[3]

[1] *Department of Biochemistry, Faculty of Science, Charles University, Albertov 2030, 128 40 Prague 2, Czech Republic*

[2] *German Cancer Research Center (DKFZ), Heidelberg, Germany*

[3] *Analytical and Environmental Sciences Division, MRC-HPA Centre for Environment and Health, King's College London, London SE1 9NH, United Kingdom*

**stiborov@natur.cuni.cz*

Abstract

Benzo[*a*]pyrene (BaP) is human carcinogen that is activated by cytochrome P450 (CYP), predominantly by CYP1A1. We found that efficiencies of this CYP in BaP oxidation and BaP-derived DNA adduct formation is dictated by its expression in prokaryotic and eukarypotic organisms, being less efficient in the prokaryotic system.

1. INTRODUCTION

Benzo[*a*]pyrene (BaP) is a human carcinogen that covalently binds to DNA after activation by cytochrome P450 (CYP) [1,2].CYP1A1 is the most important enzyme in BaP activation [2,3], in combination with microsomal epoxide hydrolase (mEH). First, CYP1A1 oxidizes BaP to an epoxide that is then converted to a dihydrodiol by mEH (*i.e.* BaP-7,8-dihydrodiol); then further bio-activation by CYP1A1 leads to the ultimately reactive species, BaP-7,8-dihydrodiol-9,10-epoxide (BPDE) that can react with DNA, forming preferentially the 10-(deoxyguanosin-N^2-yl)-7,8,9-trihydroxy-7,8,9,10-tetrahydrobenzo[*a*]py-rene adduct [4]. BaP is, however, oxidized also to other metabolites such as the other dihydrodiols, BaP-diones and hydroxylated metabolites. [5,6]. There is still limited information on the mechanim of the reaction cycle of BaP oxidation catalyzed by human CYP1A1. Here, we investigated BaP metabolism catalyzed by human CYP1A1 in prokaryotic and eukaryotic model systems.

2. MATERIAL AND METHODS

Human CYP1A1 expressed in the eukaryotic system (microsomes of insect cells transfected with human CYP1A1 and NADPH:CYP reductase, POR - Supersomes™) and in the prokaryotic system of *Escherichia coli* cells (*E. coli* membranes containing over-expressed human CYP1A1 and POR - Bactosomes) were used as models. HPLC was used to separate and identify BaP metabolites and the ^{32}P-postlabling method to detect and quantify BaP-derived DNA adducts [5,6].

3. RESULTS AND DISCUSSION

In the eukaryotic cells, CYP enzymes, including CYP1A1, are components of a mixed-function oxidase (MFO, monooxygenase) system located in the membrane of endoplasmic reticulum (microsomes). This enzymatic system also contains other enzymes, the multidomain flavoprotein POR and cytochrome b_5 accompanied by its NADH:cytochrome b_5 reductase (CBR). Because Supersomes™ are microsomes, they contain beside the over-expressed human recombinant CYP1A1 with POR, also basic levels of CBR, microsomal epoxide hydrolase (*m*EH) and cytochrome b_5. In the case of the prokaryotic cells of *E. coli* transfected with human CYP1A1 and POR, this CYP together with POR are expressed in the cell membrane that does not contain any other enzymes of the MFO monooxygenase system. BaP-9,10-dihydrodiol, BaP-7,8-dihydrodiol, BaP-1,6-dione, BaP-3,6-dione, BaP-9-ol, BaP-3-ol, a metabolite of unknown structure, and two BaP-DNA adducts were generated by the CYP1A1-Supersomes™ system, both in the presence of NADPH and in the presence of NADH. BaP-3-ol as the major metabolite, BaP-9-ol, BaP-1,6-dione, BaP-3,6-dione, an unknown metabolite, and at least three BaP-DNA adducts were observed in the system using CYP1A1 expressed with POR in *E. coli* plus NADPH, a cofactor of POR. Because of the absence of *m*EH, no dihydrodiol metabolites of BaP were formed. When CYP1A1 in *E. coli* membrane was incubated with a cofactor of CBR, NADH, no BaP metabolites as well as BaP-DNA adducts were detectable. Only low levels of BaP-DNA adducts were found in the presence of NADH when purified CBR and cytochrome b_5 were added into the *E. coli* enzymatic system. This finding suggests a role of the NADH/cytochrome b_5/CBR system as sole donor of electrons to CYP1A1 in its reaction cycle substituting the system of POR with NADPH. The results found indicate some limitation in the use of human CYP1A1 expressed in cells of the prokaryotic organism, *E. coli*. The differences between enzyme (protein) compositions of the cell membrane of *E. coli* from those of the microsomal membrane of

Supersomes™, absenting several components of the CYP monooxygenase system, seem to be responsible for the found results.

4. ACKNOWLEDGEMENT

Supported by GACR (15-02328S) and Charles University (UNCE 204025/2012)

5. REFERENCES

[1] IARC: IARC Monographs of Evaluation of Carcinogens. Risk of Chemicals for Human, 92 (2010) 1-853
[2] Baird WM, Hooven LA, Mahadevan B: Environmental and Molecular Mutagenesis, 45 (2005) 106–114
[3] Hamouchene H, Arlt VM, Giddings I, et al.: BMC Genomics, 12 (2011) 333
[4] Phillips DH, Venitt S: International Journal of Cancer, 131 (2012) 2733-2753
[5] Stiborová M., Moserová M., Cerná V., et al.: Toxicology, 318 (2014) 1-12
[6] Indra R., Moserova M., Sulc M., et al.: Neuro Endocrinology Letters, 34 Suppl. 2 (2013) 55-63

DNA BASED BIOSENSOR FOR ELECTROCHEMICAL STUDY OF AROMATIC COMPOUNDS IN BIOLOGICAL MATRIX

Veronika SVITKOVÁ[1*], Hana MACKOVÁ[1], Jana BLAŠKOVIČOVÁ[1], Ján LABUDA[1]

[1] *Institute of Analytical Chemistry, Faculty of Chemical and Food Technology, Slovak University of Technology in Bratislava, Radlinského 9, 812 37 Bratislava, Slovak Republic*

**veronika.svitkova@stuba.sk*

Abstract

The aim of this work is preparation and use of an electrochemical DNA biosensor with textured surface for the investigation of DNA interactions with specific chemicals in biological samples of complex matrix such as urine. Results obtained at the search and optimization of polymer protective films on the DNA recognition layer will be presented. Polyvinyl alcohol membrane has been found as effective barrier able to stabilize the biosensor response in the given matrix. An interaction of acridine yellow and doxorubicin as the representatives of DNA intercalators has been studied by using cyclic voltammetry with the DNA redox indicator and square wave voltammetry of the guanine and adenine moieties anodic responses.

1. INTRODUCTION

Electrochemical DNA based biosensor is an analytical device that represents the connection between the nucleic acid as a biorecognition element and the electrode made of different materials as a physicochemical transducer [1]. External protective polymer membranes have been reported to prevent the biosensor surface against the influence of interfering substances in complex matrices [2].

Intercalators are the significant class of aromatic compounds and some of them are used in the treatment of cancer. Acridine yellow (AY) is a yellow dye which damages DNA and is used as a mutagen in the microbiology. Studies show that AY is the intercalator capable of binding to the DNA double helix and change its structure [3]. Patent from 2009 (US 2009/0136933 A1) also shows possibility of the electrochemical determination of DNA damage in the presence of derivate of acridine [4]. Doxorubicin (DOX) also called daunomycin or adriamycin is an anthracycline antibiotic. It is known that DOX interacts with DNA and inhibits the function of the enzyme topoisomerase II [5]. There are also studies of the

electrochemical determination of doxorubicin and its effect on the DNA structure using biosensors [6].

The goal of the work was to compare the possibility of the detection and monitoring of the dsDNA interaction with intercalating substances in phosphate buffer and in complex biological matrix of urine.

2. MATERIAL AND METHODS

Reagents

Salmon sperm dsDNA was obtained from Sigma-Aldrich, Germany. Its stock solution was prepared in a PB. Polyvinylalcohol was obtained from Sigma-Aldrich, Germany and dissolved it nanopure water. Stock solutions of acridine yellow and doxorubicin were of concentration 2.10^{-5} mol.dm^{-3}.

Apparatus

All measurements were performed using the potentiostat Autolab and were carried out in the three-electrode system using a glassy carbon working electrode (GCE), a silver|silver chloride reference electrode (Ag/AgCl/sat KCl) and a platinum counter electrode.

Preparation of the biosensors

The GCE surface was pretreated by applying a constant potential. Chemical modification of the electrode was carried out by covering the surface of the GCE by a layer of dsDNA deposited on the electrode surface under the conditions of the adsorption potential. Then, a drop of PVA stock solution was deposited and let to evaporate to dryness.

Procedures

Cyclic voltammetry (CV): in 1 mM $[Fe(CN)_6]^{3-/4-}$ in 0.1 mol.dm^{-3} PB, potential range from -0.4 to 0.8 V, scan rate 100 mV·s^{-1}, potential step 2 mV.

Square wave voltammetry (SWV): in 0.1 mol.dm^{-3} PB pH 7.4, pulse amplitude 40 mV, frequency 100 Hz, scan rate 1.5 V.s^{-1}, potential step 15 mV.

Electrochemical impedance spectroscopy: in 1 mM $[Fe(CN)_6]^{3-/4-}$ in 0.1 mol.dm^{-3} PB, polarization potential 0.1 V, frequency range from 0,1 Hz to 5000 Hz (51 frequency steps), amplitude 10 mV.

3. RESULTS AND DISCUSSION

CV measurements indicated that the interferences in the urine were adsorbed on the surface of both the bare GCE and the DNA/GCE electrodes and reduced the redox response of the $[Fe(CN)_6]^{3-/4-}$. The surface of the biosensor was modified by selected polymer membrane of PVA to protect it against interfering substances. From the evaluation of the time and dimensional stability of the CV redox indicator it could be concluded that the PVA membrane is suitable for the protection of biosensor from high molecular weight substances in the urine. This was confirmed by electrochemical impedance spectroscopic (EIS) measurements. From the SWV measurements it was found that the membrane did not significantly change the signals of adenine and guanine base moieties.

The DNA biosensor with a protective membrane was used to test an effect of known intercalating substances AY and DOX added to the urine matrix on the structure of immobilized DNA. CV measurements confirmed the intercalation of the substances under study and SWV measurements showed a significant change in the structure of DNA after an incubation of the biosensor in intercalating substances solutions. The intercalators are detectable in buffer alone and in the biological matrix as well.

4. CONCLUSION

The goal of the work was to construct an electrochemical DNA biosensor with protective polymer membrane for an analytical examination of substances interacting with DNA in a complex biological matrix of urine. Electrochemical analysis using the biosensor is suitable for investigation of intercalators such as acridine yellow and doxorubicin with dsDNA.

5. ACKNOWLEDGEMENT

This work was supported by the Scientific Grant Agency VEGA of the Slovak Academy of Sciences and the Ministry of Education of the Slovak Republic (Project 1/0361/14), the Project of excellent teams of young researchers (Projekt excelentných tímov mladých výskumníkov) STU, and the Project of young researchers (Projekt na podporu mladých výskumníkov) STU.

6. REFERENCES

[1] Labuda J, Bakoš D, Palou M, et all.: Biomateriály a biosenzory, Vydavateľstvo STU, Bratislava, 2008, 121-144
[2] Ambrózy A, Hlavatá L, Labuda J: Acta Chim. Slovaca, 6 (2013), 35-41
[3] Long JF, Huang CHZ, Li YF: J. Phys. Chem., B 111 (2007), 4535-4538
[4] Sakomoto H: Patent App. Pub., United States, (2009). US 2009/0136933 A1.
[5] Hynek D, Krejcova L, Zitka O, et all.: Int. J. Electrochem. Sci., 7 (2012), 13-33
[6] Trnkova L, Huska D, Adam V, et all.: IEEE Sensors Conference, ISBN 978-1-4244-4548-6, (2009), 1200-1203

MATRA-A REAGENT/POLYETHYLENEIMINE COMPLEX TRANSFECTION FOR LOW TOXIC DNA PLASMID DELIVERY

Ondrej SVOBODA[1,*], Zdenka FOHLEROVA[2], Larisa BAIAZITOVA[1], Vratislav CMIEL[1], Jaromir HUBALEK[2,3], Ivo PROVAZNIK[1], Vladimir PEKARIK[4,5]

[1] *Department of Biomedical Engineering, Faculty of Electrical Engineering and Communication, Brno University of Technology, Technicka 12, 616 00, Brno*

[2] *Central European Institute of Technology, Brno University of Technology, Technicka 10, 616 00 Brno*

[3] *Department of Microelectronics, Faculty of Electrical Engineering and Communication, Brno University of Technology, Technicka 10, 616 00 Brno*

[4] *Central European Institute of Technology, Masaryk University, Kamenice 753, 625 00 Brno*

[5] *Department of Physiology, Faculty of Medicine, Masaryk University, Kamenice 753, 625 00 Brno*

** xsvobo32@stud.feec.vutbr.cz*

Abstract

The non-toxic intracellular delivery of biopolymers is very hot topic in current biology. In this work, two different MATRA-A reagent/polyethyleneimine transfection protocols were used for intracellular delivery of ChR2 DNA vector. Cell morphology changes were studied 48 hours after transfection. Our transfection efficiency is lower than normally achieved, but the rate of cells with physiological properties remains is very high: 85.34%. Therefore, these transfection protocols are very applicable for electrophysiological experiments.

1. INTRODUCTION

The agent based transfection methods for intracellular biopolymer delivery, which have increasing attention in last years has major drawbacks such as low transfection efficiency or impossible specific biopolymer targeting. Magnetofection – an approach for intracellular plasmid delivery of DNA/magnetic nanoparticle complex (MNP) can overcome these drawbacks. For proper electrophysiological experiments choose of proper transfection approach is an essential, because transfection protocol itself can significantly change the cell health, morphology and electrophysiological properties. Based on these facts magnetofection seems to be very applicable method for electrophysiological experiments because of its low cytotoxicity, high transfection efficiency and easy targeting [1–3].

In these work two magnetofection protocols are performed and transfection efficiency and toxicity are observed. The goal is to preserve physiological cell morphology with high transfection efficiency which are essential for electrophysiological experiments.

2. MATERIAL AND METHODS

For cell cultures (HEK293T) minimum essential medium eagle (EMEM, Sigma) supplemented with 10% FBS (Sigma), 1% Penicillin/Streptomicin (Sigma-Aldrich) and 1% L-glutamine (Sigma) were used. Cells were seeded at 24-well plate (TPP) with density 3-4×10^4 cells/well and cultured for 48 hours at 37 °C and 5% CO2 before each experiment.

Two transfection protocols for humanized pCAG-hChR2-YFP (Channelrhodopsin-2, Addgene) plasmide delivery were defined: In the first protocol (DNA-MATRA-PEI) DNA was resuspend in serum-free EMEM and incubated for 20 minutes with MATRA-A reagent. Afterwards PEI was added and incubated for 10 minutes. In the second protocol DNA plasmide and PEI were diluted in serum-free EMEM with 10 minutes incubation followed by addition MATRA-A reagent and 20 minutes incubation. Both protocols were optimized for high transfection efficiency and low cell morphology changes and were performed in duplicates. During the optimization different concentrations of MATRA-A reagent (2.00 to 8.00 µg×ml^{-1}) and PEI (1.00 to 6.00 µg×ml^{-1}) were used. DNA concentration was chosen as 1.10 ng×ml^{-1}. All concentrations were taken from previously used routine protocols. In each protocol positive (DNA + PEI in 150 mM NaCl and DNA + MATRA-A reagent in serum-free EMEM) and negative control (pure DNA, PEI in 150 mM NaCl and MATRA-A reagent in serum-free EMEM) were included. After the incubation, each sample was completed with 500 µl of fresh EMEM and added to seeded cells. Than the plate was placed on magnetic plate in the incubator for 20 minutes. Afterwards the plate was incubated at 37°C and 5% CO_2 outside the magnetic plate. After 48 hours from fluorescent images were taken using confocal laser scanning microscope Leica TCS SP8 X with the picosecond White Light Laser. The well-working concentrations of individual transfection components are listed in Table 1. The concentrations are selected for the best ratio of patch clamp suited cells.

For plasmid transfection efficiency MATLAB 2013b (Mathworks) script was used. Script compare quantity of ChR2-YFP expressing cells and the quantity of cells marked by DAPI. Cell morphological analysis was made as follows: the quantity of cells with rounded outline (Hough transform) is compared to the total quantity of cells stained with DAPI.

3. RESULTS AND DISCUSSION

In comparison to commonly used methods, our protocols reached lower transfection efficiencies. Nevertheless we were focused on the cell health and morphology, which corresponds to cell adhesion and viability. These indicators are very important for proper patch clamp experiments. In both protocols we received high proportion of cells which are suitable for electrophysiological experiments – 85.34% in case of the first protocol, 75.98% in case of the second protocol. In Table 1 all individual transfection components are listed with corresponding transfection efficiencies and patch clamp capability ratios. The results chose is selected for highest ratio of path clamp suitable cells.

Table 1: Concentrations of individual transfection reagents for plasmid delivery with the best ratio of transfection efficiency and cell morphology

	Transfection protocol	PEI ($\mu g \times ml^{-1}$)	MATRA-A reagent ($\mu g \times ml^{-1}$)	Tr. efficiency (%)	Patch clamp capability (%)
1.	DNA-MATRA-PEI	3.50	7.00	69.45	85.34
2.	DNA-PEI-MATRA	2.25	4.50	87.18	75.98

4. CONCLUSION

Two MATRA-A reagent/polyethyleneimine transfection protocols for humanized pCAG-hChR2-YFP are optimized in this paper. Transfection efficiency and cell morphology are studied 48 hours from transfection. In both protocols transfection efficiency is lower than commonly achieved. In the first protocol transfection efficiency is lower than in second but proportion of patch clamp suitable cells is higher – about 85%. In case of the second protocol the patch clamp capable cells ratio is more than 75%. The first transfection protocol produce better results, but both can be successfully used in electrophysiology experiments.

Our future work will be focused on the investigation of electrophysiological properties of the cells.

5. ACKNOWLEDGEMENT

The article was supported by project no. FEKT-S-14-2300 A new types of electronic circuits.

6. REFERENCES

[1] A. V. Kornev and M. V. Dubina, “Magnetic nanoparticles and intracellular delivery of biopolymers,” Ross. Fiziol. Zh. Im. I. M. Sechenova, vol. 100, no. 3, pp. 257–273, Mar. 2014.

[2] X. Wang, L. Zhou, and H. Gu, “Charged Magnetic Nanoparticles for Enhancing Gene Transfection,” IEEE Trans. Nanotechnol., vol. 8, no. 2, pp. 142–147, 2009.

[3] T. K. Kim and J. H. Eberwine, “Mammalian cell transfection: The present and the future,” Anal. Bioanal. Chem., vol. 397, pp. 3173–3178, 2010.

THE ELECTROCHEMICAL ANALYSIS OF DNA HEXAMER d(GCGAGC)

Iveta TŘÍSKOVÁ[1], Libuše TRNKOVÁ[1*]

[1] *Department of Chemistry, Faculty of Science, Masaryk University, Brno, Kamenice 5, CZ-625 00 Brno, Czech Republic*

**libuse@chemi.muni.cz*

Abstract

The aim of our research is the voltammetric analysis of the DNA hexameric mini-hairpin d(GCGAGC). The cyclic voltammetric experiment on a hanging mercury drop electrode (HMDE) yields reduction signals of adenine (A) and cytosine (C) moieties and two oxidation signals of guanine moieties (G); these signals were investigated with respect to the hexamer concentration and pH of buffered solutions (phosphate-acetate buffer). Although the character of LSV curves is similar for different concentrations and pHs, the elimination voltammograms are different and show the other character of adsorption.

1. INTRODUCTION

DNA hairpins play a key role in many biochemical processes on cellular level, because they are considered potential recognition sites for regulatory proteins operating the living cycles[1]. The shortest and the most stable DNA hairpin d(GCGAAGC) is linked with the triplet repeat expansion events in the nucleic acid chain, and therefore it is associated with many neurodegenerative disorders [2, 3]. Based on the semi-empirical structural and energetic analysis it was proposed that even the shorter hexameric hairpin, d(GCGAGC), may exist in solutions [1, 4]. From the electrochemical point of view, the DNA oligomers (hexamers and heptamers) provide the characteristic reduction adenine-cytosine (AC) signals and double-shaped oxidation signals of guanine moieties (G peak) on the mercury electrode in buffered aqueous solutions [3]. The aim of this study was the voltammetric analysis of DNA mini-hairpin d(GCGAGC).

2. MATERIAL AND METHODS

Cyclic voltammetry of DNA hexamer d(GCGAGC)

The electrochemical behavior of the DNA hexamer d(GCGAGC) (Thermo Fisher Scientific, Ulm, Germany) was investigated using the electrochemical analyzer AUTOLAB PGSTAT 20

(EcoChemie, Utrecht, The Netherlands). The measured samples with concentrations from 45nM to 855 nM in phosphate – acetate (PA) buffer (mixture of 0.4 M acetic acid, 0.4 M phosphoric acid and 2 M sodium hydroxide; pH 3.57 – 6.26) were dosed into the voltammetric cell occupied with three electrodes: a hanging mercury drop electrode (HMDE) with an effective area of 0.04 mm^2 as the working electrode, an Ag/AgCl/3M KCl and a Pt wire as the reference and auxiliary electrodes, respectively.

The experimental conditions were as follows: the potential range was changed from 0 V to -1.7 V; scan rates: 200, 400 and 800 mV/s, the accumulation potential: -0.1 V, the accumulation time was 60 s. The experiments were carried out in inert argon atmosphere (99.999 %) at room temperature. From the smoothed voltammetric curves (Savitzky–Golay filter, level 2) the elimination function E4, simultaneously eliminating kinetic and charging currents and diffusion current conserving, according to the equation $f(I) = 17.485\ I - 11.657\ I_{1/2} - 5.8584\ I_2$[5-13] was calculated.

3. RESULTS AND DISCUSSION

Cyclic voltammetry of DNA hexamer d(GCGAGC)

Similar to the DNA heptamer, the DNA hexamer with the sequence of d(GCGAGC) provided the characteristic reduction AC signals and the double–shaped oxidation signals of guanine (G) moieties on the mercury electrode (HMDE) in buffered solutions (PA buffer; pH from 3.57 to 6.26). The voltammetric experiment proved that the current intensity and potential position of redox signals is strongly dependent on the concentration and pH.

a) Effect of pH

It is obvious that in more acidic pHs (3.57 and 4.09), the hexamer studied provided only one AC reduction signal while the G oxidation signal was not detected. With increasing pH the AC reduction signals are going to separate on the electrode surface and a double–shaped G oxidation signal is observed. In addition, the elimination voltammetry revealed the adsorbed state of AC moieties in more acidic pHs. Using the elimination voltammetric procedure it was found that at higher pH values AC moieties are reduced without full adsorption on the electrode surface but G moieties are oxidized in full adsorptive state.

b) Effect of concentration

Besides the pH effect, the concentration effect on the redox responses of the DNA hexamer was monitored. The voltammetric experiments proved that the concentration change does not significantly affect the hexamer signals. Although the character of LSV curves is similar for

different concentrations and pHs, the elimination voltammograms indicate a different character of adsorption.

4. CONCLUSION

We can conclude that the DNA hexamer d(GCGAGC) yields both AC reduction and oxidation (guanine) voltammetric signals on a mercury electrode in buffered solutions, similar to DNA heptamer results. It is obvious that the pH effect on structural changes is more significant than the effect of concentration.

The application of the elimination procedure (EVP) confirms the electrode process with electron transfer in adsorbed state for both AC reduction and G oxidation signals. The EVP signals were changed significantly with pH, and at lower pH the AC counterpeaks were split.

5. ACKNOWLEDGMENT

This research has been supported by the project LH 13053 KONTAKT II (MEYS of the Czech Republic).

6. REFERENCES

[1] Rubin Y V, Belous L F, and Evstigneev M P.: Journal of Molecular Structure, 1027 (2012), 124-127.
[2] Hirao I, et al.: Nucleic Acids Research, 22 (1994), 4, 576-582.
[3] Trnkova L, Postbieglova I, and Holik M.: Bioelectrochemistry, 63 (2004),1-2, 25-30.
[4] Evstigneev M P, et al.: Biopolymers, 93 (2010),12, 1023-1038.
[5] Trnkova L.: Chemicke Listy, 95 (2001), 9, 518-527.
[6] Trnkova L.: Journal of Electroanalytical Chemistry, 582 (2005), 1-2, 258-266.
[7] TrnkovaL.: In: Utilizing of bio-electrochemical and mathematical methods in biological research (Adam V, and Kizek R, Eds.), 51 (2007), Kerala, India.
[8] Trnkova L, and Dracka O.: J. Electroanal. Chem, 413 (1996),123-129.
[9] Trnkova L, and Dracka O.: In: 59th Annual Meeting of International Society of Electrochemistry, 2008, Sevilla, Spain.
[10] Trnkova L, Friml J, and Dracka O.:Bioelectrochemistry, 54 (2001), 131-136.
[11] Trnkova L, Jelen F, and Postbieglova I.:. Electroanalysis, 15 (2002), 19, 1529-1535.
[12] Trnkova L, Jelen F, and Postbieglova I.: Electroanalysis, 18 (2006), 662 - 669.
[13] Trnkova L, Kizek R, and Dracka O.: Electroanalysis, 12 (2000), 12, 905-911.

STUDY OF THE GLASS TRANSITION OF CO-AMORPHOUS DRUG BY DMA

Irena TÜRKEOVÁ[1*], Tomáš SOLNÝ[1], Korbinian LÖBMANN[2], Thomas RADES[2], Martina KLUČÁKOVÁ[1*]

[1] *Materials Research Centre, Faculty of Chemistry, Brno University of Technology, Purkyňova 464/118, 612 00 Brno, Czech Republic*

**xcturkeovai@fch.vut.cz*

[2] *Pharmaceutical Design and Drug delivery, Department of Pharmacy, University of Copenhagen, Universitetparken 2, 2100 Copenhagen, Denmark*

Abstract

Nowadays in pharmaceutical research is problem that new chemical entities are poorly water soluble and therefore present a low dissolution rate. One approach to increase their solubility is to convert the crystalline form of a drug into the amorphous form.

In this study, the co-amorphous IND-TRY mixtures were prepared by mechanical activation – ball milling. It was given different amount of polyvinylpyrrolidon to the mixture and was characterized. Solid - state properties were analyzed by dynamic mechanical analysis (DMA). It was found that addition of polyvinylpyrrolidon improved stability compared to the pure co-amorphous form. Glass transition state is growing with addition of PVP.

1. INTRODUCTION

Approximately 90% of small molecular weight drug candidates under development have poor aqueous solubility[1]. Problems in finding an appropriate drug delivery system for poorly water soluble API can severely compromise the chance of the API to be further developed. Therefore, it is necessary to overcome problems associated with limited dissolution of an API in order to enable promising drug candidates to reach the patient[6].

One of the most promising approaches in the development of drug delivery systems to improve the efficacy of new drugs is the conversion of a crystalline drug to its respective amorphous counterpart[2]. However, the main drawback of the use of individual amorphous drugs is their physical instability during manufacturing, storage or administration with respect to their inherent tendency to recrystallize due to the fact that they are thermodynamically unstable[3]. One strategy to improve the stability of amorphous drugs is to incorporate them into amorphous polymers to create glass solutions[4], which can be described as molecular

mixtures of a drug and a hydrophilic polymer. The increased physical stability of these amorphous systems can be explained (at least in part) by their increased glass transition temperature (T_g), compared to the T_g of the pure amorphous drug, resulting from the frequently high T_g of the polymers. In this case we tried used aminoacid as stabilizer and PVP[6,7]. As drug we used Indomethacin – poorly water soluble BCS class II drug. Indomethacin is a nonsteroidal anti-inflammatory drug (NSAID) that reduces fever, pain and inflammation. We tried to prepare co-amorphous mixtures with aminoacid and polymer and will see that is working, is stable or not.

2. MATERIAL AND METHODS

Materials

Indomethacin (IND, *M*=357.79 g/mol) was purchased from Hawking, Inc. Pharmaceutical Group (Minneapolis, USA). The amino acids L-tryptophan (TRP, *M*=204.23 g/mol) was obtained from Sigma-Aldrich (St. Louis, USA). As polyvinylpyrrolidon, was selected Kollidon VA 64 from BASF (The Chemical Company, Germany). All compounds were used as received.

Methods

Preparation of the amorphous form

Co-amorphous blends of drug, amino acid and PVP were prepared by vibrational ball milling. The ball milling samples were produced by placing a total mass of 500 mg of the crystalline compounds, or the appropriate amount of drug and amino acid at the molar ratio 1:1 with 0 %, 1 %, 2 %, 5 % of PVP, respectively, into 25 ml milling jars with two 12 mm stainless steel balls, and milling at 30 Hz for 90 min in an oscillatory ball mill (Mixer Mill MM400, Retch GmbH & Co., Haan, Germany), which was placed in a cold room (+6 °C).

Dynamic mechanical analysis (DMA)

The Q800 DMA (TA instruments, New Castle) was used to measure the glass transition temperature of amorphous samples.

3. RESULTS AND DISCUSSION

All co-amorphous mixtures revealed a single glass transition temperature (T_g). We can investigate that addition of PVP has good response, because with higher addition of PVP we have higher glass transition temperature. Results are in Table 1. Type of result is in Figure 1.

Table 1.: Glass transition temperature T_g from DMA

	T_g (°C)
0 % PVP	94,06
1 % PVP	97,50
2 % PVP	99,42
5 % PVP	100,20

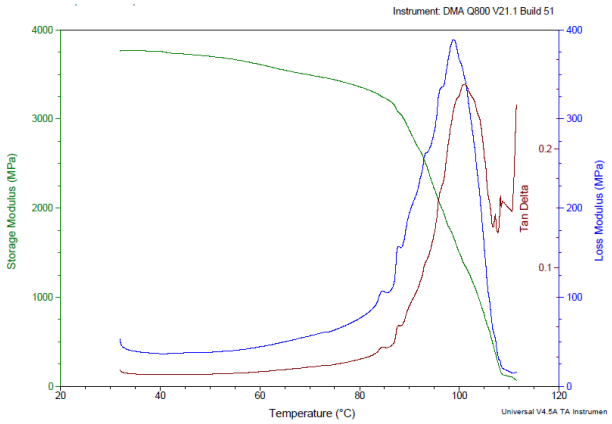

Figure 1.: DMA – addition of 2 % PVP

4. CONCLUSION

In this study mechanical activation ball milling was successfully applied to obtain co-amorphous mixtures of indomethacin and as stabilizers was used tryptophan and addition of PVP Kollidon VA 64. The improved compared to the amorphous physical mixtures stability can be attributed to the formation of an IND-TRY molecular mixture where aminoacid acts as a stabilizing component (anti-plasticizer), which is beneficial for stability even in the absence of molecular interactions.

Glass transition increases with addition of PVP. DMA is useful method for determined glass transition temperature. We can use as a complementary method for DSC (differencial scanning calorimetry).

5. ACKNOWLEDGEMENT

This work was supported by project Nr. LO1211, Materials Research Centre at FCH BUT-Sustainability and Development (National Programme for Sustainability I, Ministry of Education, Youth and Sports).

6. REFERENCES

[1] Hauss D. J: Advanced Drug Delivery Reviews, 59 (2007), 667-676
[2] Aaltonen J, Rades T: Dissolution Technologies, 16 (2009), 2, 47-54
[3] Hancock B. C, Zografi G: Journal of Pharmaceutical Sciences, 86 (1997), 1, 1-12
[4] Kauschal A. M, Gupta P, Bansal P: Critical Reviews in Therapeutic Drug Carrier Systems, 21 (2004), 3, 133-193
[5] Vasconcelos T, Sarmento B, Costa P: Drug Discovery Today, 23 (2007), 24, 1068-1075
[6] Löbmann K, Groghanz H, Laitinen R, et all.: European Journal of Pharmaceutics and Biopharmaceutics, 85 (2013), 3, 873-881
[7] Jensen K, Larsen F. H, Cornett C, et all: Molecular pharmaceutics, 12 (2015), 7, 2484-2492
[8] Taylor L. S, Zografi G: Pharmaceutical Research, 14 (1997), 12, 1691-1698

GENERATION OF OXIDATION DOUBLE PEAK OF GUANINE IN URACIL SUBSTITUTED DNA FRAGMENT

Aneta VEČEŘOVÁ, Libuše TRNKOVÁ, Iveta TŘÍSKOVÁ

[1] *Masaryk University, Faculty of Science, Department of Chemistry, Kamenice 5, CZ-62500 Brno, CZ*

Abstract

The formation of anodic guanine double peak when oxidizing reduced deoxyribonucleic oligonucleotide containing uracil DNA(U) was studied on static mercury electrode in phosphate-acetate buffer solution (pH 4.5) at different potentials of guanine residue reduction.

1. INTRODUCTION

A typical cyclic voltammogram of DNA (i.e. dependence of generated current on polarization potential) consists of reduction peaks of adenine (A) and cytosine (C) residues which often fuse together at approximately -1.4 V; under certain circumstances it is even possible to detect anodic peak corresponding to oxidation of guanine residues [1]. This anodic current is generated by reverse oxidation of dihydrogen derivative which is a product of guanine residue reduction [2]. In other words, to obtain guanine oxidation signal it is necessary to reduce relevant residue at sufficiently negative potential and to introduce reverse anodic scan after guanine reduction (e.g. by the means of cyclic voltammetry). Usually the guanine oxidation signal has form of a single peak, however, under special condition (such as the choice of phosphate-acetate buffer without ammonium formate) the anodic peak may be shaped as double peak (e.g. [3]). The mentioned formation of double peak attracts attention since the origin and formation of the second peak are unclear.

The aim of this work is to explore the behaviour of guanine oxidation double peak under different conditions and thus reveal its basic characteristics. As the examined nucleic acid an oligonucleotide (22 nt) with deoxyribonucleic backbone was used where thymines were replaced by uracil (DNA(U)).

2. MATERIAL AND METHODS

Lyophilized samples of DNA(U) of following sequence 5’-UGGCAGUGUCUUAGCUGGUUGU-3’ were purchased from Sigma Aldrich Company. Phosphate–acetate buffer was prepared as a mixture of acetic acid (glacial, Sigma Aldrich; ACS reagent), phosphoric acid (84%; p.a.; Penta Chrudim), and sodium hydroxide (Sigma

Aldrich; 97%; p.a.). The samples were measured at pH 4.5. All solutions were prepared in MILI Q water. The voltammetric experiment was realized using the electrochemical analyser μAUTOLAB TYPE III (Metrohm, Switzerland). The solution of DNA sample was dosed into the voltammetric cell with three-electrode set: the static mercury drop electrode (SMDE) as a working electrode, and Ag/AgCl/3M KCl and Pt wire as a reference and an auxiliary electrode, respectively.

3. RESULTS AND DISCUSSION

The sample of DNA(U) was diluted to the concentration of $6 \cdot 10^{-8}$ M and adsorbed on SMDE at a potential of 0 V for 120 s. Then the DNA(U) covering the mercury electrode was reduced by negative potential (from range -1.3 to -1.6 V) for 1.0 s. Subsequent anodic polarization of SMDE from -1 V to 0 V produced guanine double peak. The results indicate that the shape of double peak, especially the ratio between first (GI) and second (GII) guanine oxidation peak changes considerably with potential of guanine residue reduction (Figure 1). The first sign of guanine oxidation signal emergence is visible after the reduction at potential -1.35 V. With increasing the potential of reduction to more negative values, the first peak (GI) grows rapidly until the potential of reduction is -1.48 V. Afterwards there is a decrease in the height of the first peak (GI). At potential of reduction of -1.6 V there is a sudden shift in the ratio of the peaks (GI/GII).

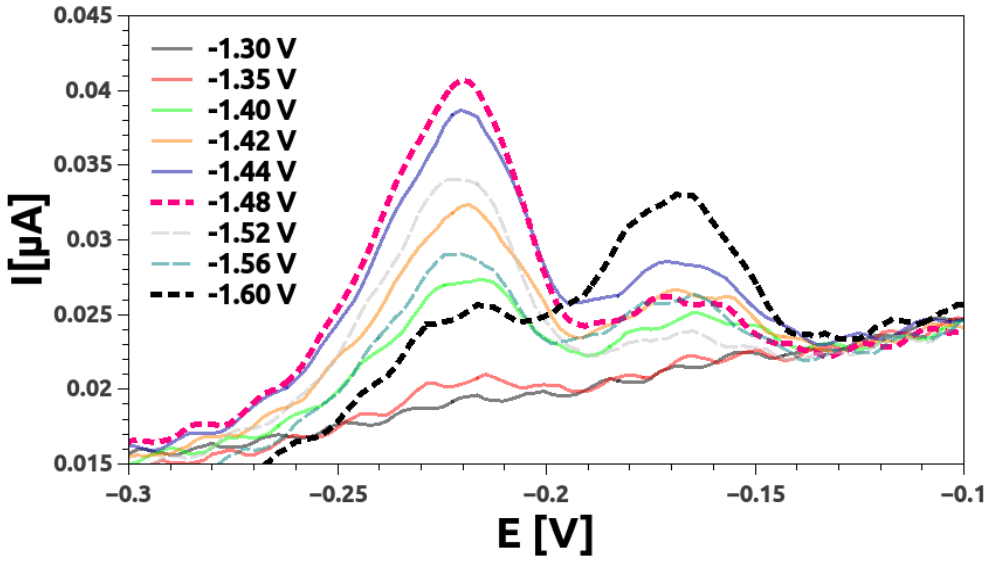

Figure 1.: LSV curves of $6 \cdot 10^{-8}$ M DNA(U) after 120 s of adsorption at 0 V with consecutive effect of reduction potential (in the legend) for 1.0 s. Measured in phosphate-acetate buffer (pH 4.5).

4. CONCLUSION

The shape dependence of guanine oxidation double peak was tested by reduction at different potentials. It may be concluded that the generation of the second (more positive) guanine peak has probably a higher energy barrier since it is sharply growing after setting the potential of reduction -1.6 V. This increase of second peak is accompanied by decrease of the first one – possibly because of conservation of the charge or because of the competition for free electrode surface sites with evolving hydrogen.

5. ACKNOWLEDGEMENT

The work has been supported by Central European Institute of Technology Project CZ 1.05/1.1.00/02.0068.

6. REFERENCES

[1] E. Palecek, F. Jelen, and L. Trnkova, “Cyclic Voltammetry of DNA at a Mercury-Electrode - an Anodic Peak Specific for Guanine,” Gen. Physiol. Biophys., vol. 5, no. 3, pp. 315–329, 1986.
[2] M. Studnickova, L. Trnkova, J. Zetek, and Z. Glatz, “Reduction of Guanosine at a Mercury-Electrode,” Bioelectrochem. Bioenerg., vol. 21, no. 1, pp. 83–86, 1989.
[3] I. Pilarova, I. Kejnovska, M. Vorlickova, and L. Trnkova, “Dynamic Structures of DNA Heptamers with Different Central Trinucleotide Sequences Studied by Electrochemical and Spectral Methods,” Electroanalysis, vol. 26, no. 10, pp. 2118–2128, 2014.

GET TO KNOW METROHM

Peter BARATH*

[1] *Metrohm Czech Republic, s.r. o.; Na Harfě 935/5c; CZ –190 00 Prague 9; Czech Republic*

**peter.barath@metrohm.cz*

REAL-TIME MONITORING OF INTERACTIONS BY EC-MP-SPR

Martin ALBERS[1], Niko GRANQVIST[1]*, Johana KUNCOVÁ-KALLIO[1]

[1] BioNavis Ltd, Hermiankatu 6-8H, 337 20 Tampere, Finland

niko.granqvist@bionavis.com

Abstract

Last few decades Surface Plasmon Resonance (SPR) has been used for label-free detection and characterization of biochemical kinetics and affinities. The physical phenomenon is not limited to biochemistry, but is also applicable for characterization of other nanoscale layers [1]. In addition to kinetic information (k_{on}, k_{off}), Multi-Parametric Surface Plasmon Resonance (MP-SPR, a novel method) quantifies also structural changes. Uniquely, two wavelength measurement allows calculation of refractive index (*RI)* and thickness (*d)* without prior knowledge of either parameter [2-3]. The measurements can be conducted on subnanometer thick (3.7 Å graphene measured in [4]) up to micrometer (drug release from 5 µm thick co-polymer measured in [5], living cells [6]) thick layers.

Here, we present a combination of MP-SPR with electrochemical methods for electrodeposition of thin films in-situ, for studies of electroswitchable surface and for validation of electrochemical biosensors. The examples include parallel measurements of MP-SPR with potentiometric, amperometric or impedance spectroscopy.

1. INTRODUCTION

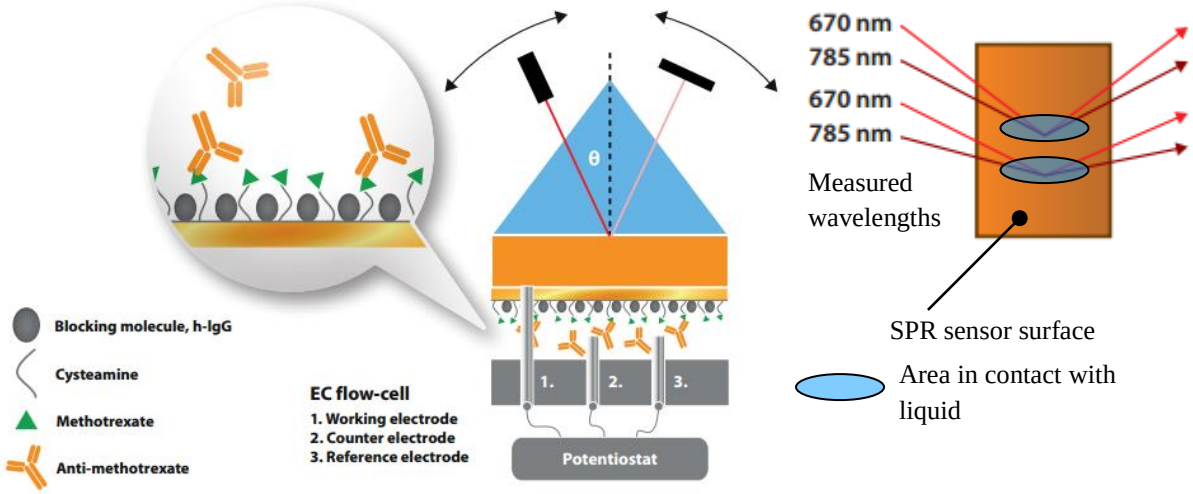

Figure 1.: Left: Set-up of EC-MP-SPR configuration. Right: In MP-SPR measurement, the changes are measured in angular scanning mode at two different wavelengths, here in a 2-channel set-up.

Metal stripping and deposition

Surface plasmon resonance is especially sensitive to changes in metal layers, such as control of thickness, cleanliness, surface roughness, doping or de-doping processes. Electrochemistry coupled to SPR (EC-MP-SPR) was employed to follow the elementary processes of electrodeposition and stripping of metals. Such combination with amperometric or coulometric methods enables analysis of the formed layers in real-time and label-free.

Electroswitchable surfaces

CP polymer poly (3,4-ethylenedioxythiphene) (PEDOT) and poly(acrylic acid) (PAA) were studied at different pH and electric potential. PEDOT is biocompatible and electroactive in aqueous solutions, while PAA brushes are pH responsive.

Biosensor development

In this experiment, binding reaction of small molecule weight drug methotrexate (MTX) to immobilized anti-methotrexate was followed.

2. MATERIAL AND METHODS

Metal stripping and deposition

MP-SPR Navi™ 200 OTSO instrument was equipped with an electrochemical flow-cell that was connected with PalmSens3 potentiostat in order to deposit copper onto a clean gold SPR sensor. The deposition was performed using a 0.1 M $CuSO_4$ solution in 0.1 M HCl at a flow-rate of 100 µL/min. A baseline was acquired during the first one minute of the measurement. After that an oxidation current of 50 µA was applied for a duration of 2.5 minutes. The measurement was performed in angular scanning mode of MP-SPR at two wavelengths simultaneously in two liquid channels (see Figure 1), in order to acquire data for thickness and refractive index analysis.

Electroswitchable surfaces

SPR Navi™ 200 with an electrochemical flow-cell was used to monitor changes in film morphology caused by changed potential (0.4, 0 and -0.25V) (CH Instruments 650). BrEDOT was polymerized using cyclic voltametry. PAA brushes were grafed onto the surface (more details in [7]) Surfaces were measured in 50mM NaCl solution at pH 4 and pH 9.

Biosensor development

In this experiment, MP-SPR Navi™ VASA was equipped with an electrochemical flow-cell (Figure 2). Solid state reference electrodes (SSRE by BioNavis) made of an Ag/AgCl wire covered with a chloride-containing PVC/PU membrane were connected to a potentiostat (PalmSens3) for potentiometric and impedance measurements. MTX (454 Da) was immobilized on a self-assembled layer of cysteamine and activated with glutar-aldehyde (GA) *ex situ*. PBS was used as a running buffer at pH 7.45. All measurements were performed in angular scanning mode of MP-SPR at two wavelengths (670 nm and 785 nm) in two fluidic channels simultaneously with electrochemical measurements (Figure 2).

The electrochemical impedance spectroscopy (EIS) measurement first cycle determined the open circuit potential (E_{oc}) and then collected an impedance spectrum in the frequency range of 1 to 20 000 Hz at this potential. The cycle time was 100 seconds. The experiment was run overnight in a fully automated mode.

3. RESULTS AND DISCUSSION

In all examples, the two wavelength MP-SPR angular scan data was analysed using LayerSolver™ to obtain thickness (*d*) and optical constants (*n*, *k*) of the formed layers. Gold sensor slide optical constants and thicknesses were fitted using Fresnel equations with background values for the calculation.

Metal stripping and deposition

The deposition of copper can be seen in the MP-SPR measurements (Figure 3 left) as shift of the peak minimum to the right (change in thickness) and as shift of the peak upwards (attributed to the light absorbance of the formed Cu layer). The resulting thickness change over time in both liquid channels can be seen in Figure 3 right. The calculated refractive index (*n*) and extinction coefficient (*k*) are shown in the insert. In theory, the optical constants should be similar to those of gold. In this case, they differ most likely due to nonhomogeneous growth, i.e. reflecting the deposition of copper intermediates or copper nanoparticles, which have a rather high *RI* and *k* [8].

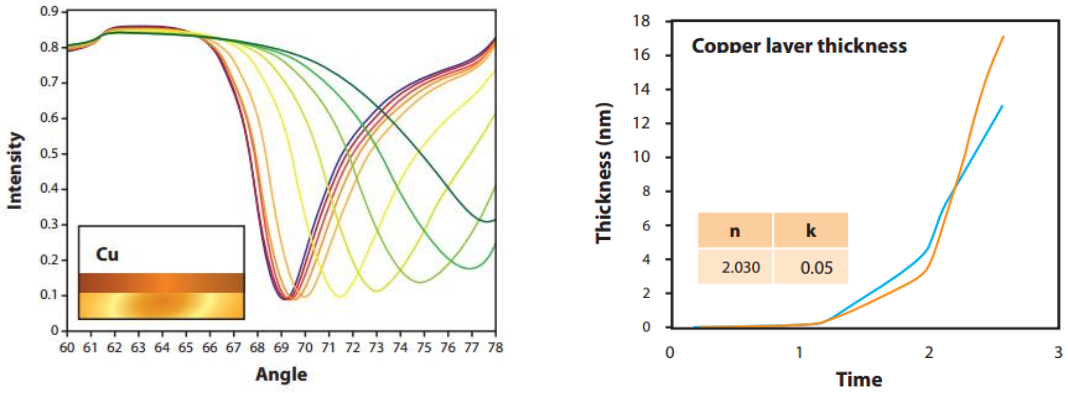

Figure 2.: Here, the measurements at 670 nm wavelength are shown for the duration of the electrodeposition of copper (2.5 minutes). Left: MP-SPR curves. Right: Calculated thickness in both liquid channels.

Electroswitchable surfaces

Using MP-SPR data analysis, the PBrEDOT layer thickness was determined as 18 nm and PAA as 15 nm thick. PEDOT shows a large response to the potential due to the changed oxidation state and therefore also in RI (Figure 3c-d). In basic environment (pH 9) PBrEDOT-g-PAA brushes shoe slow increase in SPR angle (Figure 3a), which is likely due to the PAA conformational change (collapse during polymer oxidation). At pH4, PAA brushes are already collapsed and therefore similar effect is not seen. (Figure 3b)

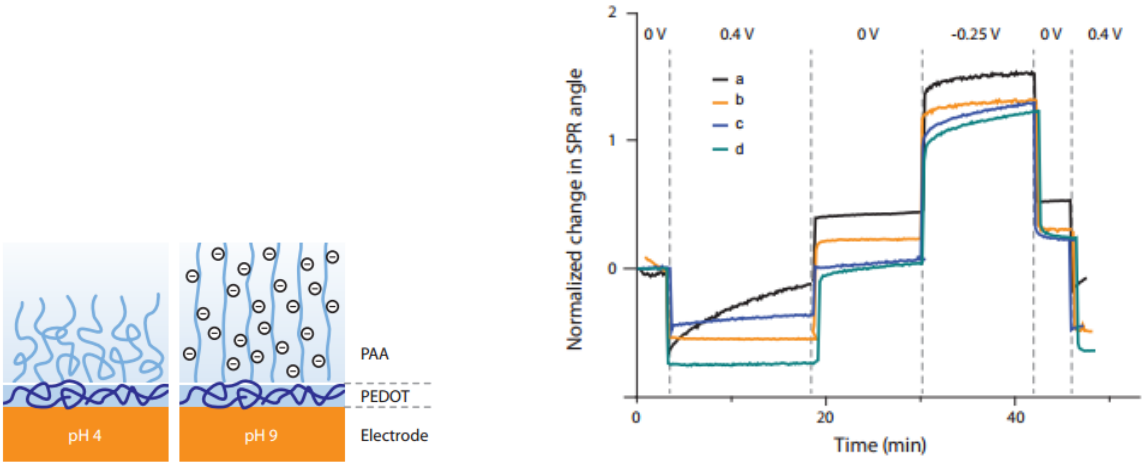

Figure 3.: MP-SPR measurement of electroswitchable surfaces.

Biosensor development

Figure 4 shows measurement results of MP-SPR and potentiometry (left) and MP-SPR and impedance spectroscopy (right). The results are in line with expectations for penetration depth of different methods. While potentiometry records only reactions at the vicinity of the surface (a few Ångströms), MP-SPR and EIS reach deeper.

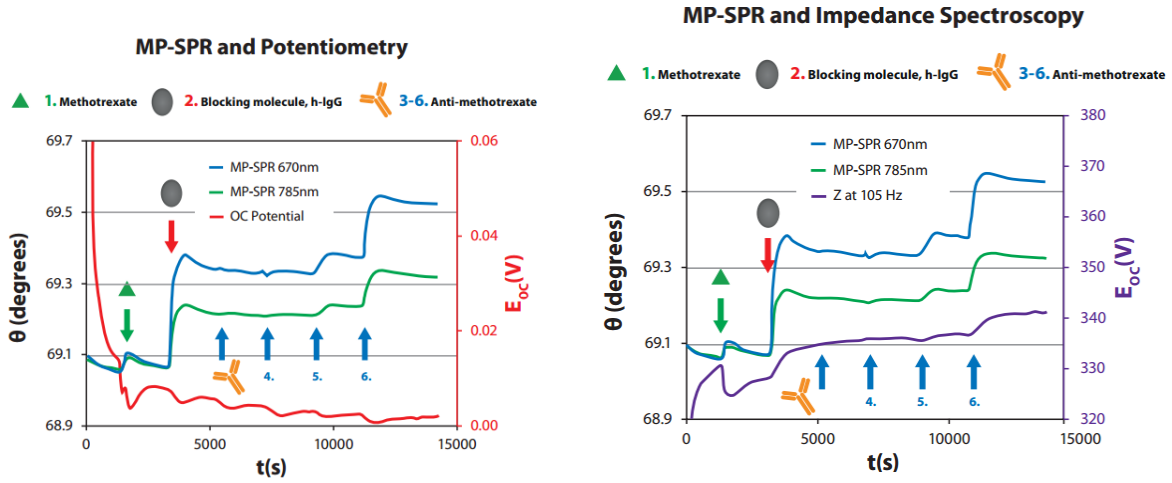

Figure 4.: Binding of anti-MTX to MTX. Injections: 1. MTX, 2. hIGg, 3. anti-MTX (0.1 µg/mL), 4. anti-MTX (1 µg/mL), 5. anti-MTX (10µg/mL) and 6. anti-MTX (100 µg/mL).

4. CONCLUSION

In this paper, MP-SPR was shown in parallel use with a variety of electrochemical techniques for following of real-time events at the surface. Three experiments were described, where EC-MP-SPR was used: (1) Metal electrodepostion, (2) Electroswitchable surfaces and (3) Biosensor development. The combinations included MP-SPR with potentiometry, impedance spectroscopy and electrodeposition. Such simultaneous measurements provide more complete analysis of surface interactions.

5. REFERENCES

[1] Albers MW, Vikholm-Lundin I, Nano-Bio-Sensing, Springer (2010)
[2] Granqvist N et al., Langmuir. 30 (2014), 10, 2799–2809
[3] Granqvist N, Liang H, Laurila T, et al., Langmuir 29 (2013), 27, 8561–8571
[4] Jussila H, Yang H, Granqvist N, Sun Z, Optica 3 (2016), 2, 151-158
[5] Korhonen K, Granqvist N, Ketolainen J, Laitinen R, Int. J. of Phramaceutics 494 (2015), 531-536
[6] Viitala T, Granqvist N, Hallila S, et al., PLoS ONE 8 (2013), 8
[7] Malmström J, Nieuwoudt MK, Strover LT, et al. Macromolecules 46 (2013), 12, 4955-4965
[8] Popov KI, Djokic SS, Nikolic ND, Jovic VD, Morphology of Electrochemically and Chemically Deposited Metals, Springer (2016)

NOVÝ ZETASIZER fy MALVERN

POSKYTUJE RYCHLOU A VYSOCE CITLIVOU CHARAKTERIZACI PROTEINŮ

Zetasizer Nano ZSP

*Nový **Zetasizer Nano ZSP** firmy Malvern navazuje na široce rozšířený a oblíbený Zetasizer ZS. Pracuje opět na principu dynamického rozptylu světla a jeho schopnosti směrem k charakterizaci proteinových molekul jsou zároveň významně posíleny. Je to především schopnost rychlého a spolehlivého měření elektroforetické mobility proteinů a následné kalkulace tak zásadního parametru, jakým je hodnota náboje na daném proteinu. Měření proteinové mobility (resp. zeta potenciálu) pomocí dynamického rozptylu světla je rychlejší a spolehlivější než konvenční metody, jako jsou kapilární elektroforéza a iso-elektrické fokusování. Navíc Zetasizer ZPS vyžaduje pouze 20 mikrolitrů vzorku a je schopen snímat koncentrace až do 1 mg/ml.*

Klíčem k těmto schopnostem je docílení vysoké citlivosti systému a schopnosti zabránit nežádoucím agregacím a samozřejmě výkonný software, který je schopen okamžitě prezentovat data v použitelném formátu. Zetasizer Nano ZSP má takovou citlivost snímání signálu, že může měřit i slabě rozptylující se vzorky, jako jsou proteiny. Proces snímání mobility proteinů tak, aby maximalizoval kvalitu naměřených dat, je postaven na 3 specifických konstrukčních momentech. Především kombinací měření velikosti a zeta potenciálu se zabrání agregaci, která se vytváří během měření. Tato, v případě že nastane, je indikována. Dále, měření mobility je prováděno v podskupinách tak, aby byla umožněna delší časová perioda chlazení a nedošlo k zahřívání, které je příčinou aglomerace. A za třetí, automatická optimalizace nastavení parametrů měření minimalizuje denaturaci a agregace během snímání mobility.
Do softwaru nového Zetasizeru Nano ZSP byla doplněna sada proteinových kalkulátorů. Je to především DLS Debye Plot, který umožnuje výpočet DLS interakčního parametru užitečného zejména při proteinové formulaci biologických terapeutických preparátů. Dále je zde možnost spočítat náboj proteinu z proteinové mobility tzv. F(ka) z Henryho rovnice, mezičásticovou vzdálenost a thermodynamický diametr (viriální radius).
Navíc ke všem těmto schopnostem a funkcím nová verze software, která je standardní výbavou nového Zetasizeru Nano ZSP, umožňuje úplně novou měřicí funkci, a to tzv. Mikroreologii. Tato optická technika postavená na dynamickém rozptylu světla DLS umožnuje reologickou charakterizaci slabě strukturovaných a při tom vysoce citlivých materiálů na namáhání, a to použitím mikrolitrových objemů vzorku. Je tak možné měřit viskozitu polymerních a proteinových roztoků a zaznamenat začátek aglomerace.
Rozšířená řada skupiny Zetasizerů je tak rozšířena o systém, který je schopen charakterizovat velikost, Mw a zetapotenciál, a navazuje tak na již vyráběné modely, jako je Zetasizer APS pro automatické měření velikosti proteinů ve vícejamkových destičkách a na Zetasizer μV, který je určen pro měření velikosti a Mw proteinů, jak v kyvetě tak i v chromatografickém módu (např. v kombinaci s s GPC/SEC systémem).

Ing. Jiří Hrdlička, anamet s.r.o., hrdlicka@anamet.cz

NTA – Nanoparticle Tracking analyzátory fy MALVERN

Pro analýzu nanočástic v rozmezí velkosti 20 – 2000 nm nabízí firma Malvern unikátní zařízení NS 300, které pracuje na bázi „Nanoparticle Tracking Analysis – NTA". Česky můžeme tento název popsat jako „Analýza Trajektorie Nanočástic". Nanočástice v laserovém paprsku rozptylují světlo a jsou viditelné jako body v mikroskopu. Pohyb a intenzita rozptýleného světla je snímána citlivou kamerou a tyto parametry jsou vyhodnocovány pomocí originálního software, který analyzuje trajektorie jednotlivých nanočástic v roztoku a na základě jejich Brownova pohybu vypočítá difusní koeficient a hydrodynamický poloměr. Měření jednotlivých individuálních nanočástic umožňuje analýzu velmi komplexních vzorků s vysokou polydispersitou (např. některé typy liposomálních preparátů, směsi nanočástic z různých materiálů, nanočástice s tendencí agregovat atd.). Takové vzorky jsou obtížně analyzovatelné jinými metodami jako například technikou DLS (dynamický rozptyl světla).
Další předností metody je možnost rychle změřit absolutní počet nanočástic v roztoku (např. viry a virům podobné částice VLP, liposomy, Q-dot) Tento zásadní údaj pro toxikologické, imunologické, virologické a farmakologické studie lze získat jen obtížně jinými metodami.
Přístroj NS 300 nabízí ještě další unikátní možnost selektivní analýzy a to využití fluorescence.
Obtížně analyzovatelné vzorky jako například viry a virům podobné částice zpravidla obsahují kontaminanty v podobě buněčného debritu, který není možné ve všech případech snadno odstranit. Viry a VLP lze snadno označit například fluorescenčně značenými protilátkami a analyzovat pouze částice, které vykazují fluorescenční signál.

Aplikace NTA analýzy na přístroji NS 300 zahrnují zejména tyto oblasti:

- Viry, virům podobné částice, vakcíny, olejová adjuvans (zejména SOP pro kontrolu kvality ve farmaceutickém průmyslu)

1. Exosomy a extracelulární vesikuly (výzkumné laboratoře zaměřené na medicínský výzkum)
2. Biokompatibilní nanočástice pro cílení léčiv (liposomy, biopolymerní nanočástice, syntetické polymerní nanočástice) – (akademický výzkum, farmaceutický a biotechnologický průmysl – výzkum a SOP pro kontrolu kvality)
3. Stanovení agregace proteinů a stability nanočásticových systémů (akademický výzkum, farmaceutický a chemický průmysl)
4. Nanotoxikologie a ekonanotoxikologie (charakterizace nanočástic – polutanty, nanopesticity, nanofungicidy adt., – jejich stabilita a distribuce v organismech a ekosystémech) – akademický a universitní výzkum
5. Charakterizace nanomateriálů dle norem a regulací EU (specializované akreditované laboratoře).
6. Genová Terapie a Nanomedicína – charakterizace genových vektorů (akademický biomedicínský výzkum, farmaceutický výzkum a průmysl)

NS 300 v kombinaci s přístrojem ZetaNanosizer tvoří ideální komplementární dvojici kombinující technologie NTA a DLS pro analýzu velmi komplexních vzorků v rozsahu velikosti částic 0.3 – 6000 nm.

TYTO PŘÍSTROJE BUDOU VYSTAVENY NA XXV. BIOCHEMICKÉM SJEZDU.

Fy MALVERN zastupuje ANAMET s.r.o., www.anamet.cz/sales@anamet.cz

DONAU LAB Prague
Member of LPPgroup

KEM KYOTO ELECTRONICS
MANUFACTURING CO.,LTD.

- Karl Fischer titrátory
- Potenciometrické titrátory
- Hustoměry
- Refraktometry

DONAU LAB, výhradní distributor produktů firmy KEM Kyoto Electronics v České republice.

DONAU LAB, s.r.o.
Třebohostická 14, 100 31 Praha 10
Tel: +420 261 305 321,
office-cz@donaulab.com
www.donaulab.cz

XVI. WORKSHOP OF PHYSICAL CHEMISTS AND ELECTROCHEMISTS

XVI. WORKSHOP OF PHYSICAL CHEMISTS AND ELECTROCHEMISTS

BRNO 2016

Excellence in Surface Plasmon Resonance
BioNavis

METODA SPR
STUDIUM VLASTNOSTÍ POVRCHOVÝCH VRSTEV A INTERAKCÍ MOLEKUL

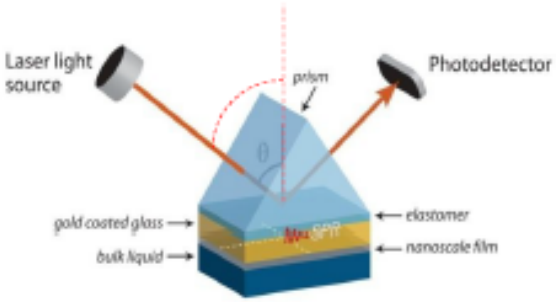

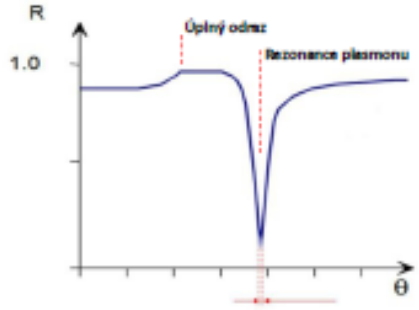

Metoda SPR

Volné elektrony tvoří zejména ve vzácných kovech elektronový plyn, který může být excitován např. světlem a tím vzniká rezonance plazmonu na površích těchto kovů. Rezonace povrchového plazmonu způsobuje při určitém úhlu dopadu pokles intenzity odraženého světla a umožňuje sledovat vlastnosti vrstvy přilehlé k rozhraní kovu, na kterém k tomuto jevu dochází. Kromě sledování vlastnosti povrchových vrstev můžeme studovat interakce (bio)molekul na těchto vrstvách a kinetiku na nich probíhajících reakcí.

Multiparametrické SPR

Oproti tradiční SPR obsahuje navíc přesný goniometr umožňující záznam kompletních křivek SPR, možnost použití laserů až o 3 různých vlnových délkách a měření absolutních hodnot, nikoli pouze relativních změn. Díky širokému úhlovému rozsahu lze charakterizovat povrchy nejen v kapalinách, ale i v plynech.

Model **SPR Navi 200** je určen pro měření jednotlivých vzorků ve dvoukanálové průtokové cele. Nový automatizovaný systém **SPR Navi 420A** je vybaven čtyřmi kanály a integrovaným autosamplerem.

Modulární
MP-SPR Navi™ 200
OTSO

Automatický
MP-SPR Navi™ 420A
ILVES

Co můžeme měřit:

Materiálový výzkum	Life Sciences	Vývoj senzorů
Index lomu (RI), komplexní RI	Kinetika vazby	Hmotnost povrchové vrstvy
Tloušťka vrstvy (zároveň s RI)	Afinita	Změna hmotnosti
Hmotnost	Specifita vazby	Afinita
Adsorpce/absorpce	Stochiometrie	Molekulární interakce
Adheze	Entalpie vazby	Elektrochemická měření
Kinetika	Aktivační energie	Tloušťka vrstvy
Elektrochemická měření	Změna hmotnosti	Optické vlastnosti
Hustota	Asociační konstanta	Hustota
Optické vlastnosti	Disociační konstanta	
Dielektrická konstanta		

CHROMSPEC SPOL. S R.O.

Mníšek pod Brdy
Brno

Tel.: 318 599 083
Tel.: 547 246 683

info@chromspec.cz
www.chromspec.cz

XVI. WORKSHOP OF PHYSICAL CHEMISTS AND ELECTROCHEMISTS

BRNO 2016

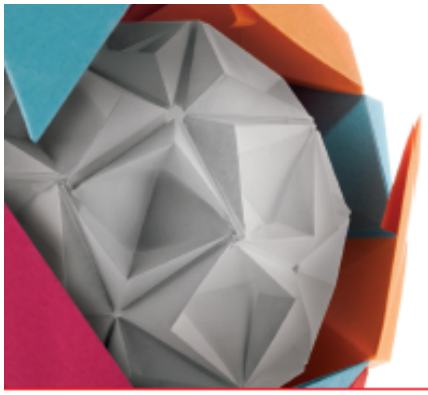

SUPELCO
Solutions within.

Ascentis® Express UHPLC Columns 30% Off

When ordering please mention Promotion Code: **U73**

Offer is valid from 01.05.2016 – 30.06.2016

Ascentis® Expres Fused Core Particles and Phases

Faster HPLC on Any System

The Ascentis® Express column line is completely scalable from UHPLC to legacy HPLC systems. Three particle sizes, 2.0, 2.7 and 5.0 µm, and nine unique chemistries are avail able making method development seamless across your organization.

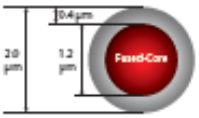

Best Fused-Core UHPLC Column
An optimized solution for high-throughput small molecule analysis

Fast HPLC on ANY System
A practical solution that delivers UHPLC performance from any HPLC

The Lab Work-Horse Column
True plug and play solution for improving existing 3 or 5 µm porous particle HPLC columns

A New Choice in Selectivity

The Ascentis® Express Biphenyl U/HPLC column offers extra separation power for the optimization of compounds that are challenging to resolve or elute early on C18 and other phenyl phases.

This new chemistry expands the selectivity choices offered in our Fused-Core® particle line-up:

- C18
- C8
- RP-Amide
- Phenyl Hexyl
- F5
- Biphenyl – **new**
- ES-Cyano
- HILIC (Si)
- OH5

To learn more about Ascentis® Express UHPLC columns, visit **sigma-aldrich.com/expres**

Ascentis® Express 2.7 µm Biphenyl U/HPLC Columns

Length	Internal Diameter		
	2.1 mm	3.0 mm	4.6mm
2 cm	64043-U	64047-U	64051-U
3 cm	64054-U	64055-U	64056-U
5 cm	64057-U	64058-U	64059-U
7.5 cm	64061-U	64062-U	64064-U
10 cm	64065-U	64066-U	64067-U
15 cm	64068-U	64069-U	64071-U
Guard Cartridges, pk 3	64074-U	64076-U	64078-U

When ordering please mention Promotion Code: U73. *Offer is valid from 01.05.2016 – 30.06.2016.*

SIGMA-ALDRICH®

XVI. WORKSHOP OF PHYSICAL CHEMISTS AND ELECTROCHEMISTS

BRNO 2016

XVI. Workshop of Physical Chemists and Electrochemists

Book of abstracts

Editor: Libuše Trnková

Technical adjustment: Iveta Třísková

Published by Masaryk University, Brno 2016

1th edition

ISBN 978-80-210-8267-0

XVI. WORKSHOP OF PHYSICAL CHEMISTS AND ELECTROCHEMISTS

BRNO
2016

muni
PRESS